MB 2025-04

U-Pb geochronology of samples from Québec by laser ablation inductively coupled plasma mass spectrometry (LA-ICPMS)

Documents complémentaires

Additional Files

Licence

License

Ressources naturelles et Forêts
Québec

U-Pb geochronology of samples from Québec by laser ablation inductively coupled plasma mass spectrometry (LA-ICPMS)

Heriberto Rochín-Banaga and Donald W. Davis

MB 2025-04

Ressources naturelles et Forêts
Québec

U-Pb geochronology of samples from Québec by laser ablation inductively coupled plasma mass spectrometry (LA-ICPMS)

January 2025

Heriberto Rochín-Banaga and Donald W. Davis
Jack Satterly Geochronology Laboratory, Department of Earth Sciences, University of Toronto, 22 Ursula Franklin St., Toronto ON Canada M5S 3B1

SAMPLES

New U-Pb geochronological data are reported for 24 Precambrian rock samples from northern Québec. U-Pb ages were determined on selected grains of zircon and monazite using laser ablation inductively coupled plasma mass spectrometry (LA-ICPMS). A sample list, grouped by project, is given below (Table 1). Sample locations are presented in Table 2 ("Autres données numériques" folder). No datable minerals were found in sample 2023-WM-5082A (volcanoclastite felsique à intermédiaire). Samples 2023-GM-1685A, 2023-MV-1114A, and 2023-MV-1169A were put on hold before U-Pb dating by James Moorhead.

Table 1. List of samples.

	Numéro d'échantillon	Lithologie	Résultats
1.	**Churchill - Baie Déception**		
1.1	2023-MV-1021A	Granite rose à biotite et magnétite	zircon: 2801.6 ±3.3 Ma
1.2	2023-MV-1049A	Granite à muscovite et grenat	zircon: 1749 ±6 Ma monazite: 1702 ±6 Ma
1.3	2023-MV-1052A	Gneiss tonalitique à biotite et hornblende	zircon: 2813 ±4.4 Ma
1.4	2023-MV-1083A	Gneiss tonalitique à biotite et hornblende	zircon: 2823 ±2.7 Ma

1.5	2023-MV-1178A	Gneiss tonalitique à biotite et hornblende	zircon: 2753.5 ±2.3 Ma
1.6	2023-MV-1187A	Diorite	zircon: 1841 ±2Ma
1.7	2023-CB-2031A	Gneiss tonalitique à biotite	zircon: 2760 ±3Ma
1.8	2023-CB-2035B	Granite	zircon: 1758 ±4.6 Ma - 2732 ±8 Ma
1.9	2023-CB-2120A	Diorite quartzifère	zircon: 1831.3 ±1.7 Ma
1.10	2023-GC-3082A	Paragneiss quartzitique	zircon: 1863 ±5 Ma
1.11	2021-TG-4060A	Paragneiss à grenat et biotite	zircon: 1843 ±3.8 Ma; 1859.2 ±2.1 Ma; 1885.2 ±3.3 Ma
2.	**Churchill - Est du Domaine Nord**		
2.1	2023-GM-1624B	Gneiss tonalitique à biotite et muscovite	zircon: 2747 ±4 Ma
2.2	2023-MV-1170D	Gneiss tonalitique à biotite et muscovite	zircon: 1781 ±37 Ma
2.3	2023-TD-2588A	Diorite quartzifère à grenat	zircon: 1840 ±2 Ma
2.4	2023-TD-2546C	Conglomérat à granules	zircon: 1875 ±9 Ma
2.5	2023-GM-1679B	Diorite quartzifère	zircon: 1899 ±2 Ma
2.6	2023-GM-1620A	Granite gris à biotite	zircon: 1882 ±3 Ma
2.7	2019-SM-6104A	Gabbro grossier	zircon: 1861 ±2.5 Ma
2.8	2022-TD-2084A	Wacke lithique	zircon: 1991 Ma to 2200 Ma
2.9	2022-MV-1044B	Arkose lithique	zircon: 1950-2100 Ma
3.	**Baie-James - Lac Michaux**		
3.1	2023-GS-4071A	Volcanoclastite intermédiaire	zircon: 2713 ±12 Ma; 2639 ±3 Ma

3.2	2023-DB-1059A	Quartzite	monazite: 2550 ±4 Ma
3.3	2023-NT-2078A	Gneiss tonalitique	titanite: 2587 ±9.5 Ma
3.4	2023-DB-1057A	Diatexite dérivée de paragneiss	monazite: 2658 ±5 Ma
3.5	2023-WM-5082A	Volcanoclastite felsique à intermédiaire	No zircon

METHODS

Following crushing and pulverization, initial separation of heavy minerals was carried out on a Wilfley table. This was followed by paramagnetic separations with the Frantz isodynamic separator and density separations using methylene iodide. Final sample selection for geochronology was by hand picking under a microscope, choosing the freshest, least cracked grains of zircon and monazite. Grains were mounted in epoxy, polished and imaged with backscattered electrons (BSE) using a JEOL JSM6610-Lv scanning electron microscope in order to detect zones of alteration, cracks, or inclusions and/or phases of growth that may have different ages.

U–Pb isotopic analyses were conducted at the University of Toronto using an Agilent 7900 ICPMS and an NWR193 excimer laser system. Data were collected using spot analyses conducted with laser wavelength of 193 nm, fluence of about 4 J/cm^2 and frequency of 10 Hz at a rate of 20 µm/s with typical beam diameter of 20-30 µm, depending on the sample. He flow from the ablation chamber was set a 100 liters/min.

Data were collected on ^{88}Sr (10 ms), ^{206}Pb (30 ms), ^{207}Pb (70 ms), ^{232}Th (10 ms), and ^{238}U (20 ms). Prior to analyses, spots were pre-ablated with a larger beam diameter for 1-2 s to clean the surface. Following a 10 s period of baseline accumulation, the laser sampling beam was turned on and data were collected for 20 s followed by a washout period of 10 s.

All results are based on ^{207}Pb/^{206}Pb ratios, which are much better estimators than ^{206}Pb/^{238}U ratios for Mesoproterozoic and older samples. ^{207}Pb/^{206}Pb data profiles are usually flat throughout the ablation process, whereas ^{206}Pb/^{238}U ratios increase due to

downhole elemental fractionation. This ratio is also subject to bias due to oxidation of U. Because of this, running conditions were optimized for $^{207}Pb/^{206}Pb$. ThO/Th was set at about 5% during tuning, which leads to a substantial enhancement of Pb sensitivity but may result in percent biases in $^{206}Pb/^{238}U$.

Data were edited and reduced using custom VBA software (UtilLAZ program) written by D. W. Davis. $^{206}Pb/^{238}U$ ratios show increasing fractionation for zircon caused by loss of refractory U with increasing penetration depth through the run while the $^{207}Pb/^{206}Pb$ profile is usually flat. No corrections were made for common Pb, because the ^{204}Pb peak is too small to be measured precisely in LA-ICPMS and common Pb is insignificant for unaltered Precambrian zircon and monazite. If present, as in other minerals such as titanite, common Pb would have the effect of pushing data to the right, away from the concordia curve along a shallow mixing line with slope determined by the isotopic composition of the common Pb contaminant. ^{88}Sr was monitored from zircon in order to detect intersection of the beam with zones of alteration or inclusions. Data showing high Sr signal accompanied by discordance or irregular time resolved profiles were either averaged over restricted time windows or rejected. In some cases, high Sr is due to ablation of apatite inclusions, and does not significantly affect the U-Pb analysis or ages.

The Th/U ratio of zircon can be a useful petrogenetic indicator and was also measured, although it is only a rough estimate because the ratio is not constant in the standard. Low Th/U (<0.1) is characteristic of metamorphic and hydrothermal zircon whereas most zircon crystallized from felsic melts has Th/U>0.1.

U-Pb LA-ICPMS RESULTS

Results of U-Pb isotopic analyses by LA-ICPMS are given in Table 3 (“Autres données numériques” folder) and data are plotted on Wetherill concordia. Average age errors are given at 95% confidence levels and error ellipses on figures are given at 2 sigma (2σ). These were calculated and plotted using the Isoplot program of Ludwig (1998, 2003). U decay constants are from Jaffey et al. (1971). Representative images

for individual samples are presented in the sections below. The notations on the BSE images are z - oscillatory zoning; c - core; m - mantle; k – cracked; U - high uranium (bright); L - low uranium.

1. Churchill - Baie Déception

1.1. 2023-MV-1021A
Granite rose à biotite et magnétite

This sample yielded large, generally cracked zircon grains with variable brownish coloration and subhedral to rounded morphology (Fig. 1.1.1). BSE images show unzoned domains with thin, slightly higher U overgrowths that are weakly zoned or unzoned (Fig. 1.1.2). Most analyses were carried out on the cores and even those targeting overgrowths may have largely penetrated into cores. U-Pb analyses show diverse ages ranging from 1969 Ma to 2921 Ma, but most define a major peak at an age of 2801.6 ±3.3 Ma (MSWD = 1.9) (Fig. 1.1.3 and 1.1.4). The peak has a younger tail consisting of variable Neoarchean ages that may indicate partial resetting (Fig. 1.1.4). A few slightly older ages may represent Archean inheritance. A single concordant analysis from grain 1, which may be on an overgrowth, gives a significantly younger age of 1969 ±46 Ma. This analysis also shows that lowest Th/U ratio suggesting that it may be metamorphic in origin. Th/U ratios of the other grains are typical of magmatic zircon (Th/U> 0.1). The most likely interpretation is that the pluton represents a late Mesoarchean granite metamorphosed and possibly remobilized during the Paleoproterozoic.

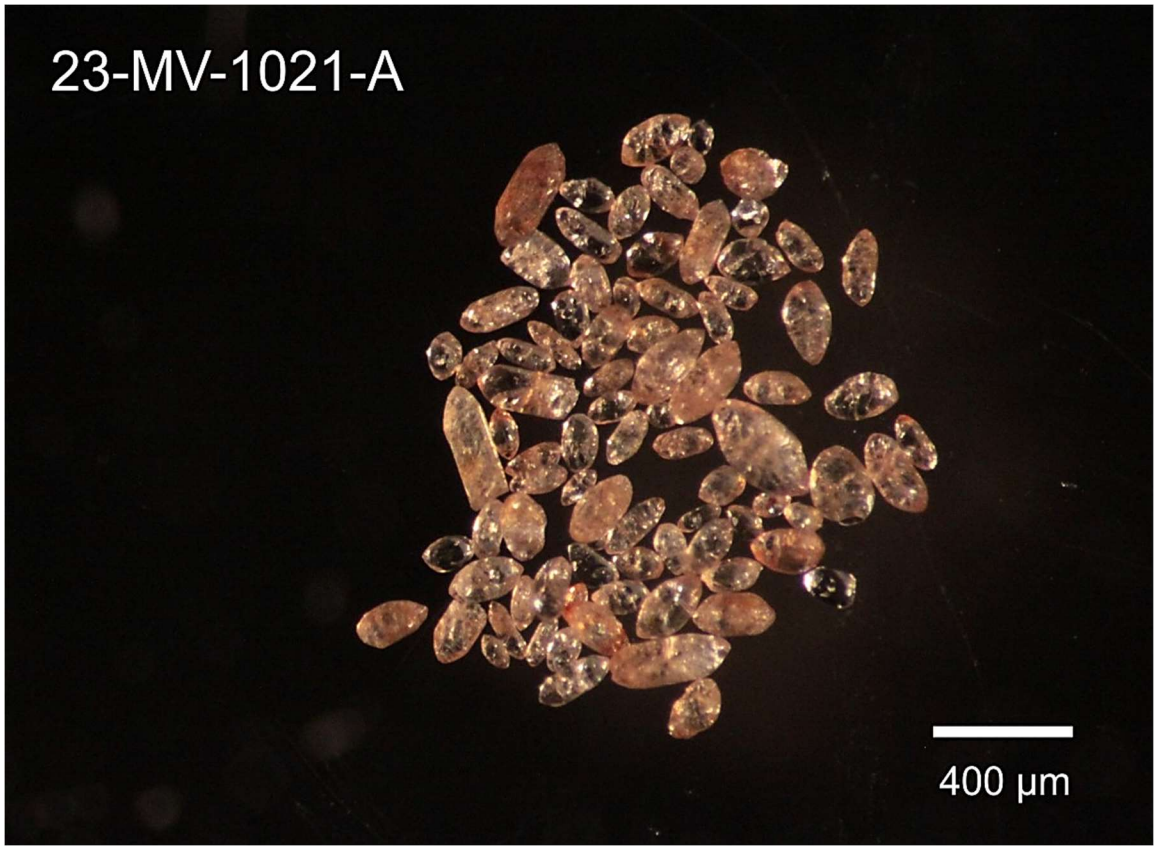

Figure 1.1.1. Picked zircon from granite sample 2023-MV-1021A.

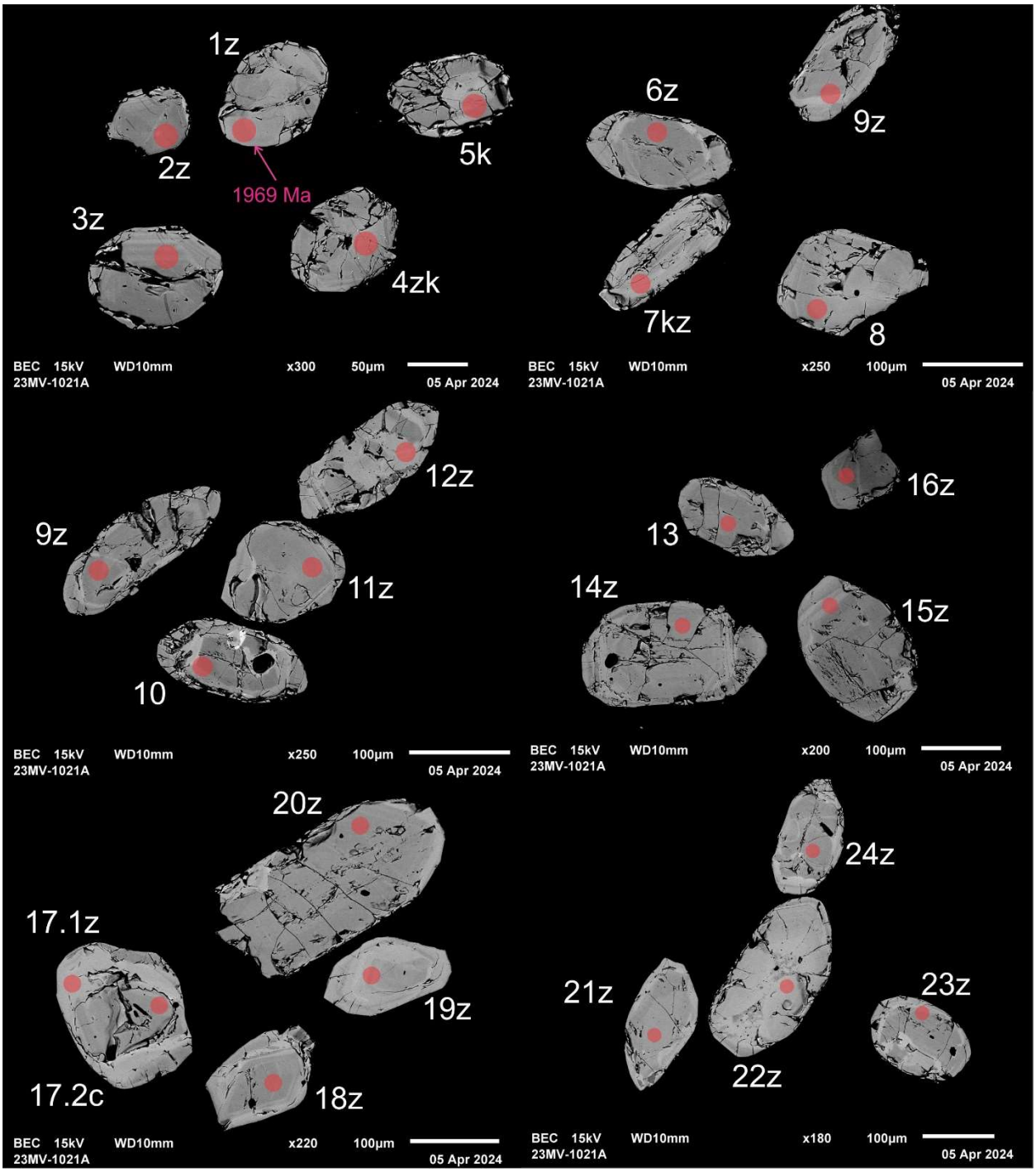

Figure 1.1.2. BSE images of selected grains from sample 2023-MV-1021A. The red circles represent the approximate locations of laser ablation spots.

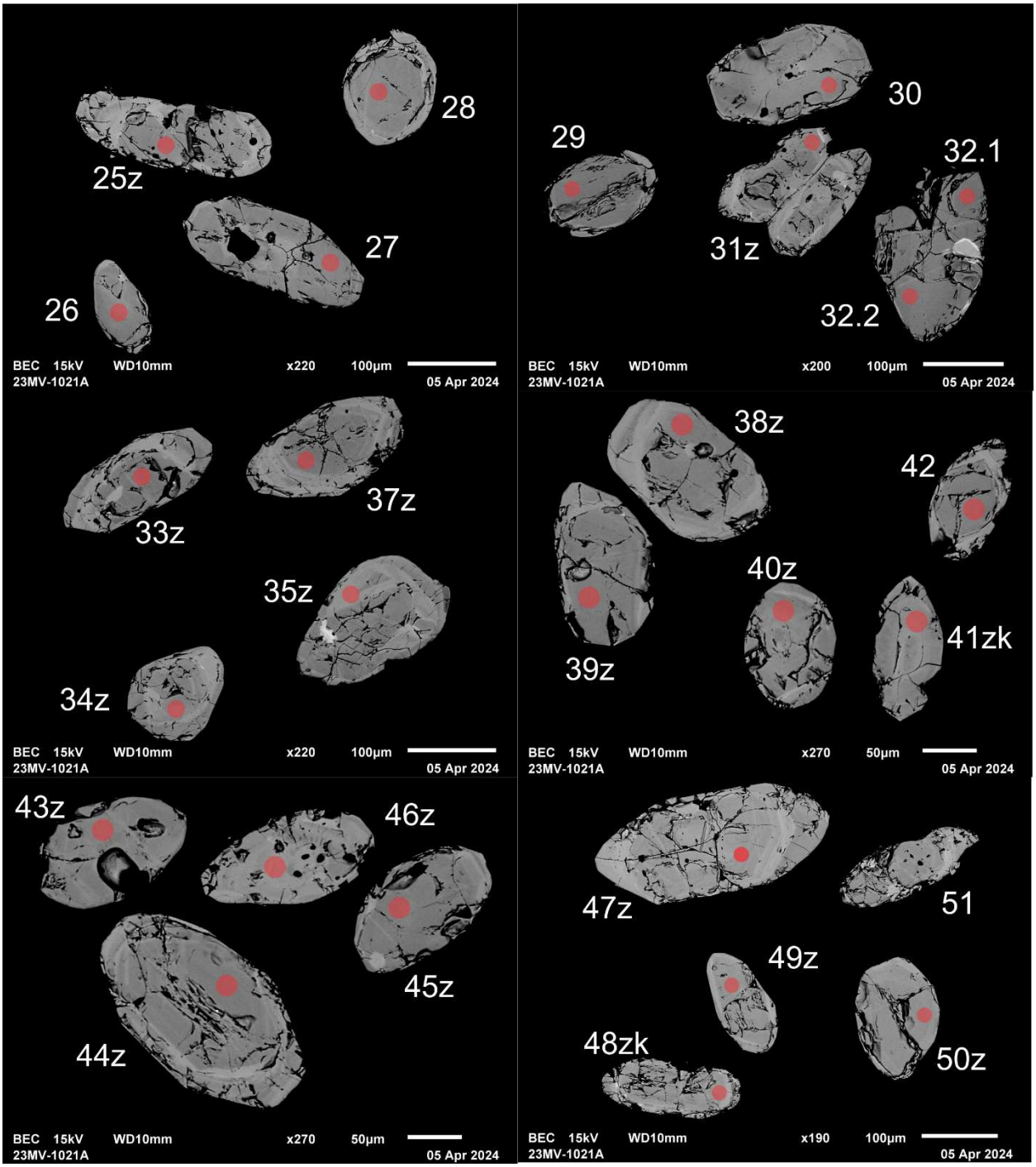

Figure 1.1.2 (cont.). BSE images of selected grains from sample 2023-MV-1021A. The red circles represent the approximate locations of laser ablation spots.

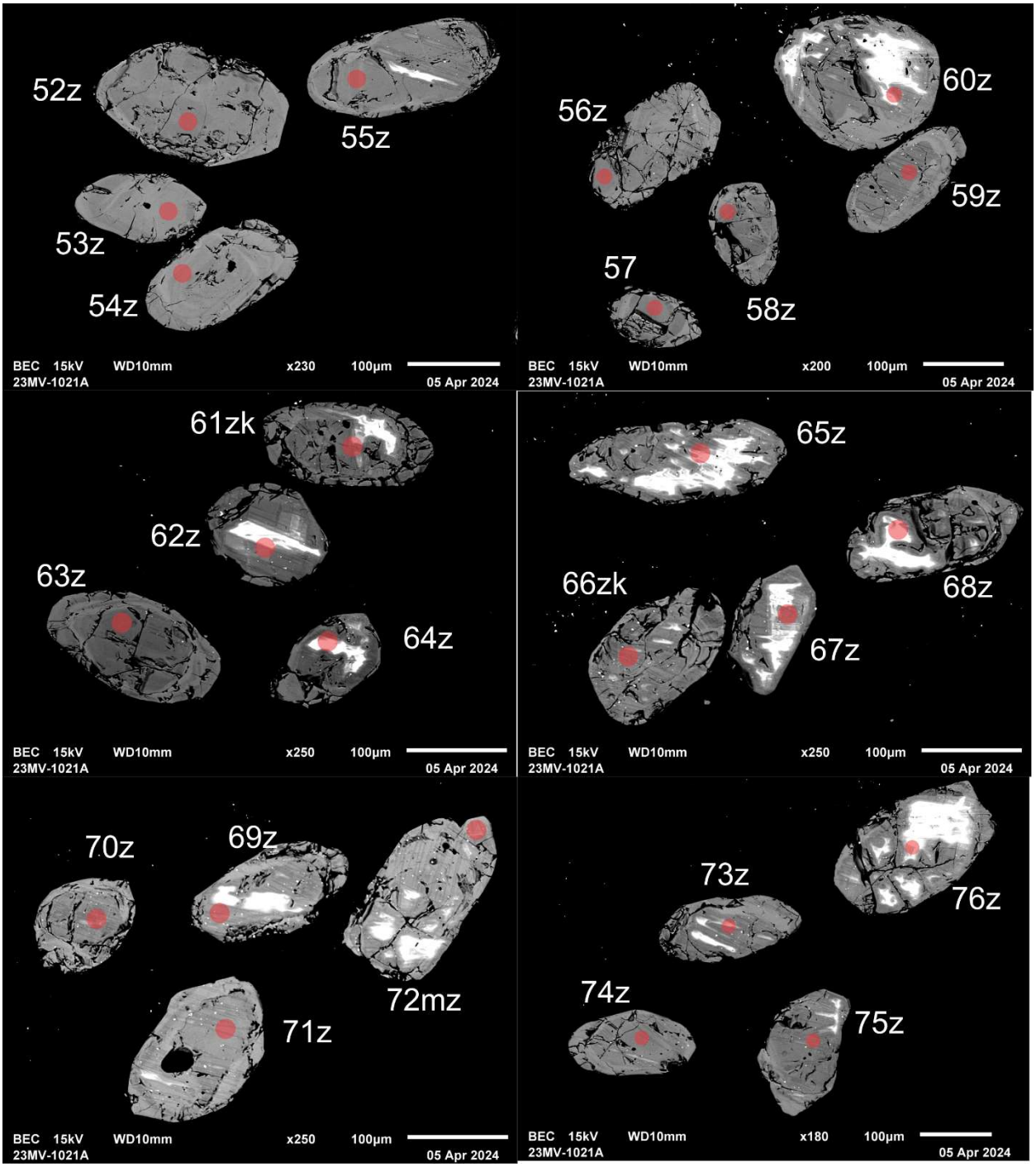

Figure 1.1.2 (cont.). BSE images of selected grains from sample 2023-MV-1021A. The red circles represent the approximate locations of laser ablation spots.

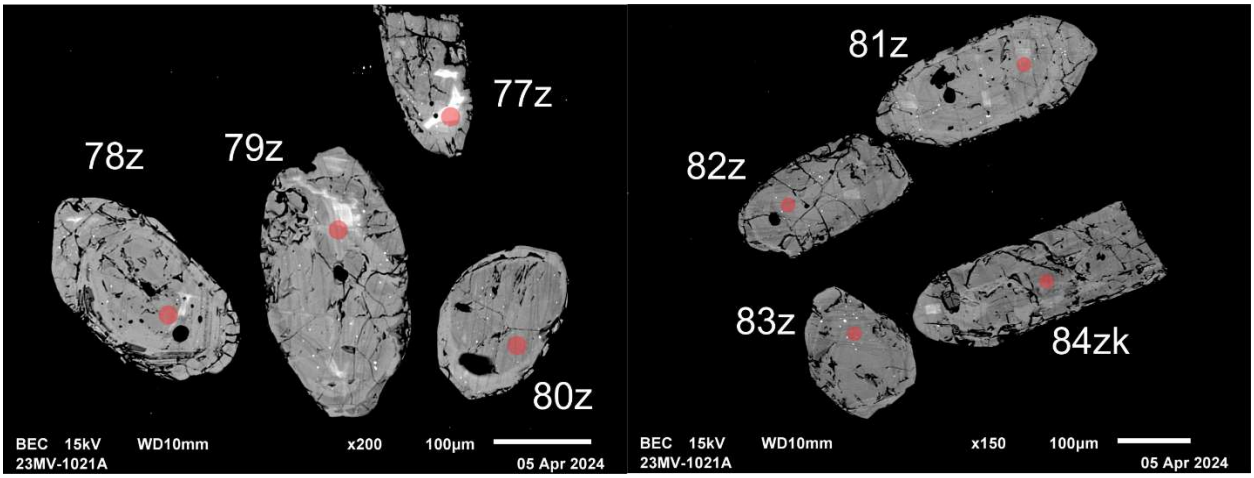

Figure 1.1.2 (cont.). BSE images of selected grains from sample 2023-MV-1021A. The red circles represent the approximate locations of laser ablation spots.

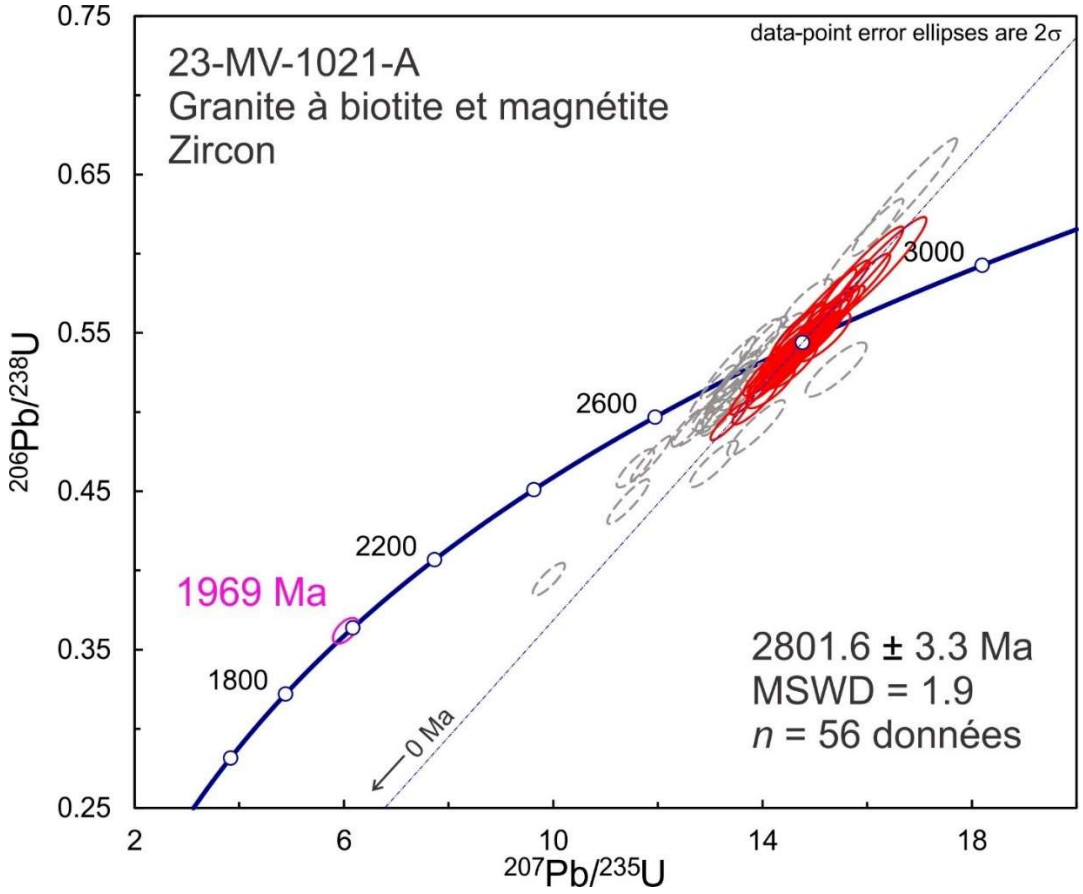

Figure 1.1.3. Concordia plot showing U-Pb isotopic data on polished zircon from granite sample 2023-MV-1021A. Red ellipses correspond to spots considered in the age model whereas gray-dashed ellipses correspond to the omitted spots. Magenta ellipse corresponds to the youngest analysis.

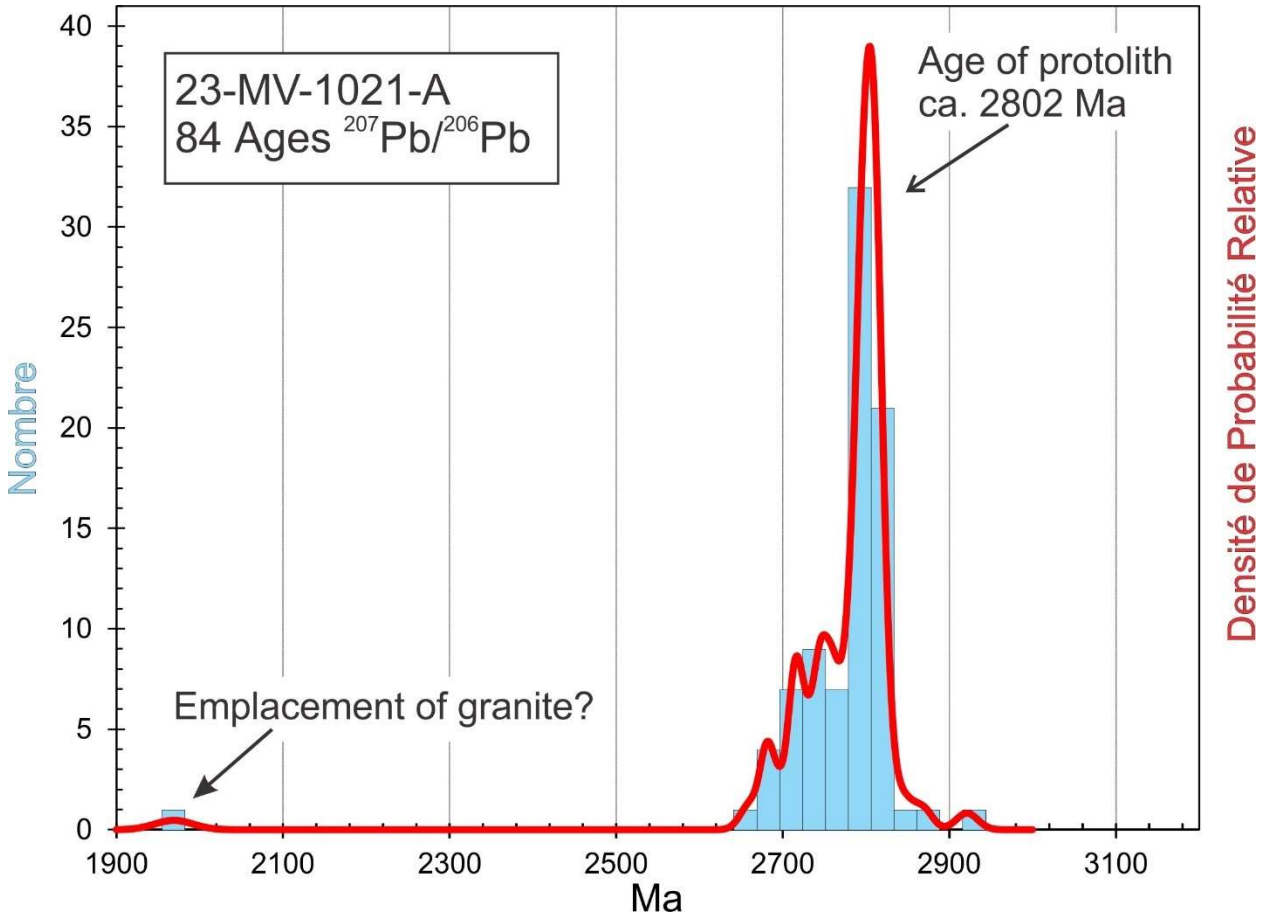

Figure 1.14. Combined age relative probability density plot and histogram showing the distribution of $^{207}Pb/^{206}Pb$ ages on polished zircon from granite sample 2023-MV-1021A.

1.2. 2023-MV-1049A
Granite à muscovite et grenat

This sample yielded euhedral large zircon grains with a variety of shapes and brownish coloration (Fig. 1.2.1). BSE images show a variety of zoning patterns, some inclusions, altered zones, cracks, and some grains show possible cores (Fig. 1.2.2). U-Pb analyses show diverse ages ranging from 1578 Ma to 3293 Ma (Fig. 1.2.3 and 1.2.4). All grains show Th/U ratios> 0.1. A relative probability density plot of $^{207}Pb/^{206}Pb$ ages reveals a major age peak at 1749 ±6 Ma (MSWD = 2.4) with numerous older ages spanning much of the Archean (Fig. 1.2.4). The youngest 1.57 Ga age is from a discordant grain and should be discounted. S-type granites (containing peraluminous minerals like muscovite and garnet) usually result from melting of sediments so much of the zircon may consist of detrital grains overgrown by a magmatic phase that is normally high in U. The detrital component is Archean while the age of emplacement of the pluton should be given by the major zircon peak at around 1720-1800 Ma, however analyses on monazite grains recovered from this sample give a better estimate of emplacement of the pluton at 1702 ±6 Ma (MSWD = 2.1) (Fig. 1.2.5). The youngest zircon (except for the discordant 1.58 Ga point that we omit because the high Sr content) is all a bit older than this. Since inheritance is rare in monazite but common in zircon, it makes sense to use the monazite to date crystallization. The monazite data show a bit of scattered, suggesting that the rock melted and crystallized very slowly.

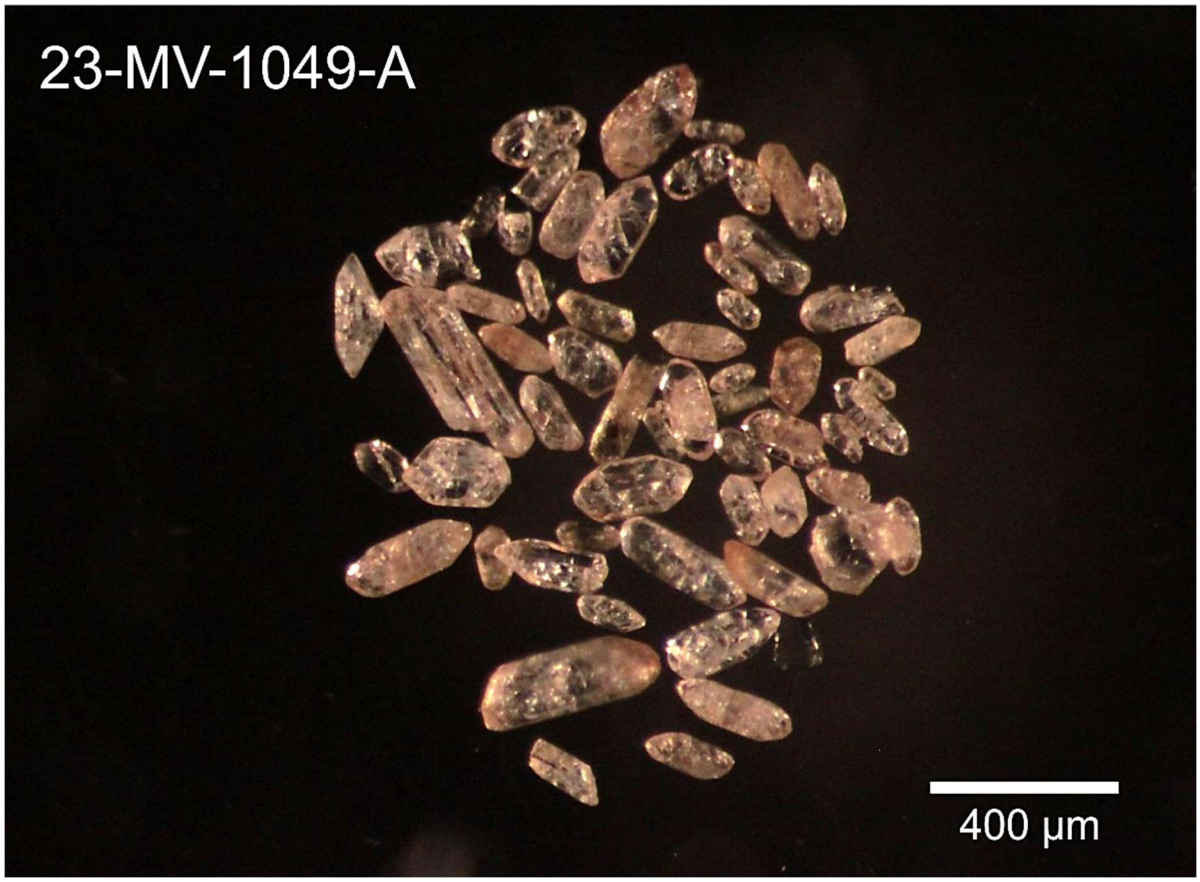

Figure 1.2.1. Picked zircon from granite sample 2023-MV-1049A.

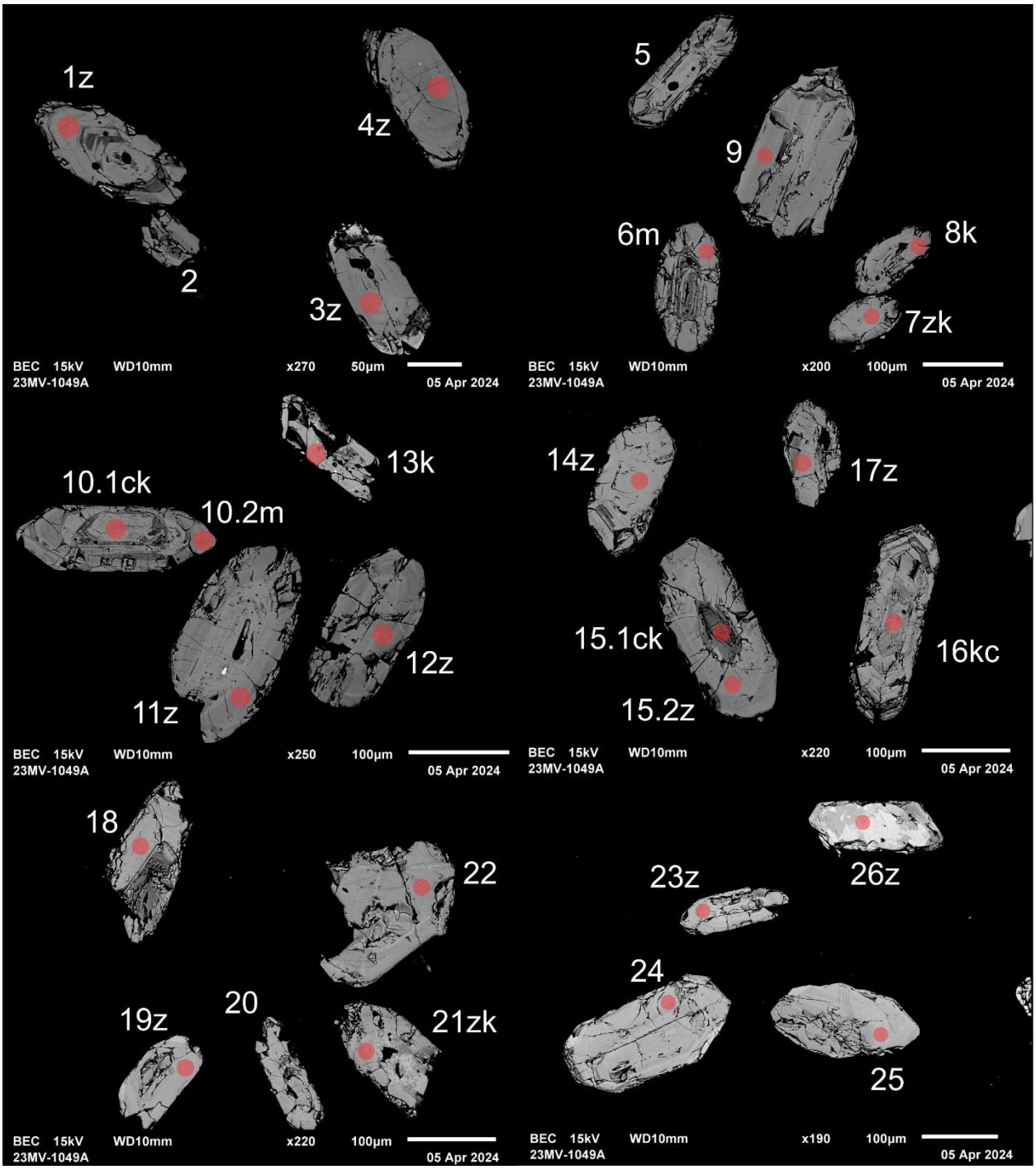

Figure 1.2.2. BSE images of selected grains from sample 2023-MV-1049A. The red circles represent the approximate locations of laser ablation spots.

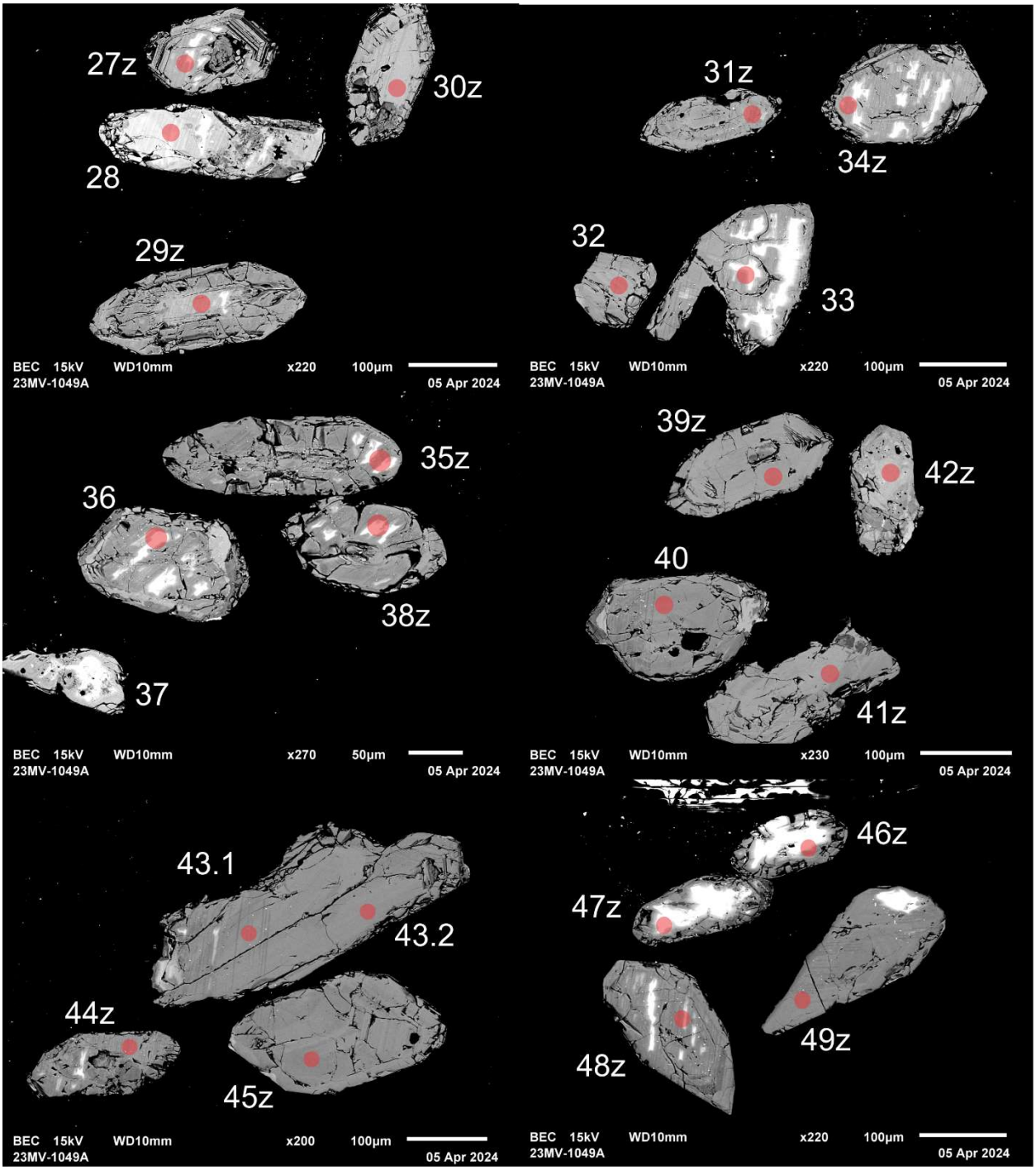

Figure 1.2.2 (cont.). BSE images of selected grains from sample 2023-MV-1049A. The red circles represent the approximate locations of laser ablation spots.

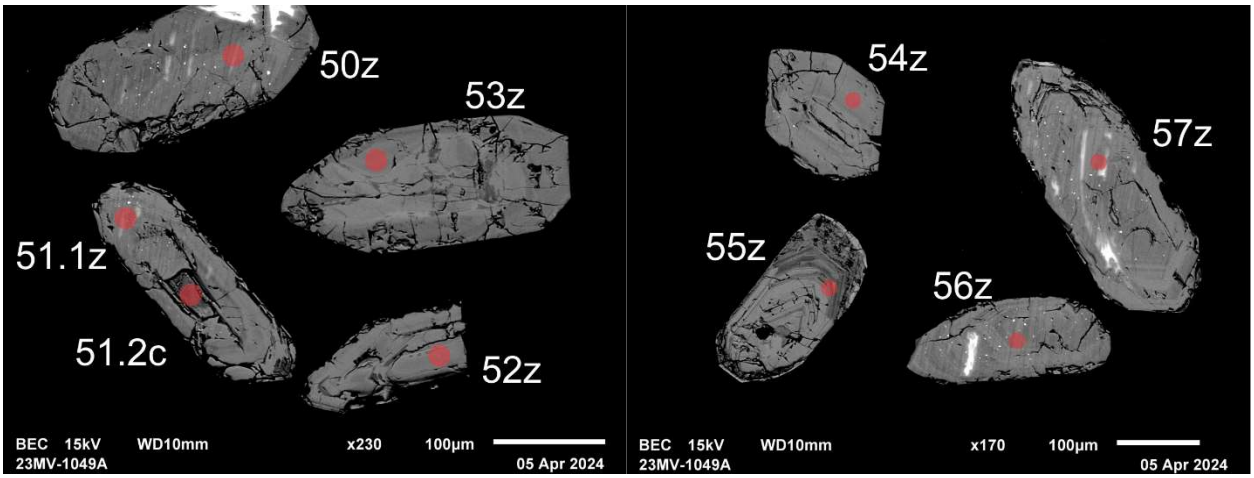

Figure 1.2.2 (cont.). BSE images of selected grains from sample 2023-MV-1049A. The red circles represent the approximate locations of laser ablation spots.

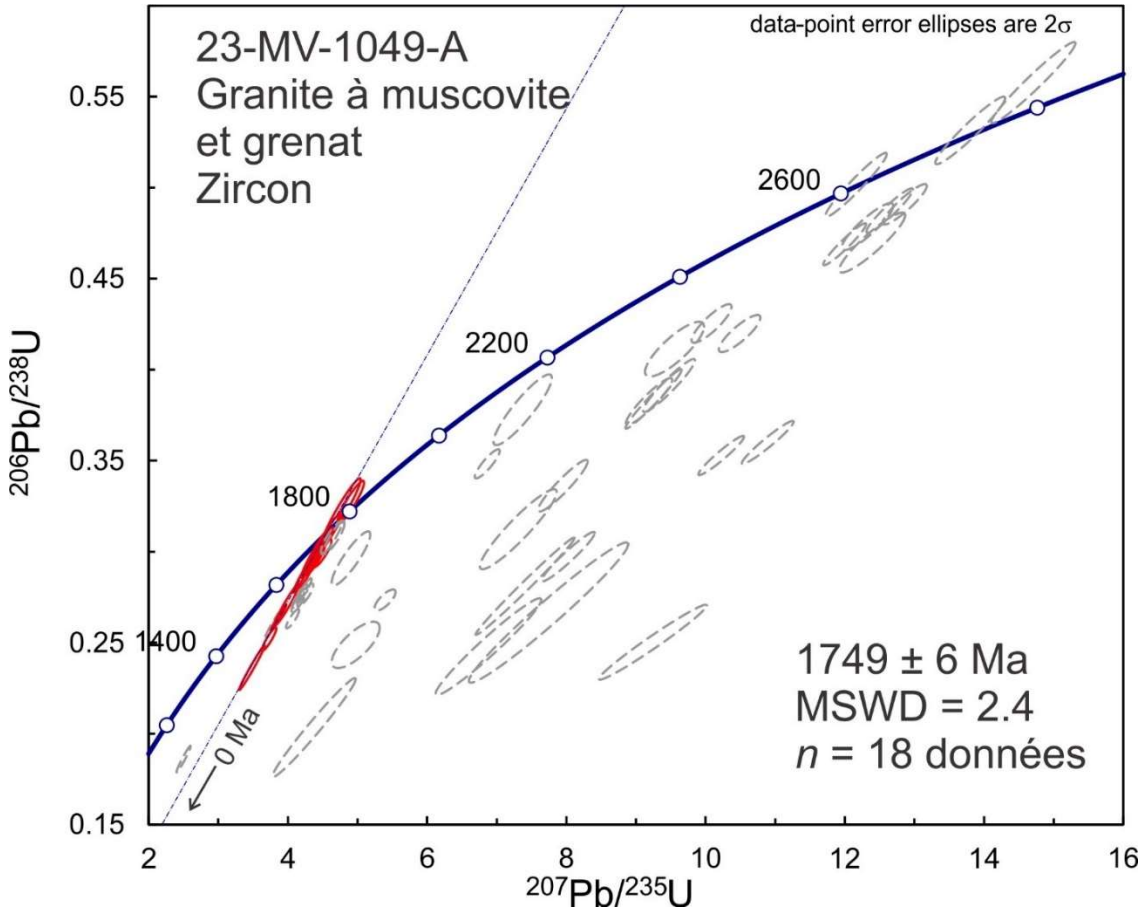

Figure 1.2.3. Concordia plot showing U-Pb isotopic data on polished zircon from granite sample 2023-MV-1049A. Red ellipses correspond to spots considered in the age model whereas gray ellipses correspond to the omitted spots.

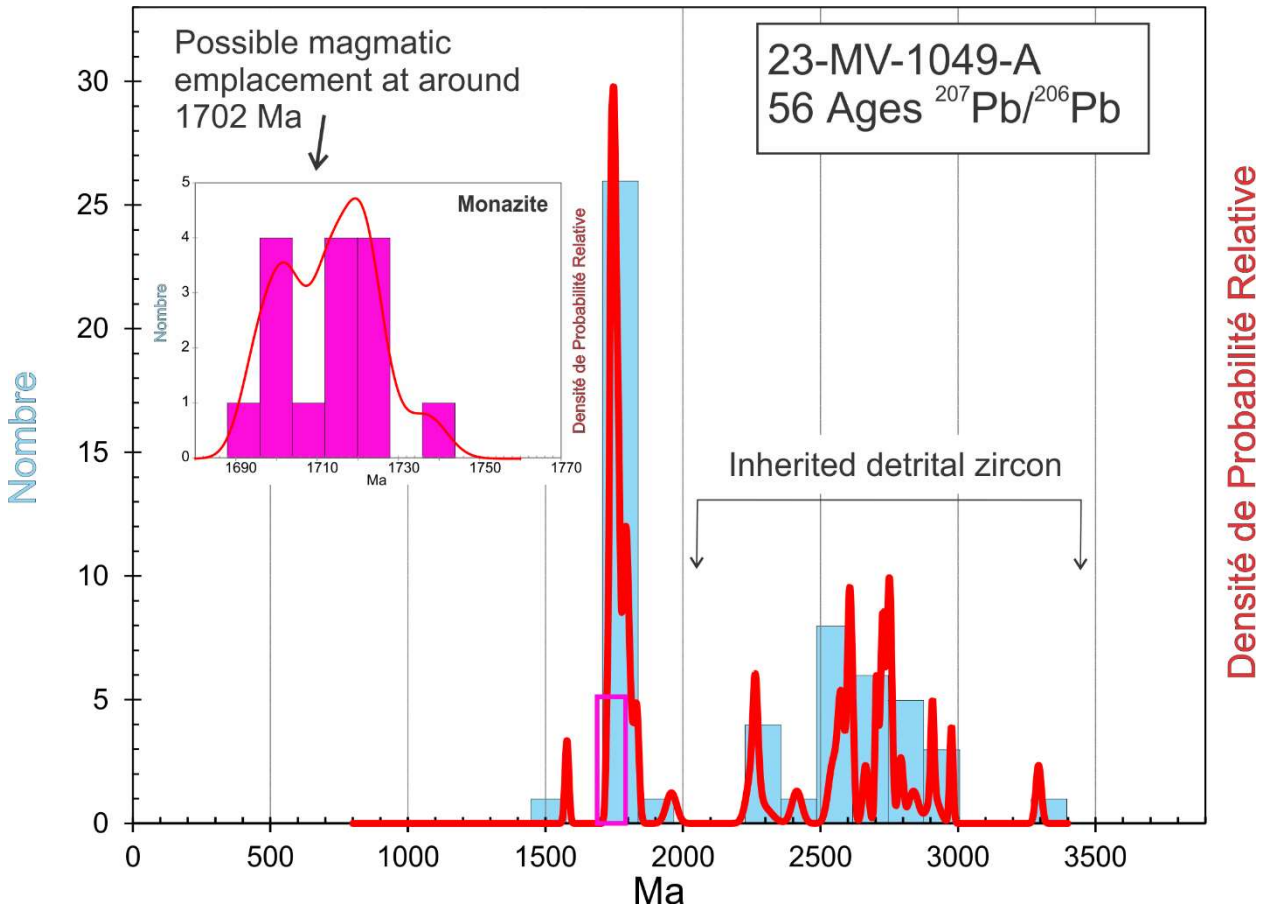

Figure 1.2.4. Combined age relative probability density plot and histogram showing the distribution of $^{207}Pb/^{206}Pb$ ages on polished zircon and monazite (magenta bars) from granite sample 2023-MV-1049A.

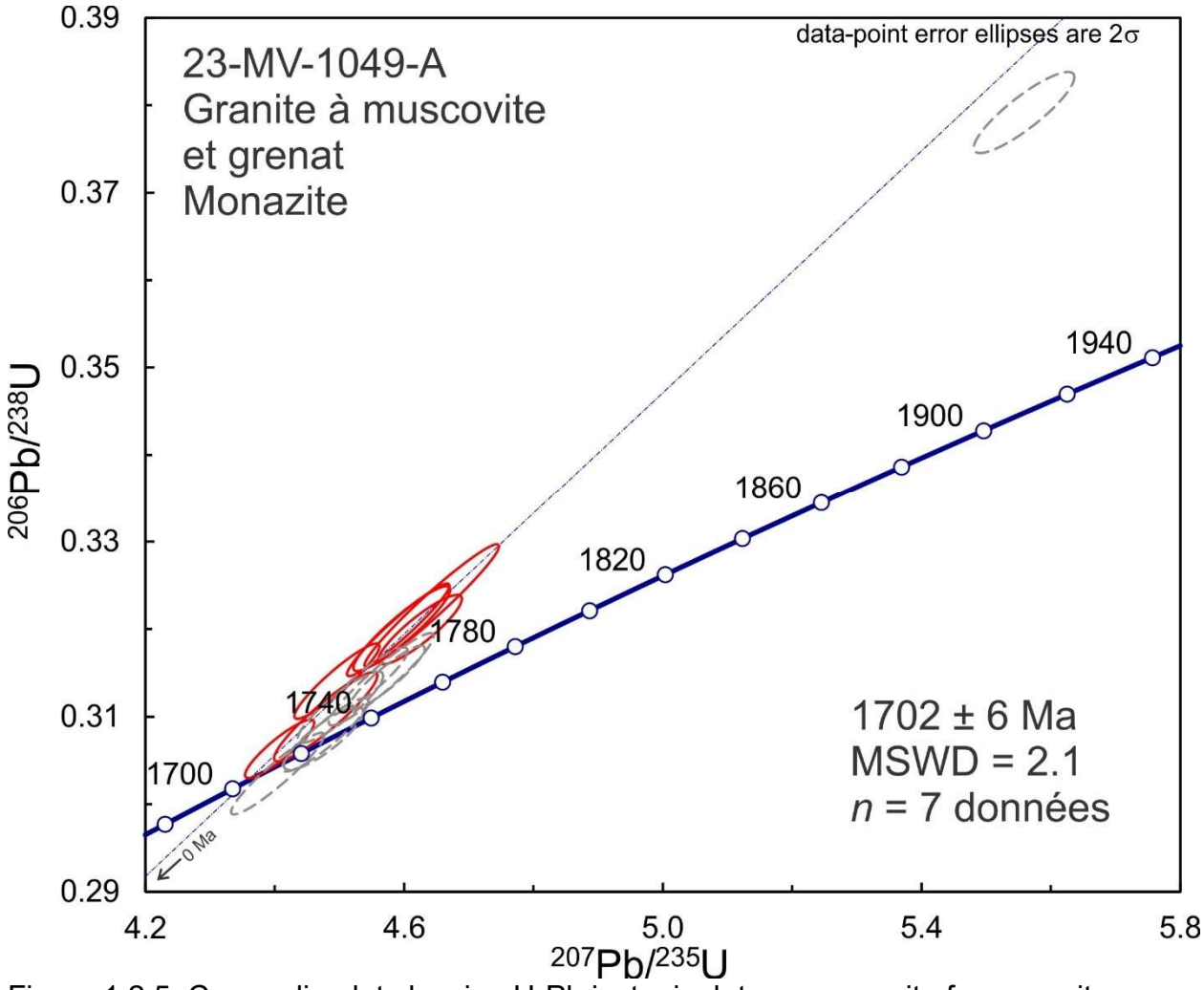

Figure 1.2.5. Concordia plot showing U-Pb isotopic data on monazite from granite sample 2023-MV-1049A. Red ellipses correspond to spots considered in the age model whereas gray ellipses correspond to the omitted spots.

1.3. 2023-MV-1052A
Gneiss tonalitique à biotite et hornblende

This sample yielded a moderate amount of cracked zircon with variable brownish coloration and euhedral to rounded shapes (Fig. 1.3.1). BSE images show cracks, alteration zones, oscillatory zoning with evidence of cores in some grains (Fig. 1.3.2). U-Pb results indicate dates ranging from 1806 Ma to 2831 Ma. A relative probability density plot of $^{207}Pb/^{206}Pb$ ages shows clustered Archean age peaks with the oldest giving an average age of 2813 ±4 Ma (Figs. 1.3.3 and 1.3.4). Th/U ratios on most of the zircon indicate a magmatic origin. The four youngest grains show low Th/U and probably represent metamorphic phases. Only the youngest is concordant within error, giving an age of 1806 ±14 Ma (Figs. 1.3.3). The most likely interpretation is that the rock represents an Archean tonalite that was metamorphosed at 1.8 Ga when it may have acquired its fabric. It may have remained at high temperature for a substantial period of time (10s of Ma) to partially reset much of the Archean zircon.

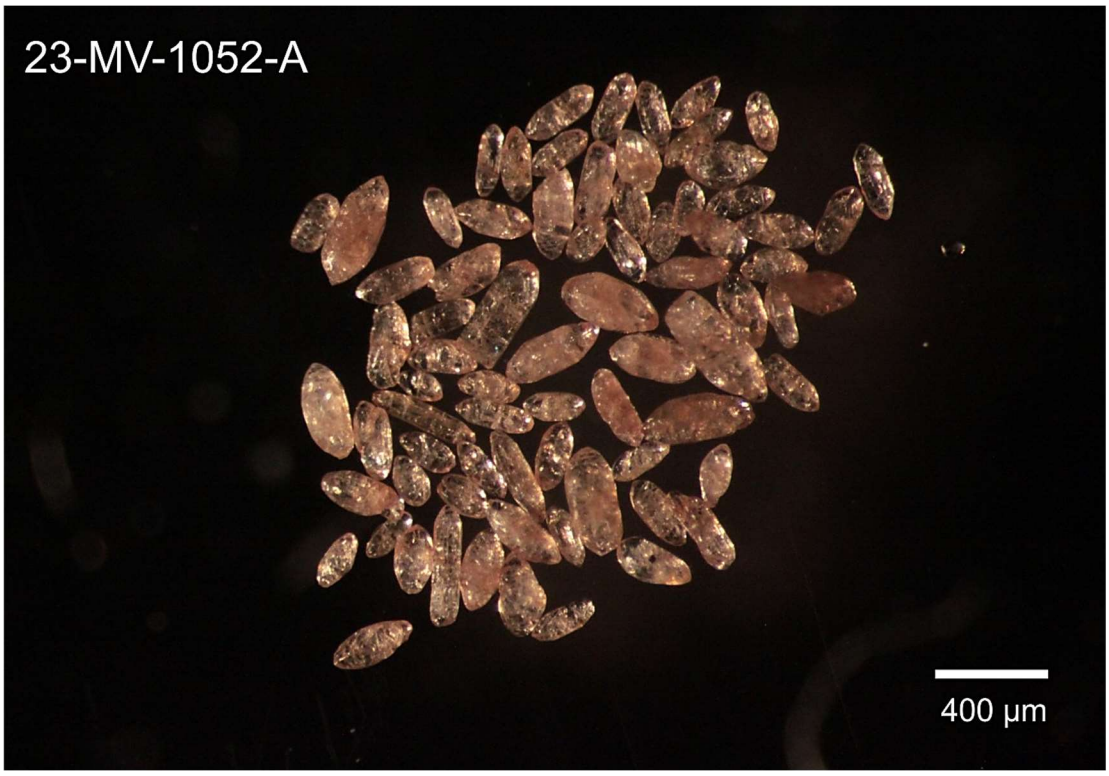

Figure 1.3.1. Picked zircon from gneiss sample 2023-MV-1052A.

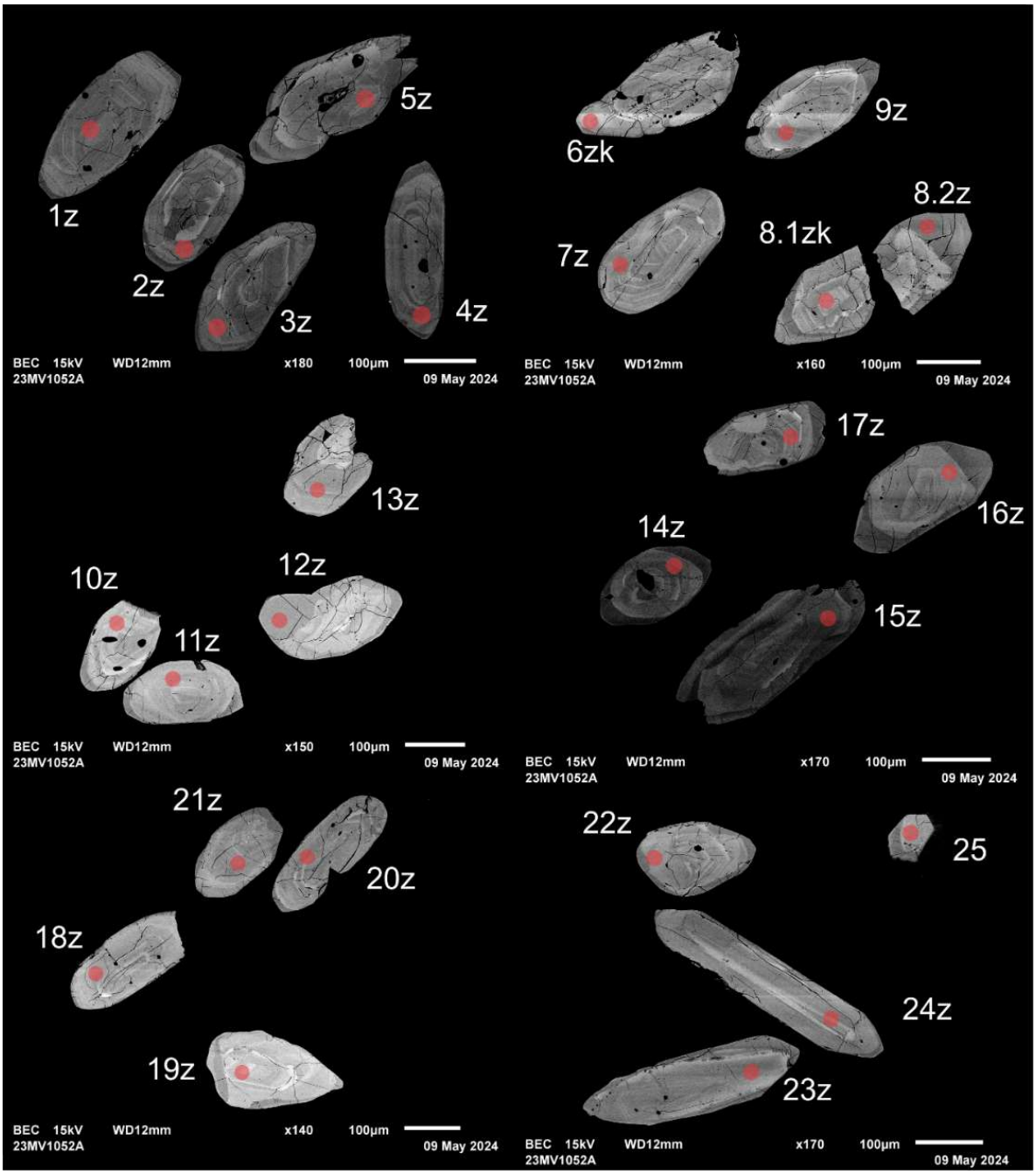

Figure 1.3.2. BSE images of selected grains from sample 2023-MV-1052A. The red circles represent the approximate locations of laser ablation spots.

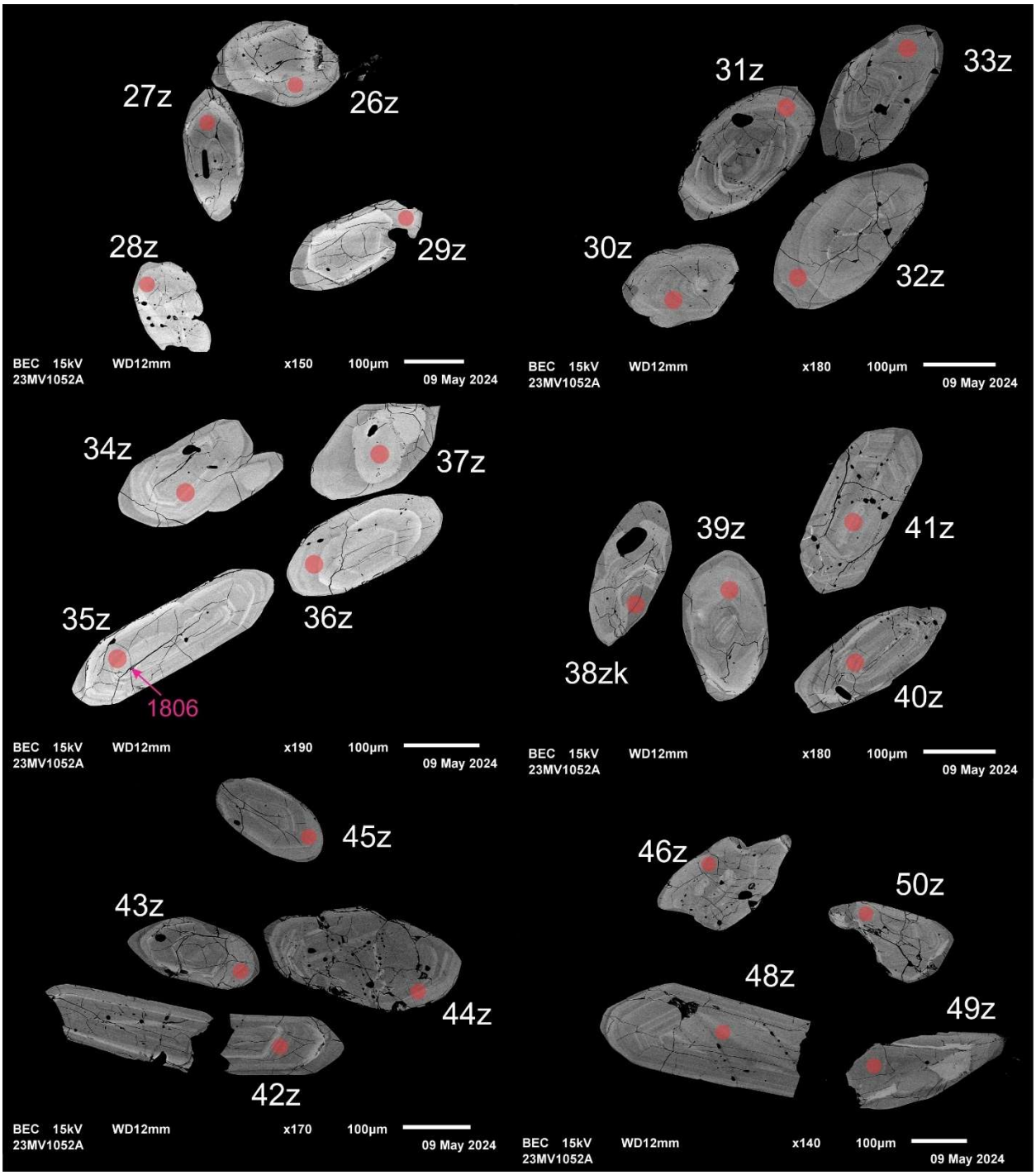

Figure 1.3.2 (cont.). BSE images of selected grains from sample 2023-MV-1052A. The red circles represent the approximate locations of laser ablation spots.

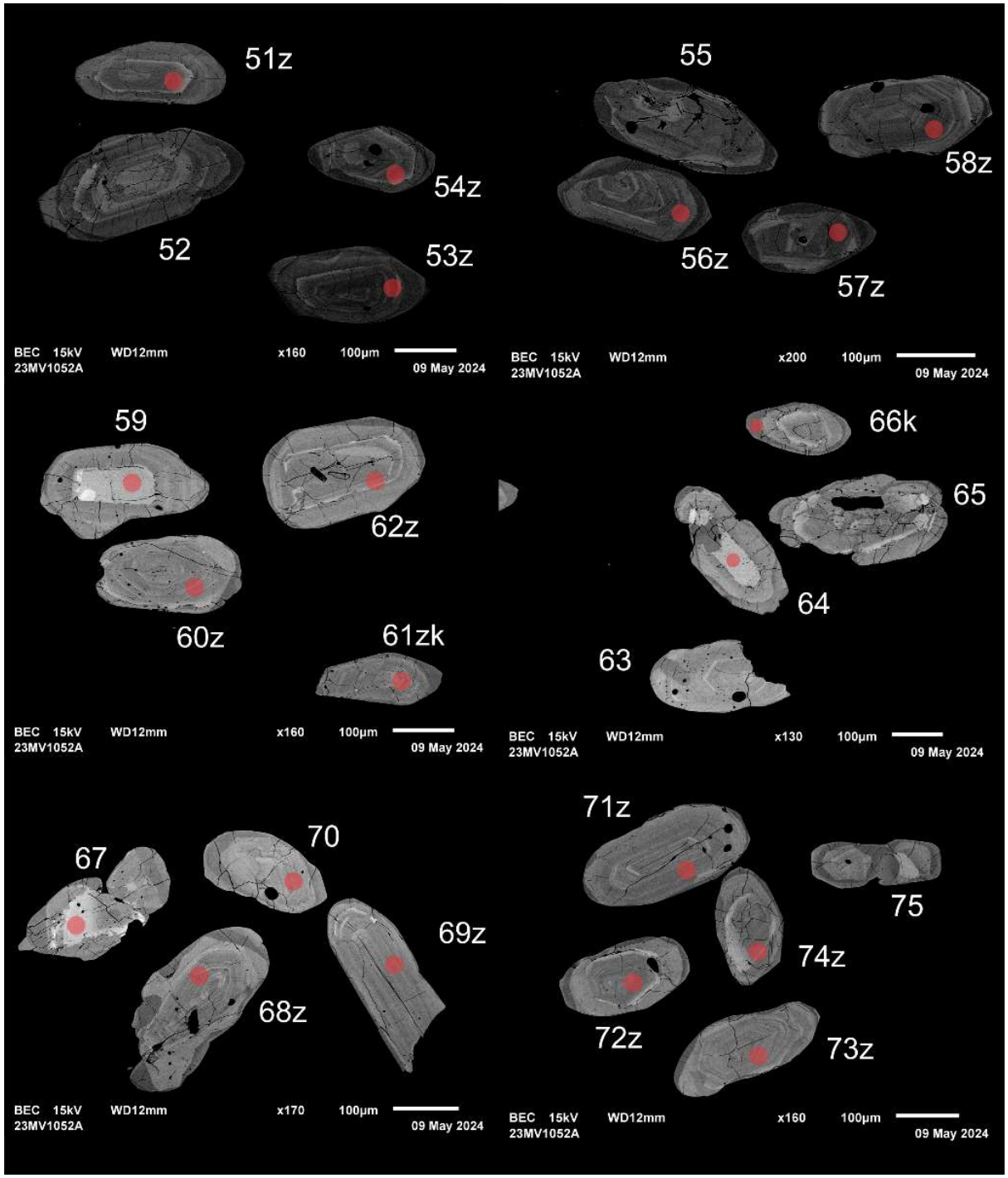

Figure 1.3.2 (cont.). BSE images of selected grains from sample 2023-MV-1052A. The red circles represent the approximate locations of laser ablation spots.

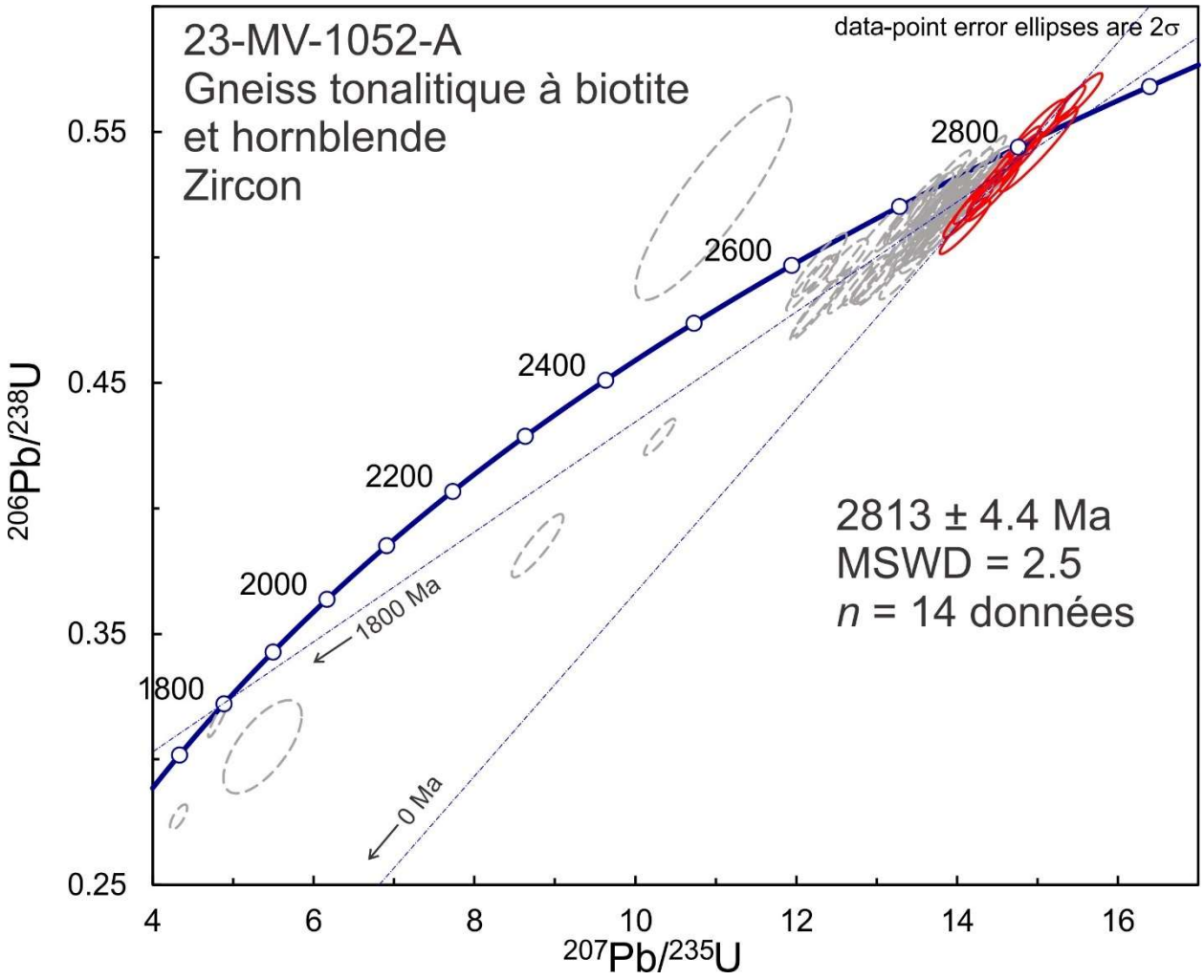

Figure 1.3.3. Concordia plot showing U-Pb isotopic data on polished zircon from gneiss sample 2023-MV-1052A. Red ellipses correspond to spots considered in the age model whereas gray-dashed ellipses correspond to the omitted spots.

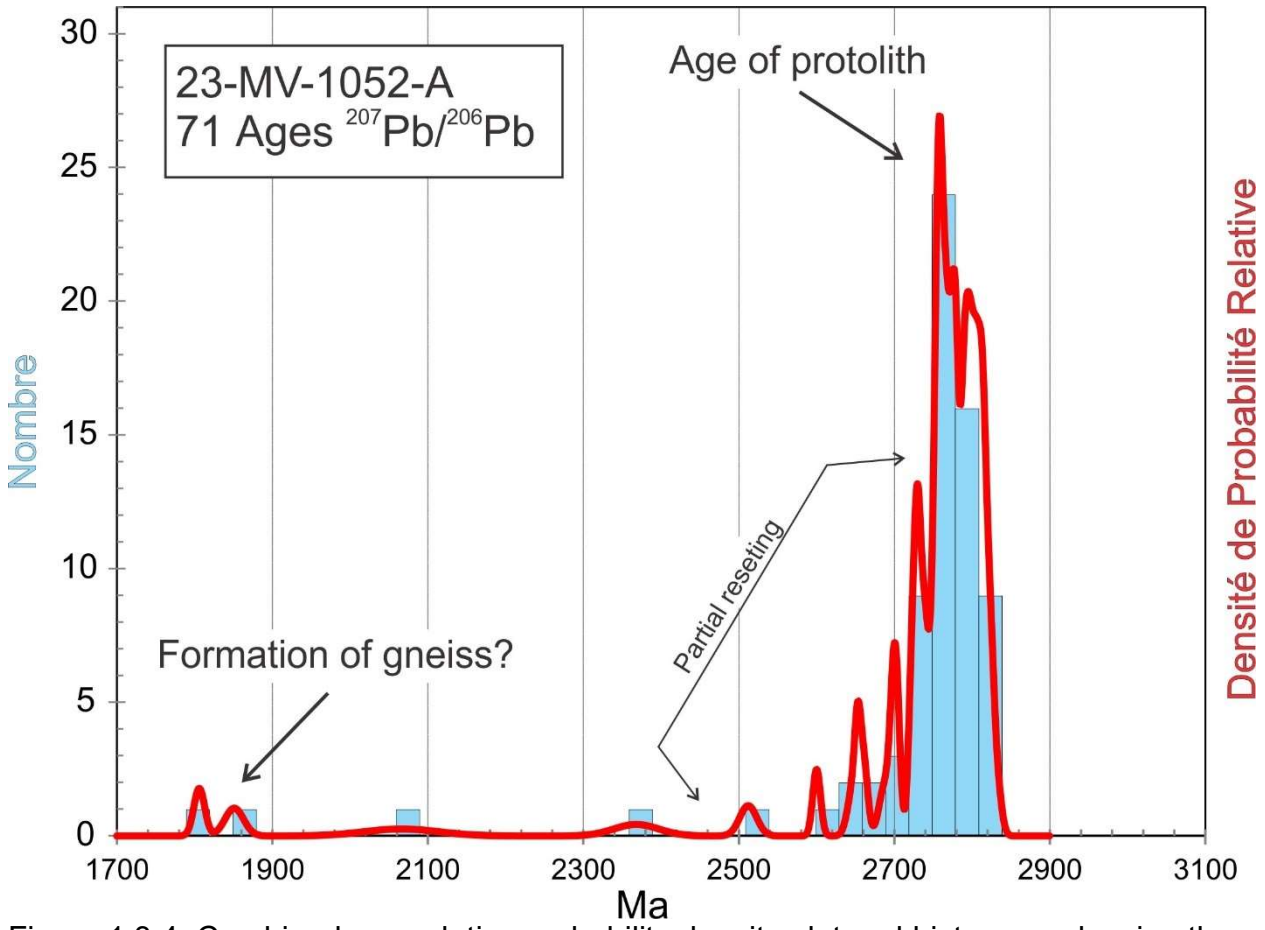

Figure 1.3.4. Combined age relative probability density plot and histogram showing the distribution of $^{207}Pb/^{206}Pb$ ages on polished zircon from gneiss sample 2023-MV-1052A.

1.4. 2023-MV-1083A
Gneiss tonalitique à biotite et hornblende

This sample yielded a moderate amount of zircon variably cracked, stubby grains with brownish coloration and euhedral to rounded morphology (Fig. 1.4.1). BSE images show cracks, alteration zones, oscillatory zoning, and thin higher U (brighter) rims (Fig. 1.4.2). U-Pb analyses show a range of near-concordant ages from 1862 Ma to 2851 Ma (Fig. 1.4.3 and 1.4.4). A relative probability density plot of $^{207}Pb/^{206}Pb$ ages shows a principal peak age at the older limit of the range, around 2810 Ma (Fig. 1.4.4). Interior spots on grains show Th/U ratios> 0.1 while rims, which are difficult to measure, show values <0.1, indicating a metamorphic origin. U-Pb data of the 46 oldest grains give overlapping $^{207}Pb/^{206}Pb$ ages with an average of 2823 ±2.7 Ma (2σ, MSWD = 1.8) (Fig. 4-3). Similar to the previous sample, this is the most likely the age of the protolith whereas the ages from the rims indicate that the metamorphic event occurred around 1862–2015 Ma. The near-concordant distribution of data for this sample shows either that the Archean magmatic zircon underwent partial diffusive loss of Pb during the Paleoproterozoic metamorphic event or analyses sampled both rims and interiors. If the first case, Pb may have partially diffused into the metamorphic rims, causing them to appear older. The closest estimate for the age of metamorphism is probably the age of the youngest near-concordant datum of 1862 Ma.

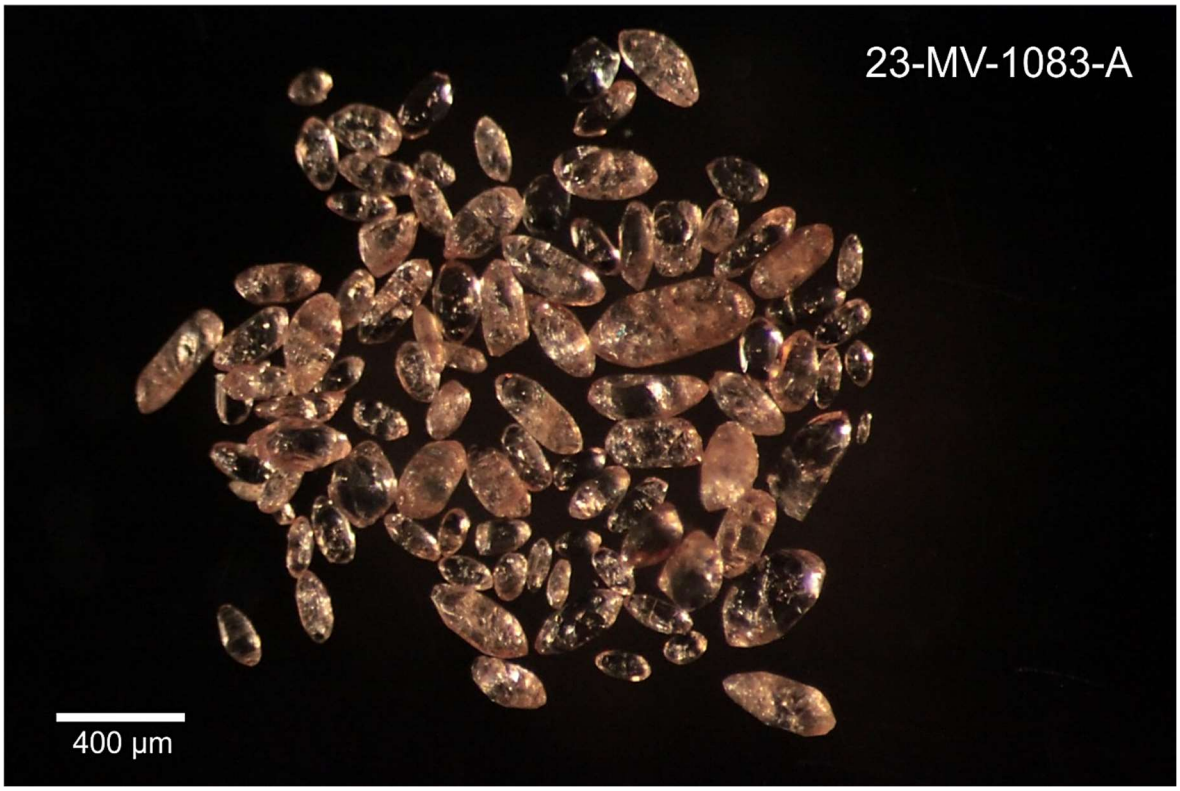

Figure 1.4.1. Picked zircon from gneiss sample 2023-MV-1083A.

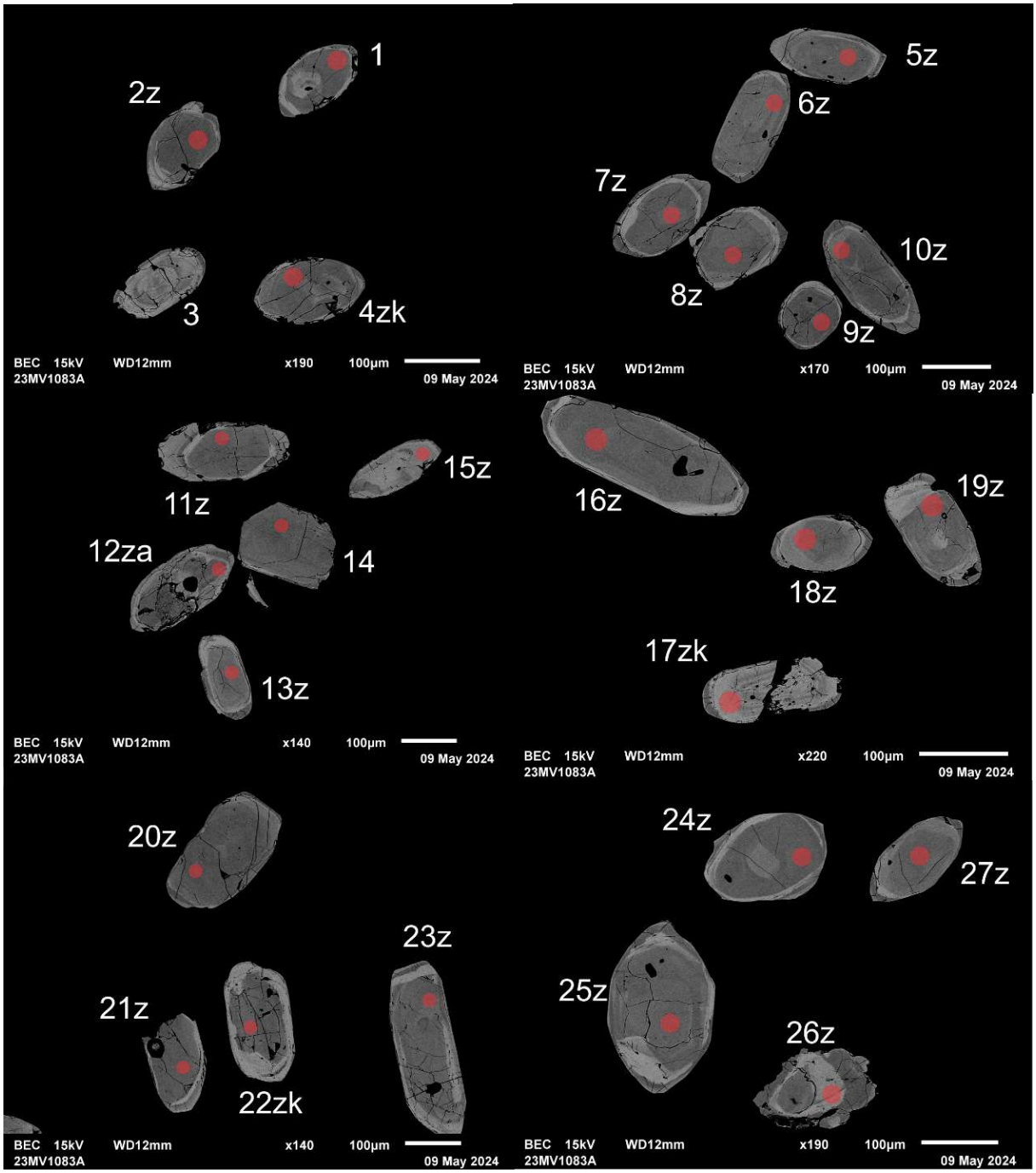

Figure 1.4.2. BSE images of selected grains from sample 2023-MV-1083A. The red circles represent the approximate locations of laser ablation spots.

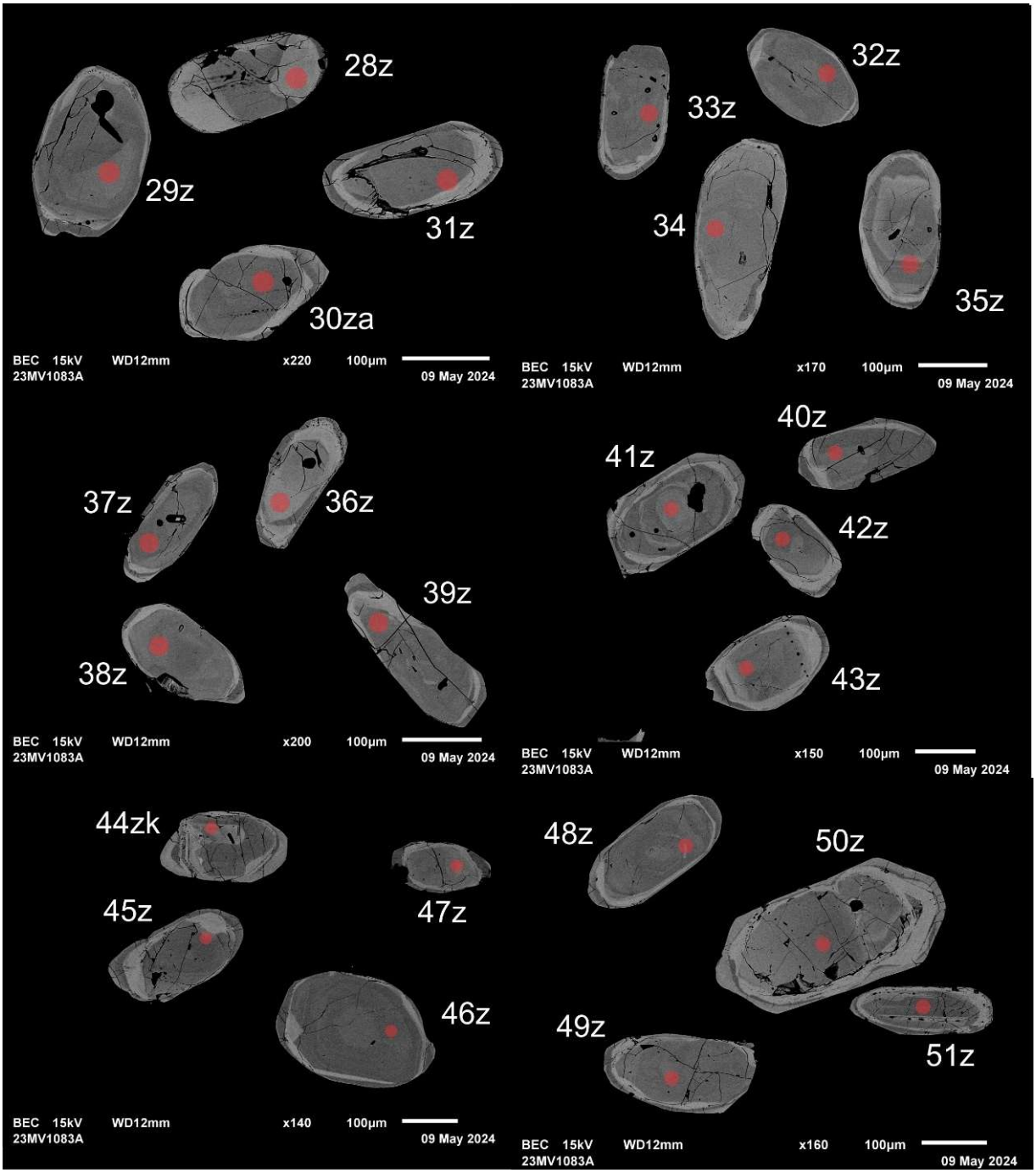

Figure 1.4.2 (cont.). BSE images of selected grains from sample 2023-MV-1083A. The red circles represent the approximate locations of laser ablation spots.

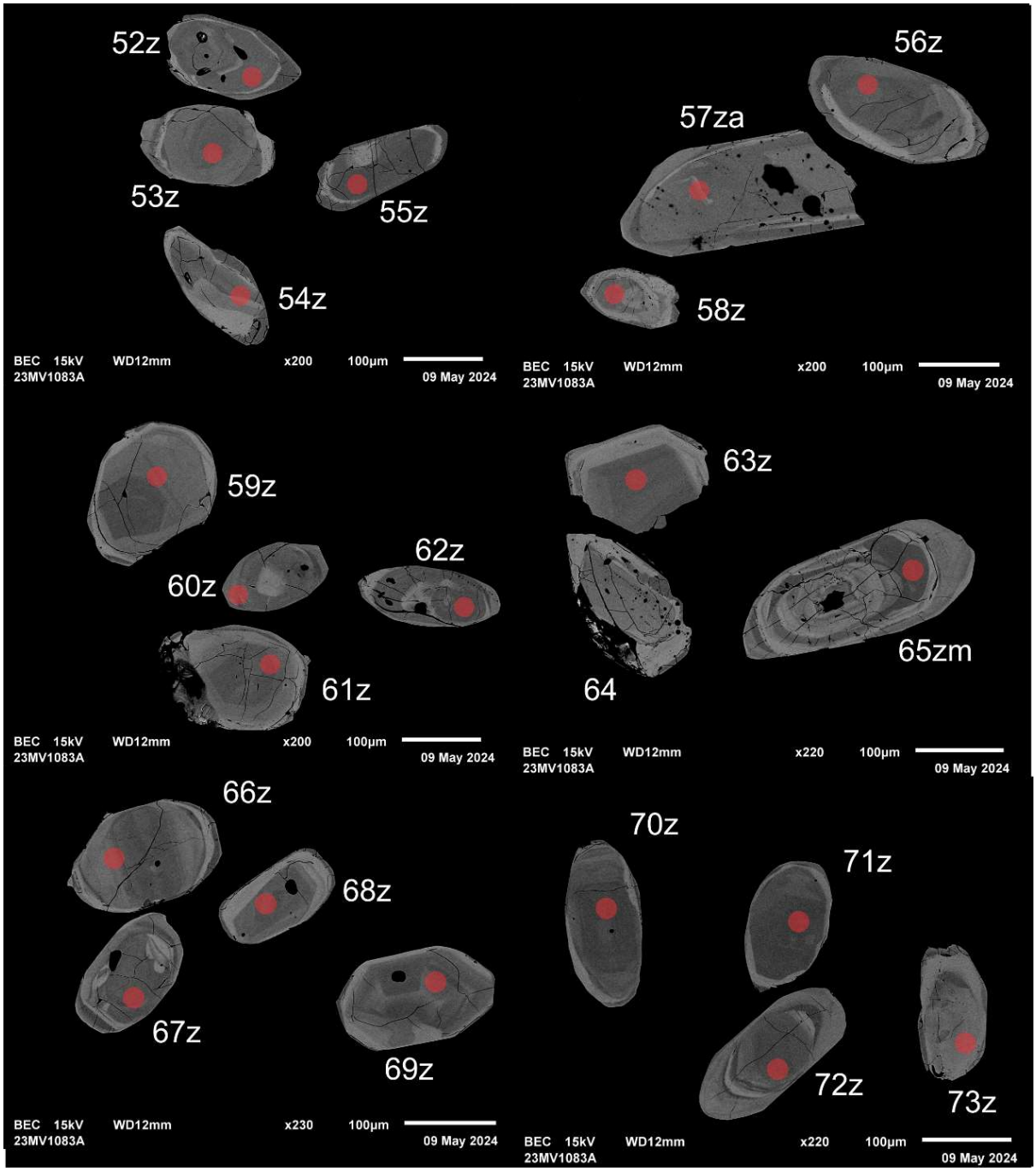

Figure 1.4.2 (cont.). BSE images of selected grains from sample 2023-MV-1083A. The red circles represent the approximate locations of laser ablation spots.

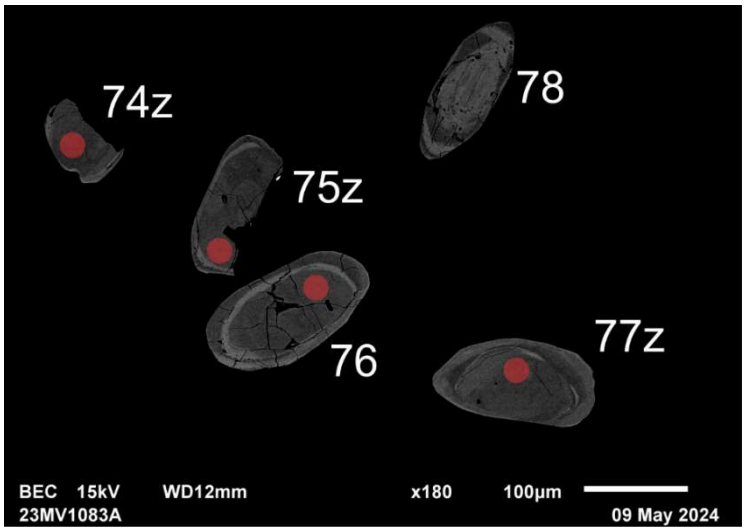

Figure 1.4.2 (cont.). BSE images of selected grains from sample 2023-MV-1083A. The red circles represent the approximate locations of laser ablation spots.

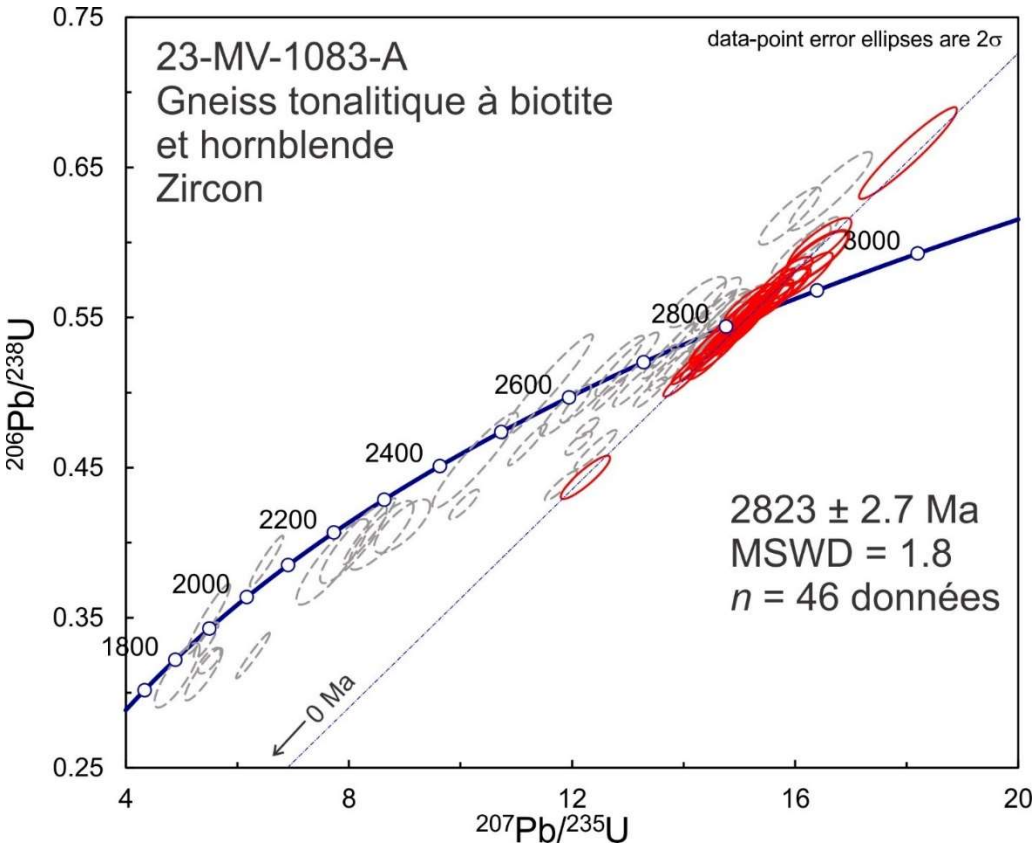

Figure 1.4.3. Concordia plot showing U-Pb isotopic data on polished zircon from gneiss sample 2023-MV-1083A. Red ellipses correspond to spots considered in the age model whereas gray-dashed ellipses correspond to the omitted spots.

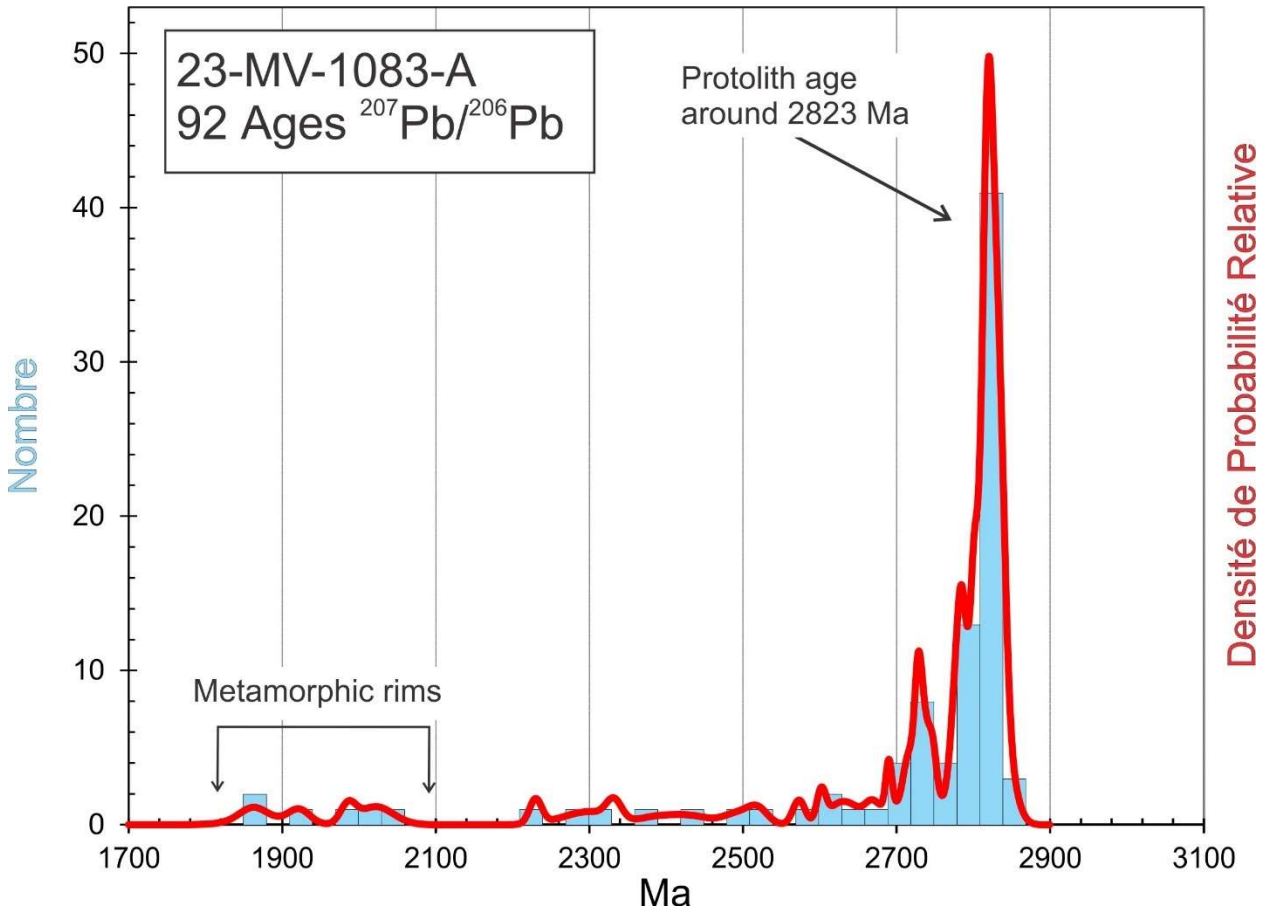

Figure 1.4.4. Combined age relative probability density plot and histogram showing the distribution of $^{207}Pb/^{206}Pb$ ages on polished zircon from gneiss sample 2023-MV-1083A.

1.5. 2023-MV-1178A
Gneiss tonalitique à biotite et hornblende

This sample yielded abundant clear zircon as fresh multifaceted prisms (Fig. 1.5.1). BSE images show faint zoning with the possibility of thin overgrowths and cores in some grains (Fig. 1.5.2). U-Pb analyses show a range of dates ranging from 2689 Ma to 2924 Ma (Fig. 1.5.3 and 1.5.4). Dates older than 2800 Ma correspond to analyses with high Sr signal (possibly altered domains). All grains show magmatic Th/U ratios (> 0.1). The major peak gives an average age of 2753.5 ±2.3 Ma (2σ, MSWD = 2.1) (Fig. 1.5.3). This is most likely to be the magmatic crystallization age. The overgrowths are too thin and altered to date.

Figure 1.5.1. Picked zircon from gneiss sample 2023-MV-1178A.

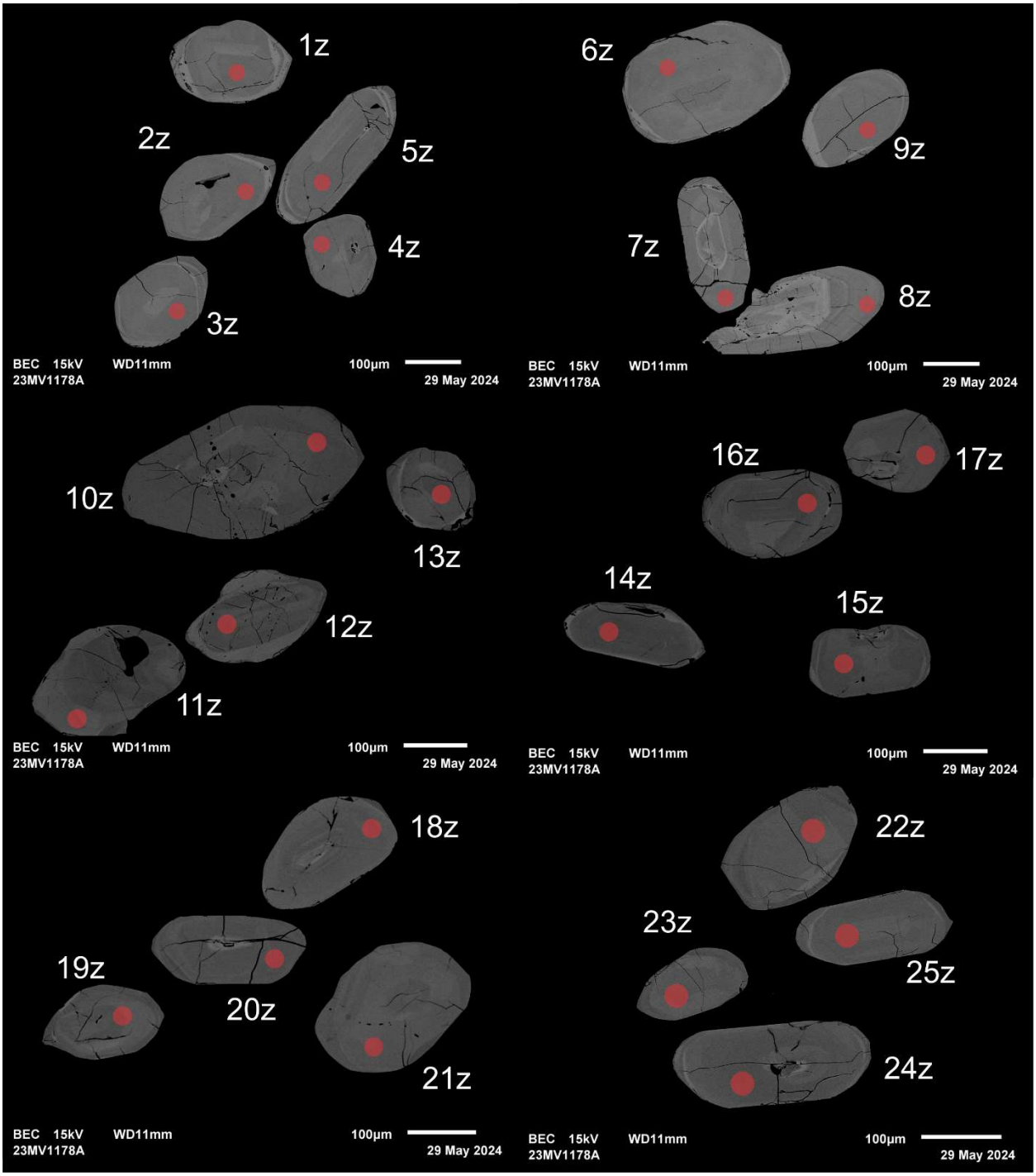

Figure 1.5.2. BSE images of selected grains from sample 2023-MV-1178A. The red circles represent the approximate locations of laser ablation spots.

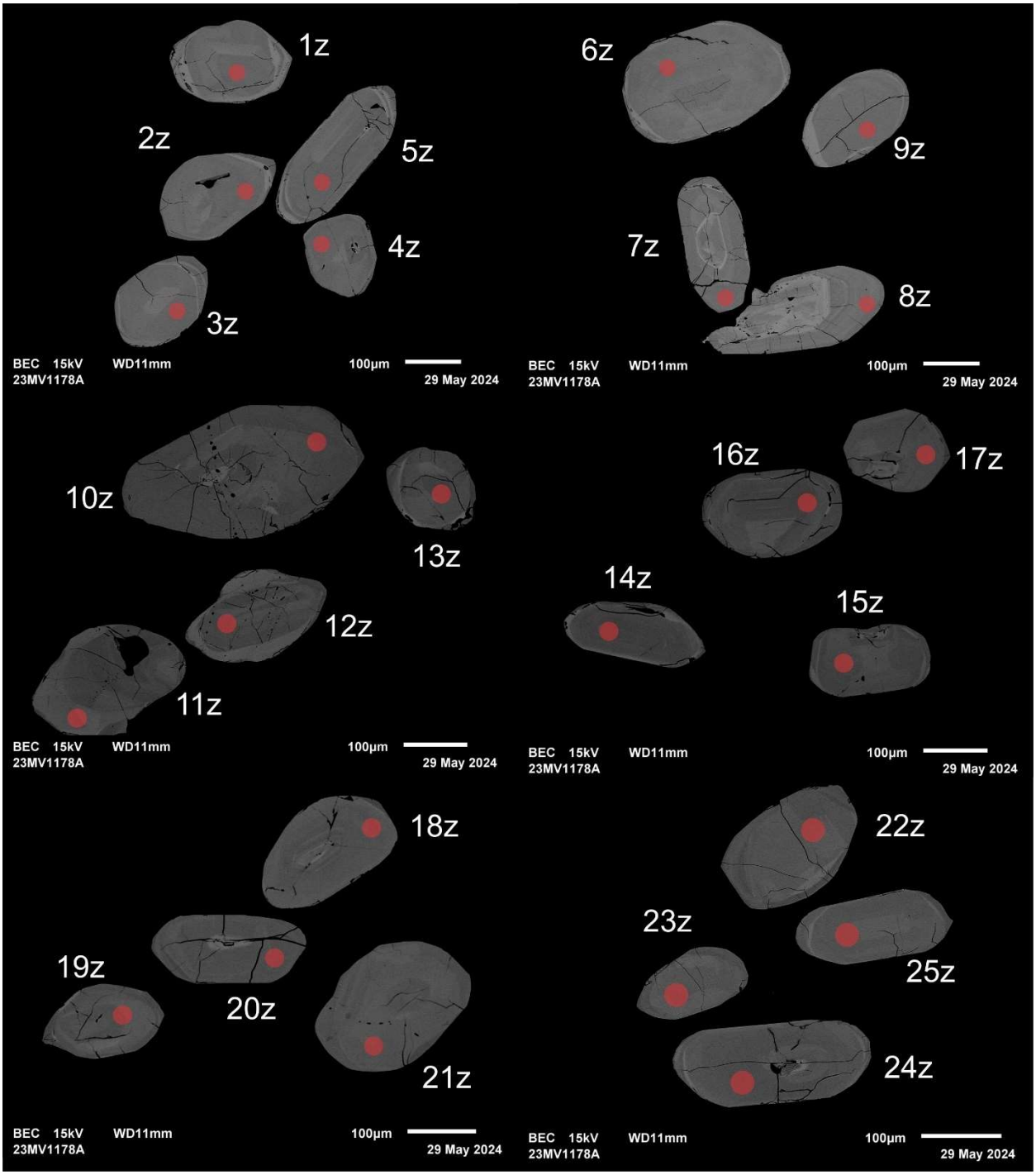

Figure 1.5.2 (cont.). BSE images of selected grains from sample 2023-MV-1178A. The red circles represent the approximate locations of laser ablation spots.

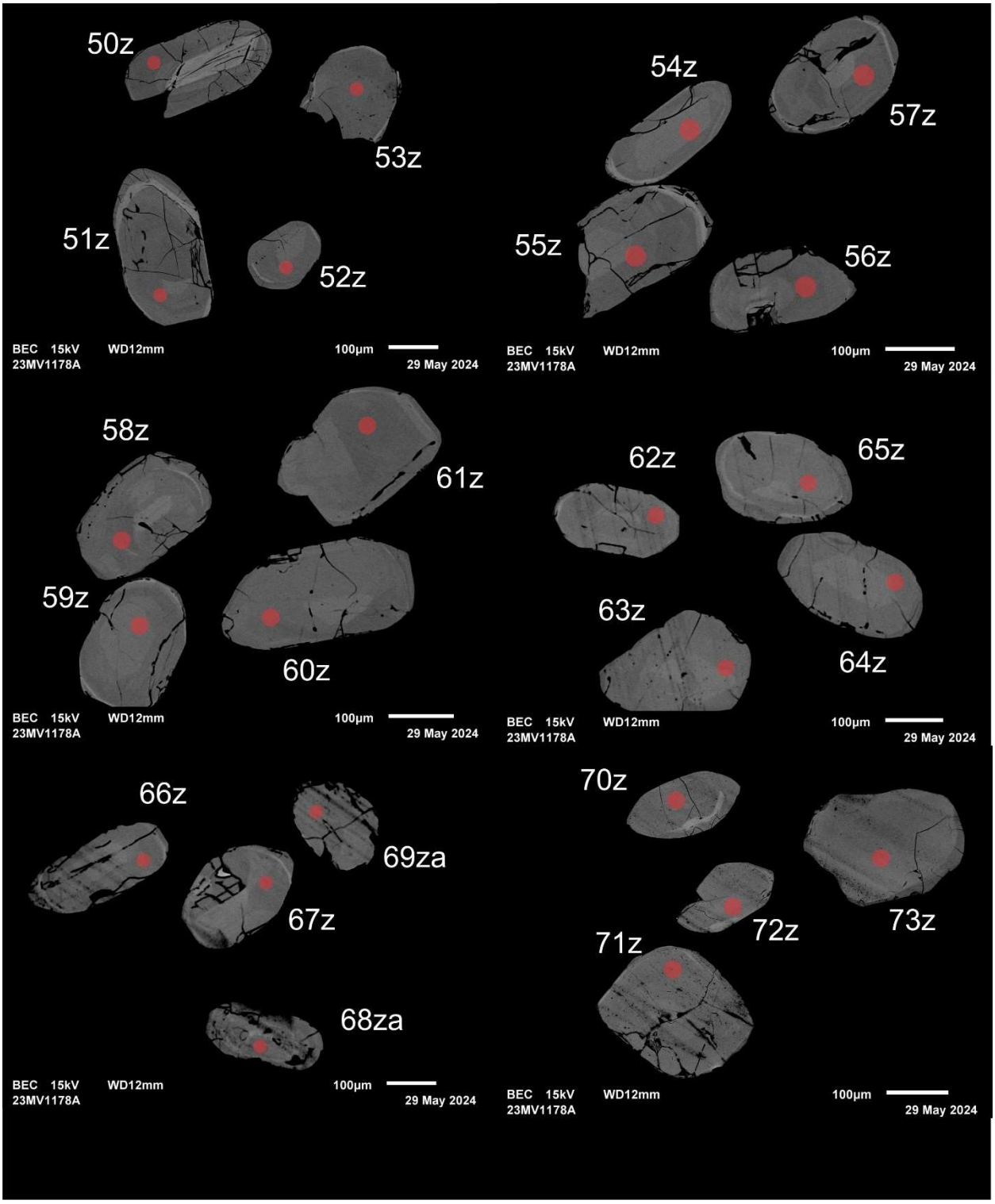

Figure 1.5.2 (cont.). BSE images of selected grains from sample 2023-MV-1178A. The red circles represent the approximate locations of laser ablation spots.

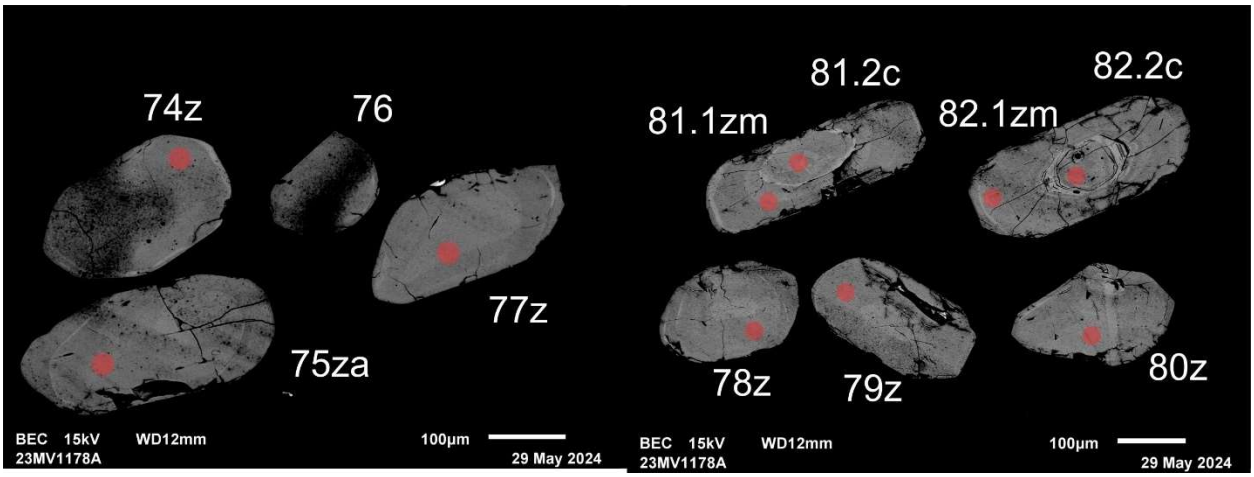

Figure 1.5.2 (cont.). BSE images of selected grains from sample 2023-MV-1178A. The red circles represent the approximate locations of laser ablation spots.

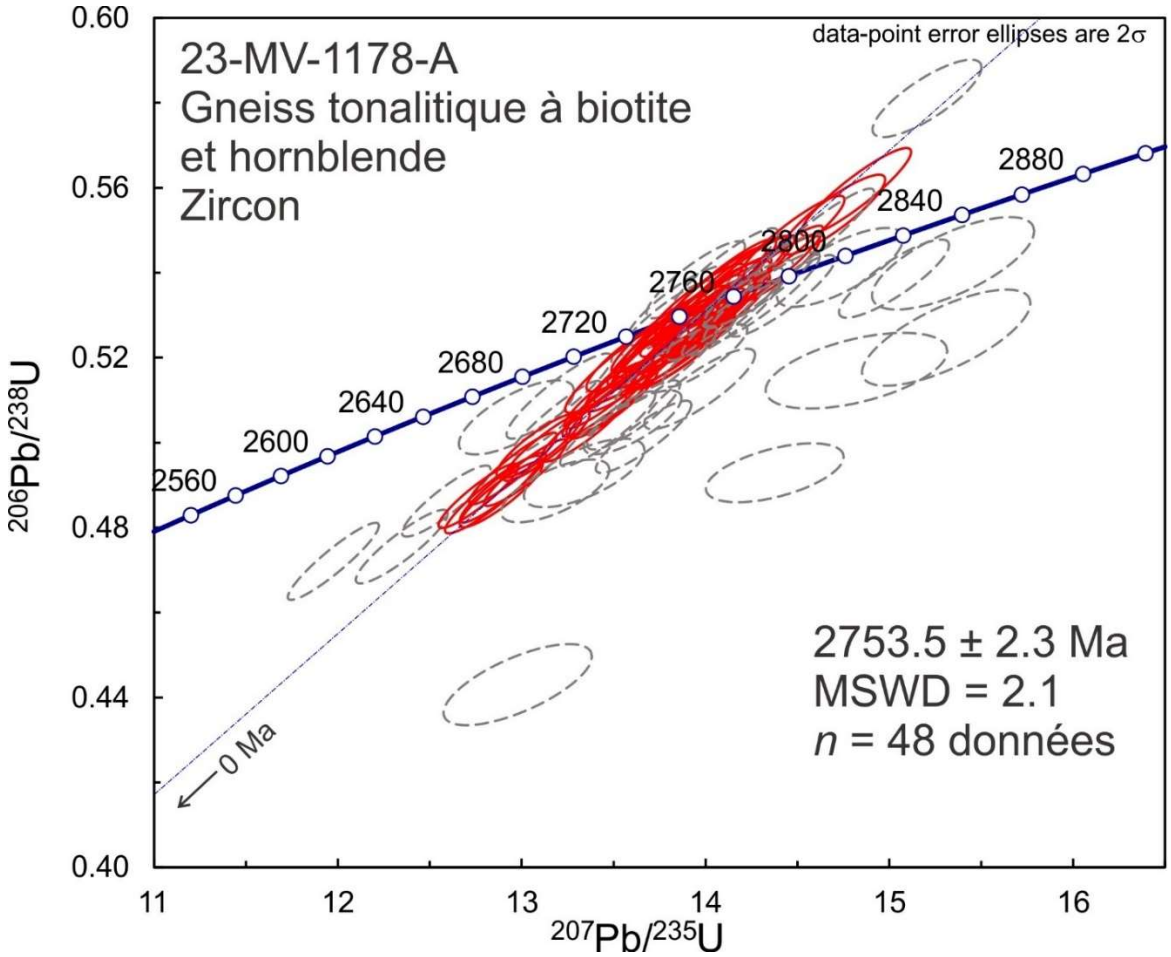

Figure 1.5.3. Concordia plot showing U-Pb isotopic data on polished zircon from gneiss sample 2023-MV-1178A. Red ellipses correspond to spots considered in the age model whereas gray-dashed ellipses correspond to the omitted spots.

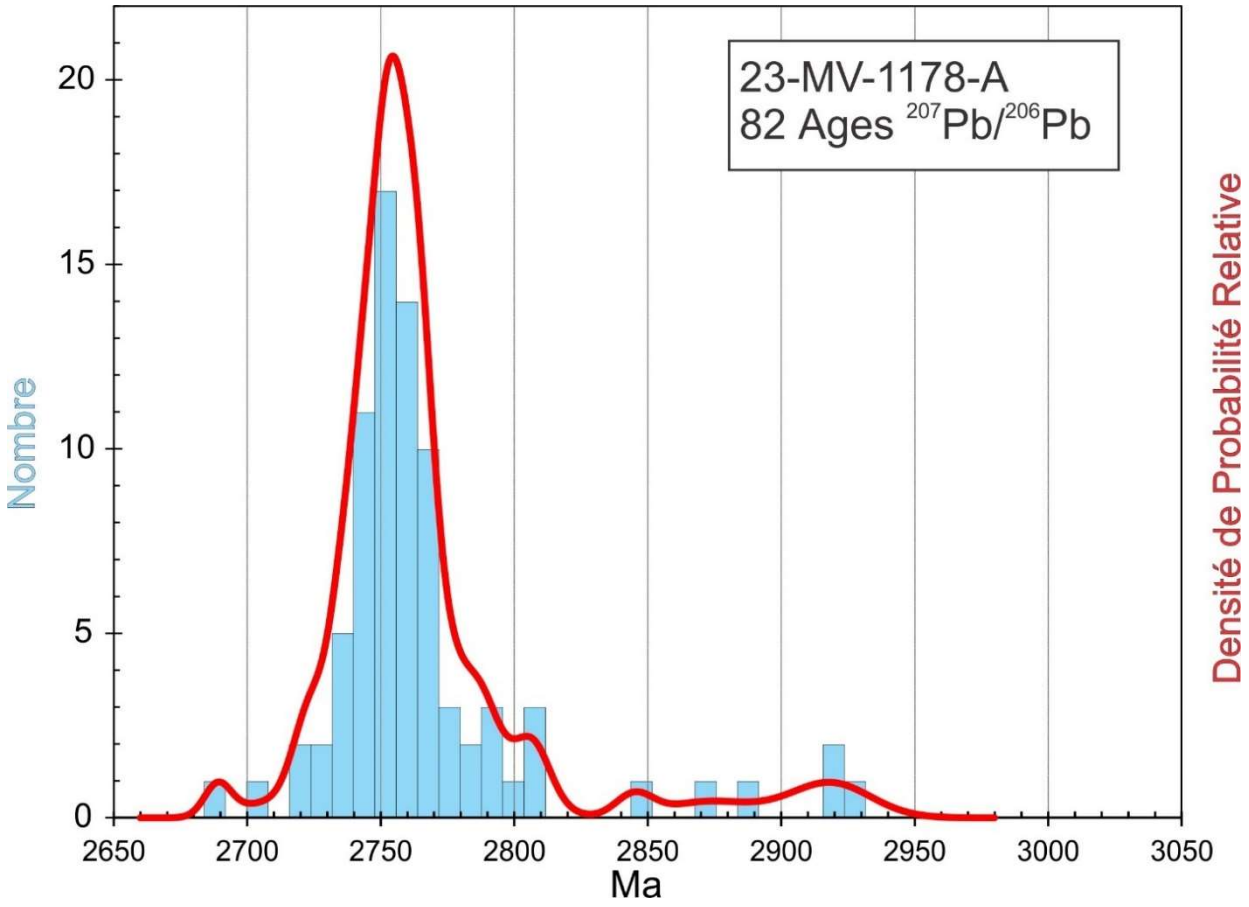

Figure 1.5.4. Combined age relative probability density plot and histogram showing the distribution of $^{207}Pb/^{206}Pb$ ages on polished zircon from gneiss sample 2023-MV-1178A.

1.6. 2023-MV-1187A
Diorite

This sample yielded abundant zircon as subhedral to rounded grains with cracks and inclusions (Fig. 1.6.1). BSE images show fairly consistent broad zoning with little evidence of cores (Fig. 1.6-2). U-Pb analyses show a bimodal age pattern with a range from 1799 Ma to 1862 Ma (Fig. 1.6-3 and 1.6.4). If there are two populations the Unmix application in Isoplot gives ages and proportions of 1841 ±2.3 Ma representing 67% of the entire set of analyses, and a second class of 1815 ±3.7 Ma that representing 33%. However, there is no systematic difference in U content or Th/U between the populations so the youngest grains may represent partial resetting during prolonged metamorphism.

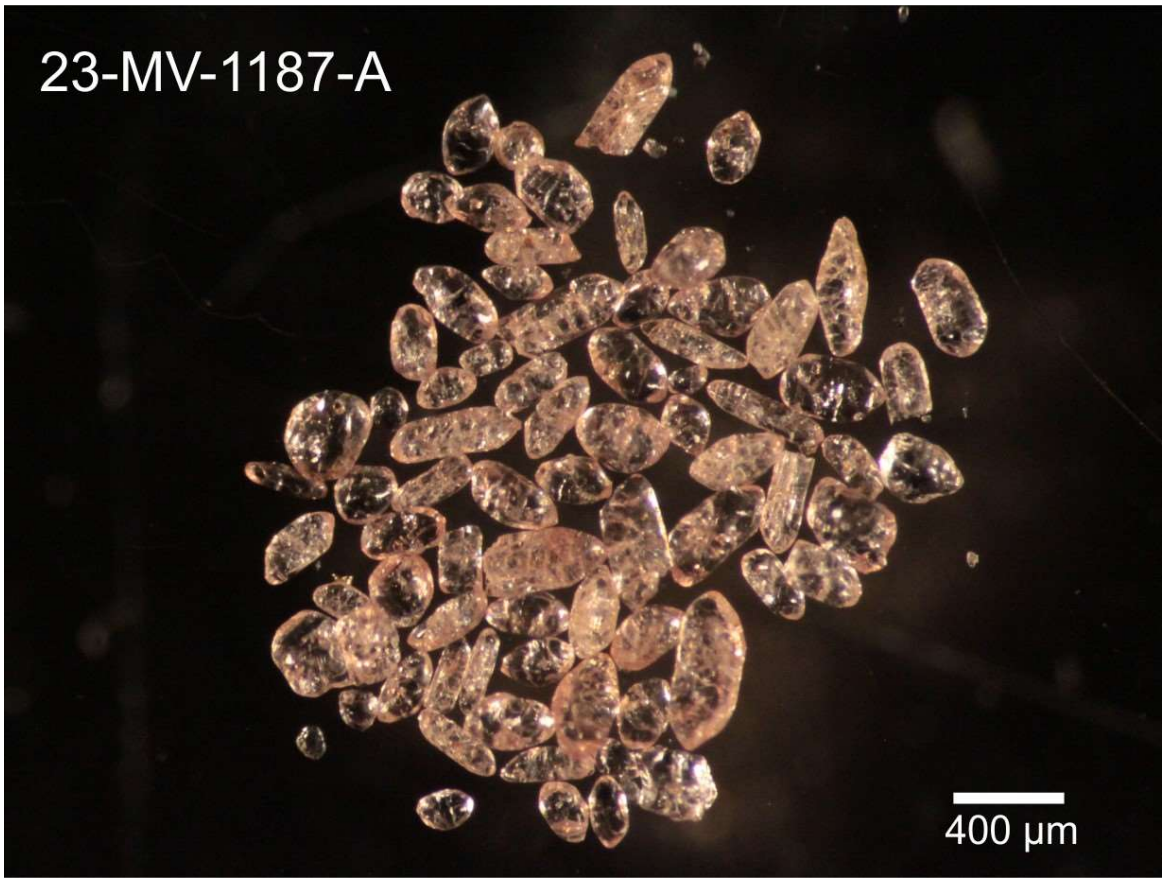

Figure 1.6.1. Picked zircon from diorite sample 2023-MV-1187A.

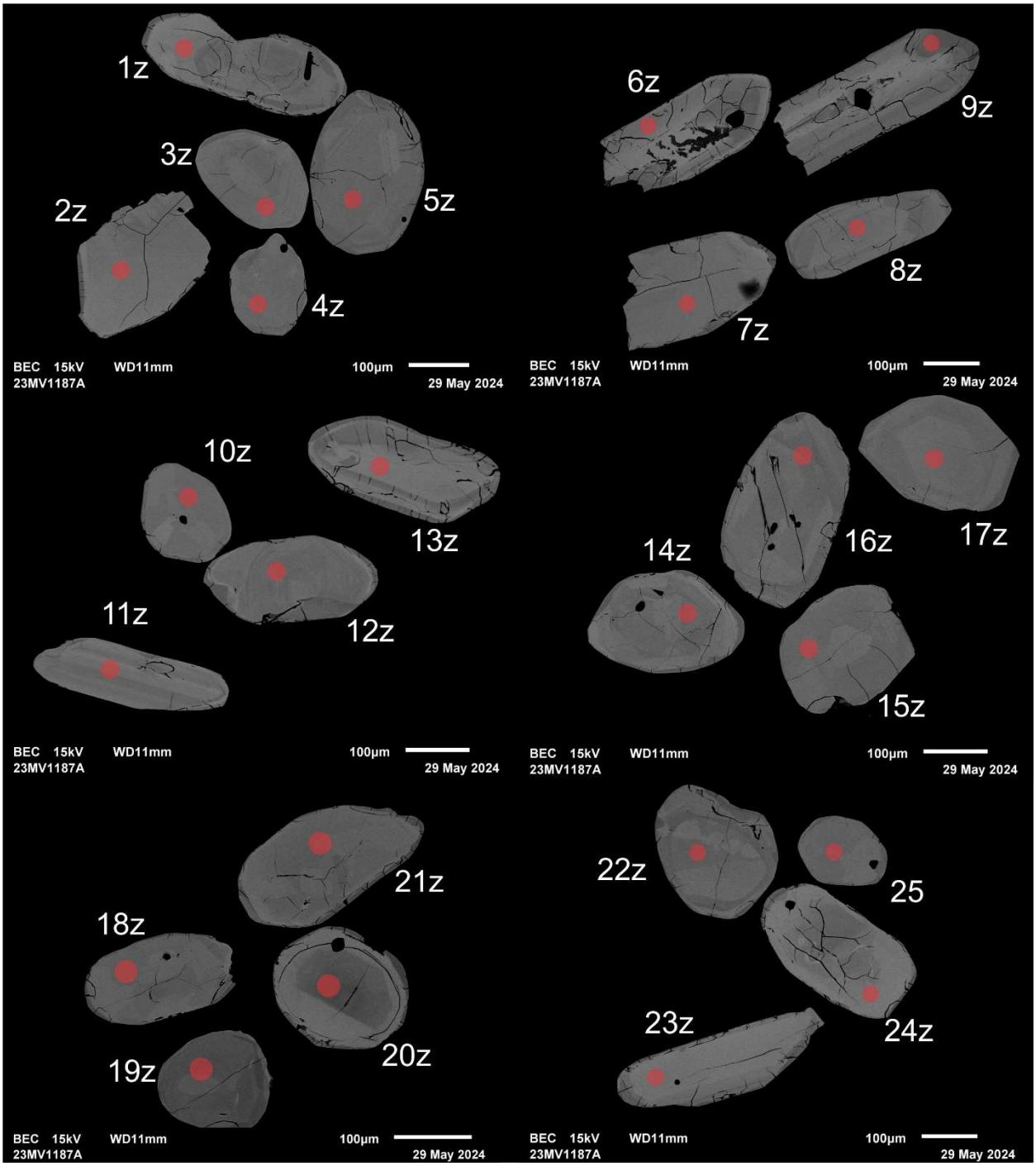

Figure 1.6.2. BSE images of selected grains from sample 2023-MV-1187A. The red circles represent the approximate locations of laser ablation spots.

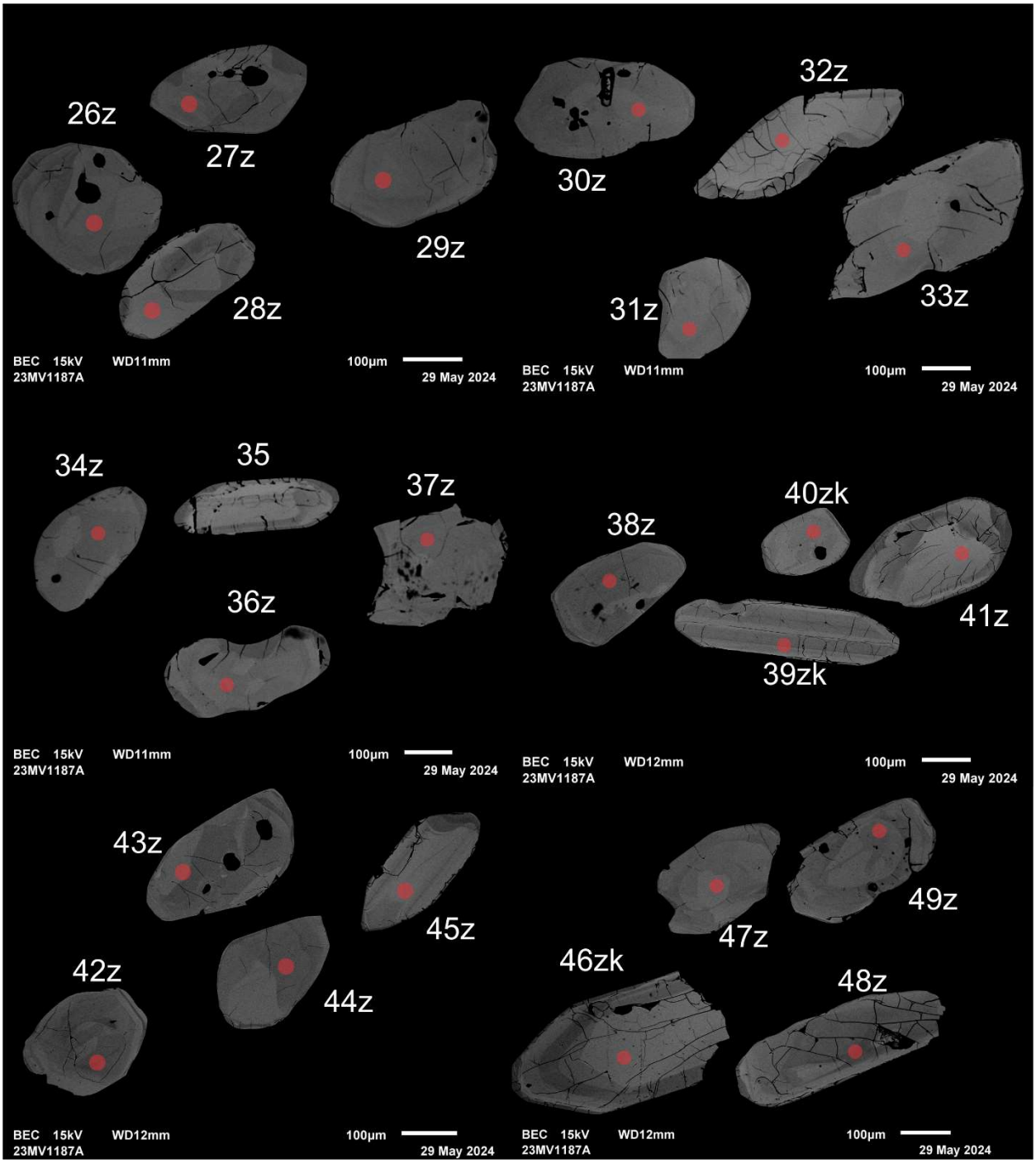

Figure 1.6.2 (cont.). BSE images of selected grains from sample 2023-MV-1187A. The red circles represent the approximate locations of laser ablation spots.

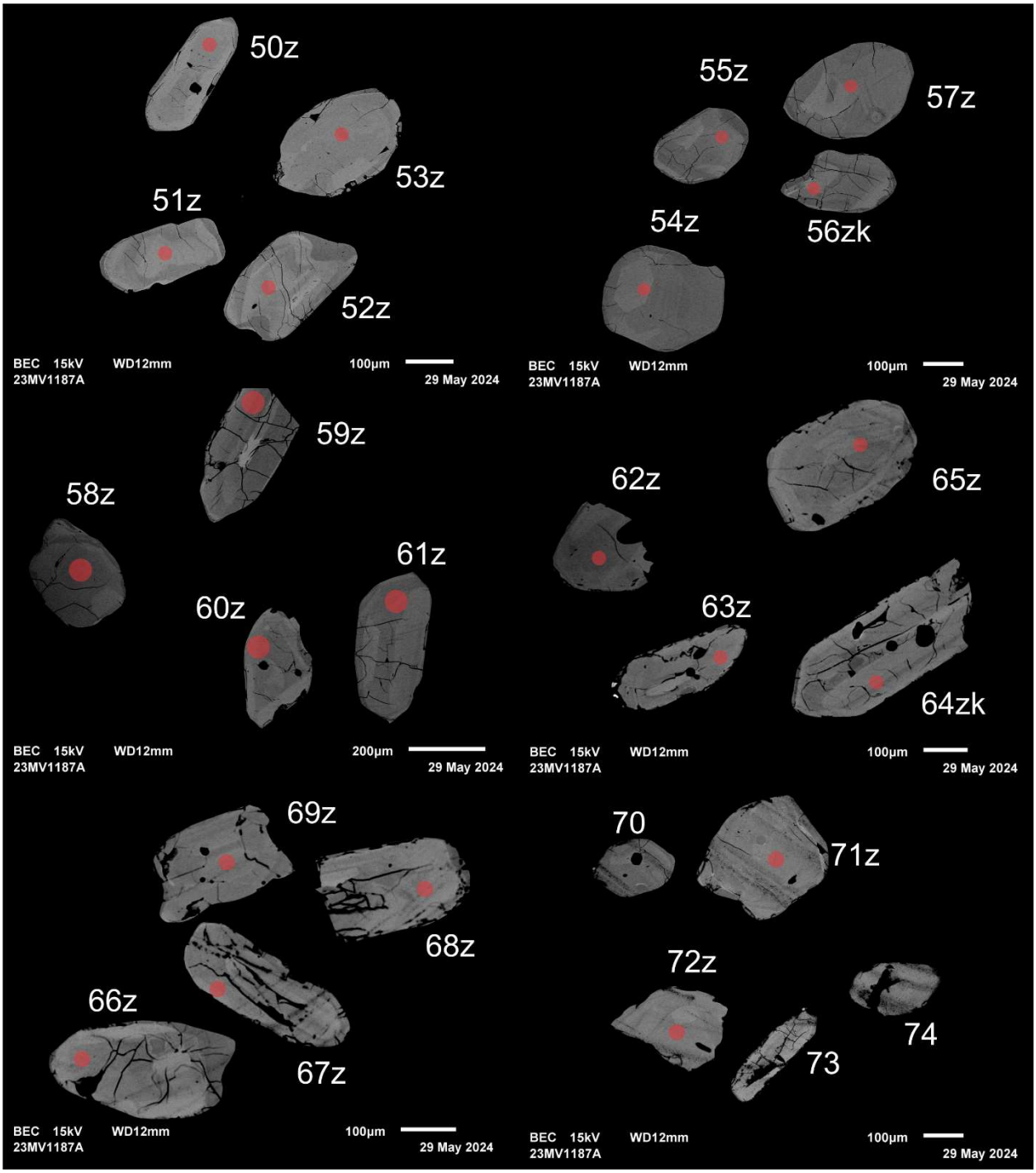

Figure 1.6.2 (cont.). BSE images of selected grains from sample 2023-MV-1187A. The red circles represent the approximate locations of laser ablation spots.

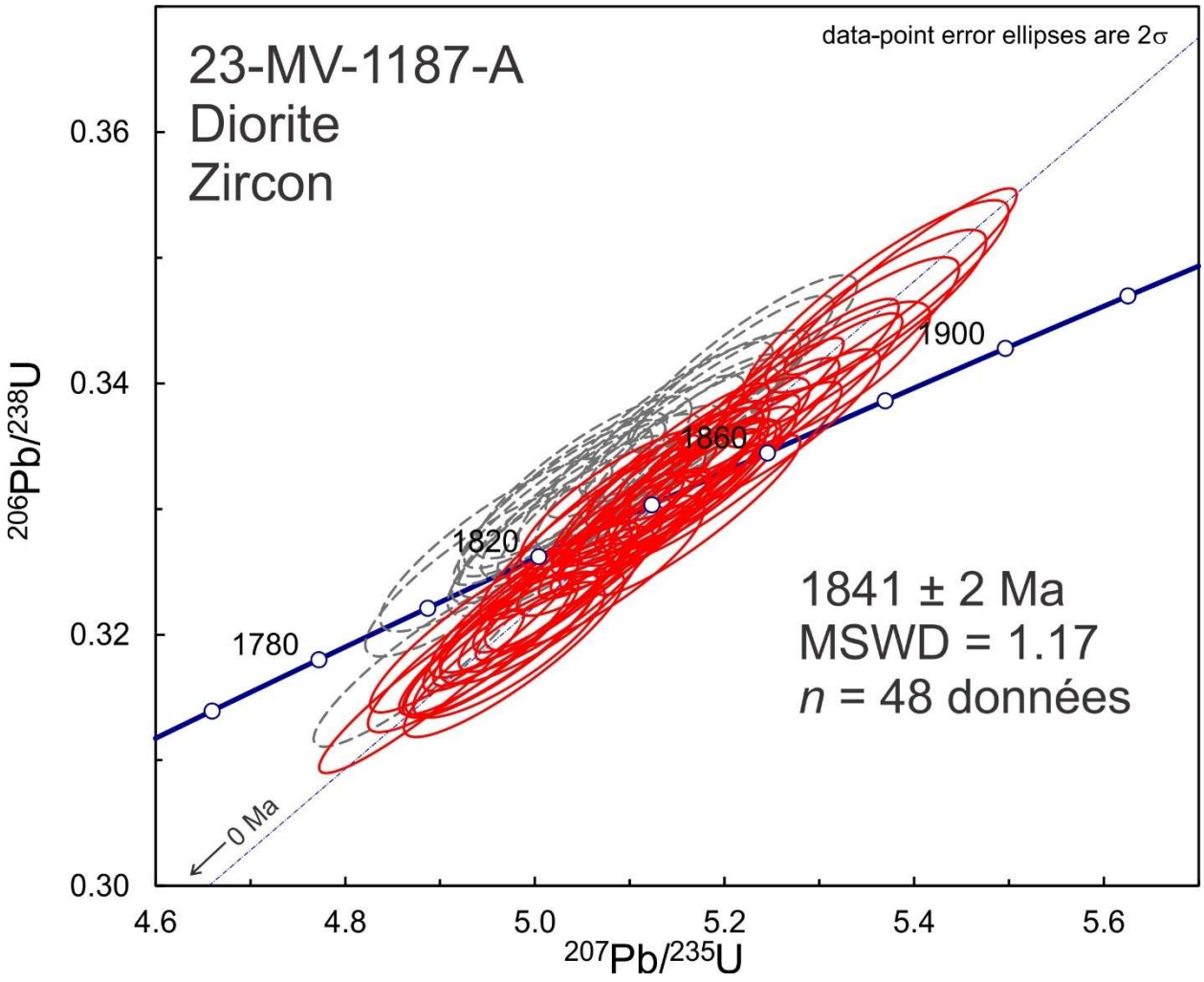

Figure 1.6.3. Concordia plot showing U-Pb isotopic data on polished zircon from diorite sample 2023-MV-1187A. Red ellipses correspond to spots considered in the age model whereas gray-dashed ellipses correspond to the omitted spots.

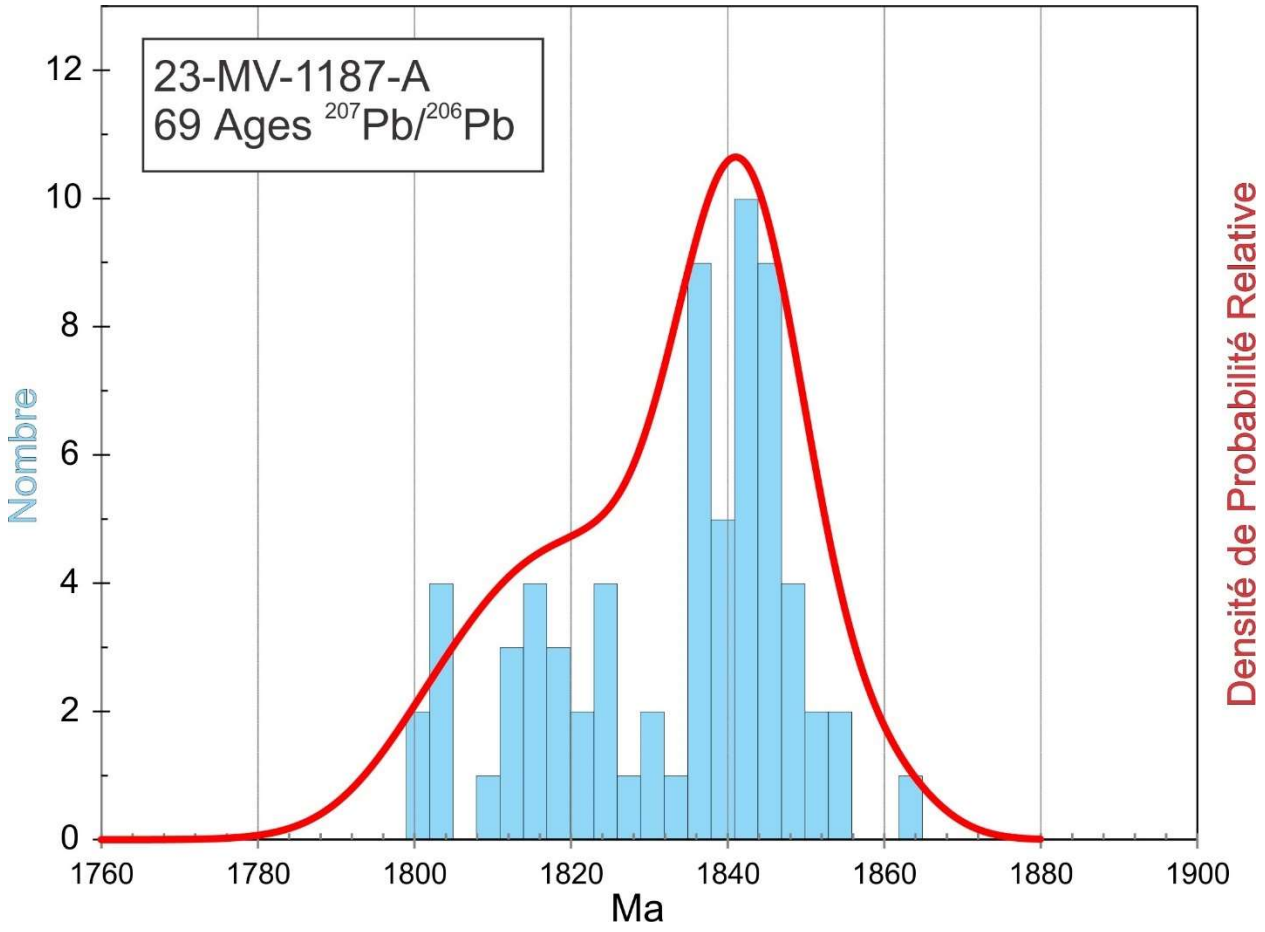

Figure 1.6.4. Combined age relative probability density plot and histogram showing the distribution of $^{207}Pb/^{206}Pb$ ages on polished zircon from diorite sample 2023-MV-1187A.

1.7. 2023-CB-2031A
Gneiss tonalitique à biotite

This sample yielded subhedral zircon with stubby to long prismatic morphologies. Many grains are highly cracked and altered but many have clear domains (Fig. 1.7.1). BSE images show a variety of zoning patterns around possible higher U cores (Fig. 1.7.2). All analyses show magmatic Th/U ratios (>0.1). Most of them are on mantle phases and the few analyses on cores do not show evidence of being older. Most $^{207}Pb/^{206}Pb$ ages occupy a peak around 2760 Ma that is skewed toward younger ages (Fig 1.7.3 and 1.7.4). A single analysis at 2446 Ma shows high Sr signal suggesting alteration, while an older analysis at 2850 Ma may represent inheritance (Fig. 1.7.4). The Unmix algorithm in Isoplot indicates that the principal peak has an age of 2760 ±3 Ma. This is the most likely age for emplacement of the pluton. Given the geological history of the area, the younger ages may reflect a small amount of Pb loss during Paleoproterozoic metamorphism.

Figure 1.7.1. Picked zircon from gneiss sample 2023-CB-2031A.

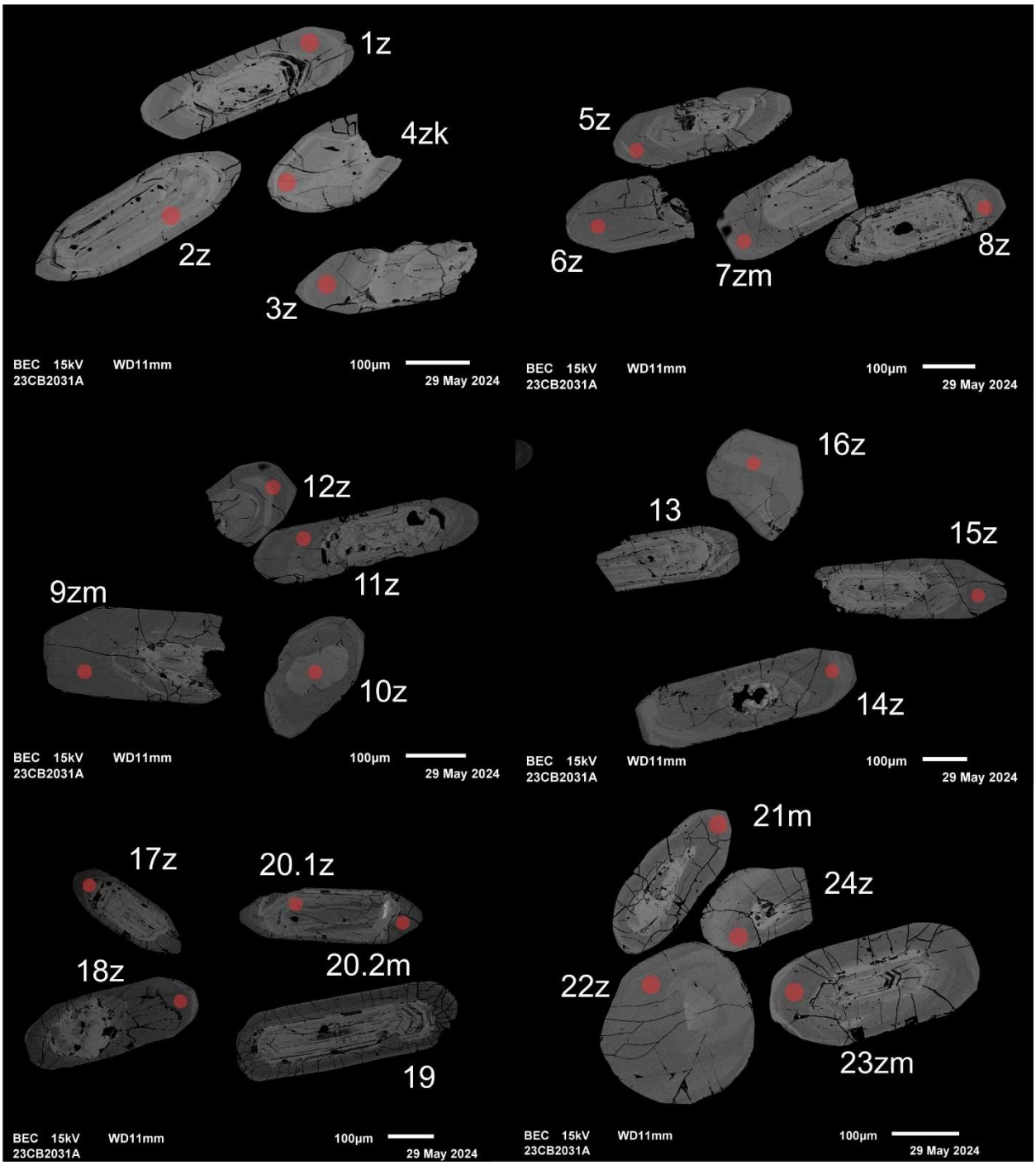

Figure 1.7.2. BSE images of selected grains from sample 2023-CB-2031A. The red circles represent the approximate locations of laser ablation spots.

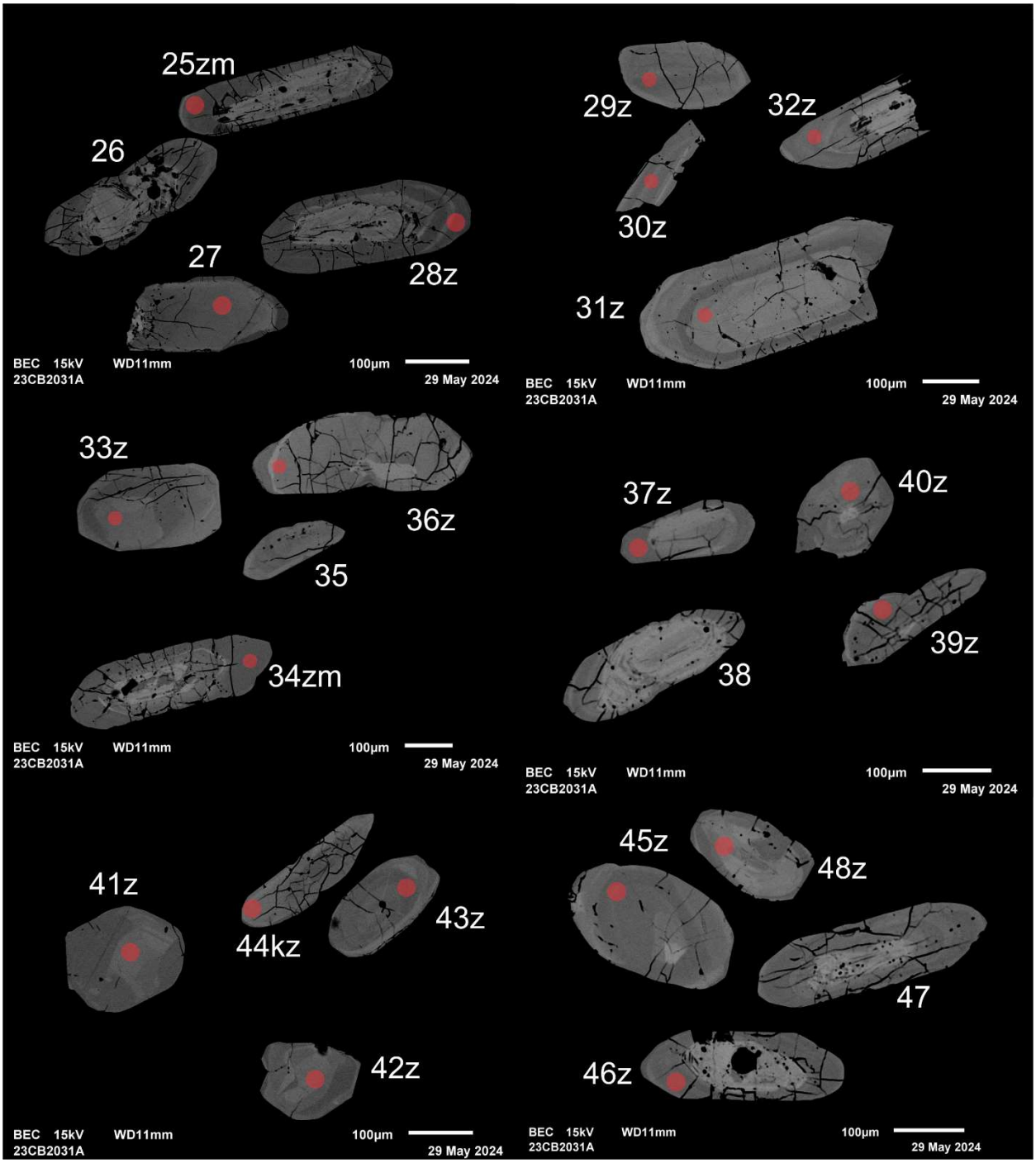

Figure 1.7.2 (cont.). BSE images of selected grains from sample 2023-CB-2031A. The red circles represent the approximate locations of laser ablation spots.

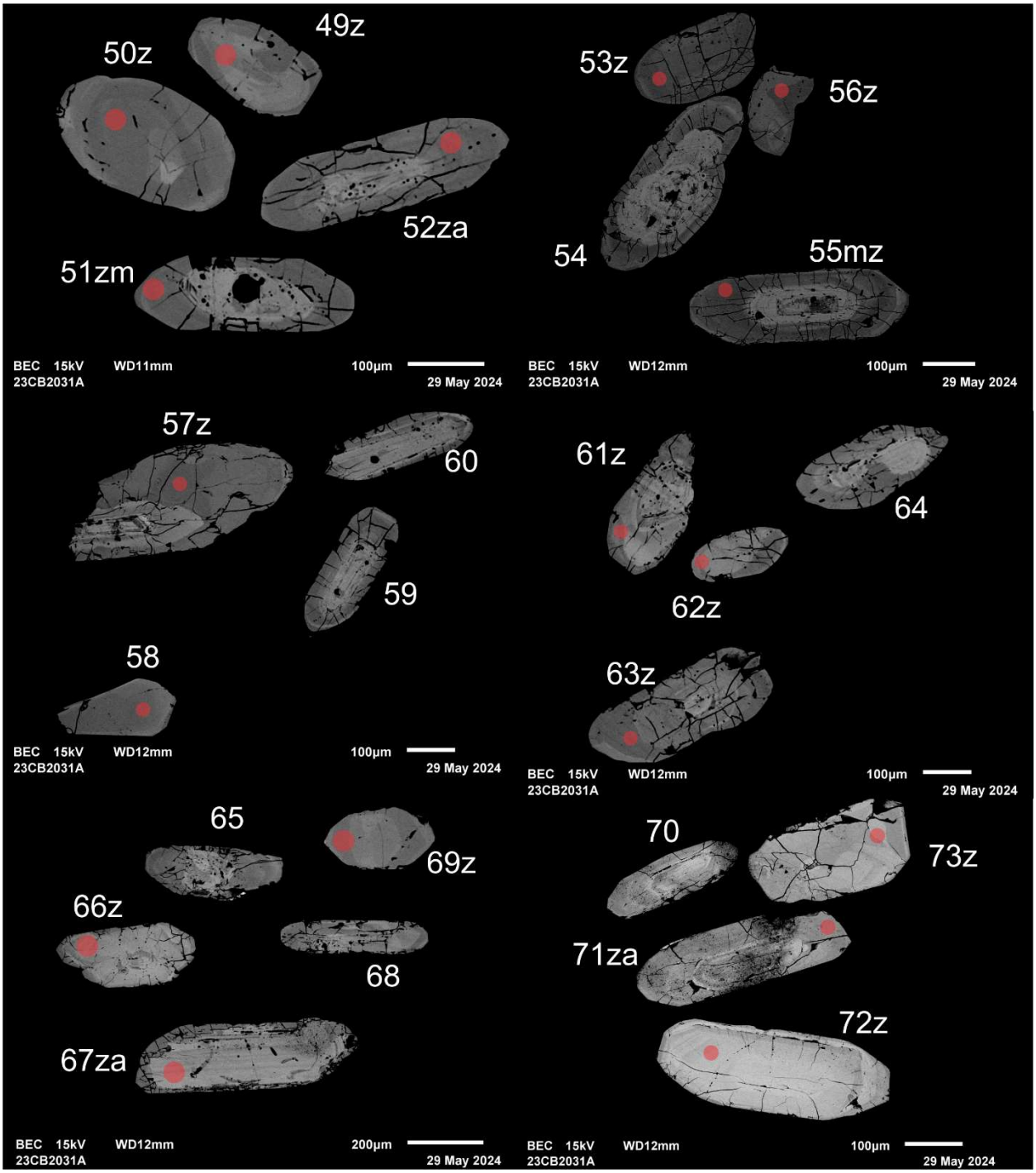

Figure 1.7.2 (cont.). BSE images of selected grains from sample 2023-CB-2031A. The red circles represent the approximate locations of laser ablation spots.

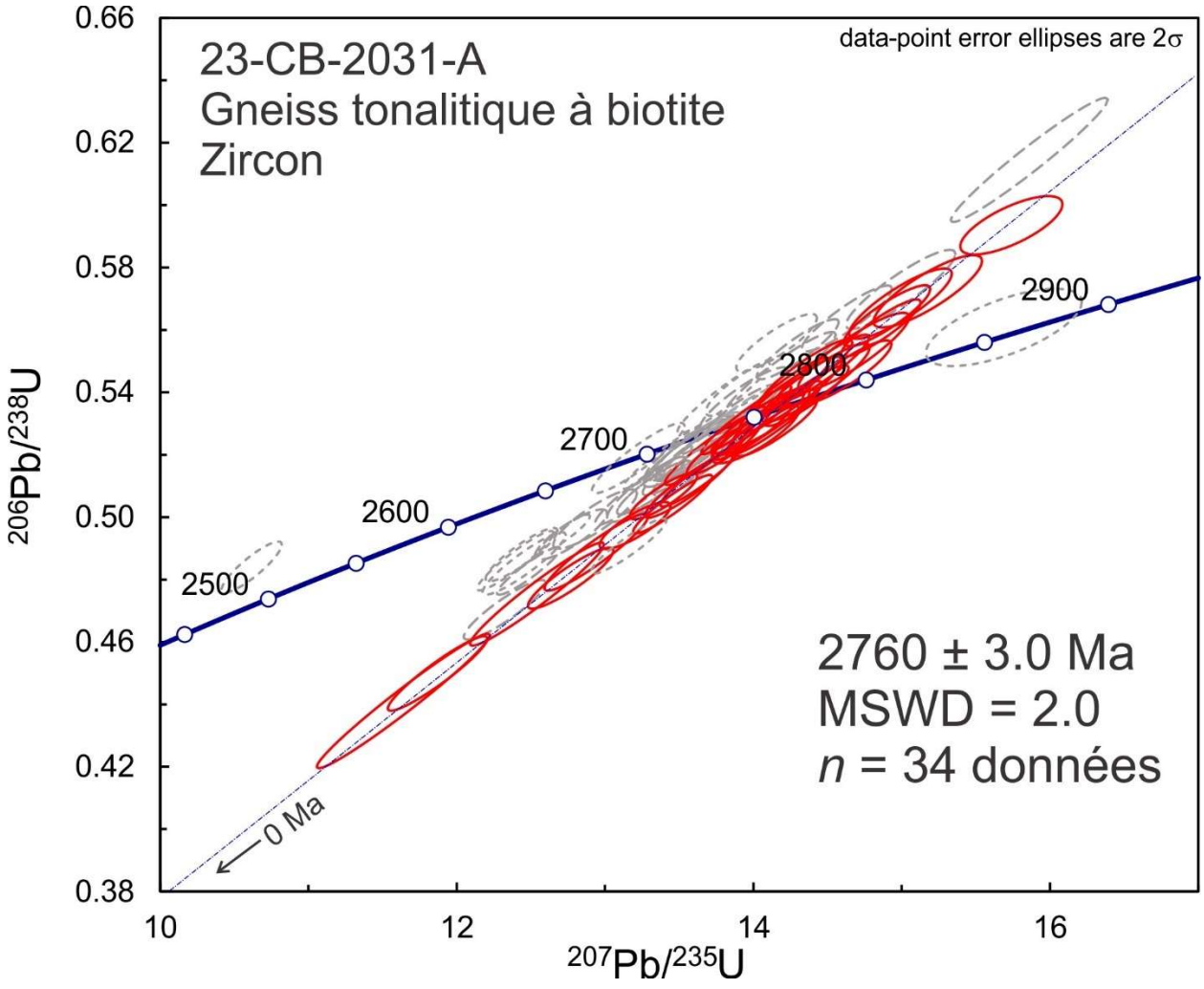

Figure 1.7.3. Concordia plot showing U-Pb isotopic data on polished zircon from gneiss sample 2023-CB-2031A. Red ellipses correspond to spots considered in the age model whereas gray-dashed ellipses correspond to the omitted spots.

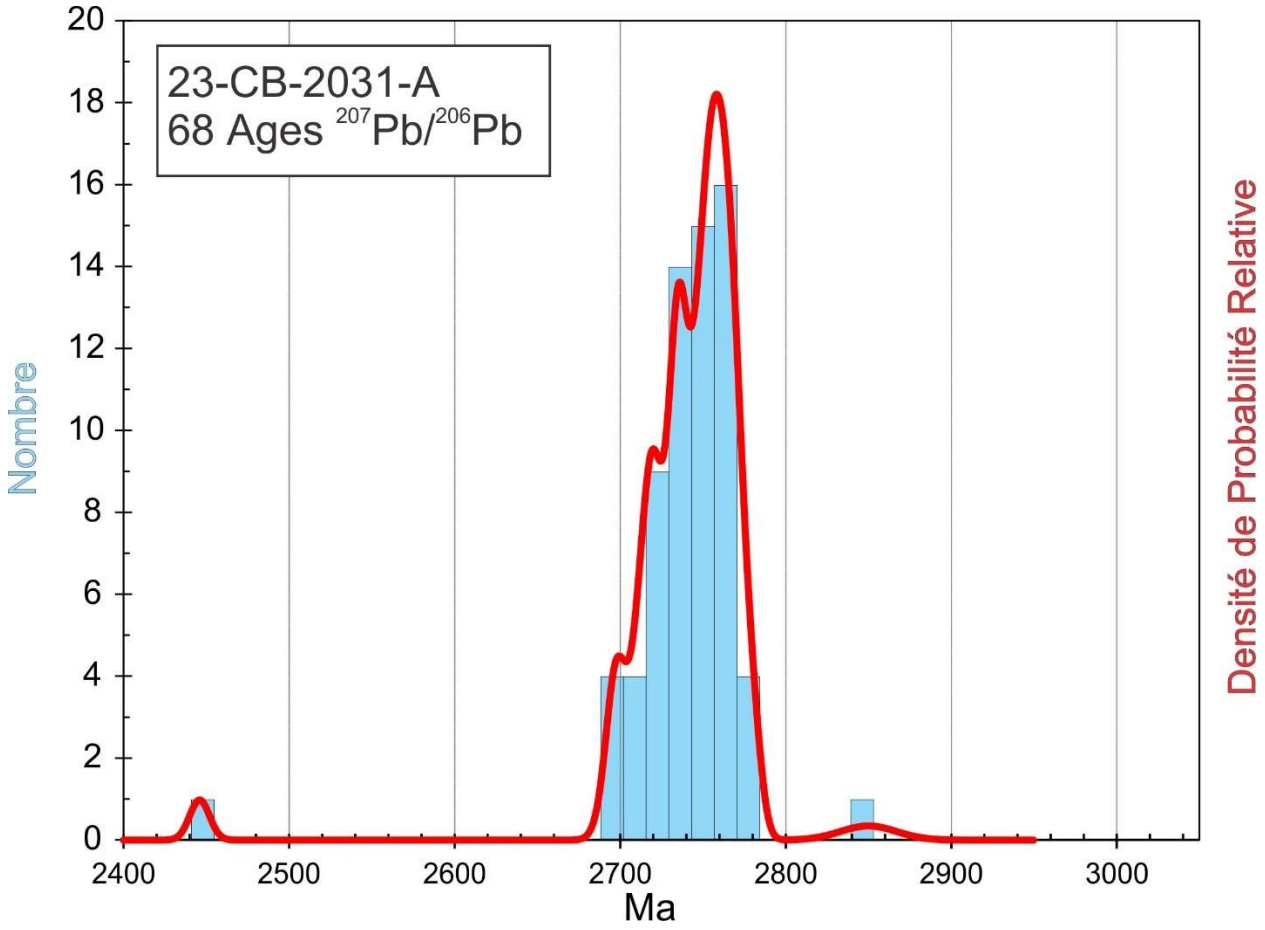

Figure 1.7.4. Combined age relative probability density plot and histogram showing the distribution of $^{207}Pb/^{206}Pb$ ages on polished zircon from gneiss sample 2023-CB-2031A.

1.8. 2023-CB-2035B
Granite

This sample yielded a small amount of zircon as subhedral and subrounded grains that are variably fractured (Fig. 1.8.1). BSE images show possible cores mantled by oscillatory zoned zircon (Fig. 1.8.2). All analyses show magmatic Th/U ratios (> 0.1). U-Pb analyses show two principal peaks corresponding to analyses on overgrowths and cores, respectively (Fig. 1.8.3 and 1.8.4). The Unmix age relative probability data show a Paleoproterozoic age peak of 1762 ±3 Ma (60%) and an Archean peak at 2723 ±3 Ma (32%). A few intermediate ages may be from spots that straddled the boundary between phases. Regressing the two clusters individually defines average ages of 1758 ±4.6 Ma (2σ, MSWD = 2.2), and 2732 ±8 Ma (2σ, MSWD = 2.5) (Fig. 1.8.3), respectively. The Archean age is probably that of the protolith whereas the Paleoproterozoic age likely represents crustal melting to form the granite.

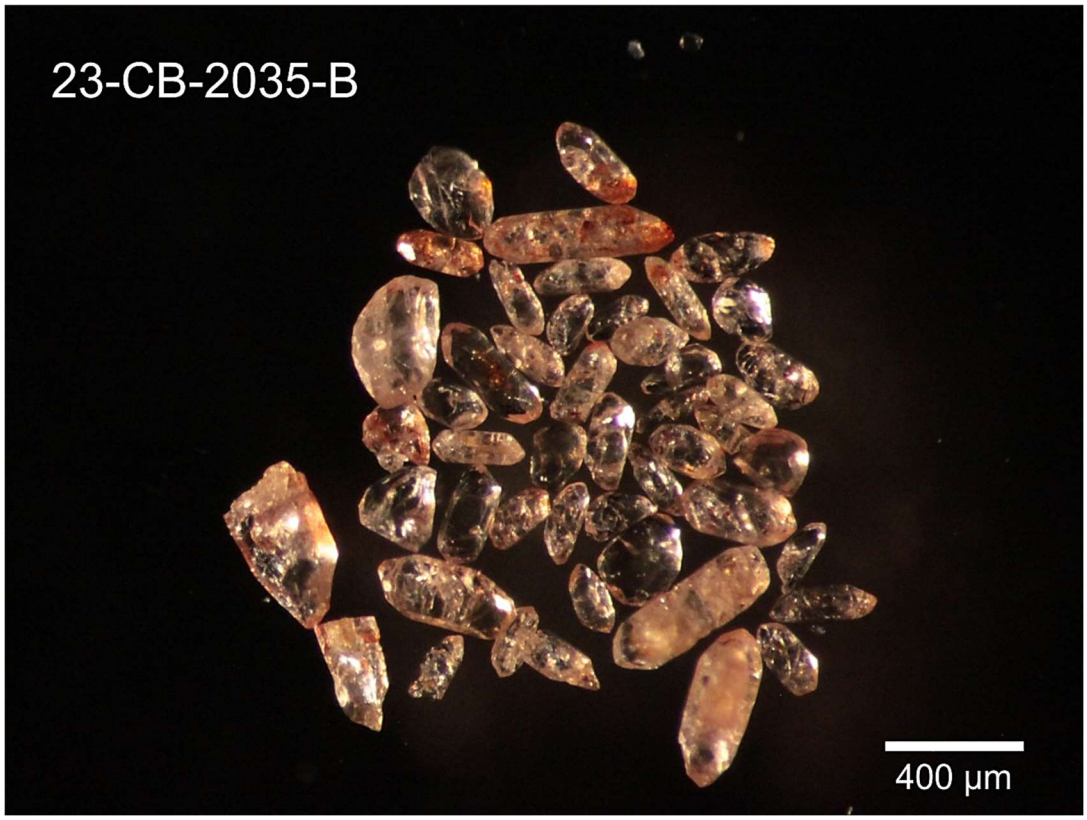

Figure 1.8. Picked zircon from granite sample 2023-CB-2035B.

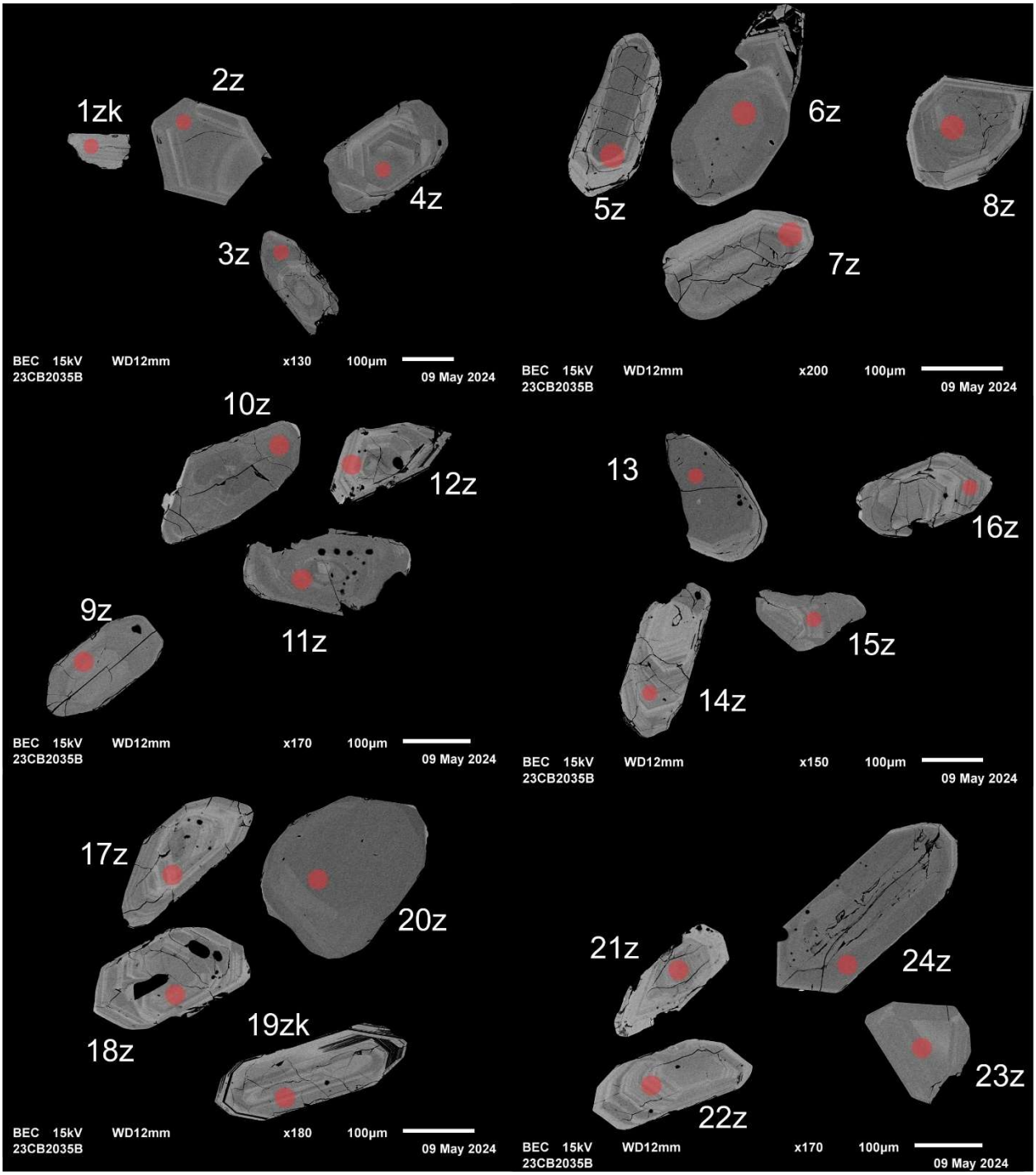

Figure 1.8.2. BSE images of selected grains from sample 2023-CB-2035B. The red circles represent the approximate locations of laser ablation spots.

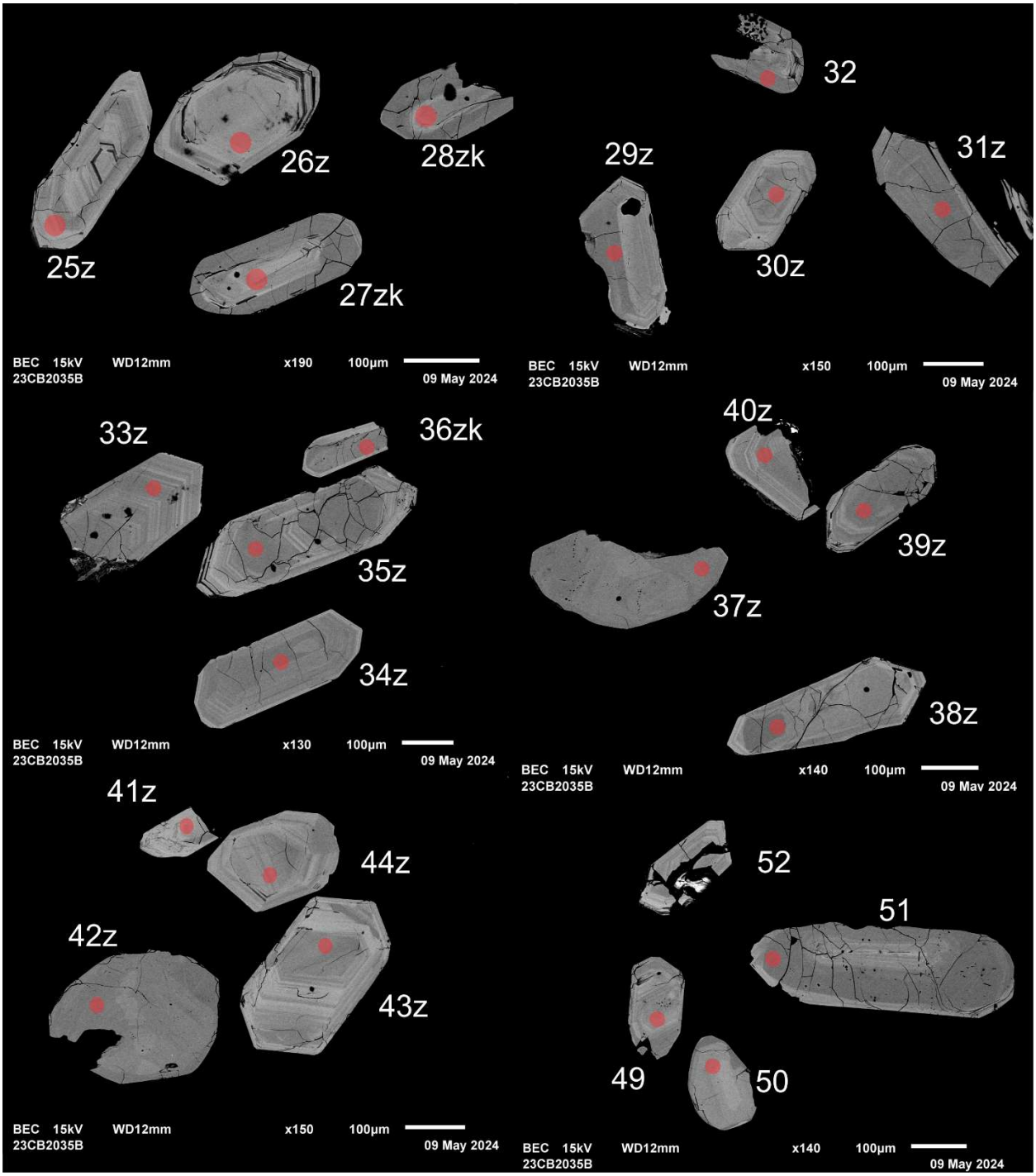

Figure 1.8.2 (cont.). BSE images of selected grains from sample 2023-CB-2035B. The red circles represent the approximate locations of laser ablation spots.

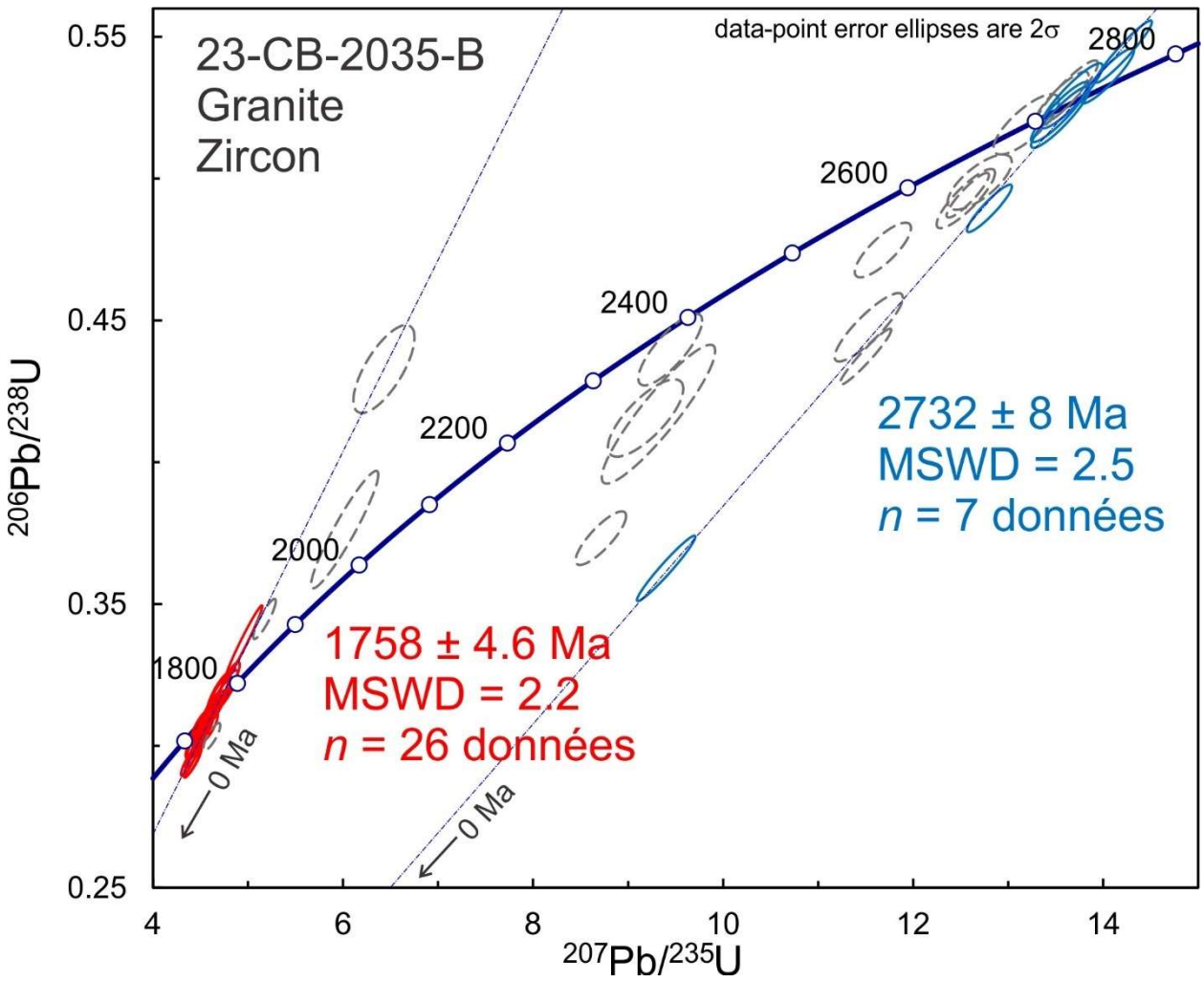

Figure 1.8.3. Concordia plot showing U-Pb isotopic data on polished zircon from granite sample 2023-CB-2035B. Red and blue ellipses correspond to spots considered in the age model whereas gray-dashed ellipses correspond to the omitted spots. Two possible ages are shown.

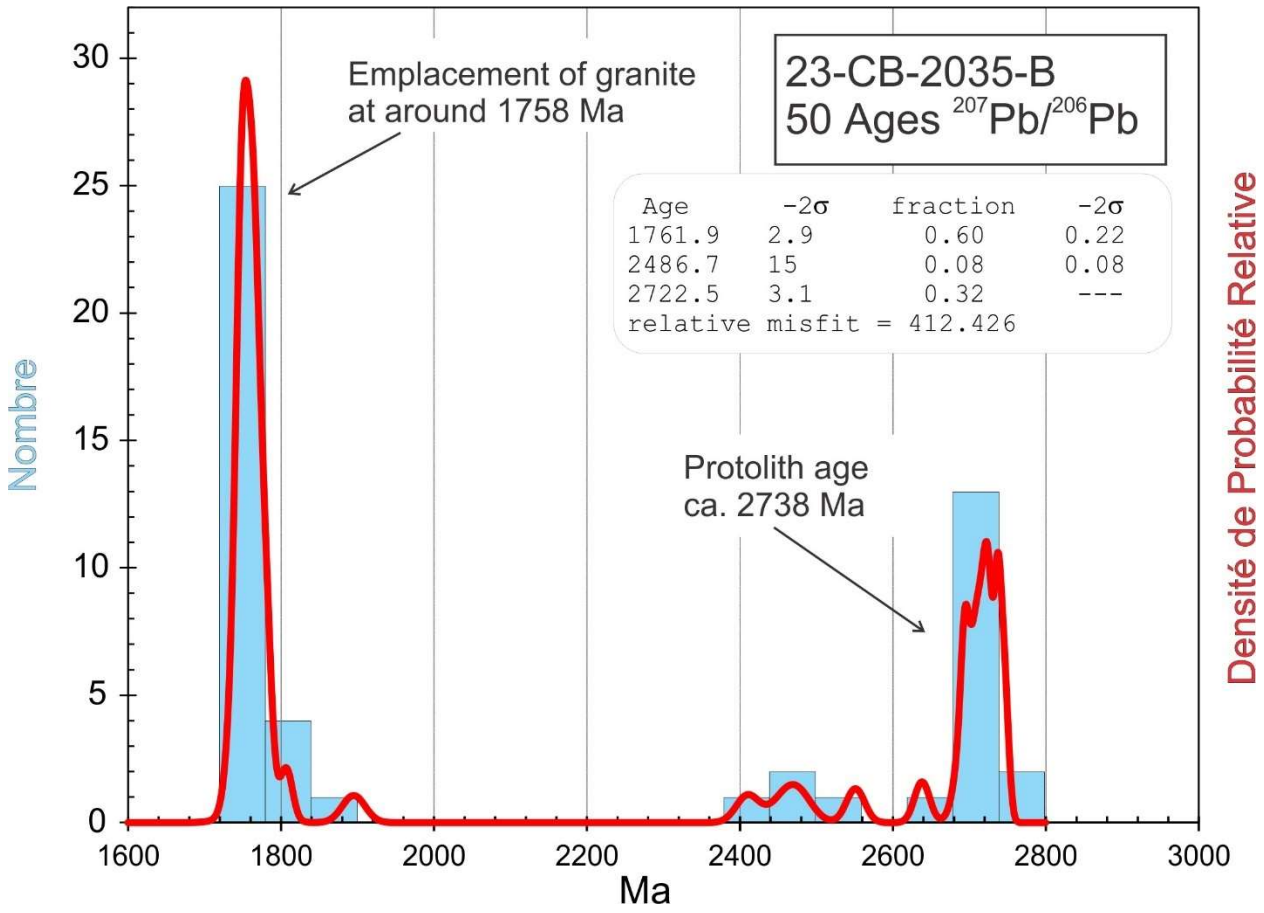

Figure 1.8.4. Combined age relative probability density plot and histogram showing the distribution of $^{207}Pb/^{206}Pb$ ages on polished zircon from granite sample 2023-CB-2035B.

1.9. 2023-CB-2120A
Diorite quartzifère

This sample yielded a small amount of zircon consisting mostly of fragments (Fig. 1.9.1). BSE images show broad zoning with no evidence for older cores (Fig 1.9.2). U-Pb analyses on 42 spots scatter within error with an average age of 1831.3 ±1.7 Ma (2σ, MSWD = 1.2) (Fig. 1.9.3). All analyses show magmatic Th/U ratios (> 0.1), therefore the age of 1831.3 ±1.7 Ma represents emplacement of the diorite.

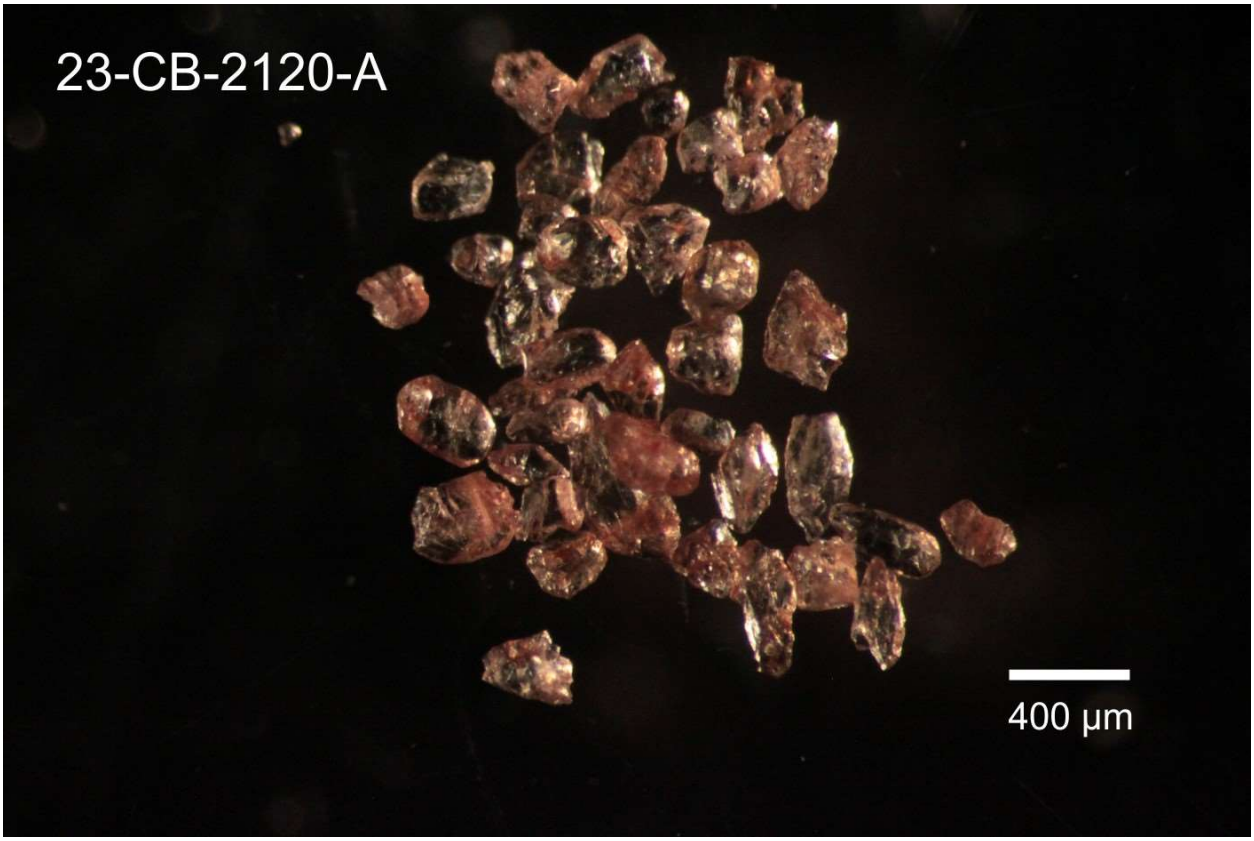

Figure 1.9.1. Picked zircon from diorite sample 2023-CB-2120A.

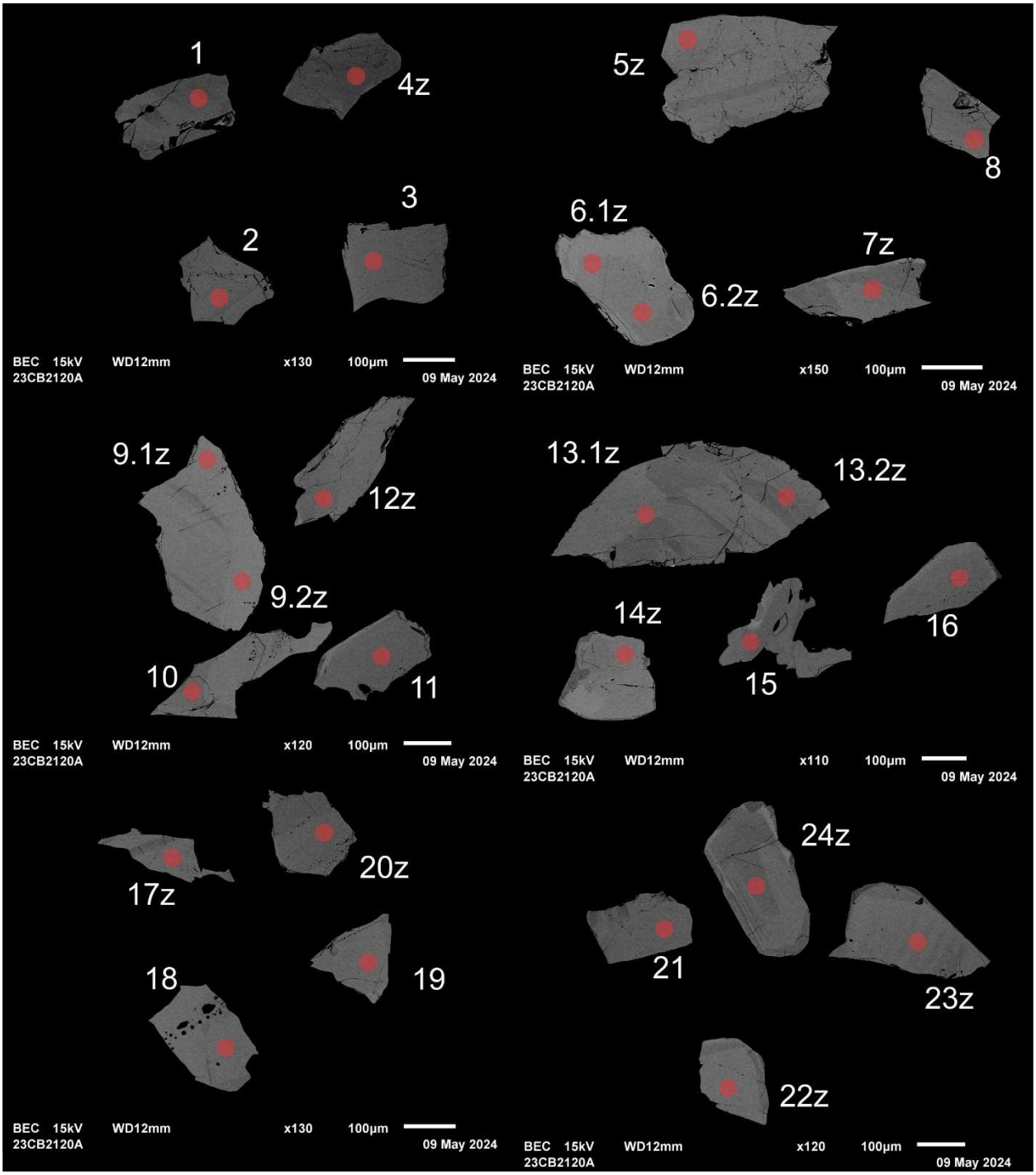

Figure 1.9.2. BSE images of selected grains from sample 2023-CB-2120A. The red circles represent the approximate locations of laser ablation spots.

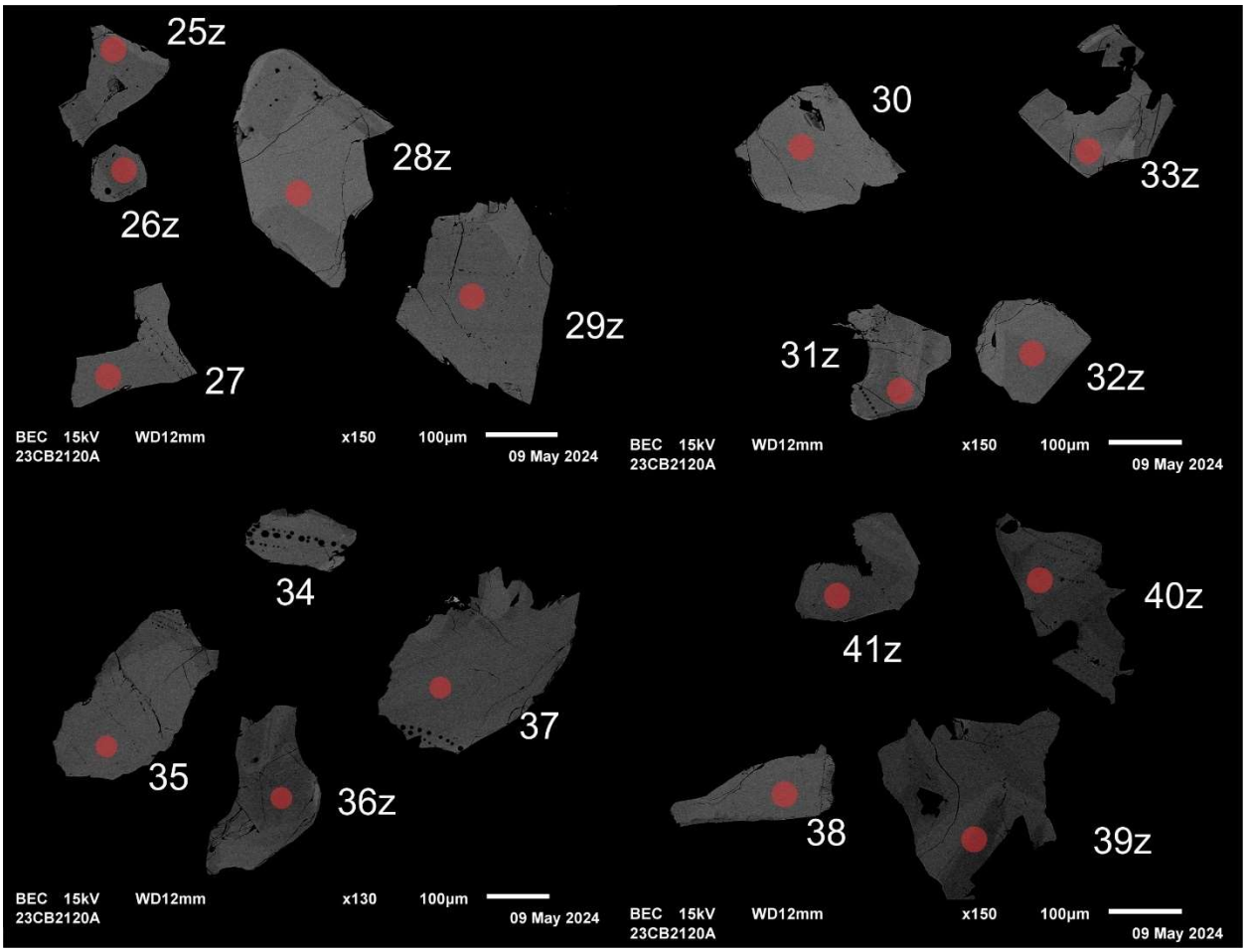

Figure 1.9.2 (cont.). BSE images of selected grains from sample 2023-CB-2120A. The red circles represent the approximate locations of laser ablation spots.

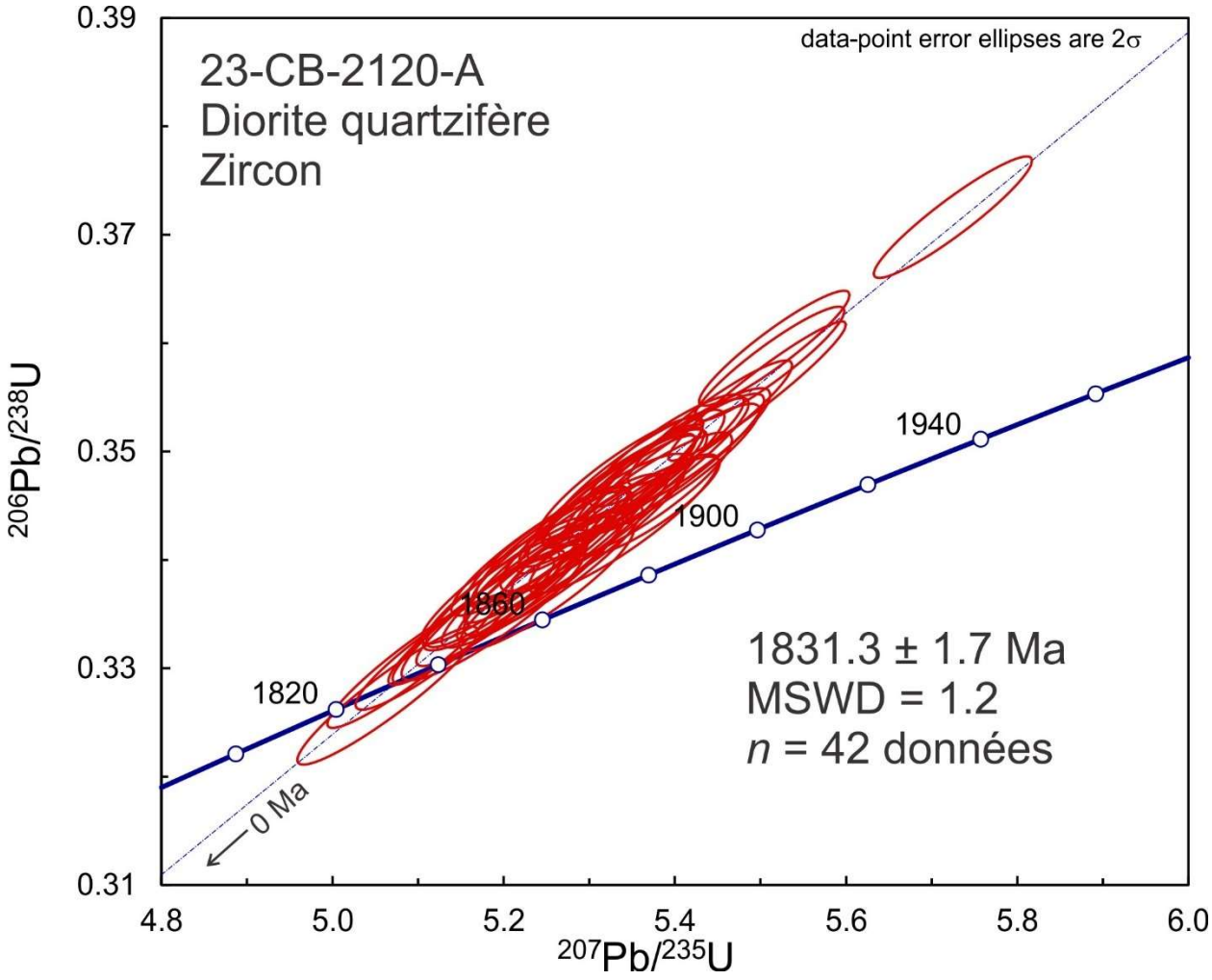

Figure 1.9.3. Concordia plot showing U-Pb isotopic data on polished zircon from diorite sample 2023-CB-2120A.

1.10. 2023-GC-3082A
Paragneiss quartzitique

This sample yielded mostly small zircon grains with a variety of brownish coloration from subhedral to well-rounded morphology (Fig. 1.10.1). Due to their size, the grains were mounted on double-sided tape and analyzed on natural surfaces. U-Pb analyses show diverse ages ranging from 1842 Ma to 2744 Ma (Fig. 1.10.2 and 1.10.3) but with a peak at the younger end. All analyses show Th/U> 0.1. U-Pb ages on the 30 youngest spots scatter within error with an average age of 1863 ±5 Ma (2σ, MSWD = 2.1, Fig. 1.10.2). This is likely the age of the formation of the paragneiss, whereas the oldest analyses correspond to inherited detrital zircon, which may or may not have been partially reset.

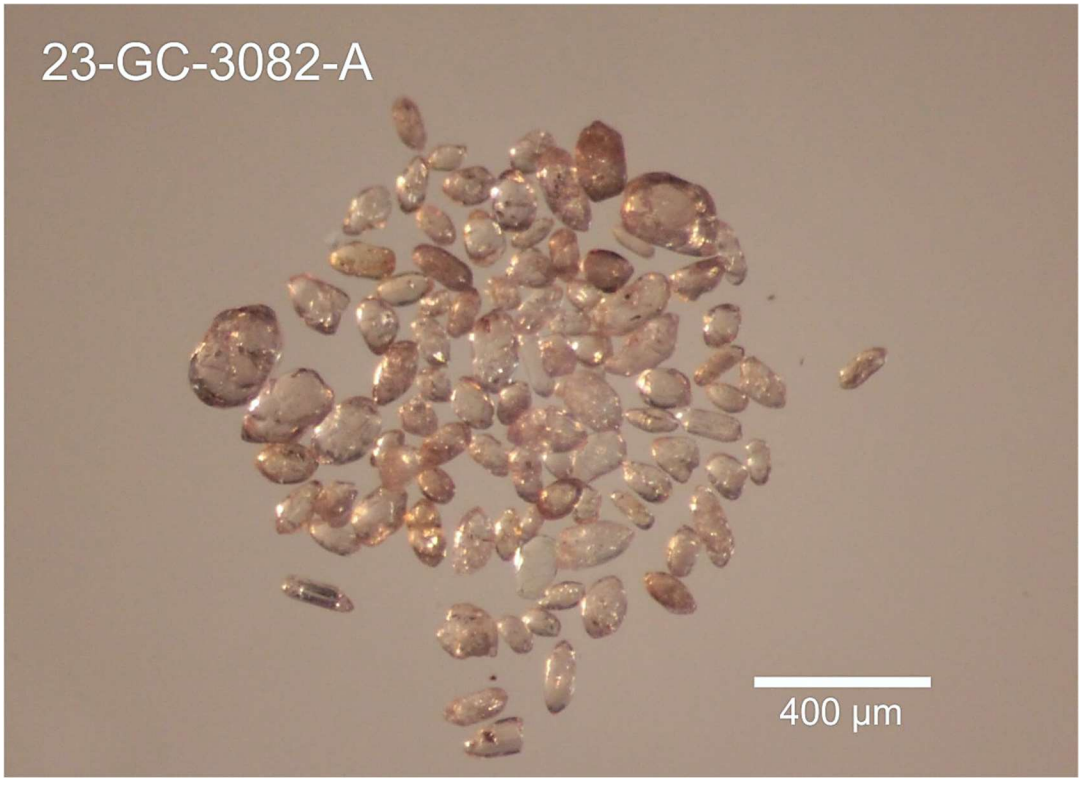

Figure 1.10.1. Picked zircon from paragneiss sample 2023-CG-3082A.

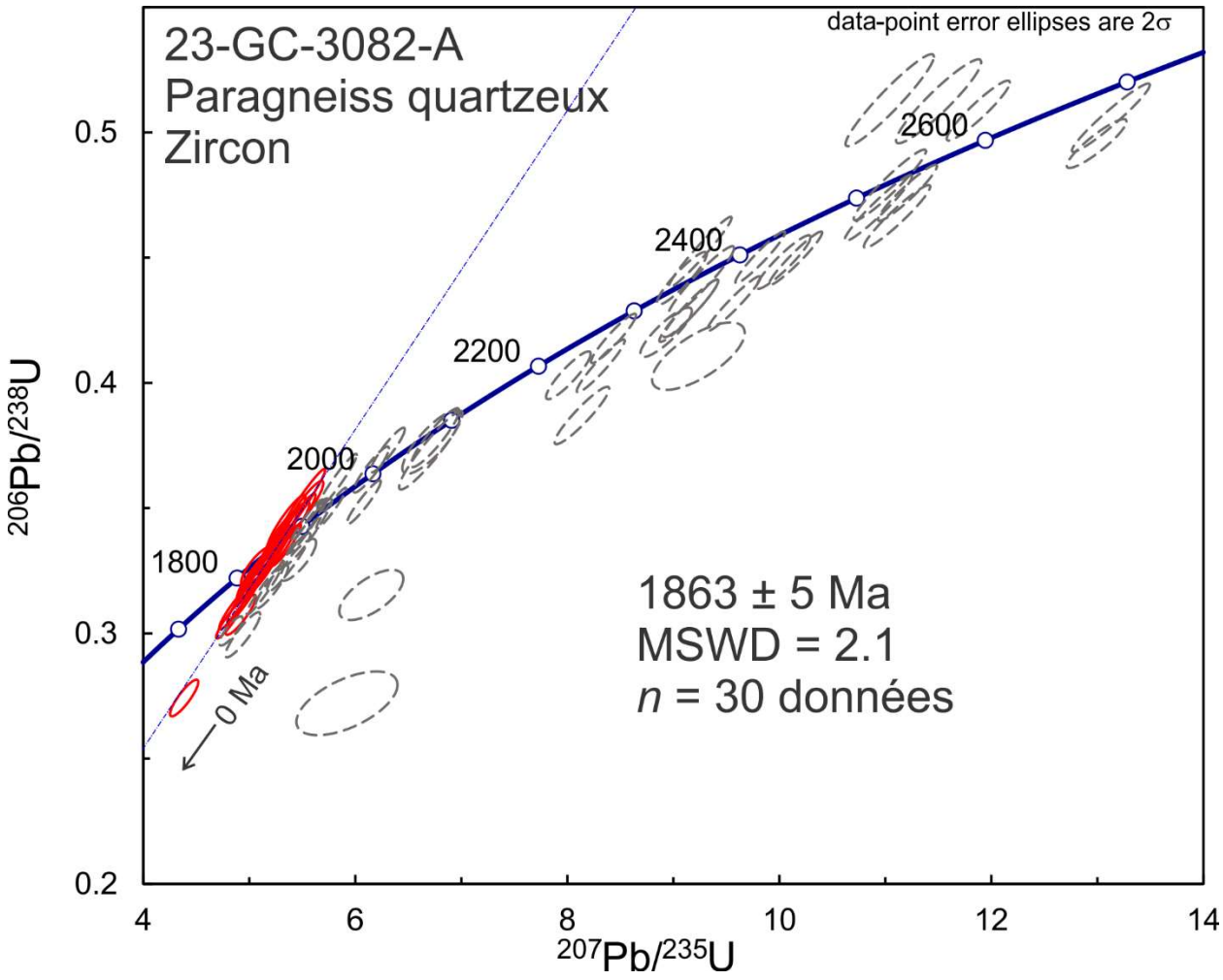

Figure 1.10.2. Concordia plot showing U-Pb isotopic data on polished zircon from paragneiss sample 2023-CG-3082A. Red ellipses correspond to spots considered in the age model whereas gray-dashed ellipses correspond to the omitted spots.

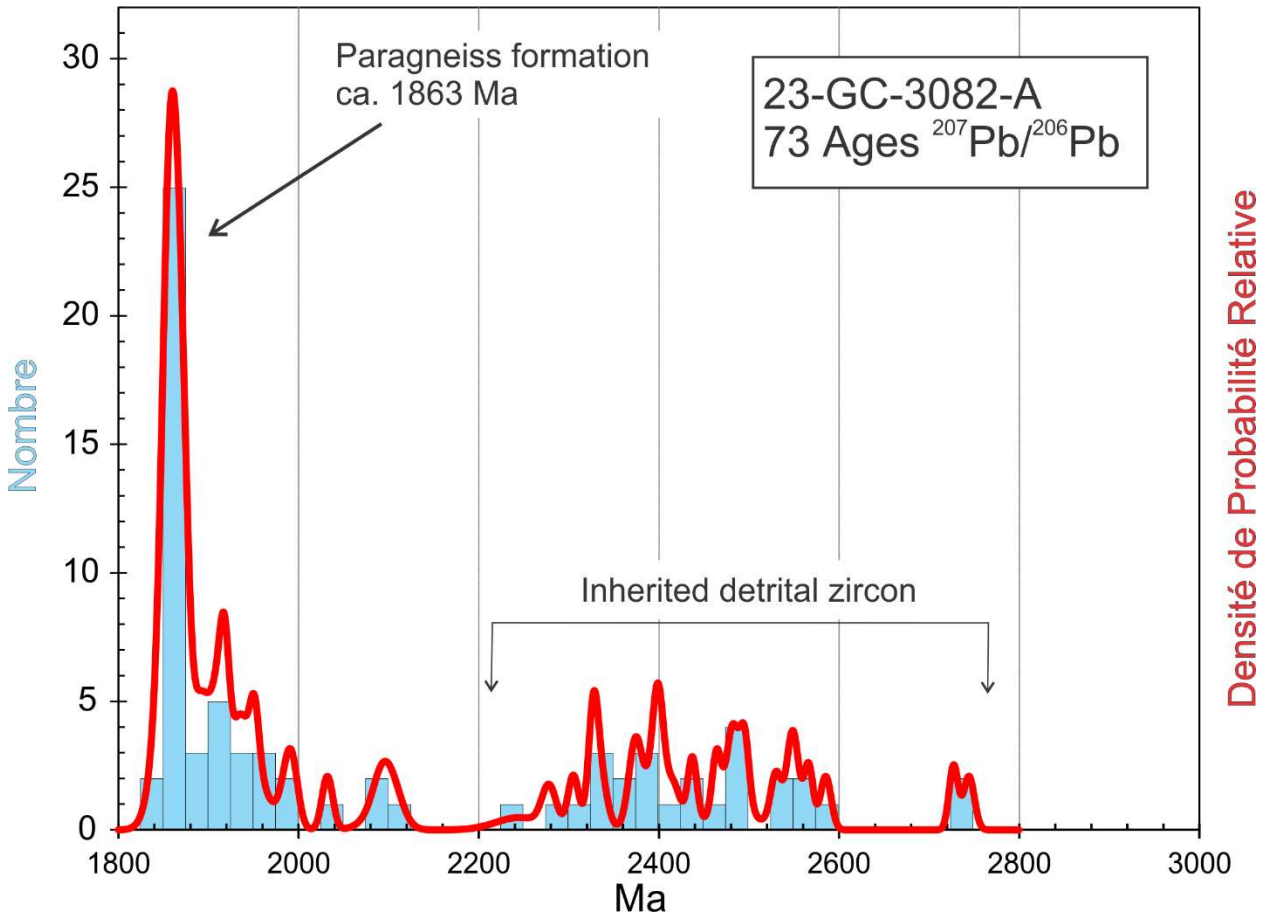

Figure 1.10.3. Combined age relative probability density plot and histogram showing the distribution of $^{207}Pb/^{206}Pb$ ages on polished zircon from paragneiss sample 2023-CG-3082A.

1.11. 2021-TG-4060A
Paragneiss à grenat et biotite

This sample yielded a diverse population of zircon grains with variable brownish coloration and euhedral to well-rounded morphology (Fig. 1.11-1). BSE images show abundant evidence of cores surrounded by higher U (brighter) overgrowths that in some cases show broad zonation (Fig. 1.11.2). Analyses on overgrowths show Th/U <0.1, indicating a metamorphic origin, while those on cores give a magmatic signature (Th/U>0.1). Given the rock type, the cores are probably of detrital origin. U-Pb analyses on the low Th/U zircon scatter well outside of error but give an average of 1852 Ma (1771-1971 Ma), whereas the high Th/U spots also scatter well outside of error with an average of 1879 Ma (1821-1914 Ma) (Fig. 1.11.3 and 1.11.4). U-Pb analyses of 80 grains, three subgroups, give an average age of 1861 ±3.3 Ma (2σ, MSWD = 9.2) (Fig. 1.11.3). The distributions overlap. Prolonged metamorphism may have extended the age range of the overgrowths and partially reset detrital ages but it is probable that the detrital zircon was deposited only a few tens of Ma before burial and metamorphism.

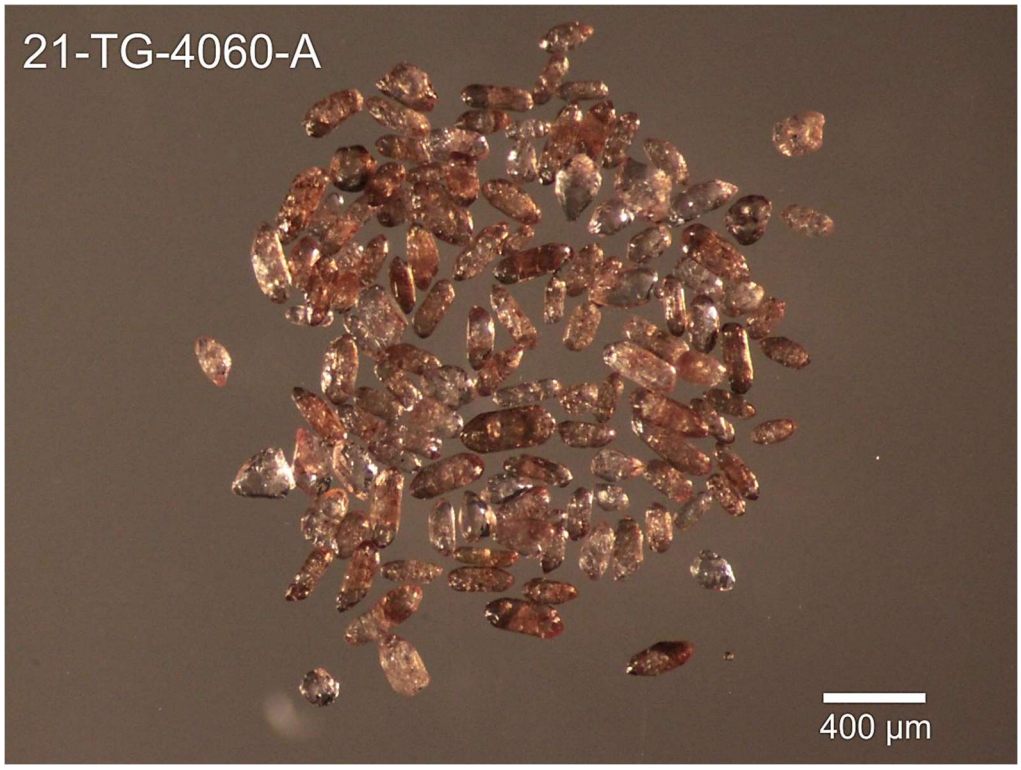

Figure 1.11.1. Picked zircon from paragneiss sample 2021-TG-4060A.

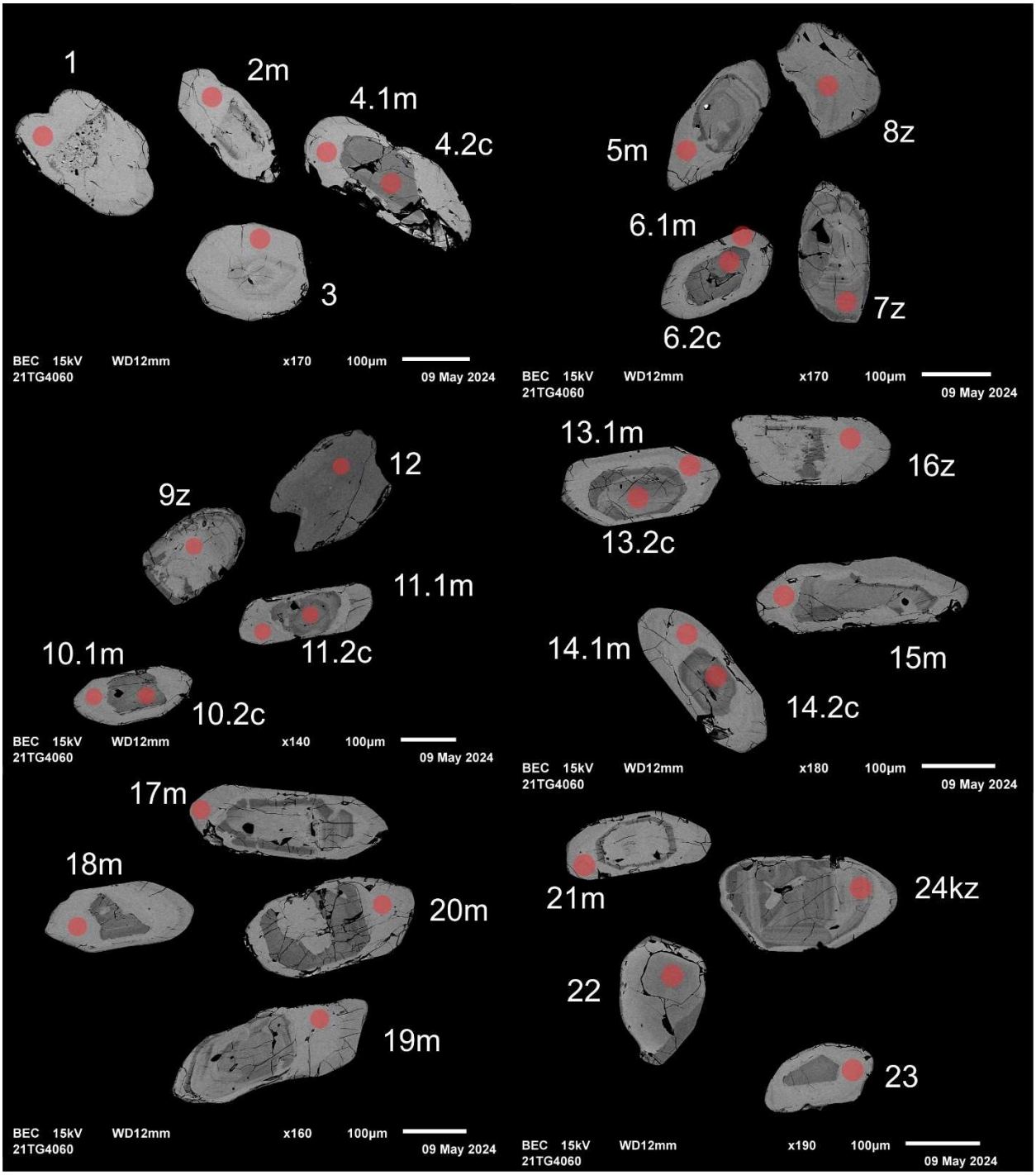

Figure 1.11.2. BSE images of selected grains from sample 2021-TG-4060A. The red circles represent the approximate locations of laser ablation spots.

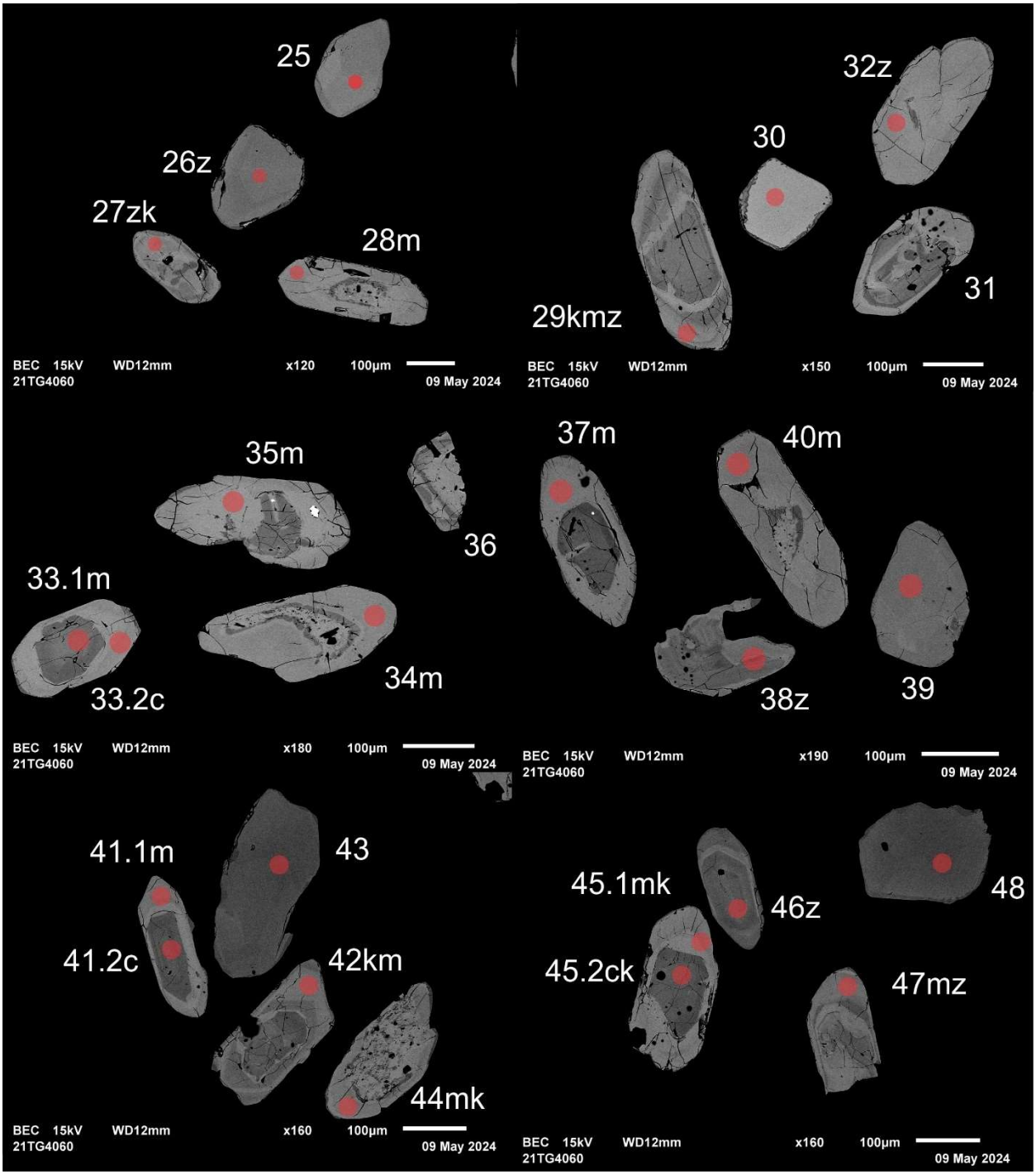

Figure 1.11.2 (cont.). BSE images of selected grains from sample 2021-TG-4060A. The red circles represent the approximate locations of laser ablation spots.

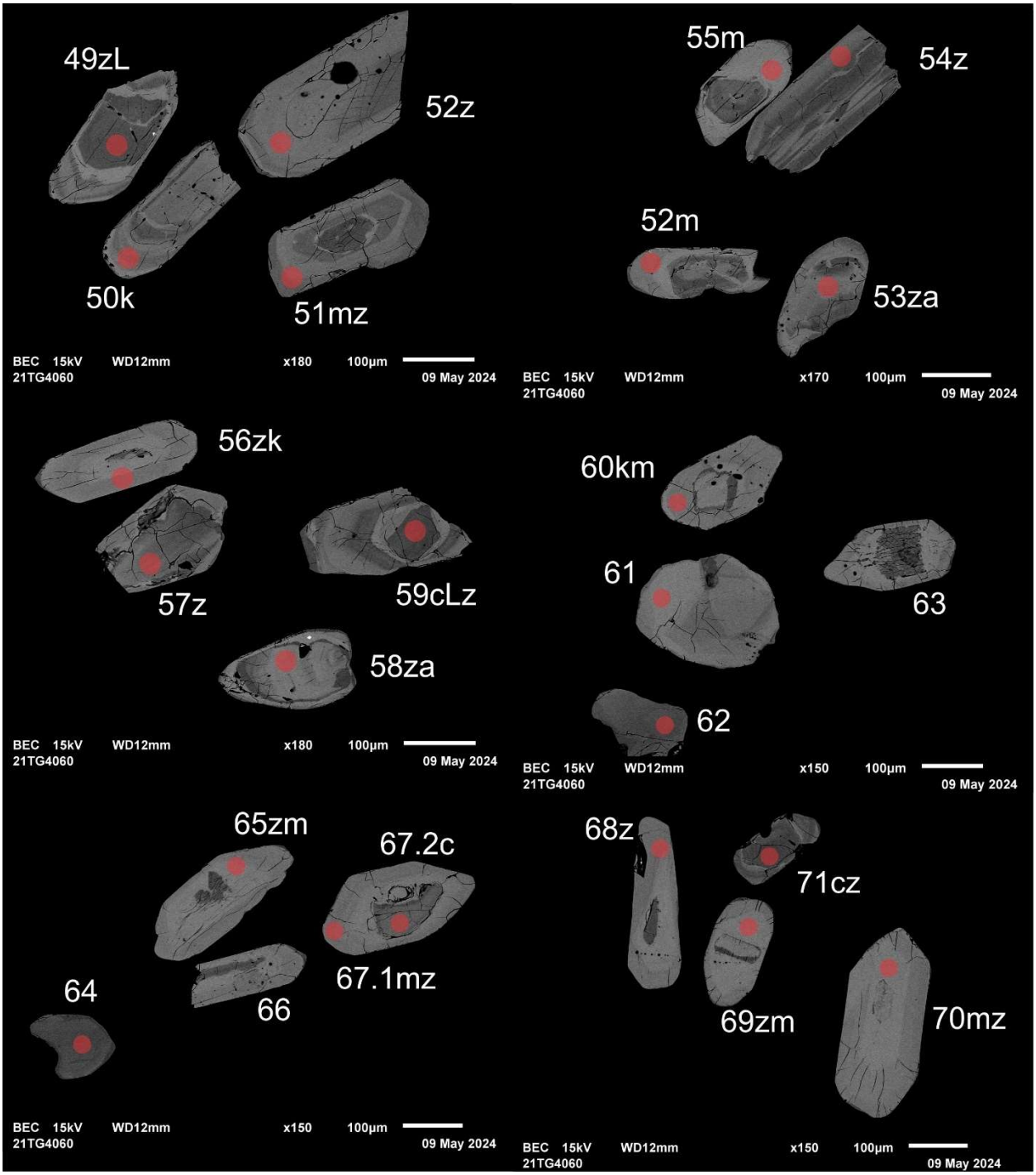

Figure 1.11.2 (cont.). BSE images of selected grains from sample 2021-TG-4060A. The red circles represent the approximate locations of laser ablation spots.

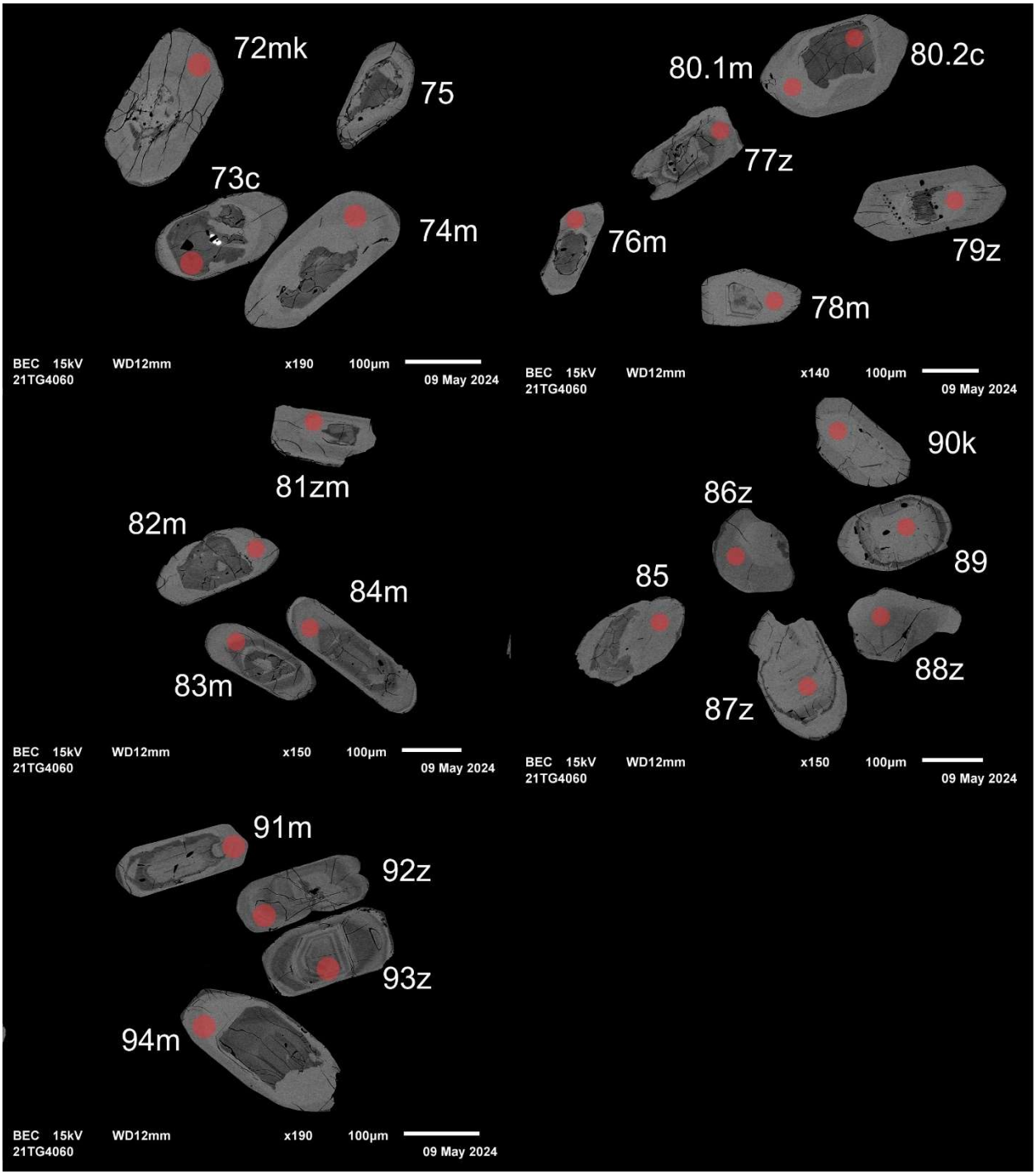

Figure 1.11.2 (cont.). BSE images of selected grains from sample 2021-TG-4060A. The red circles represent the approximate locations of laser ablation spots.

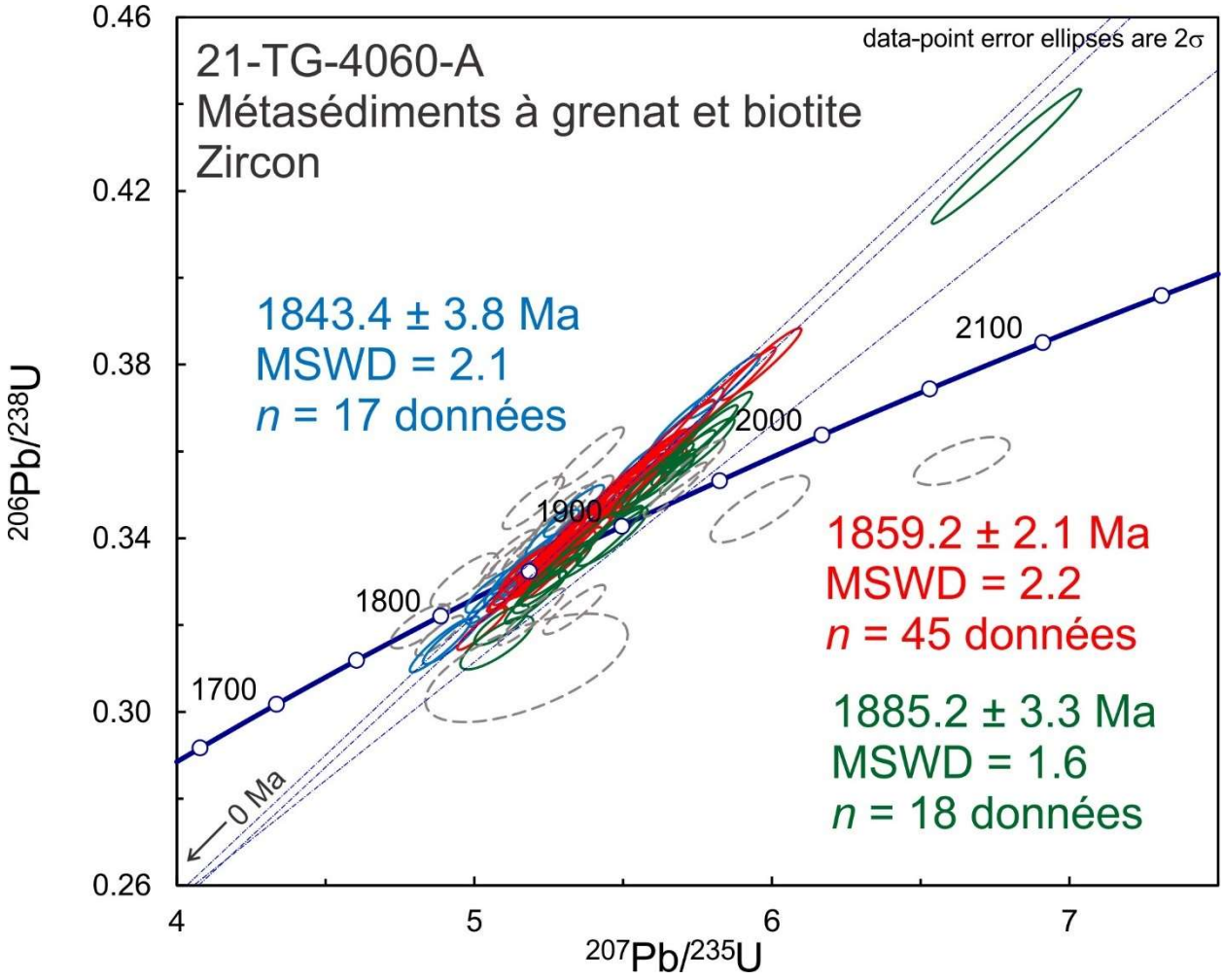

Figure 1.11.3. Concordia plot showing U-Pb isotopic data on polished zircon from paragneiss sample 2021-TG-4060A. Red, blue, and green ellipses correspond to spots considered in the age model whereas gray-dashed ellipses correspond to the omitted spots. Three possible ages are shown.

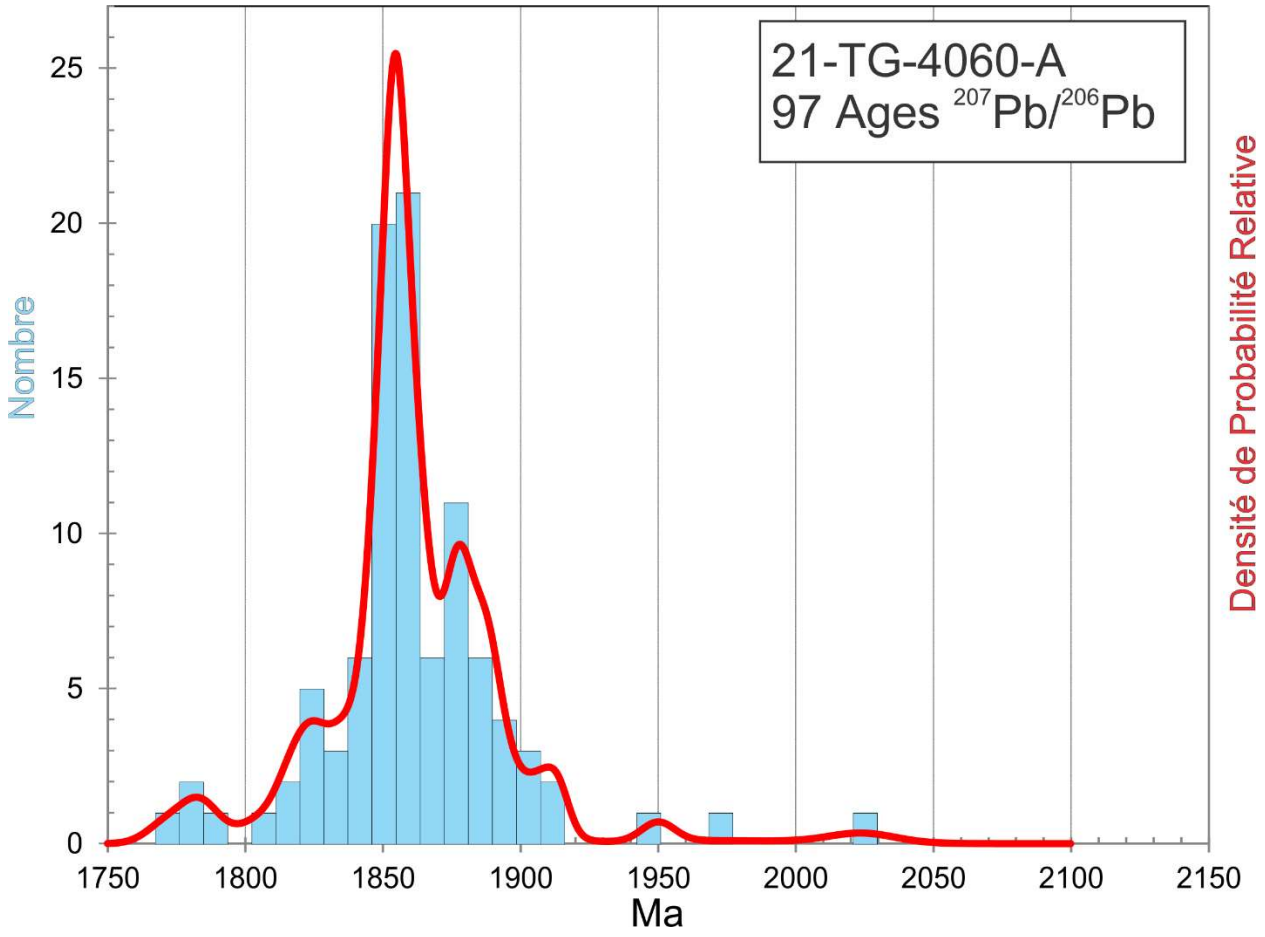

Figure 1.11.4. Combined age relative probability density plot and histogram showing the distribution of $^{207}Pb/^{206}Pb$ ages on polished zircon from paragneiss sample 2021-TG-4060A.

2. Churchill - Est du Domaine Nord

2.1. 2023-GM-1624B
Gneiss tonalitique à biotite et muscovite

This sample yielded abundant zircon consisting generally of stubby multifaceted grains that are cracked and partially altered (Fig. 2.1.1). BSE images show that alteration generally follows cracks and help in avoiding it, at least on the targeted surface (Fig. 2.1.2). U-Pb analyses show diverse ages ranging from 2422 Ma to 3066 Ma (Archean provenance) which Th/U ratios> 0.1 (magmatic). Ages of 42 spots (excluding the youngest and oldest ages because of their high Sr signal) give an average of 2747 ±4 Ma (2σ, MSWD = 2.1), which is the age of the principal component (Fig. 2.1.3). A relative probability density plot of $^{207}Pb/^{206}Pb$ ages reveals a major age peak at around 2740 Ma (Fig. 2.1.4) but there are at least six possible age peaks. Older and younger ages may represent various degrees of inheritance and Pb loss, respectively.

Figure 2.1.1. Picked zircon from gneiss tonalitique à biotite et muscovite sample 2023-GM-1624B.

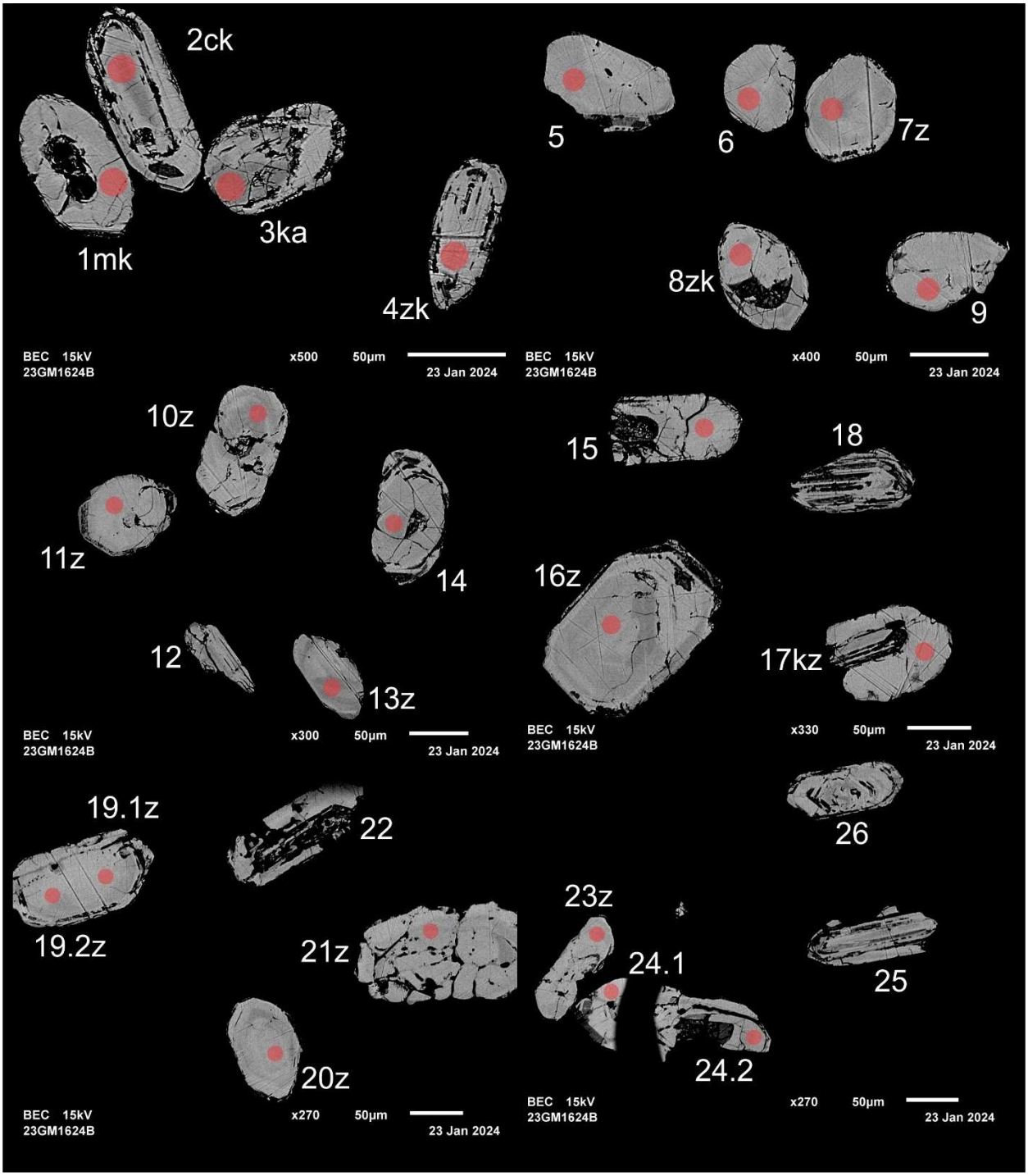

Figure 2.1.2. BSE images of selected grains from sample 2023-GM-1624B. The red circles represent the approximate locations of laser ablation spots.

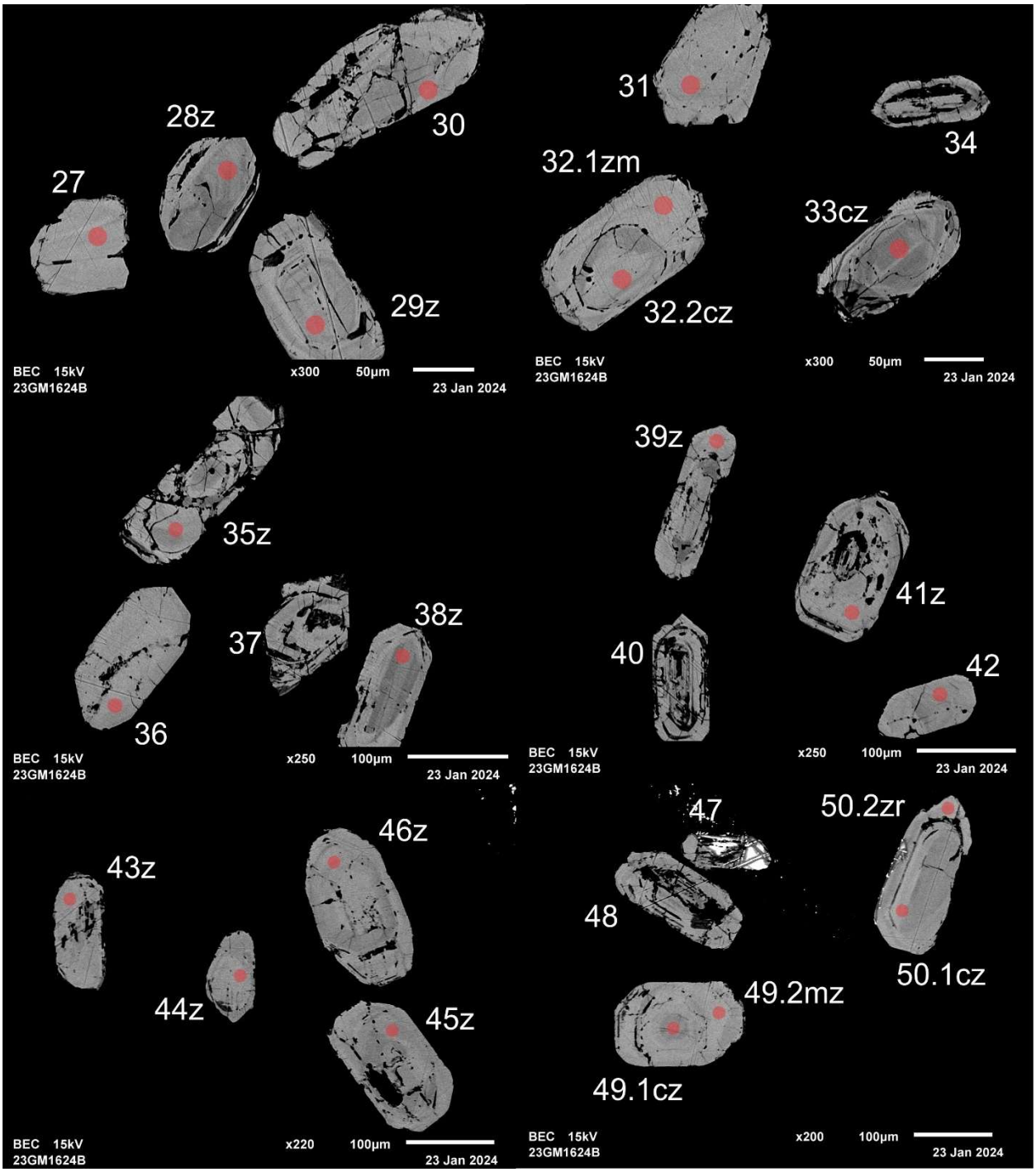

Figure 2.1.2 (cont.). BSE images of selected grains from sample 2023-GM-1624B. The red circles represent the approximate locations of laser ablation spots.

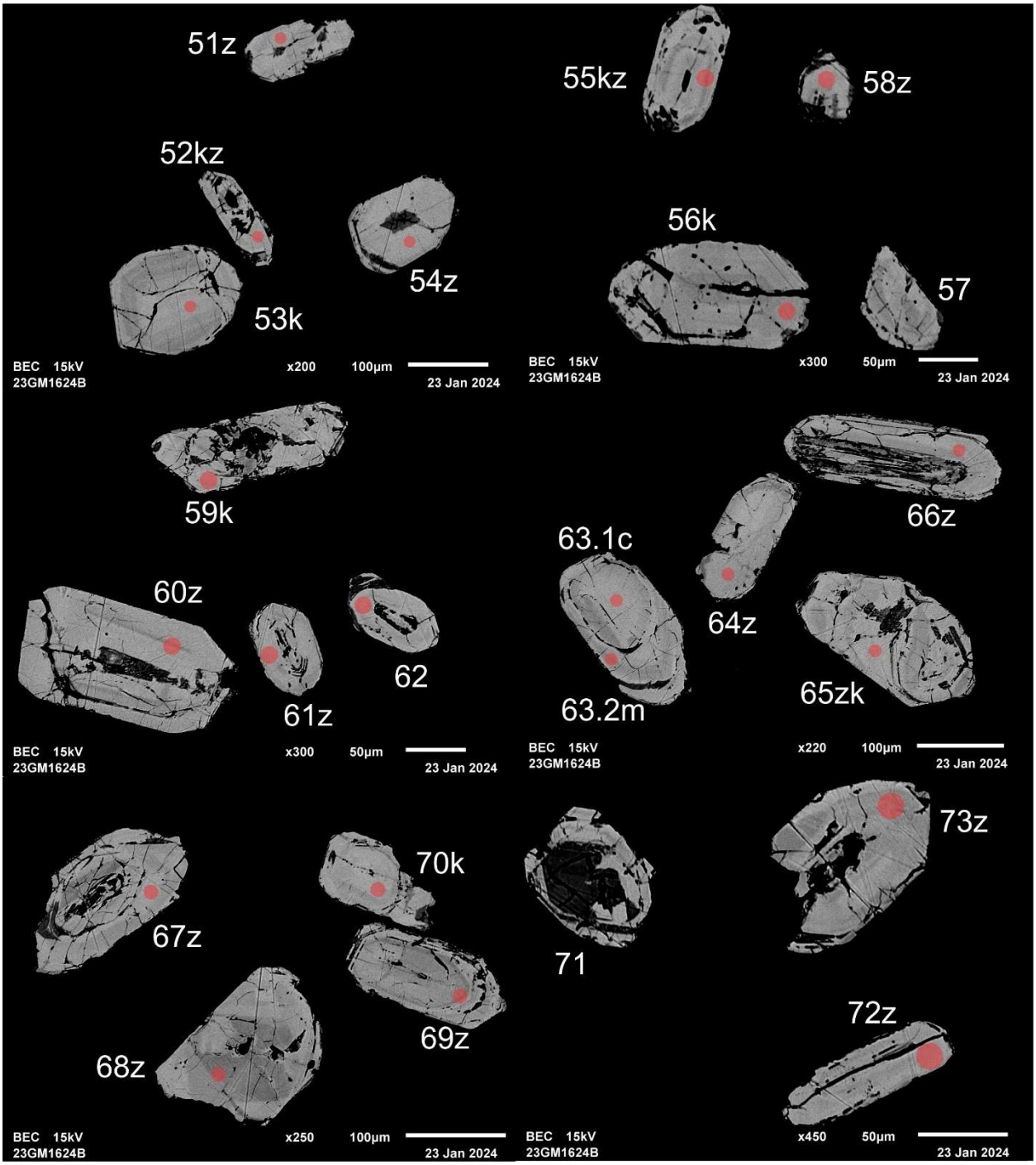

Figure 2.1.2 (cont.). BSE images of selected grains from sample 2023-GM-1624B. The red circles represent the approximate locations of laser ablation spots.

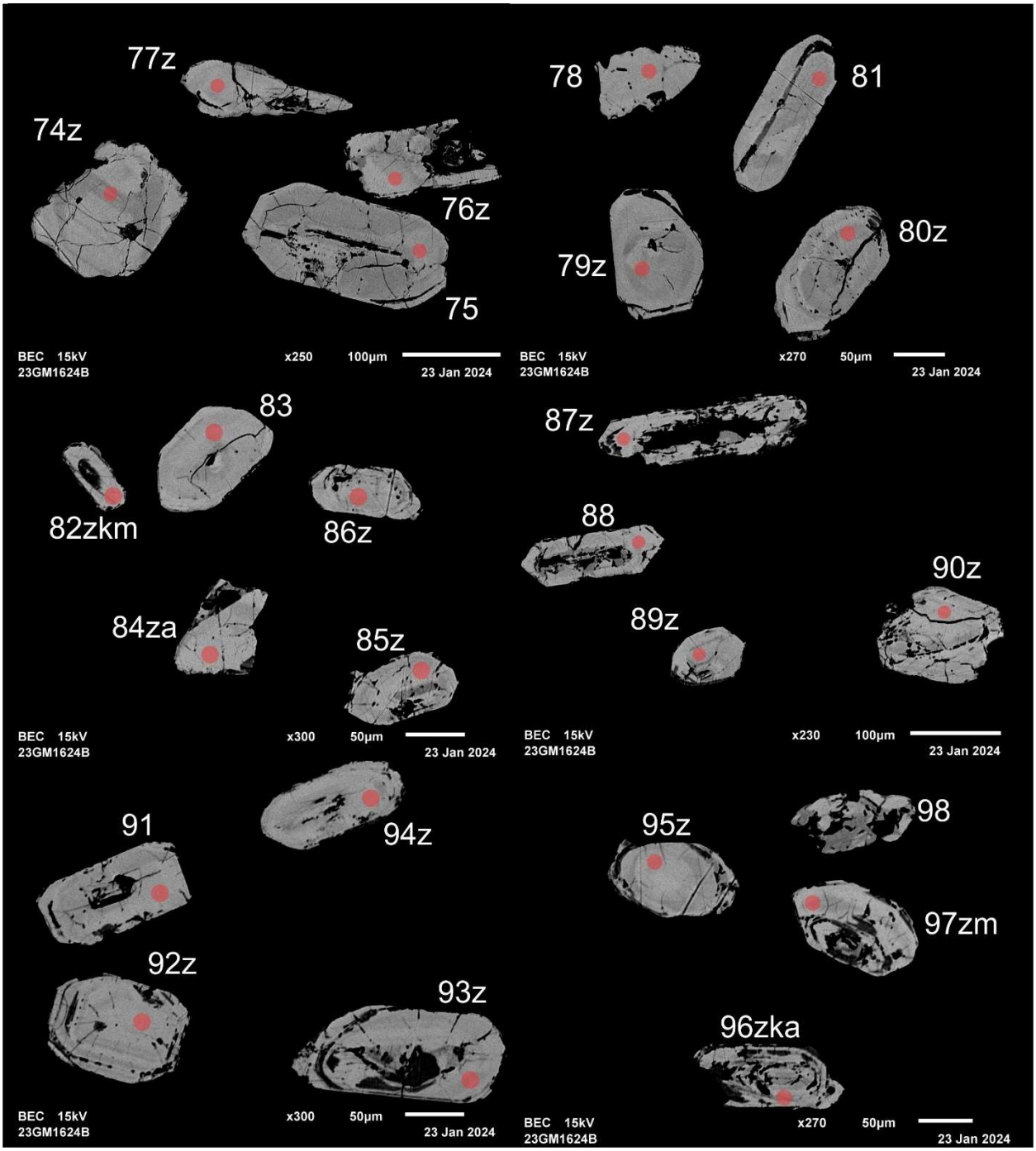

Figure 2.1.2 (cont.). BSE images of selected grains from sample 2023-GM-1624B. The red circles represent the approximate locations of laser ablation spots.

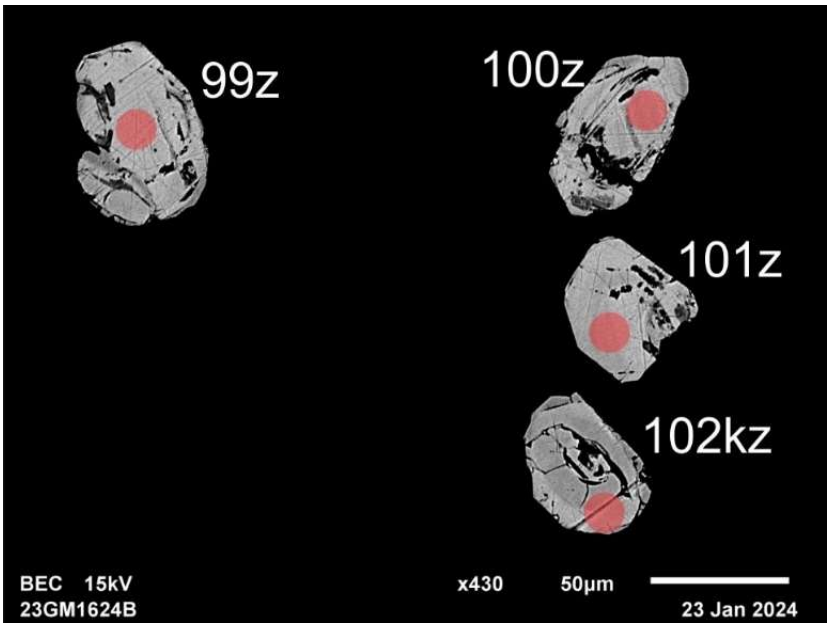

Figure 2.1.2 (cont.). BSE images of selected grains from sample 2023-GM-1624B. The red circles represent the approximate locations of laser ablation spots.

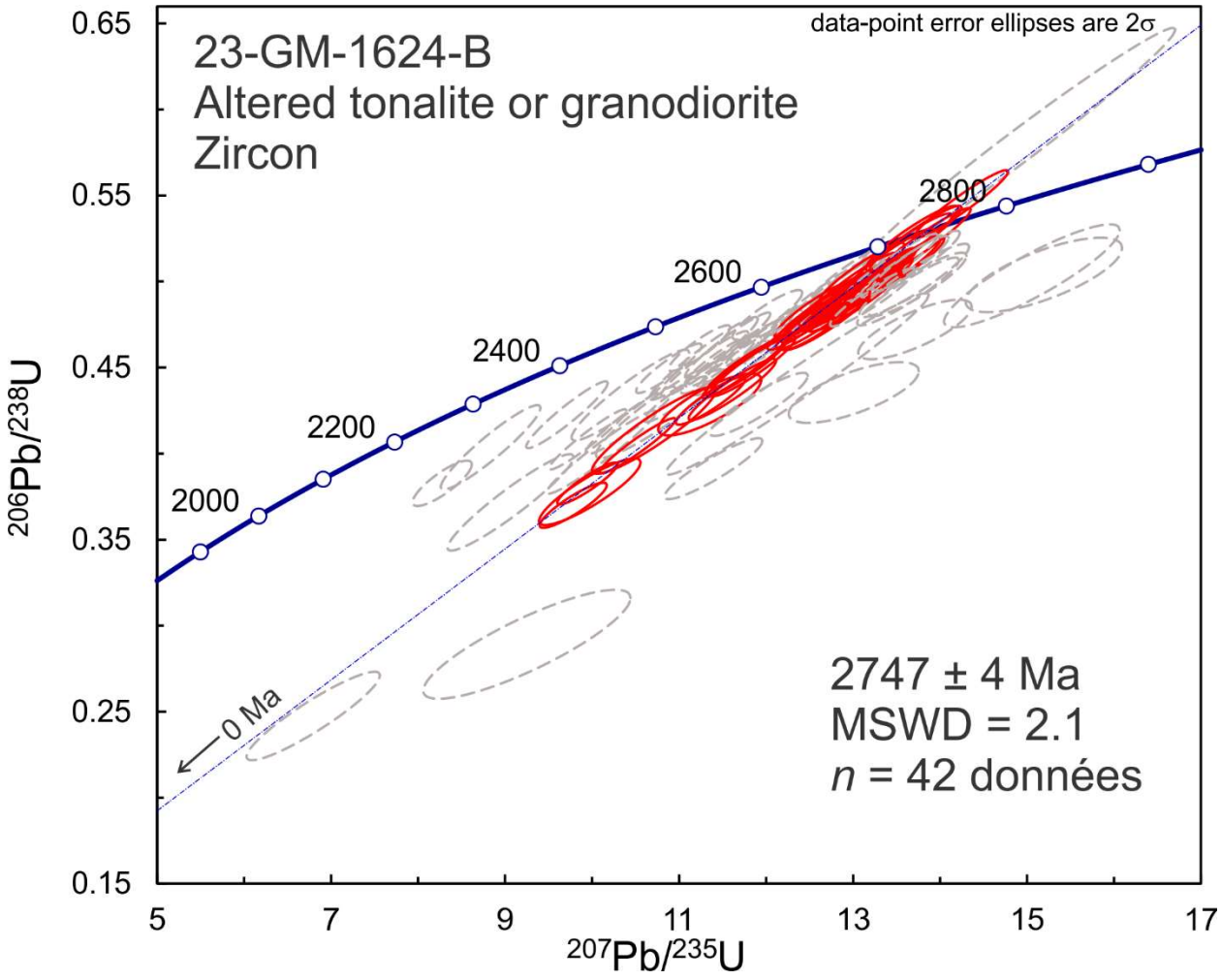

Figure 2.1.3. Concordia plot showing U-Pb isotopic data on polished zircon from gneiss tonalitique à biotite et muscovite sample 2023-GM-1624B. Red ellipses correspond to spots considered in the age model whereas gray-dashed ellipses correspond to the omitted spots.

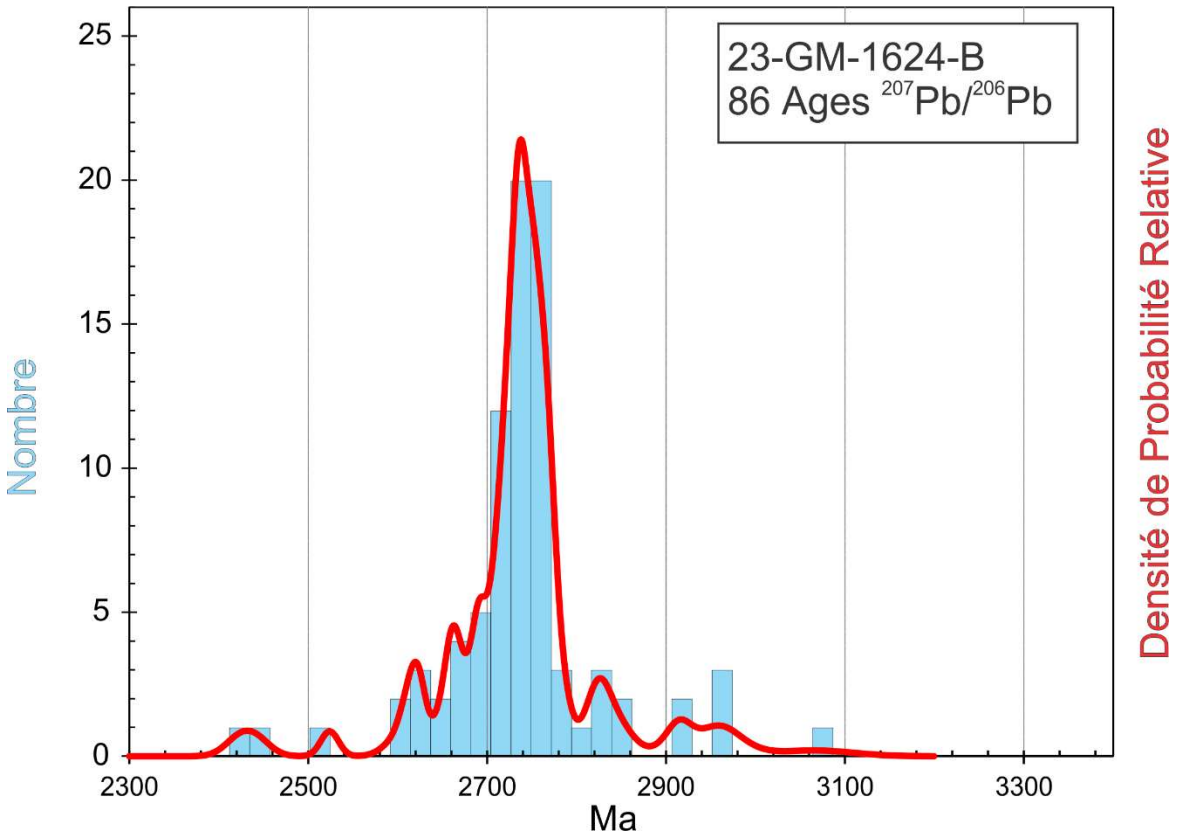

Figure 2.1.4. Combined age relative probability density plot and histogram showing the distribution of $^{207}Pb/^{206}Pb$ ages on polished zircon from gneiss tonalitique à biotite et muscovite sample 2023-GM-1624B.

2.2. 2023-MV-1170D
Gneiss tonalitique à biotite et muscovite

This sample yielded generally altered zircon with stubby to short-prismatic shapes (Fig. 2.2.1). BSE images show that alteration follows high-U zones and most strongly affects the cores of crystals (Fig. 2.2.2). U-Pb analyses show ages ranging from 1781 Ma to 3025 Ma with most of the analyses between about 2.2 Ga and 2.7 Ga (Fig. 2.2.3 and 2.2.4). All analyses give Th/U ratios within or near the range for metamorphic zircon. U concentrations are relatively high (generally >2000 ppm), which is also characteristic of metamorphic zircon. The grains are therefore metamict, which accounts for the high degree of alteration. Selective analyses on relatively unaltered domains limits Pb loss although it is still generally significant (>10%). Most of the age data are probably affected by Pb loss and therefore not reliable except to confirm an Archean age for the protolith.

Figure 2.2.1. Picked zircon from gneiss tonalitique à biotite et muscovite sample 2023-MV-1170D.

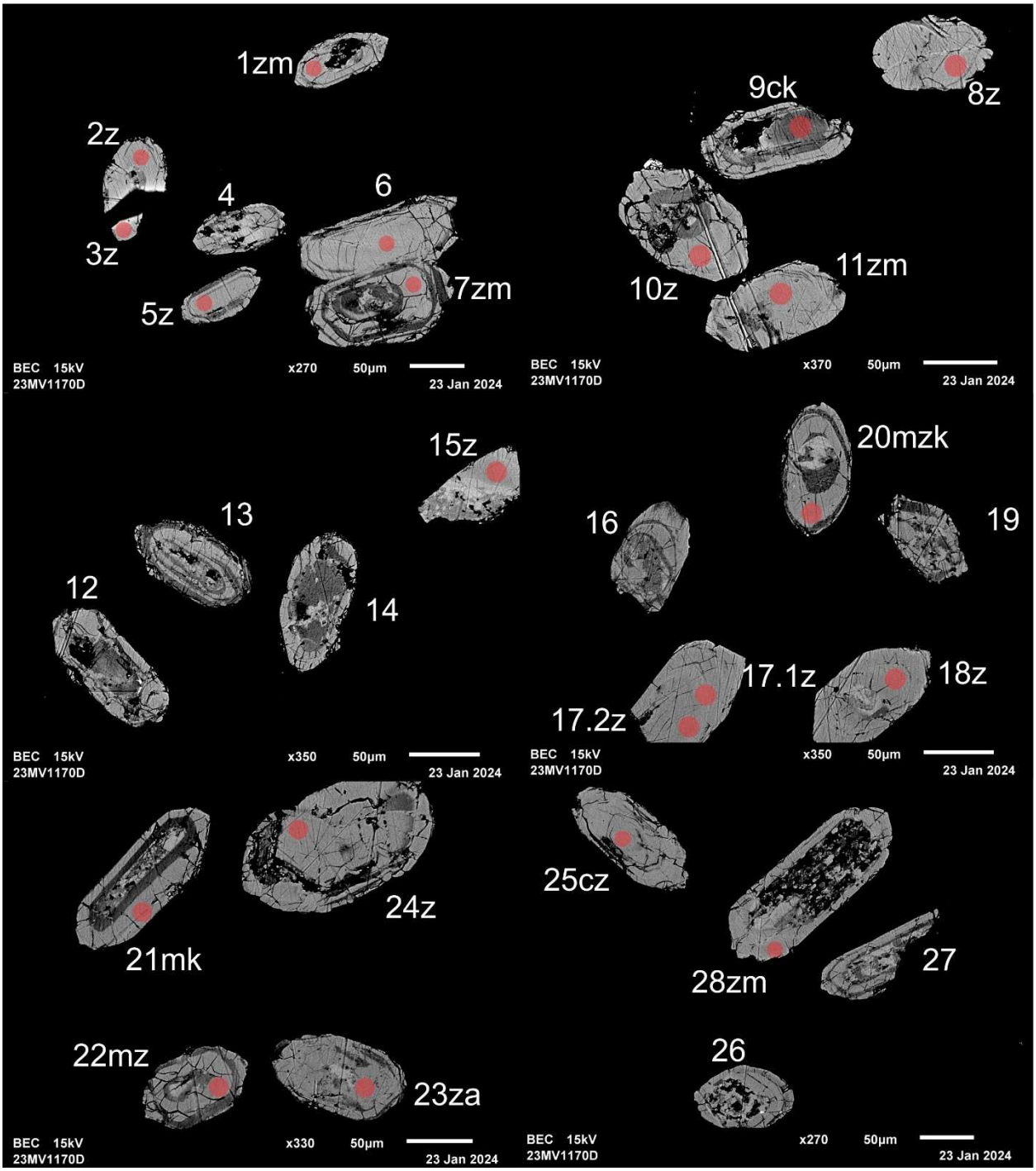

Figure 2.2.2. BSE images of selected grains from sample 2023-MV-1170D. The red circles represent the approximate locations of laser ablation spots.

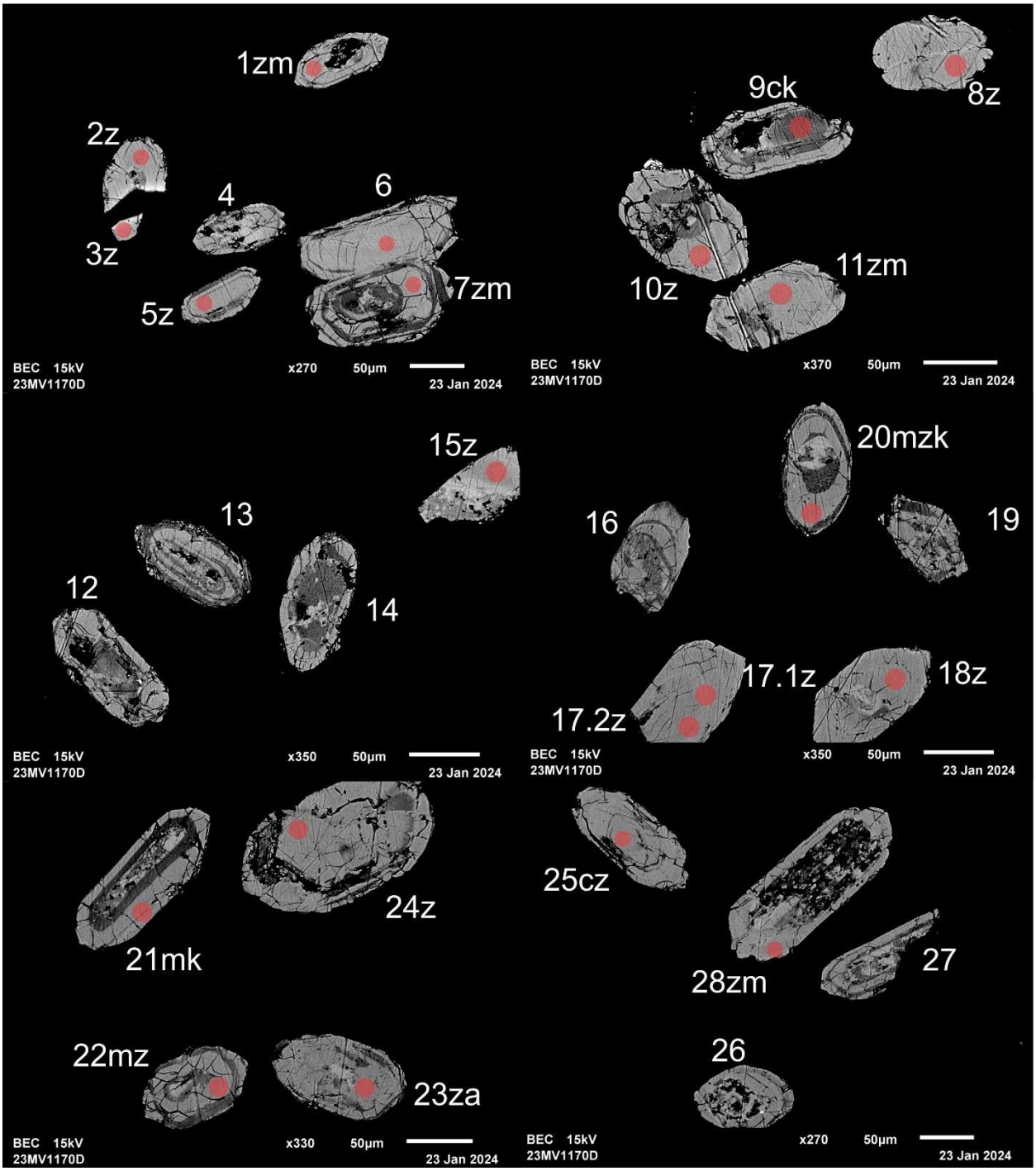

Figure 2.2.2 (cont.). BSE images of selected grains from sample 2023-MV-1170D. The red circles represent the approximate locations of laser ablation spots.

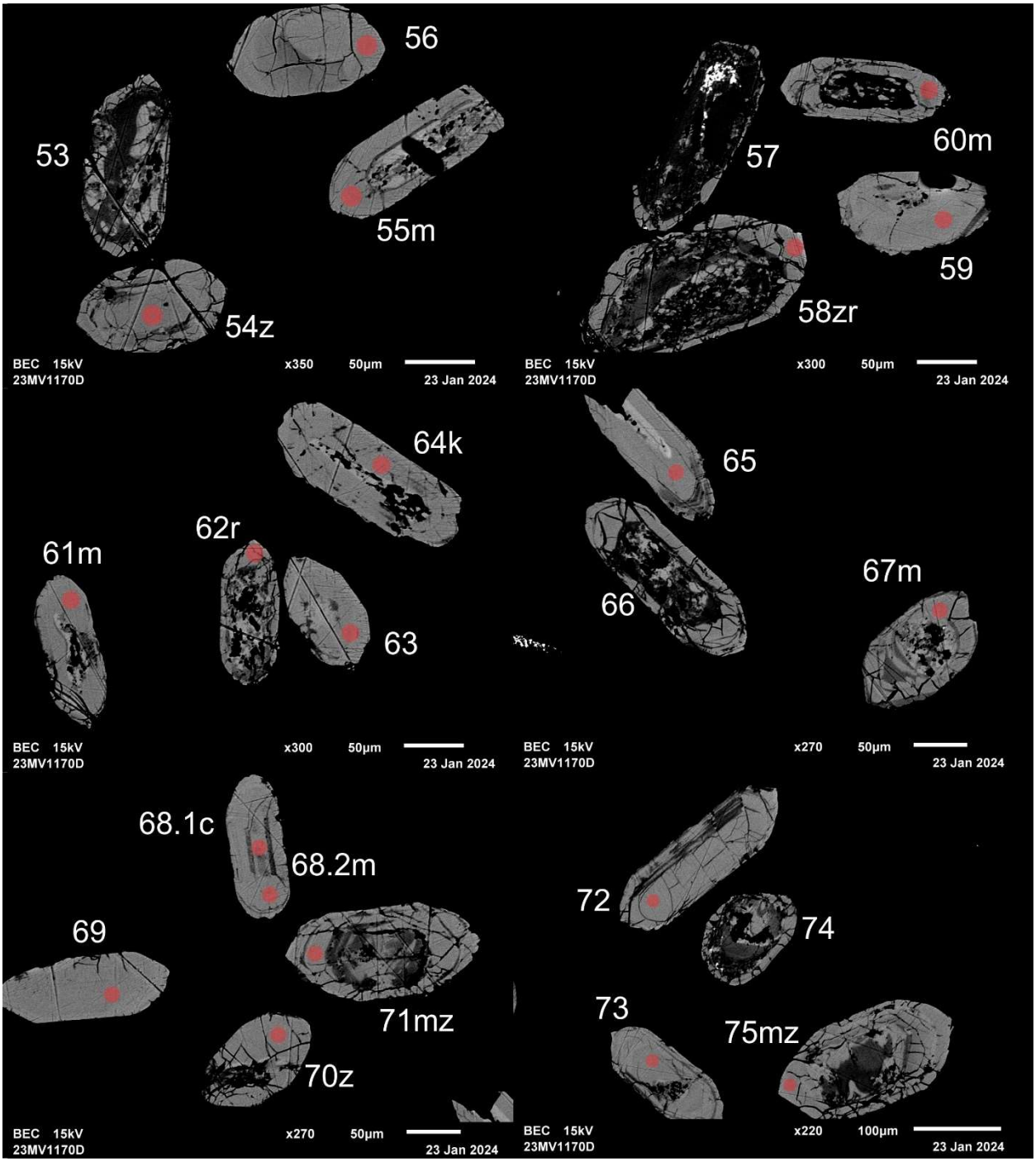

Figure 2.2.2 (cont.). BSE images of selected grains from sample 2023-MV-1170D. The red circles represent the approximate locations of laser ablation spots.

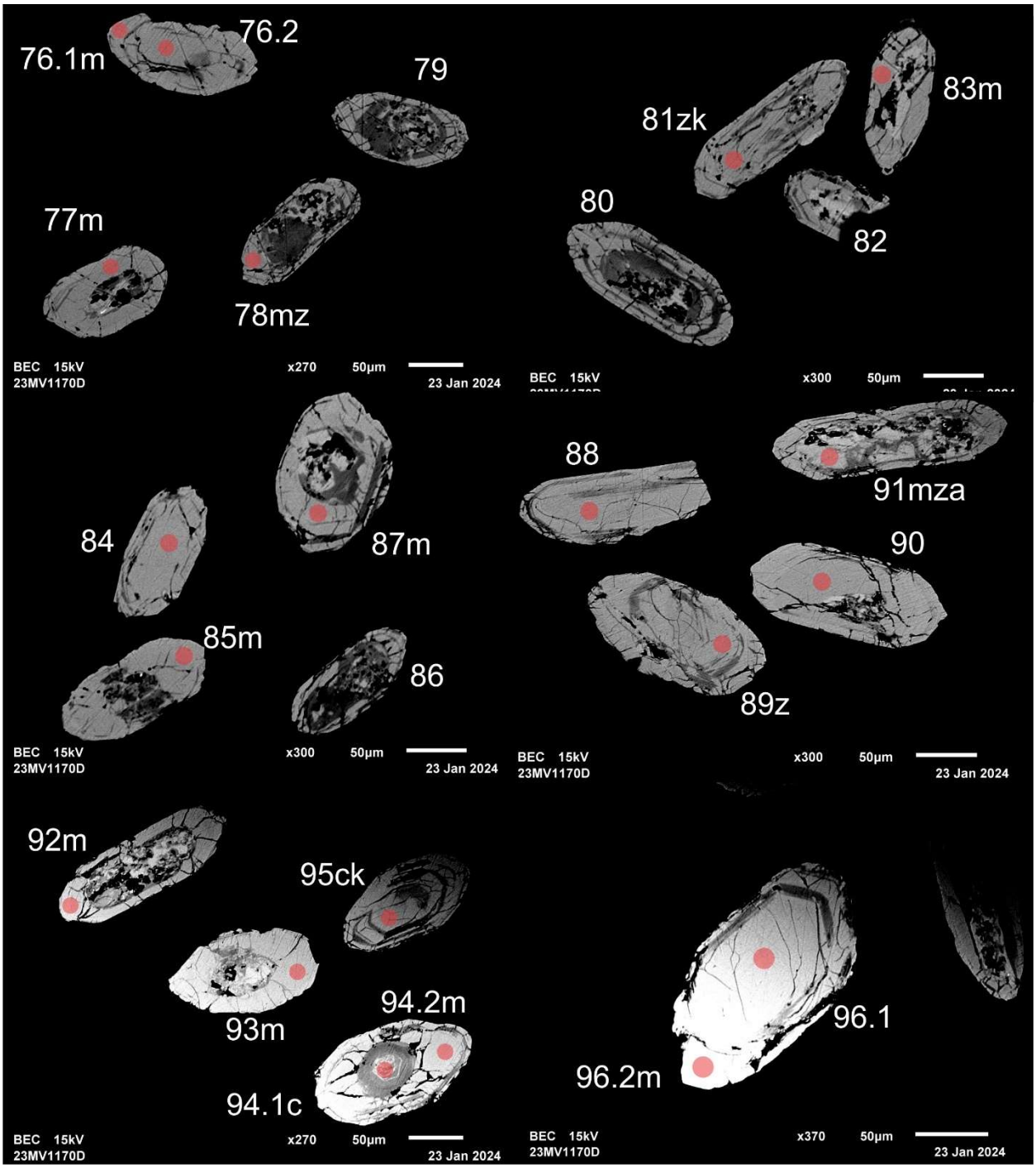

Figure 2.2.2 (cont.). BSE images of selected grains from sample 2023-MV-1170D. The red circles represent the approximate locations of laser ablation spots.

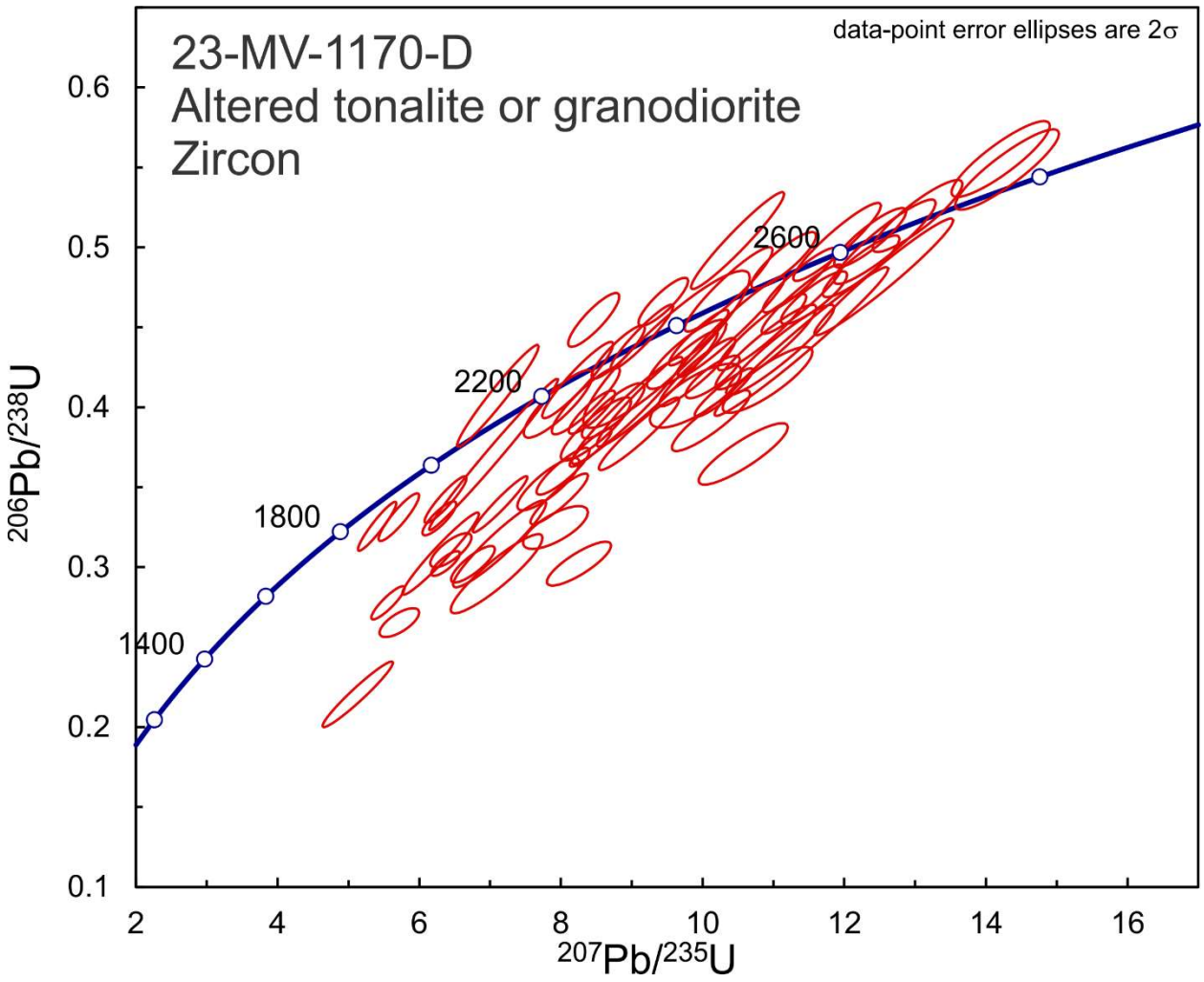

Figure 2.2.3. Concordia plot showing U-Pb isotopic data on polished zircon from gneiss tonalitique à biotite et muscovite sample 2023-MV-1170D.

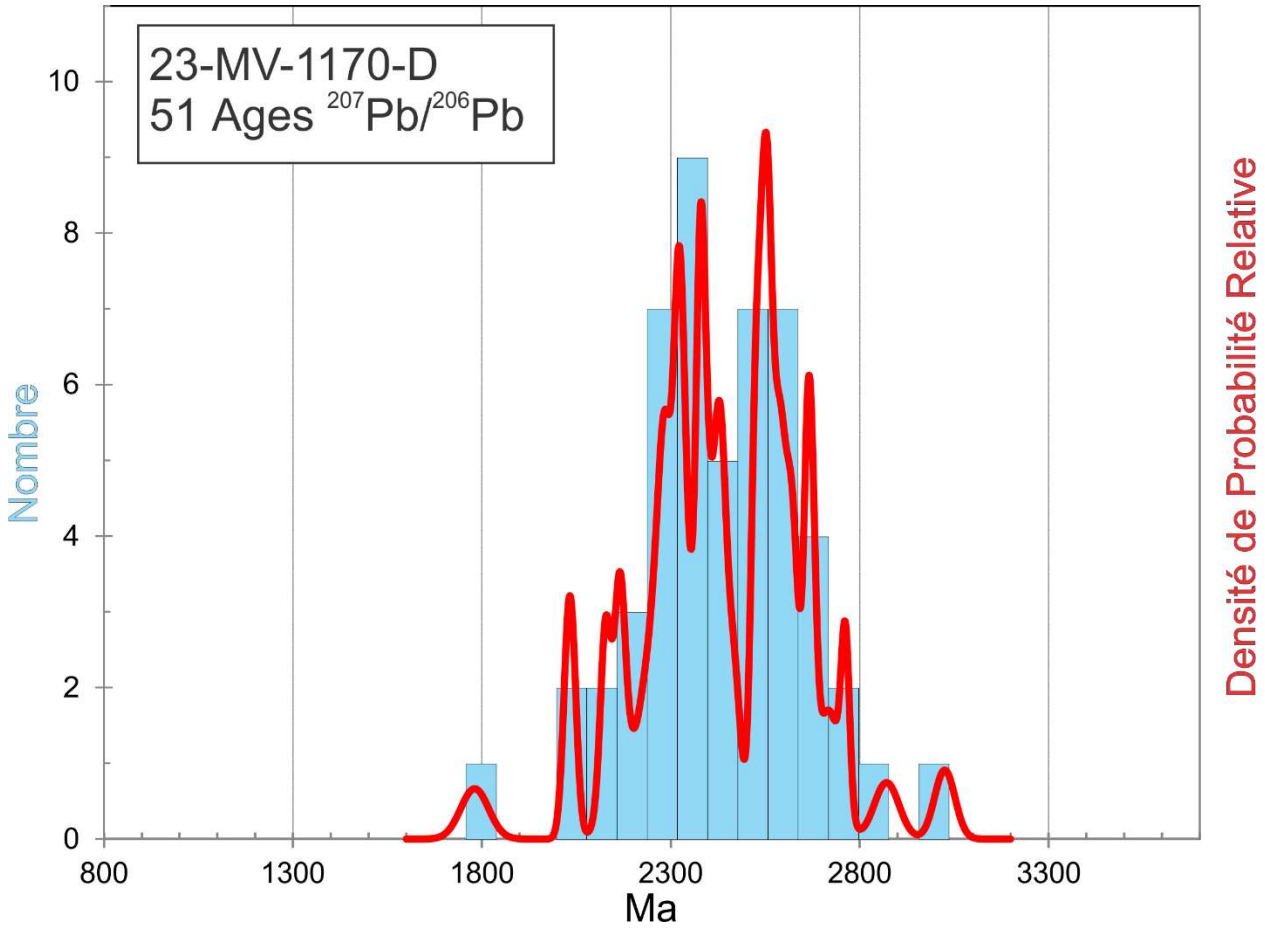

Figure 2.2.4. Combined age relative probability density plot and histogram showing the distribution of $^{207}Pb/^{206}Pb$ ages on polished zircon from gneiss tonalitique à biotite et muscovite sample 2023-MV-1170D.

2.3 2023-TD-2588A
Diorite quartzifère à grenat

This sample yielded a small amount of zircon with a uniform-looking population of fragment grains (Fig. 2.3.1). BSE images show broad sector zoning with no evidence for older cores (Fig 2.3.2). U-Pb analyses give overlapping ages between 1822 Ma and 1840 Ma (Fig. 2.3.3 and 2.3.4). U-Pb analyses on 54 spots scatter within error with an average age of 1840 ±2 Ma (2σ, MSWD = 1.1, Fig. 2.3.3).

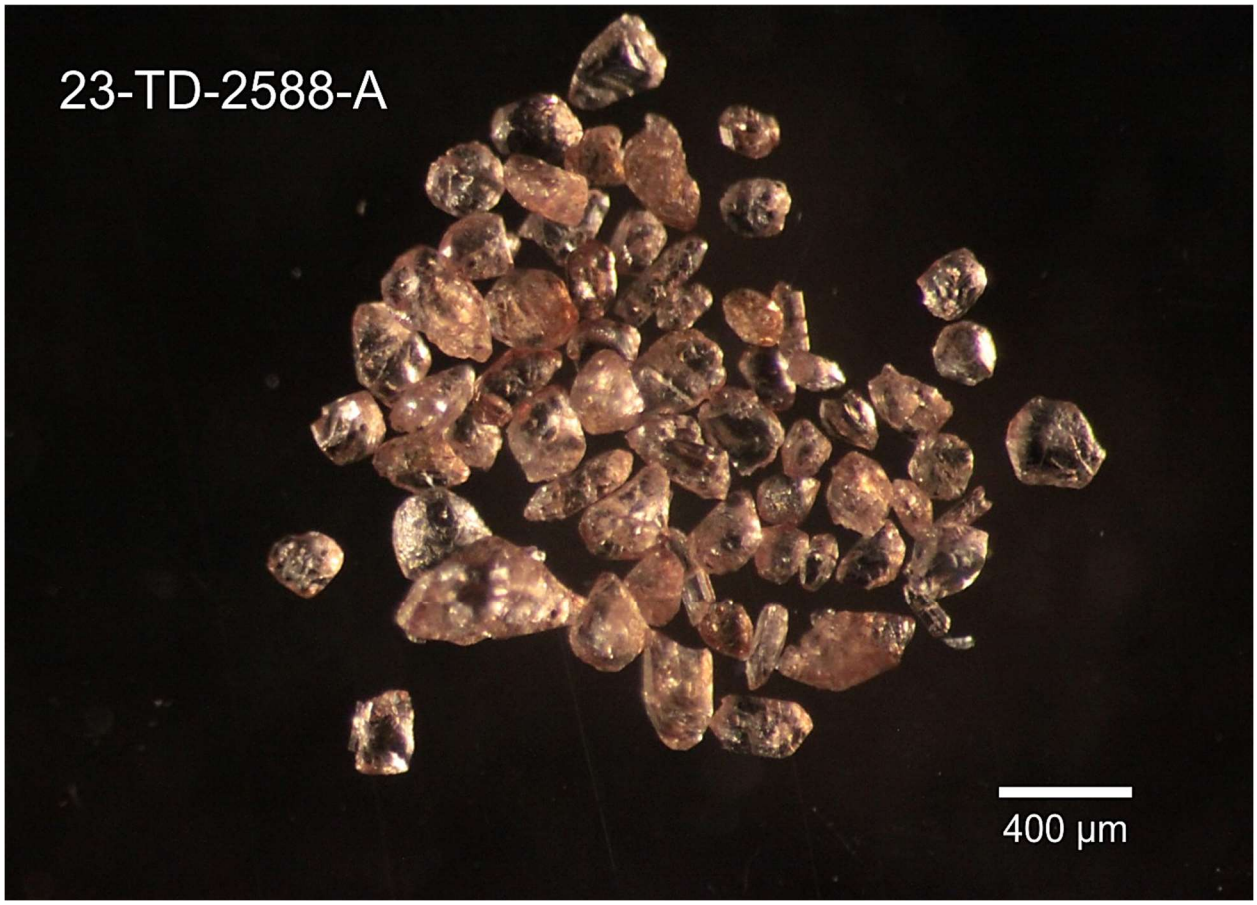

Figure 2.3.1. Picked zircon from diorite sample 2023-TD-2588A.

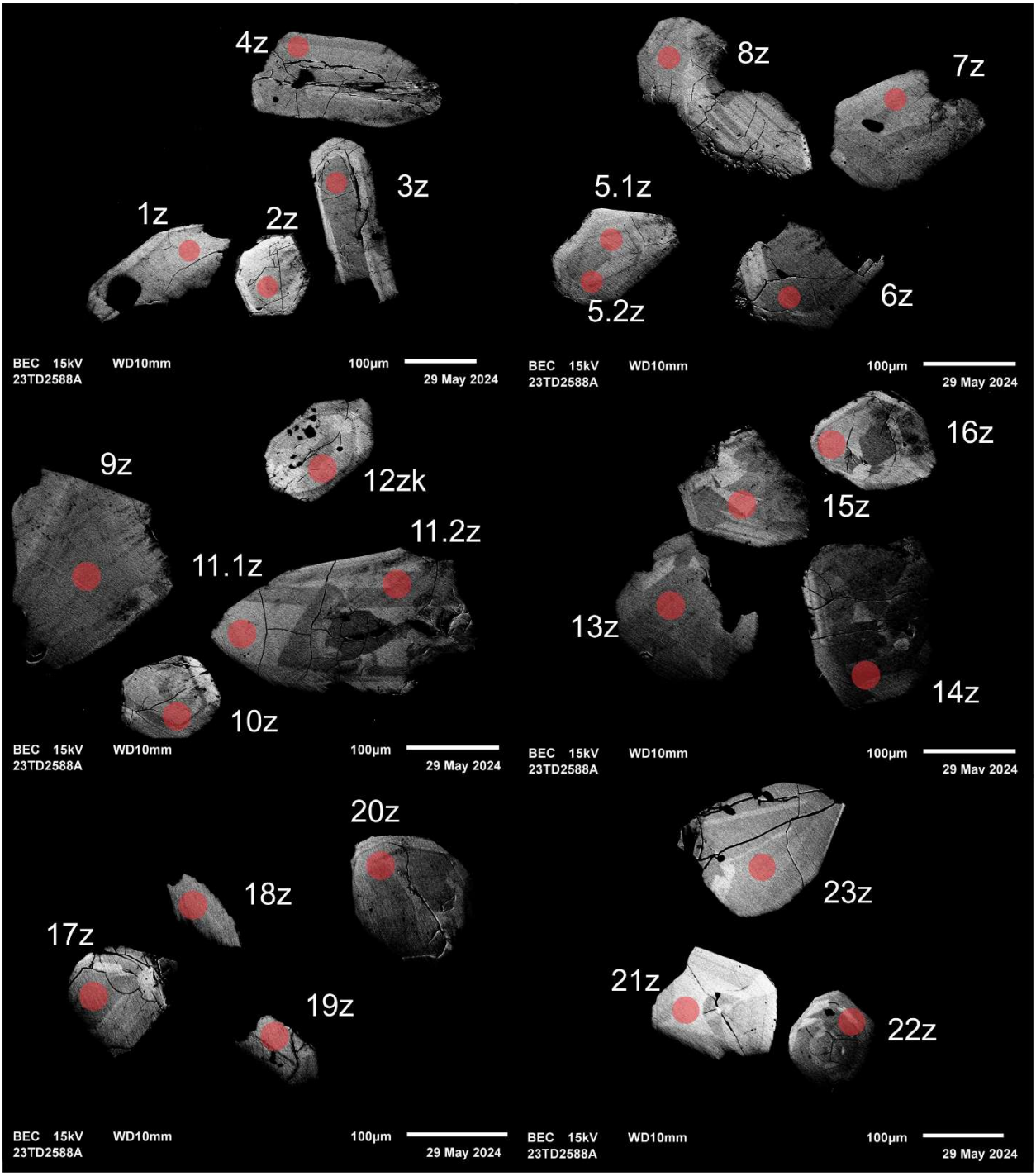

Figure 2.3.2. BSE images of selected grains from sample 2023-TD-2588A. The red circles represent the approximate locations of laser ablation spots.

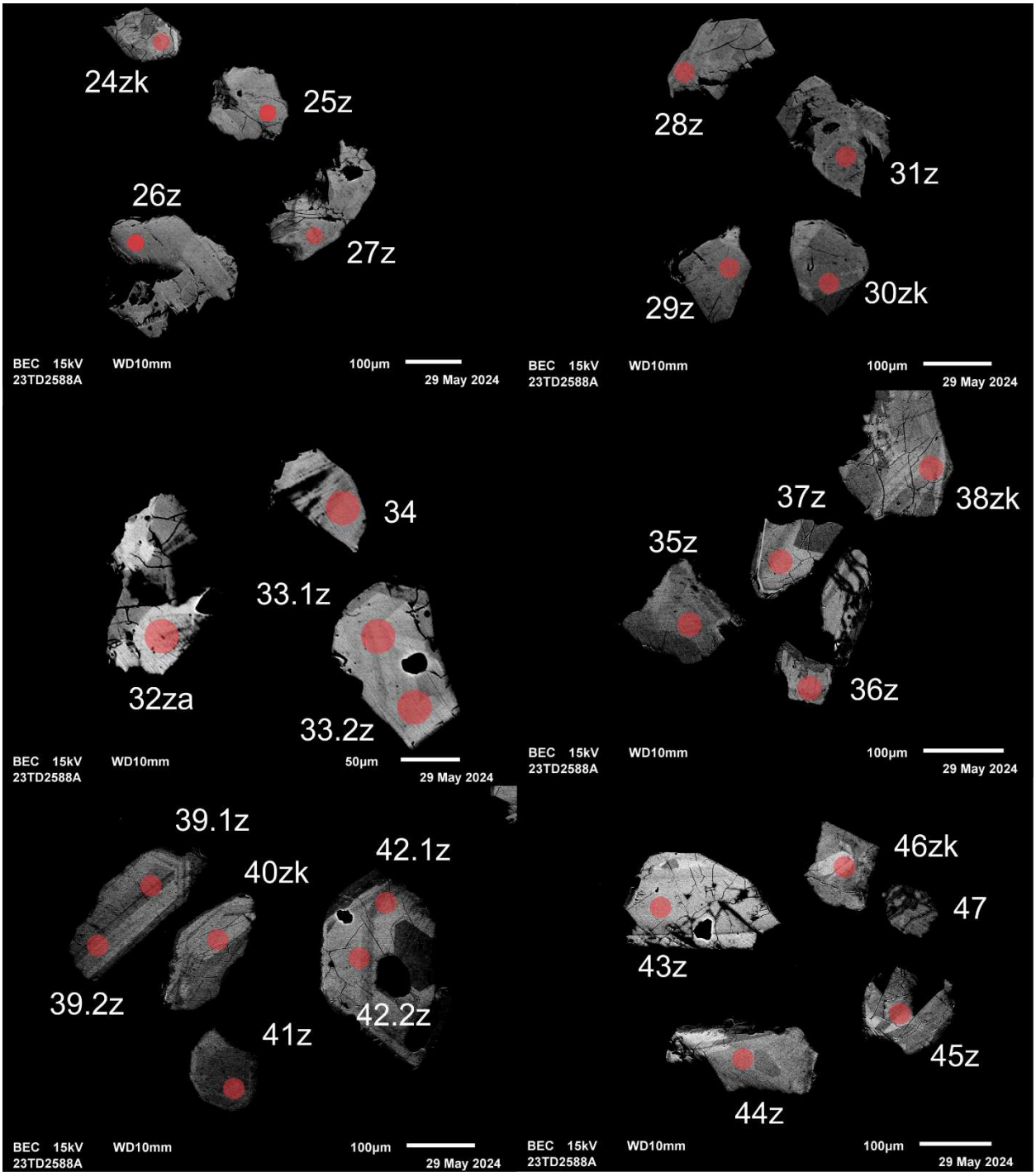

Figure 2.3.2 (cont.). BSE images of selected grains from sample 2023-TD-2588A. The red circles represent the approximate locations of laser ablation spots.

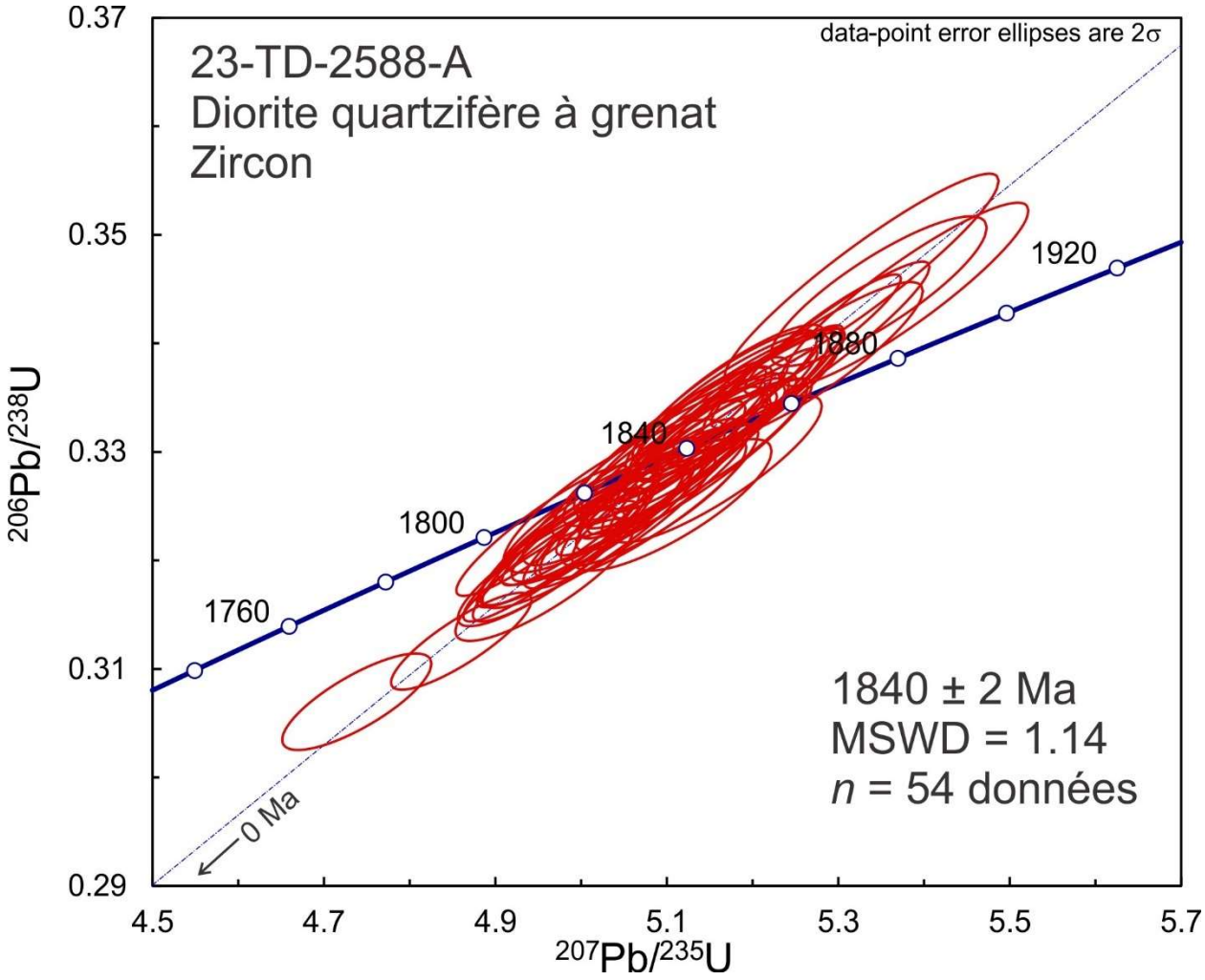

Figure 2.3.3. Concordia plot showing U-Pb isotopic data on polished zircon from diorite sample 2023-TD-2588A.

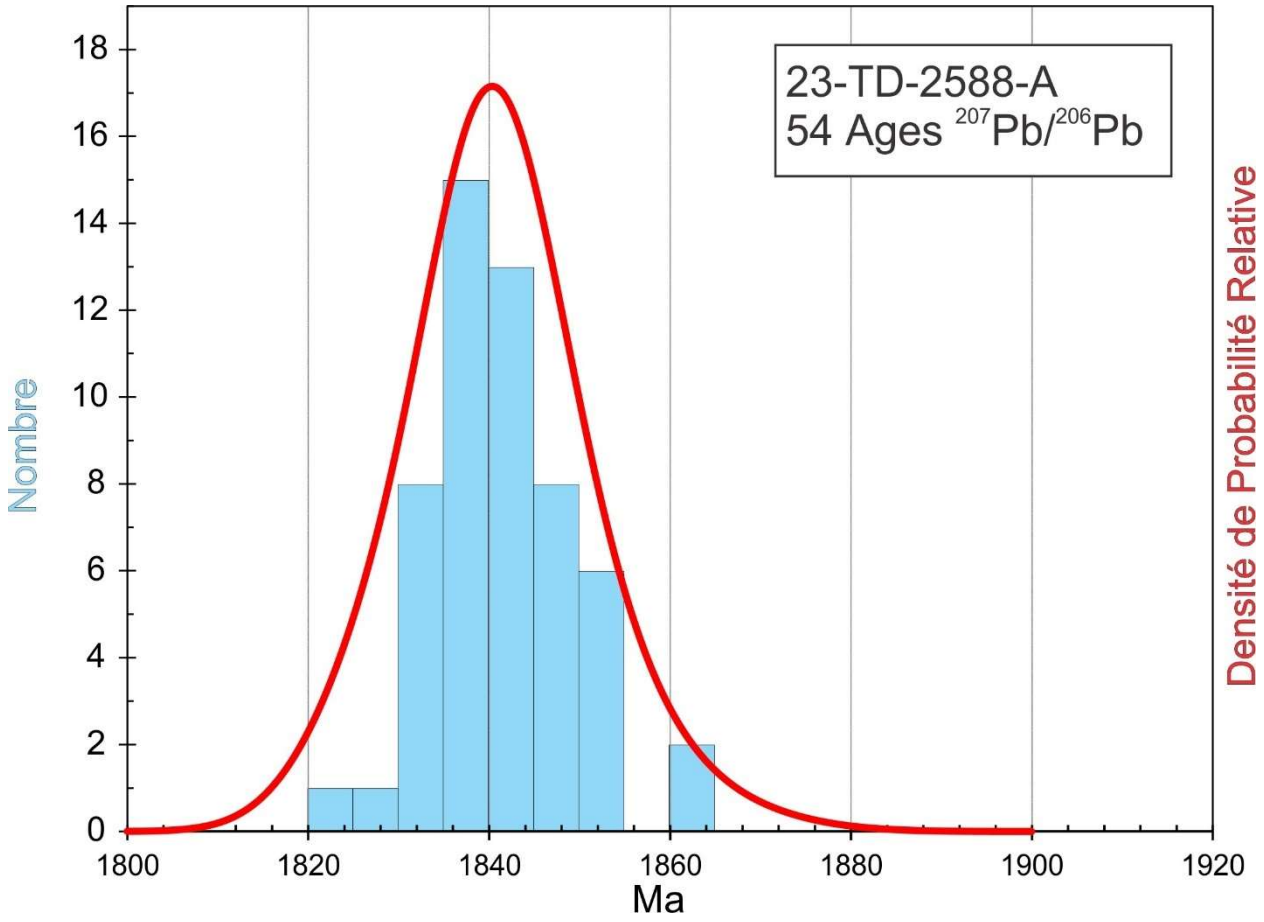

Figure 2.3.4. Combined age relative probability density plot and histogram showing the distribution of $^{207}Pb/^{206}Pb$ ages on polished zircon from diorite sample 2023-TD-2588A.

2.4. 2023-TD-2546C
Conglomérat à granules

This sample yielded a small amount of zircon as euhedral, short to long prismatic grains (Fig. 2.4.1). Due to their small size, the grains were mounted on double-sided tape and analyzed on natural surfaces. U-Pb analyses show roughly overlapping ages for most of the spots (Fig. 2.4.2 and 2.4.3). U-Pb data give $^{207}Pb/^{206}Pb$ ages with an average of 1876 ±11 Ma but with a high MSWD of 3.2 (Fig. 2.4.2). One distinctly older spot gives about 2180 ±140 Ma. After excluding the outlier, the U-Pb data results in an average age of 1875 ±9 Ma (2σ, MSWD = 2.5). Most of the analytical profiles show a thin surface layer with Th/U <0.1 suggesting a metamorphic overgrowth. This layer usually shows relatively low U concentration, but in some cases it is high. The interiors of grains give Th/U ratios that usually straddle the Th/U boundary or are slightly above it, suggesting that these represent magmatic detrital cores. It is not possible to distinguish cores and overgrowth ages suggesting that the provenance of the detrital component was only slightly older than deposition, burial and metamorphism.

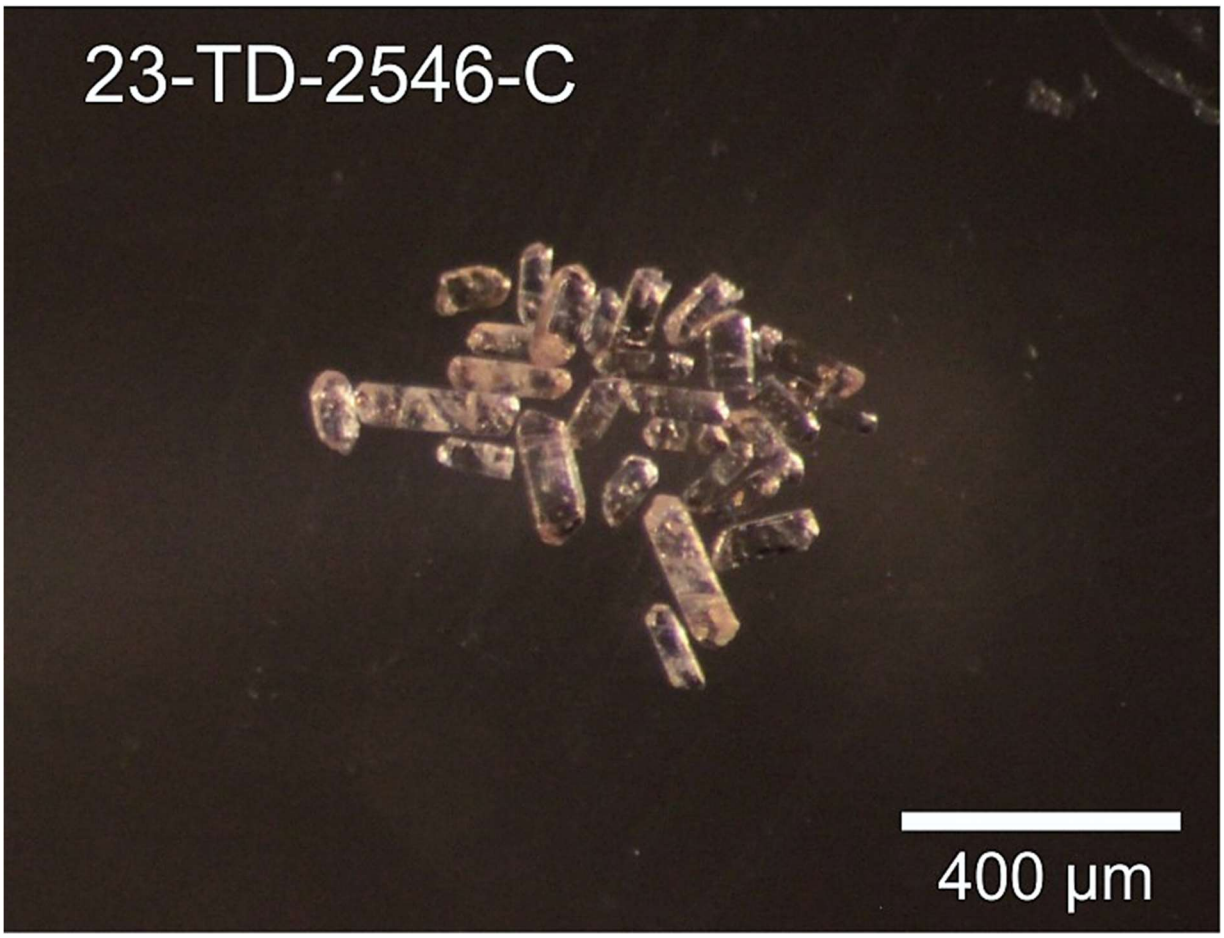

Figure 2.4.1. Picked zircon from conglomérat à granules sample 2023-TD-2546C.

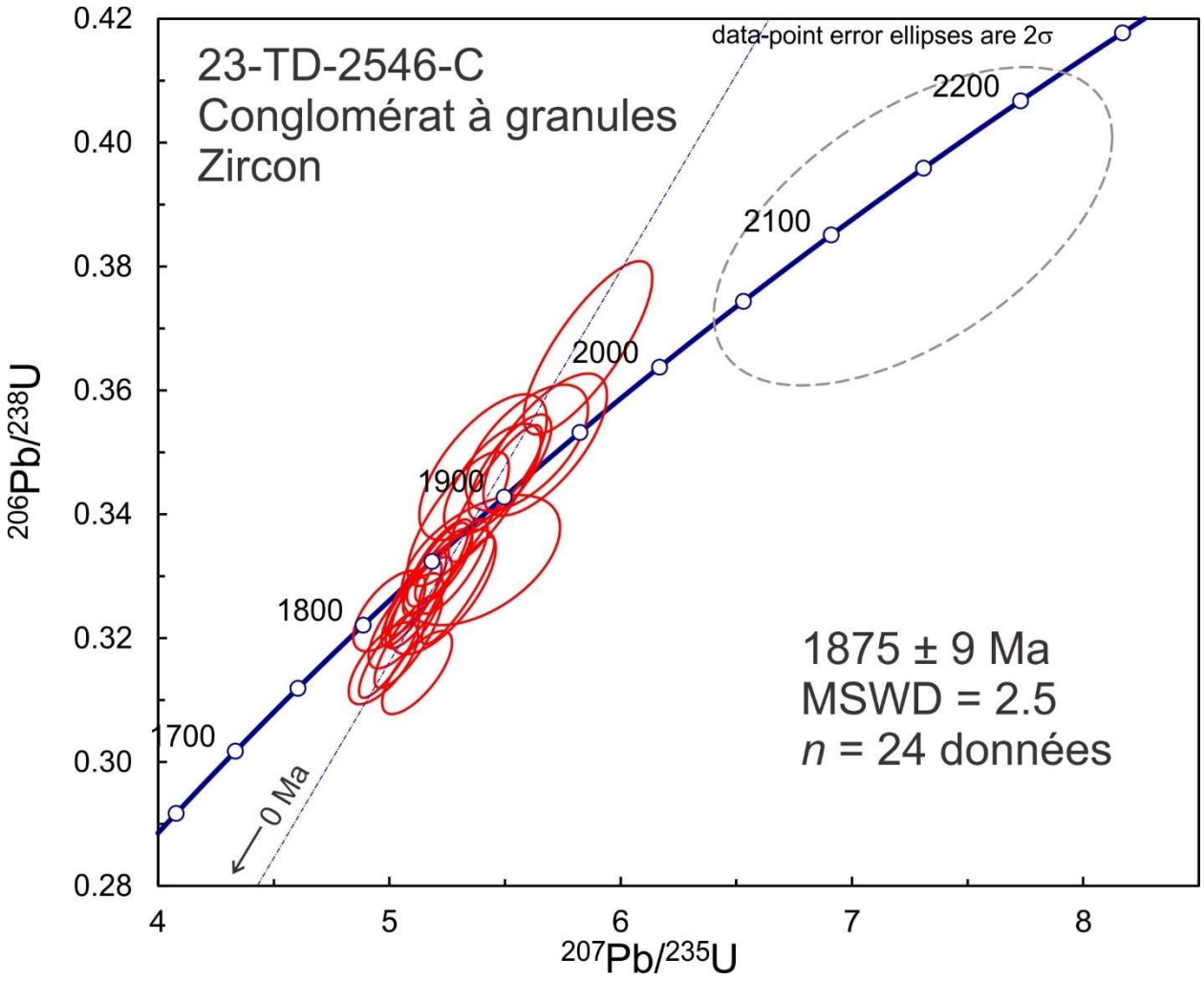

Figure 2.4.2. Concordia plot showing U-Pb isotopic data on zircon from conglomérat à granules sample 2023-TD-2546C. Red ellipses correspond to spots considered in the age model whereas gray-dashed ellipses correspond to the omitted spots.

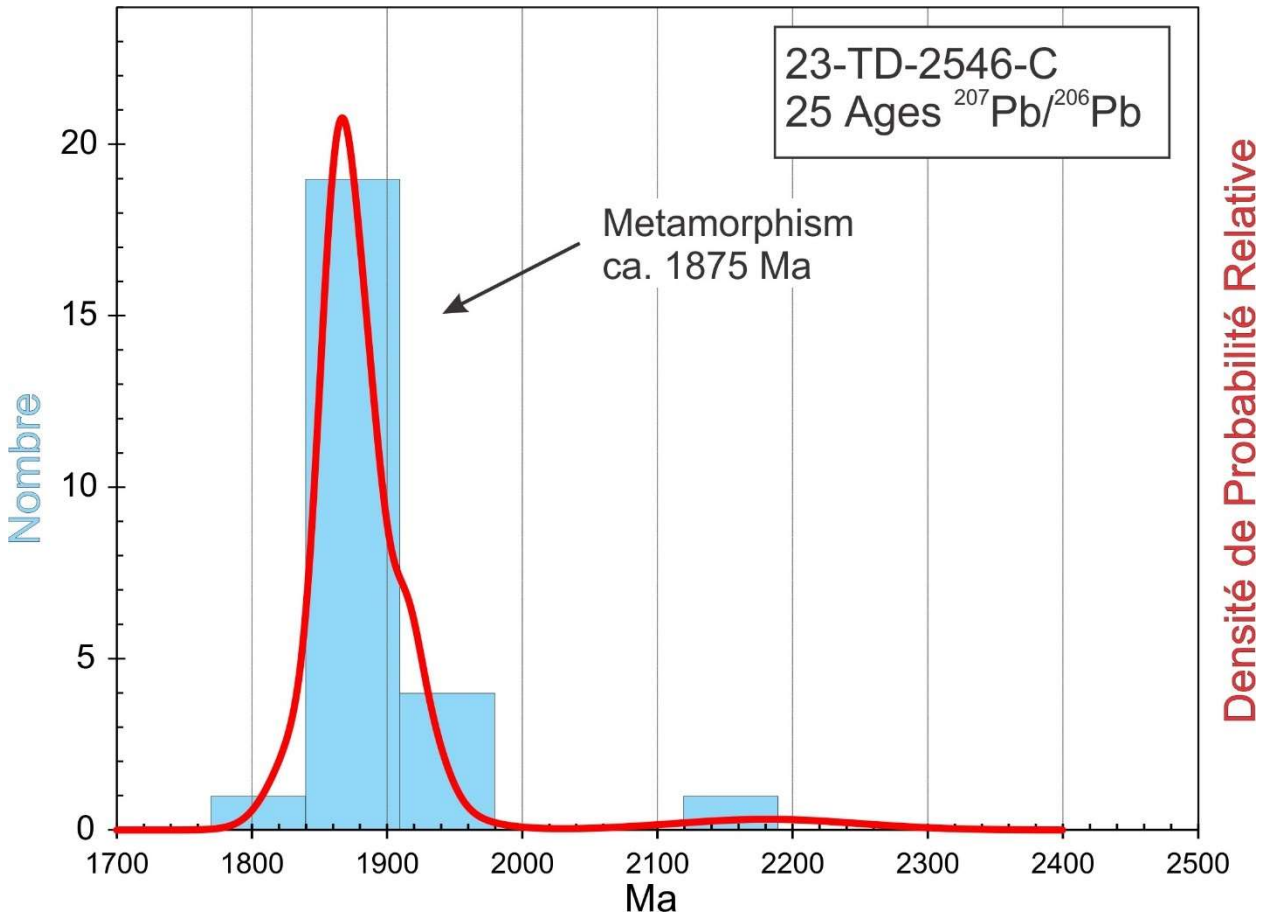

Figure 2.4.3. Combined age relative probability density plot and histogram showing the distribution of $^{207}Pb/^{206}Pb$ ages on zircon from conglomérat à granules sample 2023-TD-2546C.

2.5. 2023-GM-1679B
Diorite quartzifère

This sample yielded a diverse population of zircon grains with morphologies varying from stubby multifaceted to long prismatic (Fig. 2.5.1). BSE images show a pattern of broad zoning with fractures, inclusions, and no evidence for older cores (Fig. 2.5.2). Omitting high-Sr discordant data, U-Pb analyses show a single age peak of 1899 ±2 Ma (2σ, MSWD = 1.5, Figs. 2.5.3 and 2.5.4). Th/U ratios are in the magmatic range (>0.1) so this probably represents the age of emplacement.

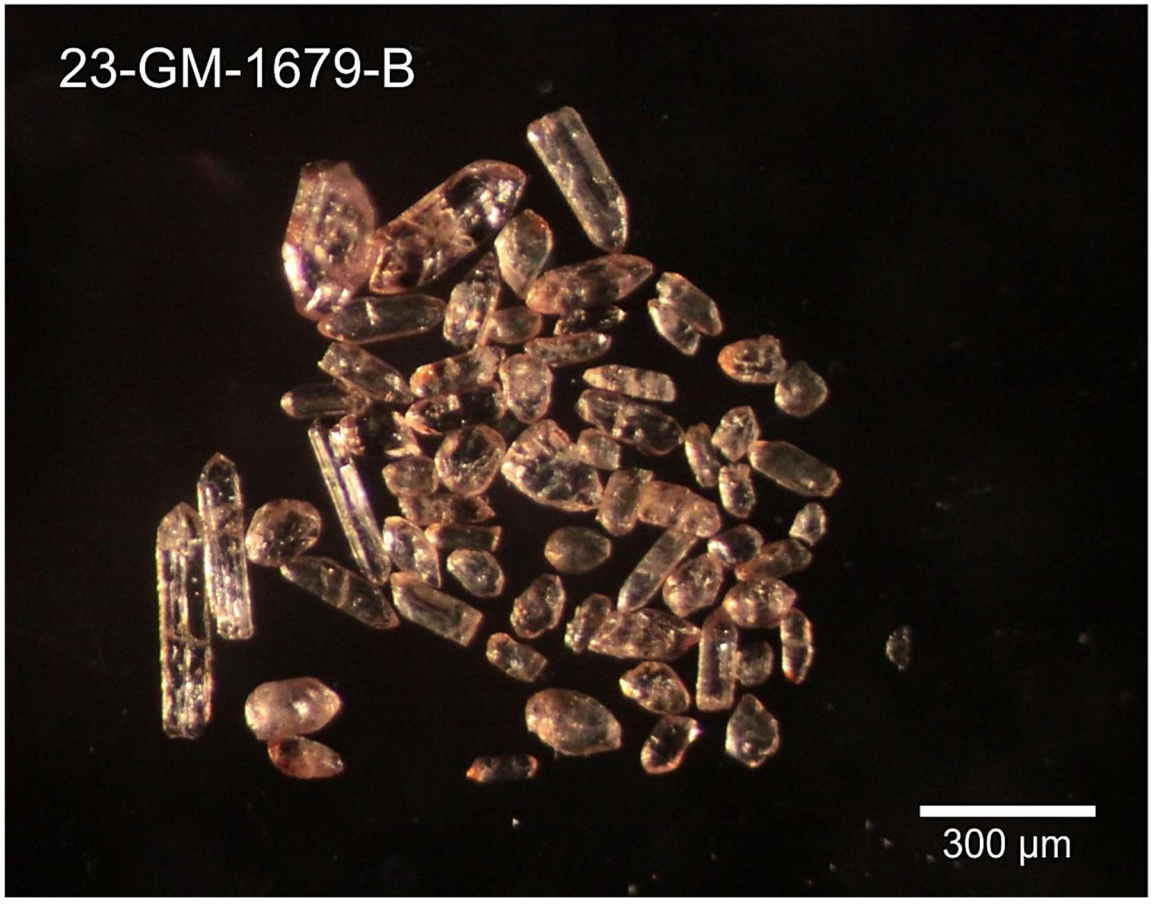

Figure 2.5.1. Picked zircon from diorite quartzifère sample 2023-GM-1679B.

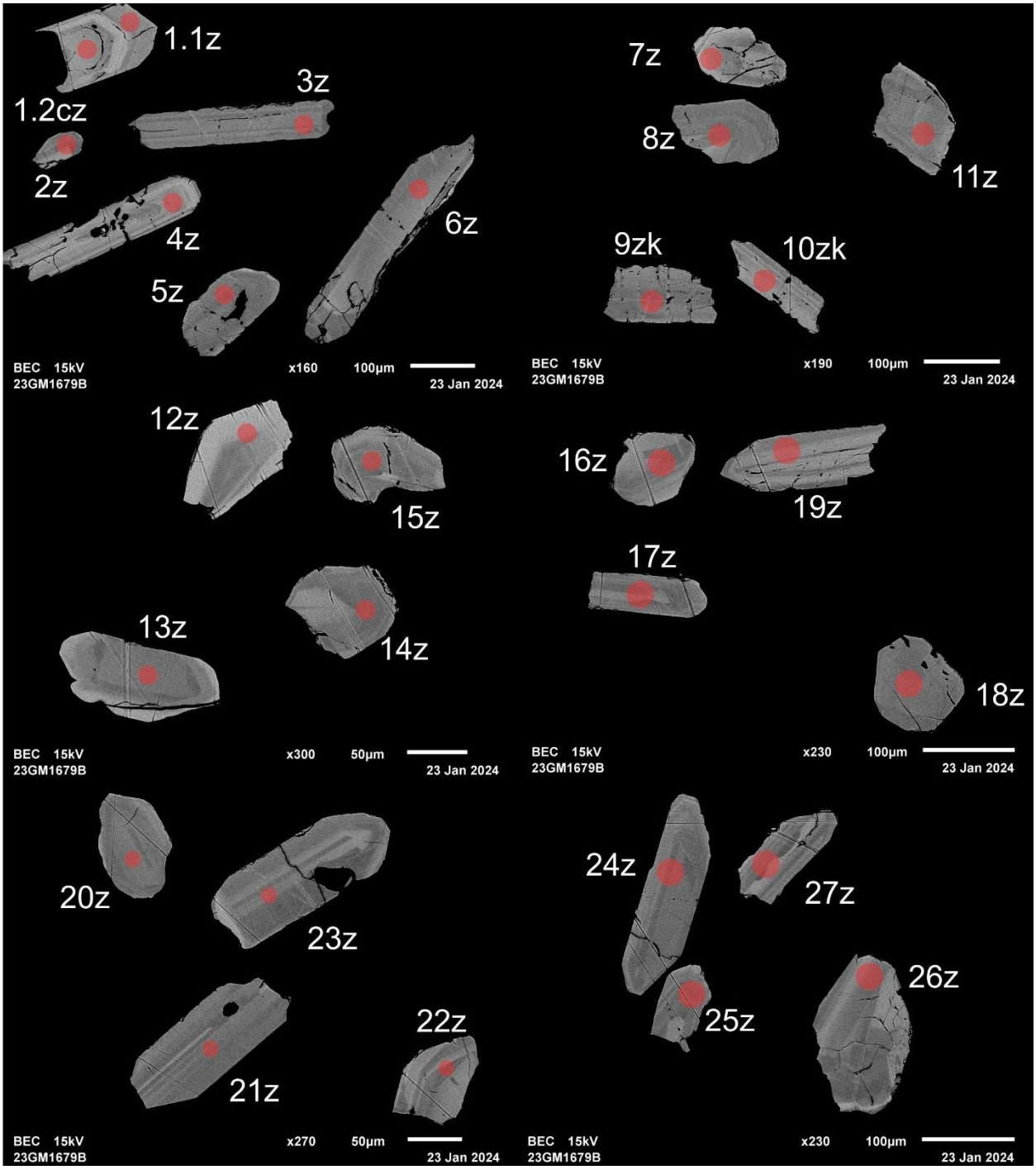

Figure 2.5.2. BSE images of selected grains from sample 2023-GM-1679B. The red circles represent the approximate locations of laser ablation spots.

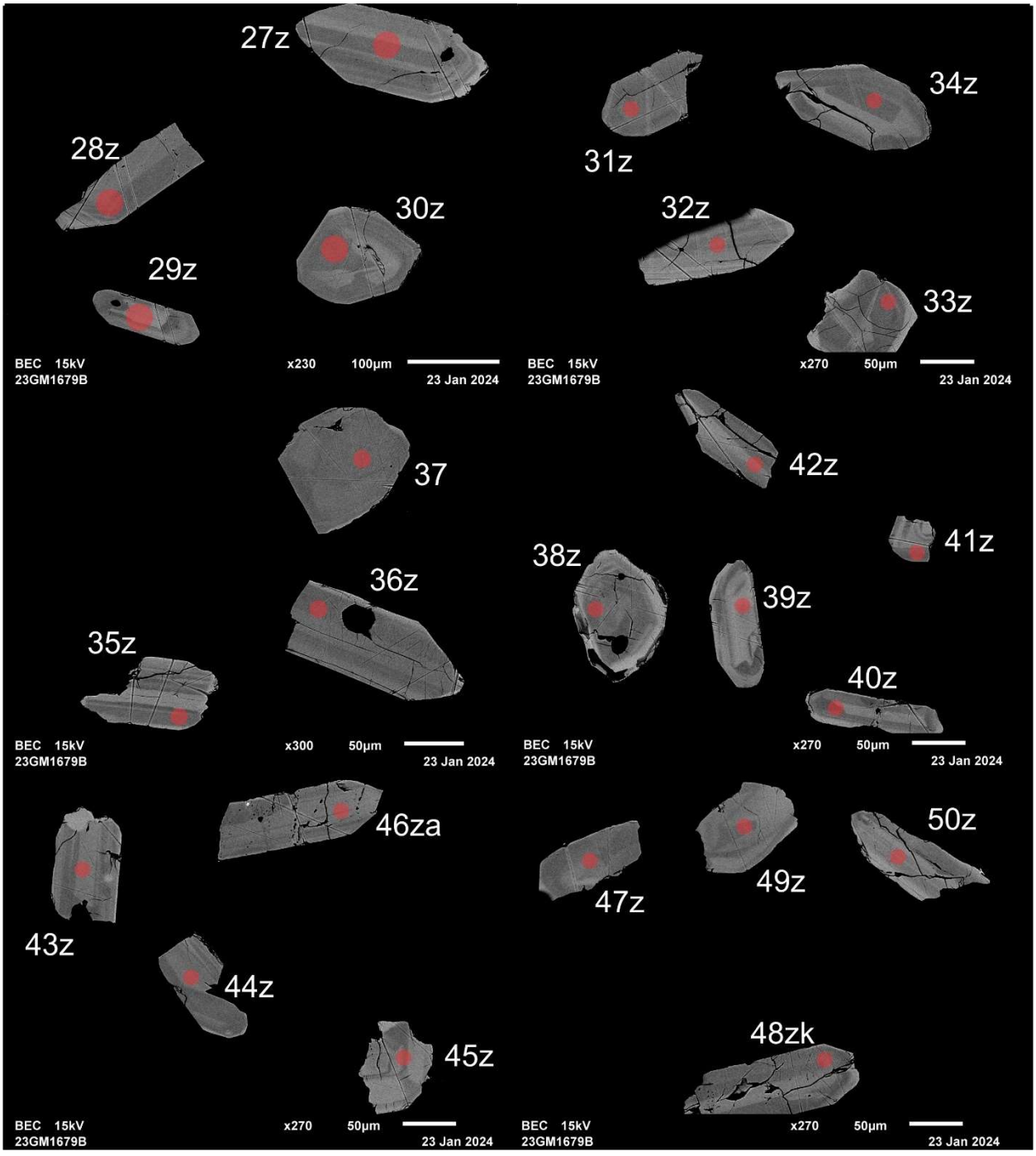

Figure 2.5.2 (cont.). BSE images of selected grains from sample 2023-GM-1679B. The red circles represent the approximate locations of laser ablation spots.

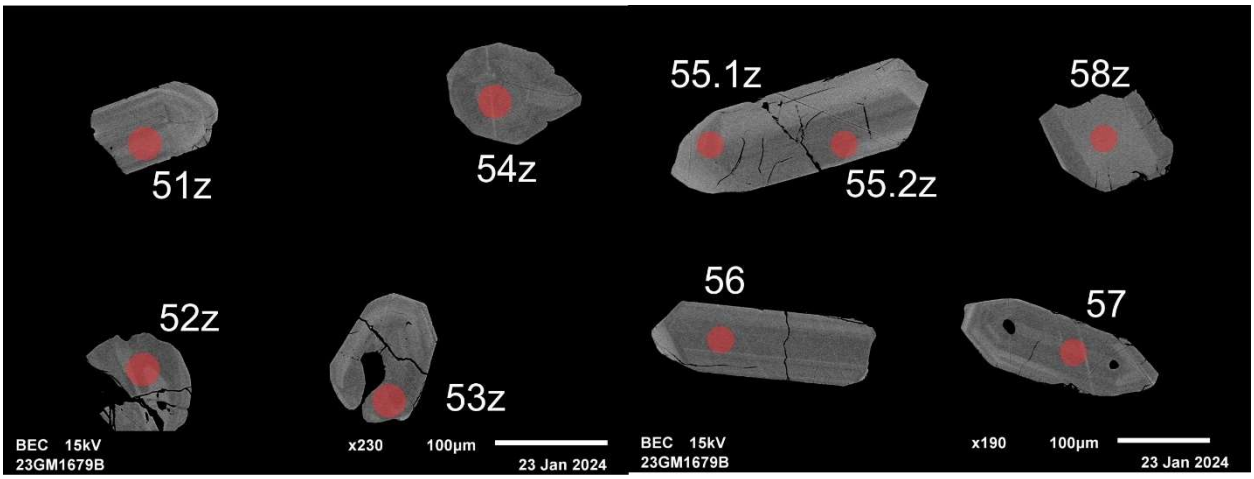

Figure 2.5.2 (cont.). BSE images of selected grains from sample 2023-GM-1679B. The red circles represent the approximate locations of laser ablation spots.

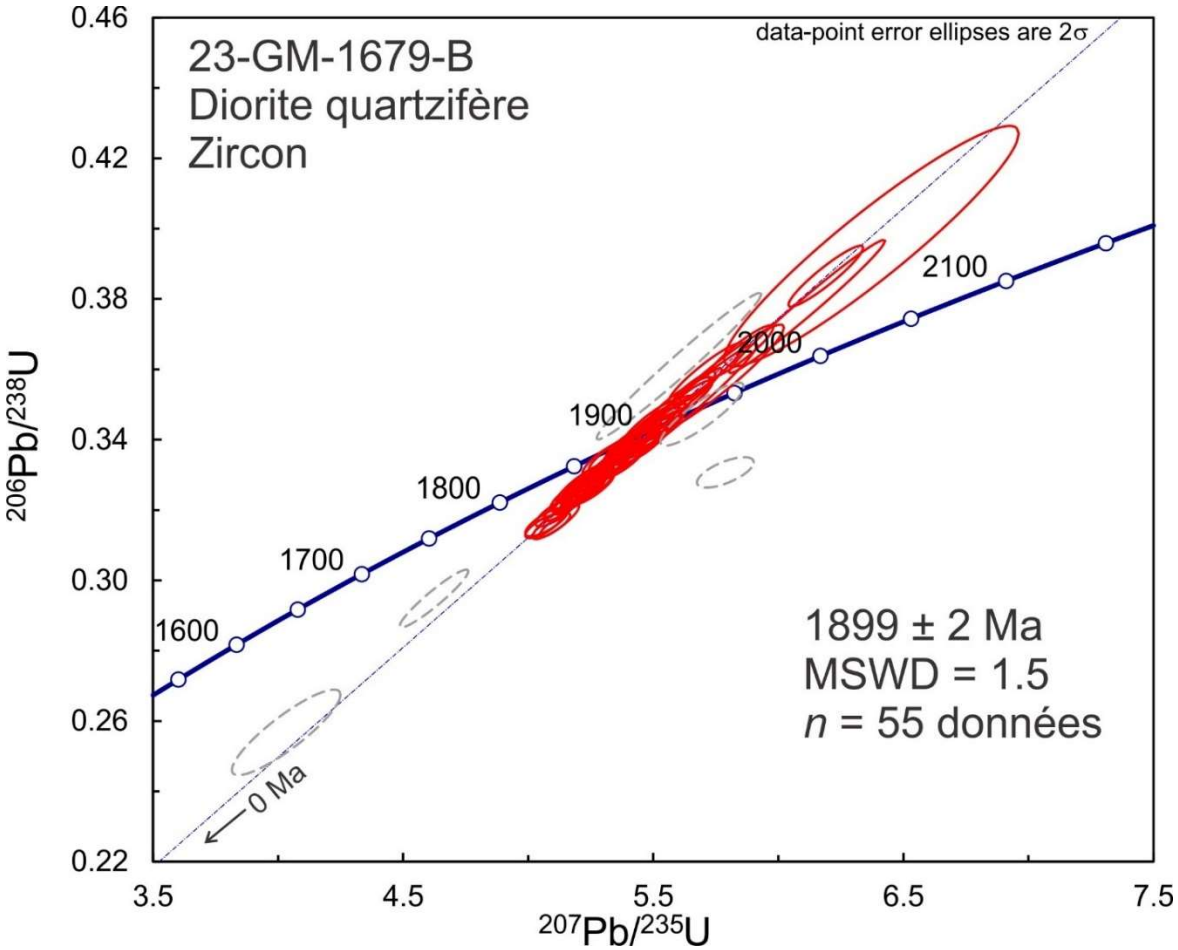

Figure 2.5.3. Concordia plot showing U-Pb isotopic data on polished zircon from diorite quartzifère sample 2023-GM-1679B. Red ellipses correspond to spots considered in the age model whereas gray-dashed ellipses correspond to the omitted spots.

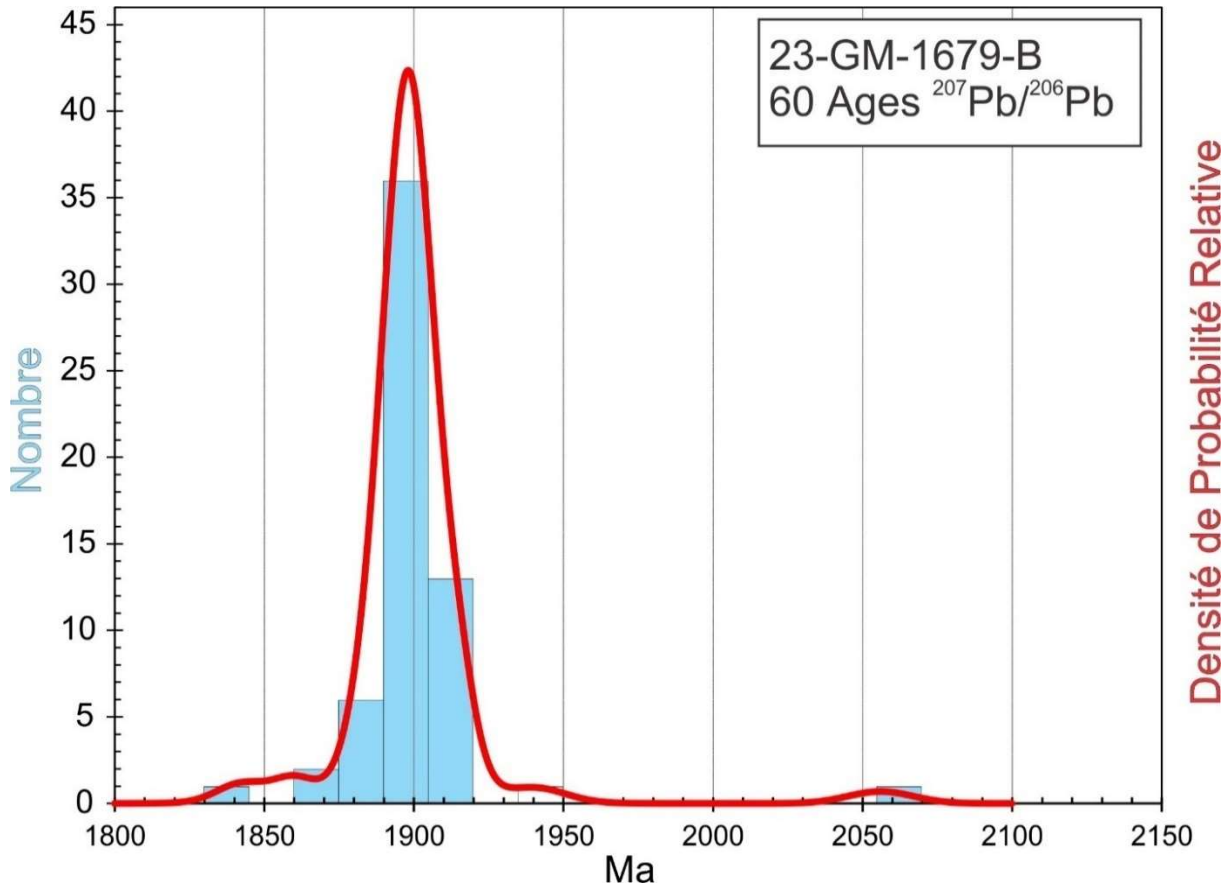

Figure 2.5.4. Combined age relative probability density plot and histogram showing the distribution of $^{207}Pb/^{206}Pb$ ages on polished zircon from diorite quartzifère sample 2023-GM-1679B.

2.6. 2023-GM-1620A
Granite gris à biotite

This sample yielded a small amount of zircon generally as short to long prisms and fragments. (Fig. 2.6.1). BSE images show pervasive alteration following cracks and affecting what may be higher U cores (Fig 2.6.2). U concentrations are highly variable ranging from 5300 ppm to 100 ppm. All Th/U ratios are within the range of magmatic zircon. With the exception of analyses showing high Sr and possible alteration, $^{207}Pb/^{206}Pb$ ages overlap with an average of 1882 ±3 Ma (2σ, MSWD = 1.9, Fig. 2.6.3). A relative probability density plot of $^{207}Pb/^{206}Pb$ ages reveals a resolved age peak at around 1880 Ma (Fig. 2.6.4).

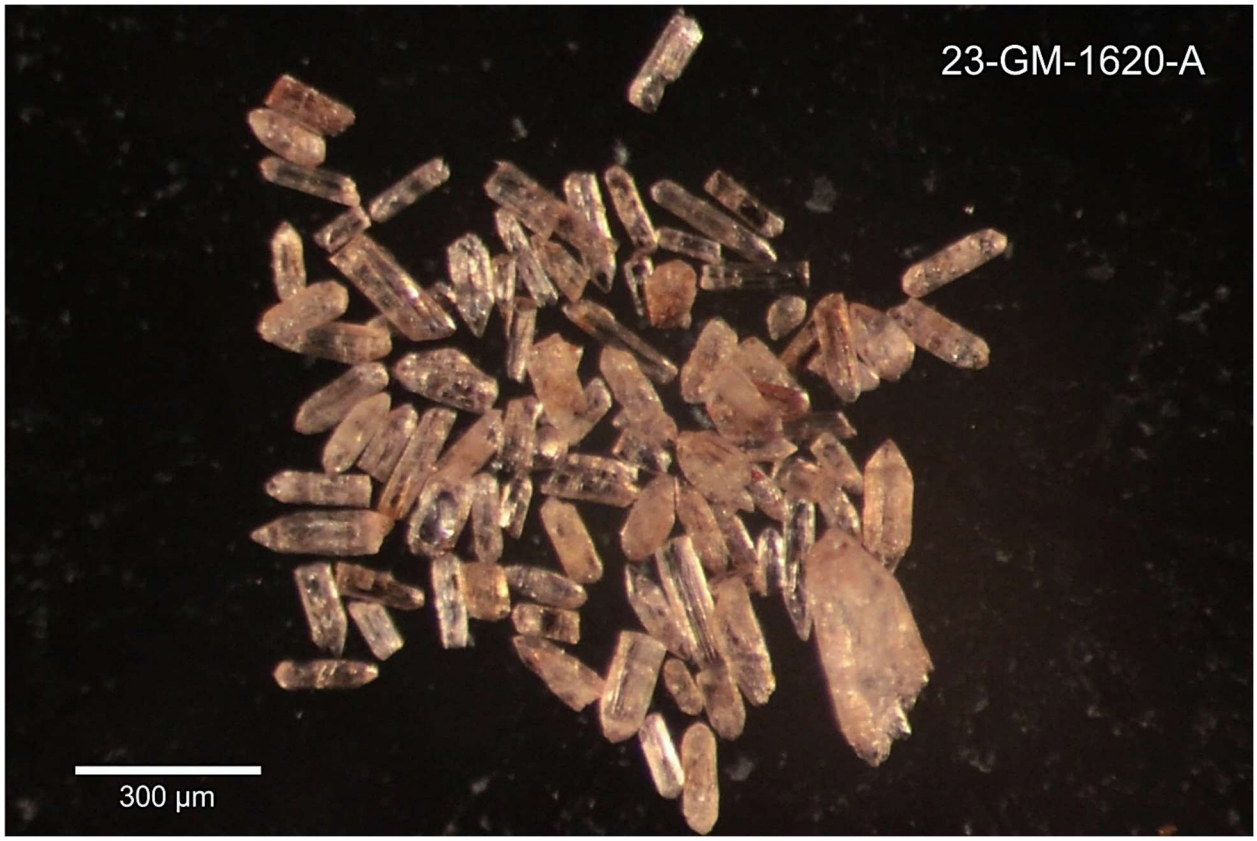

Figure 2.6.1. Picked zircon from granite sample 2023-GM-1620A.

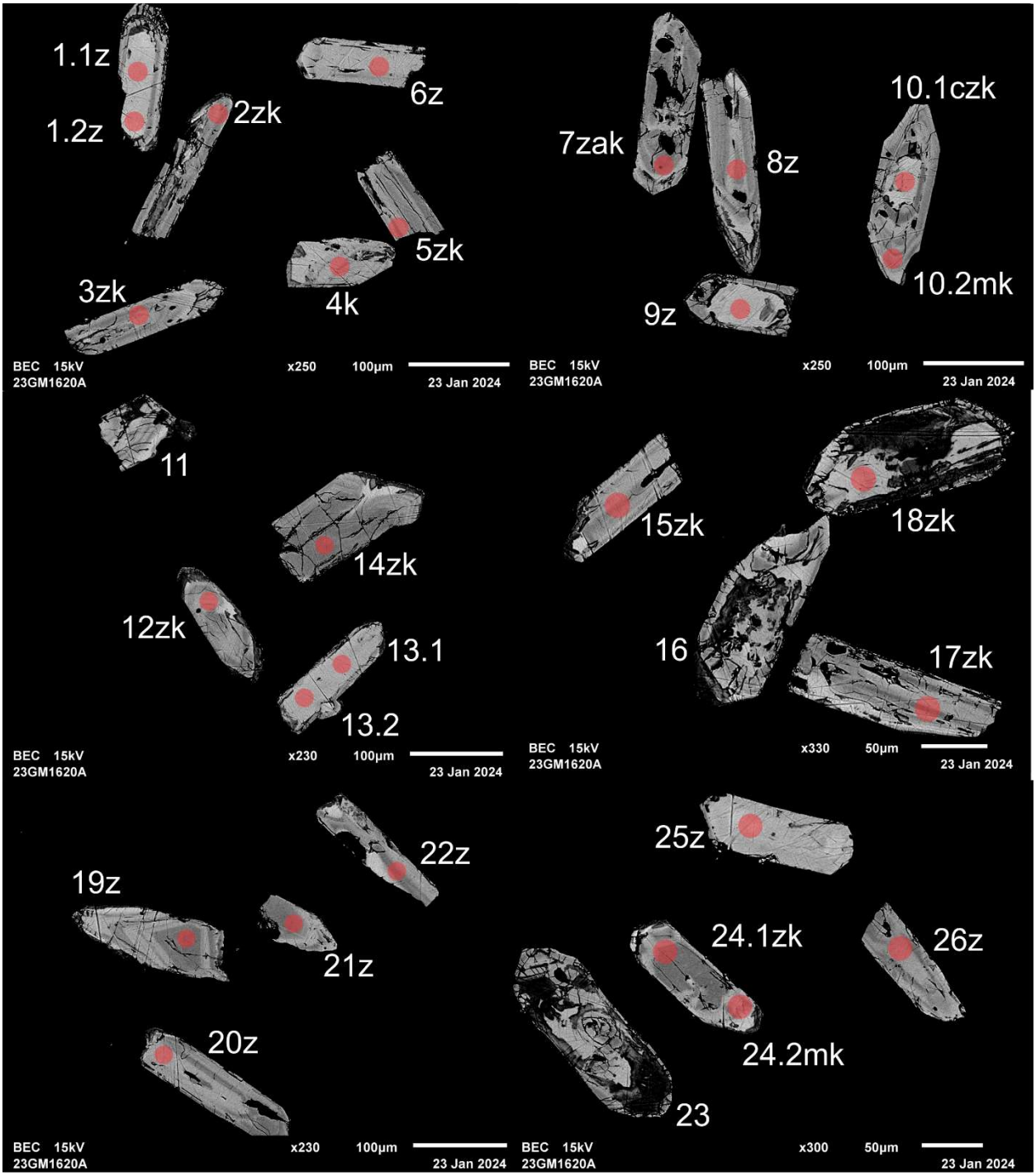

Figure 2.6.2. BSE images of selected grains from sample 2023-GM-1620A. The red circles represent the approximate locations of laser ablation spots.

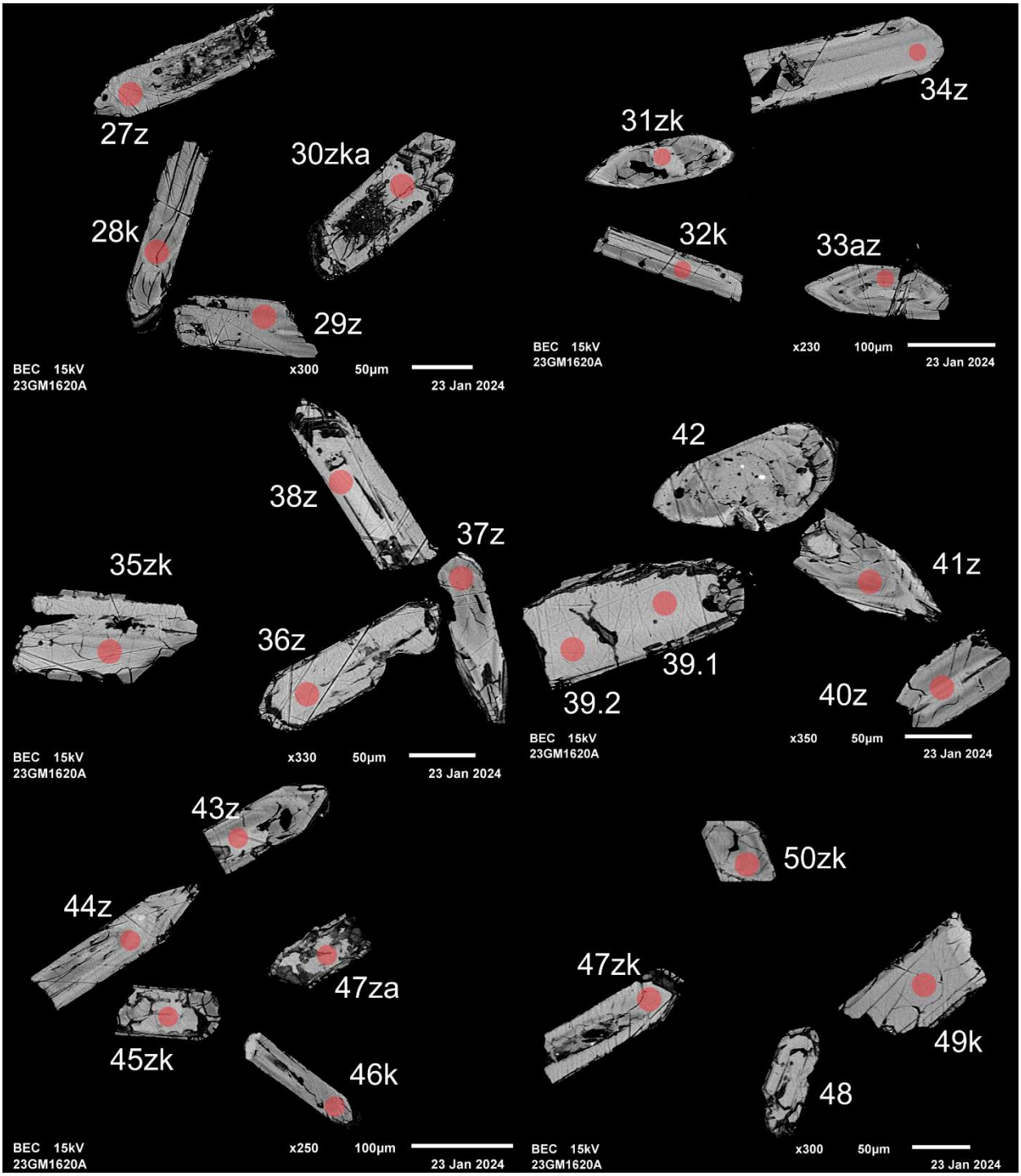

Figure 2.6.2 (cont.). BSE images of selected grains from sample 2023-GM-1620A. The red circles represent the approximate locations of laser ablation spots.

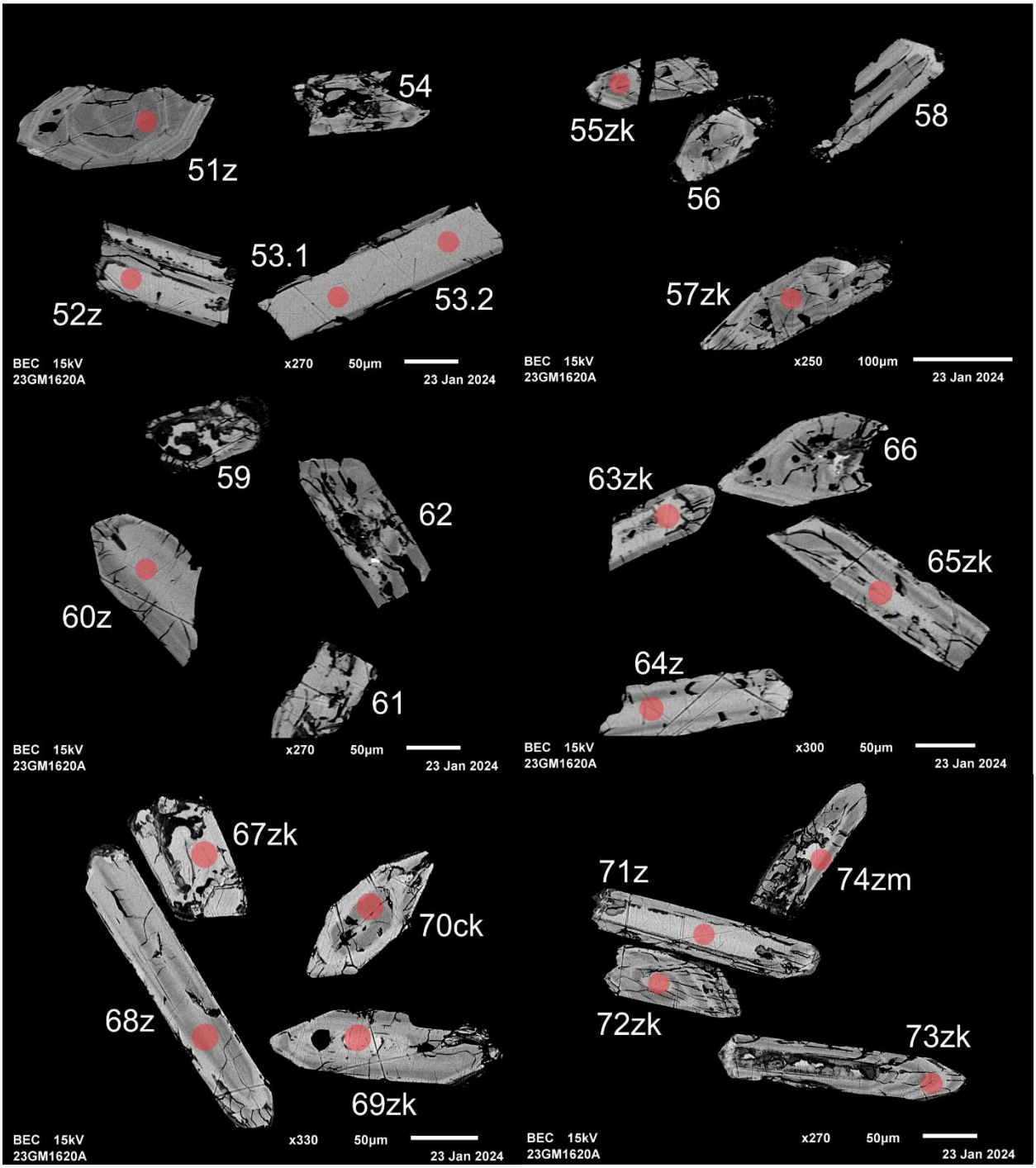

Figure 2.6.2 (cont.). BSE images of selected grains from sample 2023-GM-1620A. The red circles represent the approximate locations of laser ablation spots.

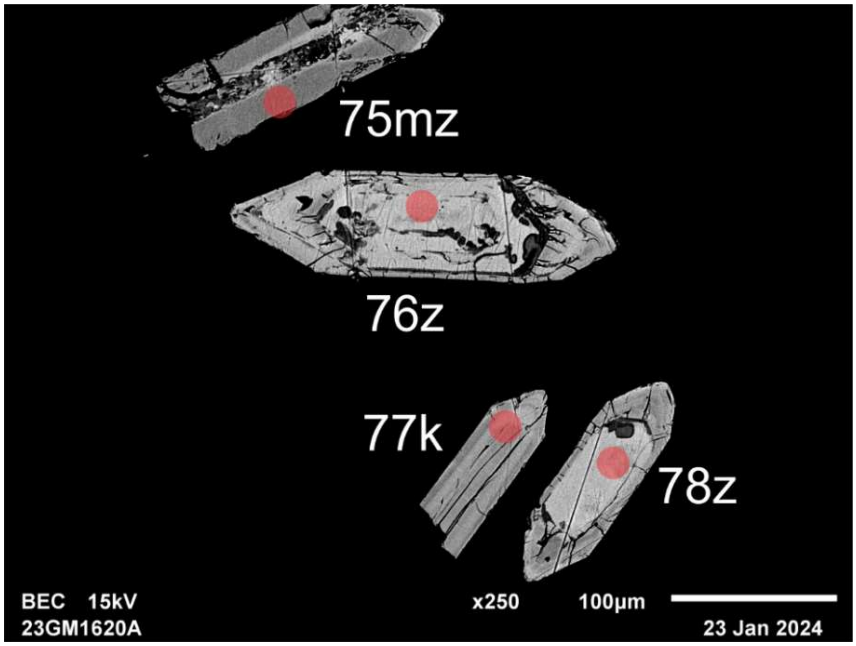

Figure 2.6.2 (cont.). BSE images of selected grains from sample 2023-GM-1620A. The red circles represent the approximate locations of laser ablation spots.

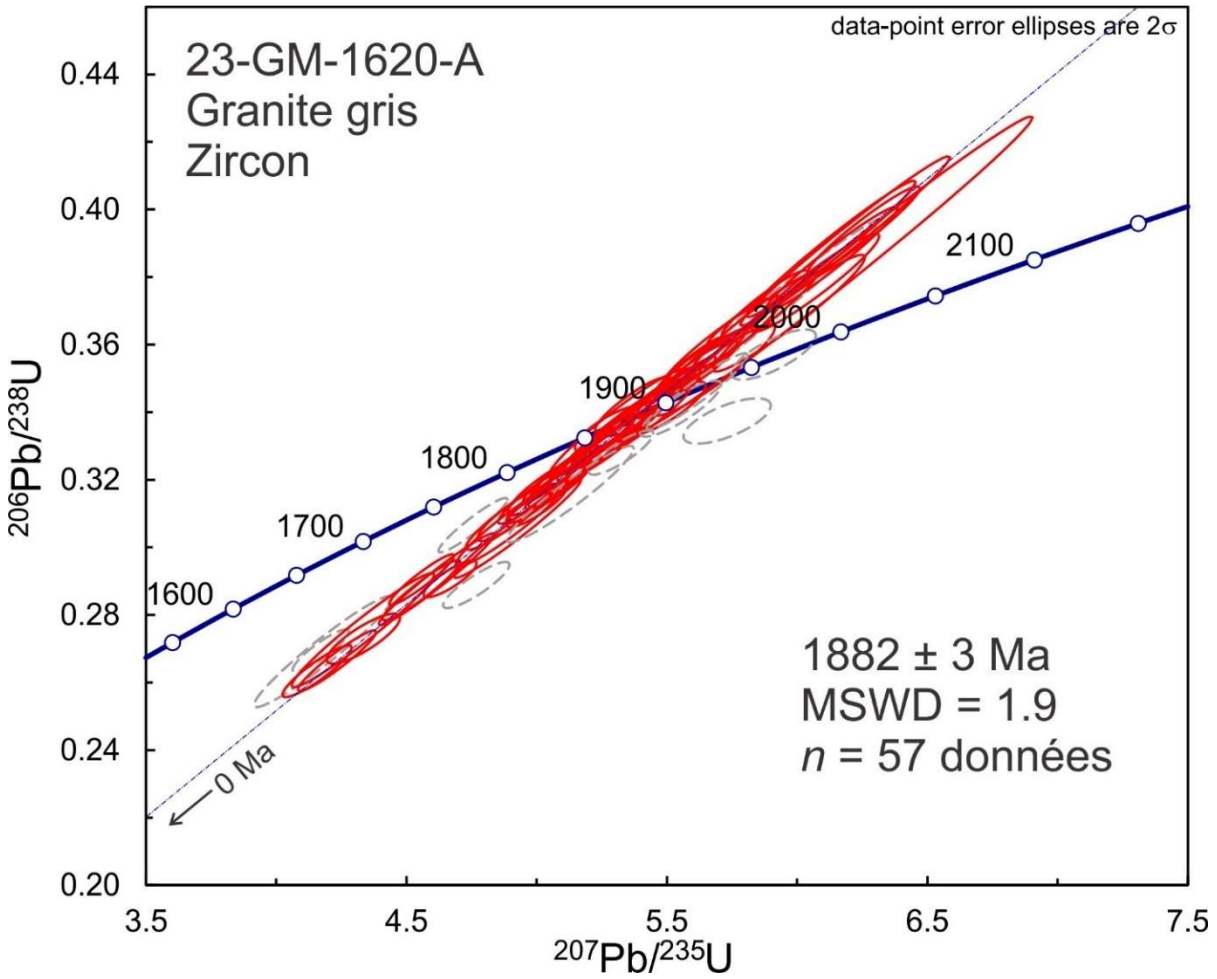

Figure 2.6.3. Concordia plot showing U-Pb isotopic data on polished zircon from granite sample 2023-GM-1620A. Red ellipses correspond to spots considered in the age model whereas gray-dashed ellipses correspond to the omitted spots.

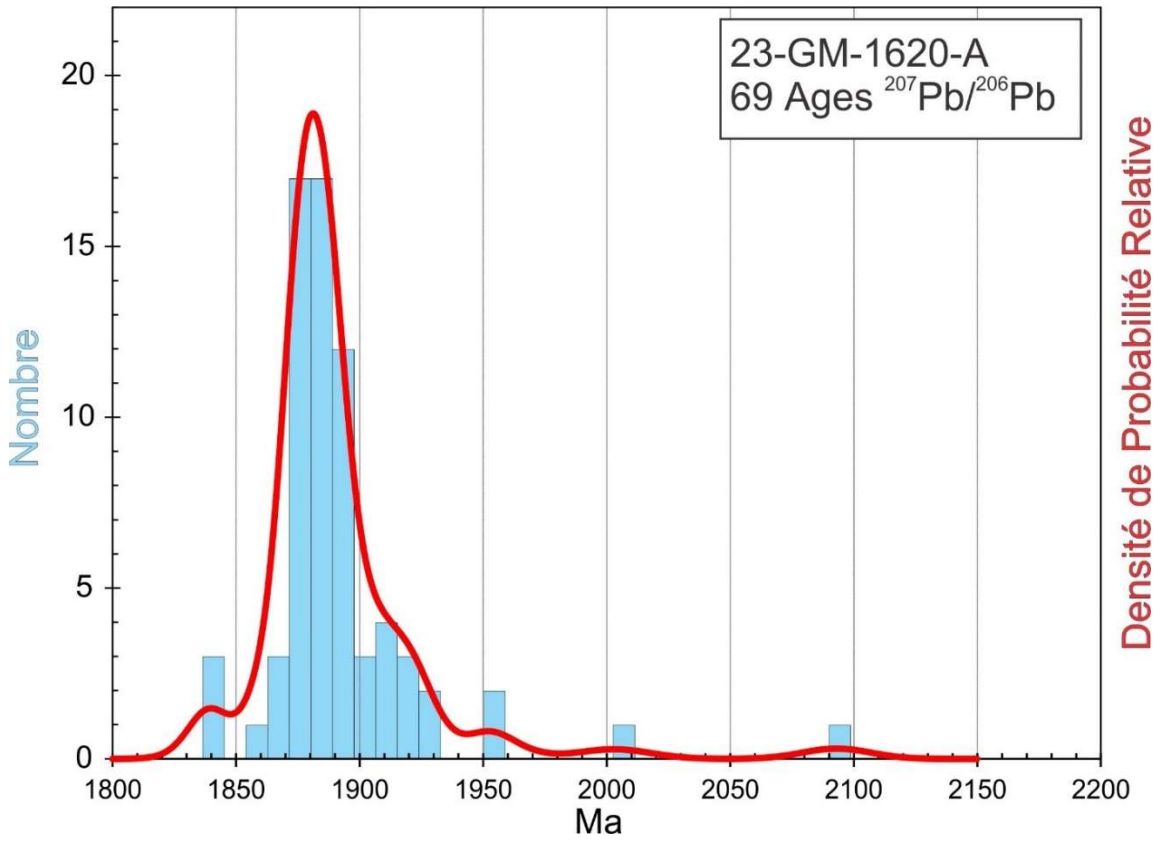

Figure 2.6.4. Combined age relative probability density plot and histogram showing the distribution of $^{207}Pb/^{206}Pb$ ages on polished zircon from granite sample 2023-GM-1620A.

2.7. 2019-SM-6104A, Gabbro grossier

This sample yielded abundant zircon with a uniform-looking population of rounded to subrounded fragments with brownish coloration (Fig. 2.7.1). BSE images show faint broad zoning with no evidence of older cores (Fig 2.7.2). Most U-Pb analyses overlap within error (Fig. 2.7.3). A relative probability density plot of $^{207}Pb/^{206}Pb$ ages reveals a resolved age peak at around 1860 Ma (Fig. 2.7.4). After excluding the outliers, the U-Pb data results in an average age of 1861 ±2.5 Ma (2σ, MSWD = 1.4, Fig. 2.7.3). This is the most likely the age of igneous crystallization of the unit.

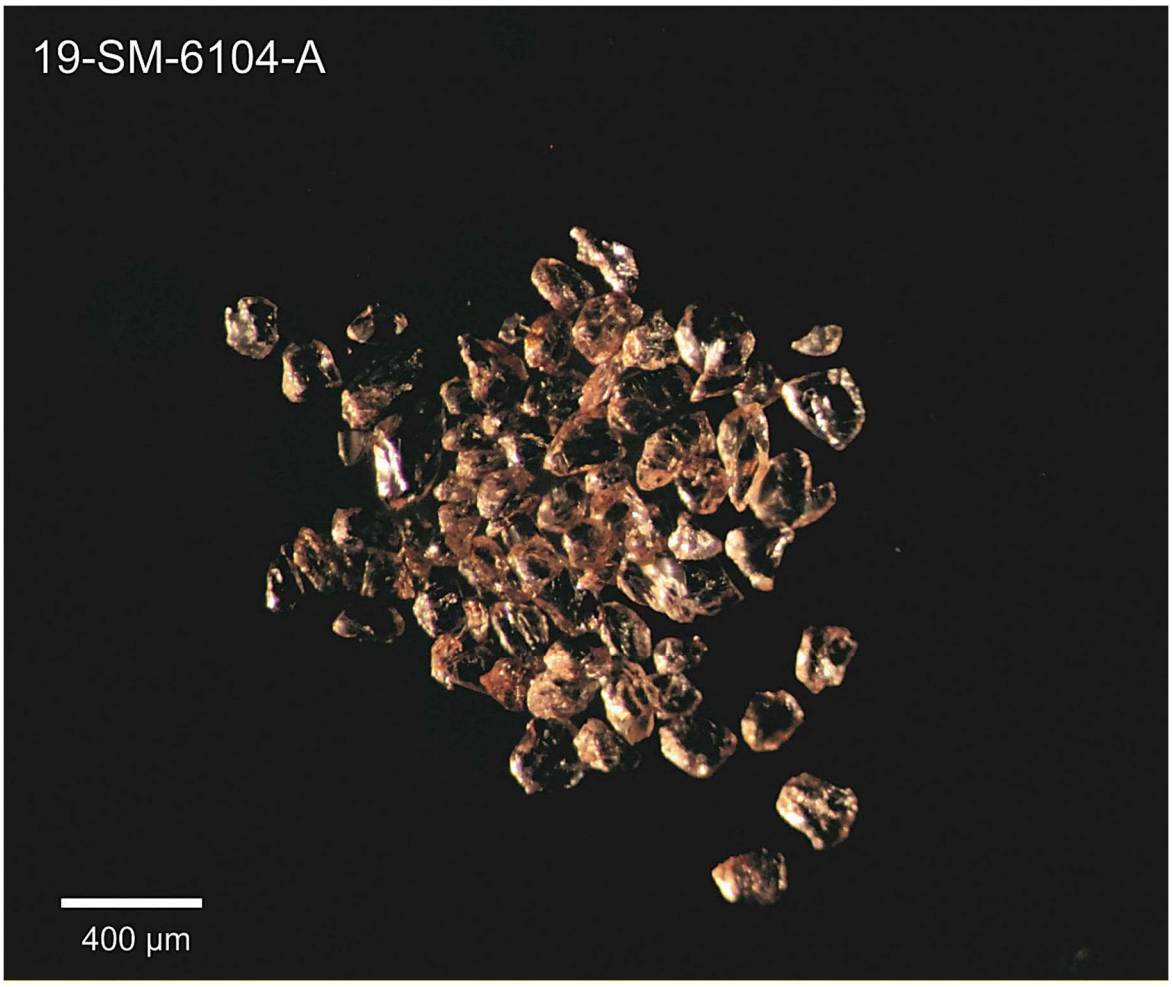

Figure 2.7.1. Picked zircon from gabbro sample 2019-SM-6104A.

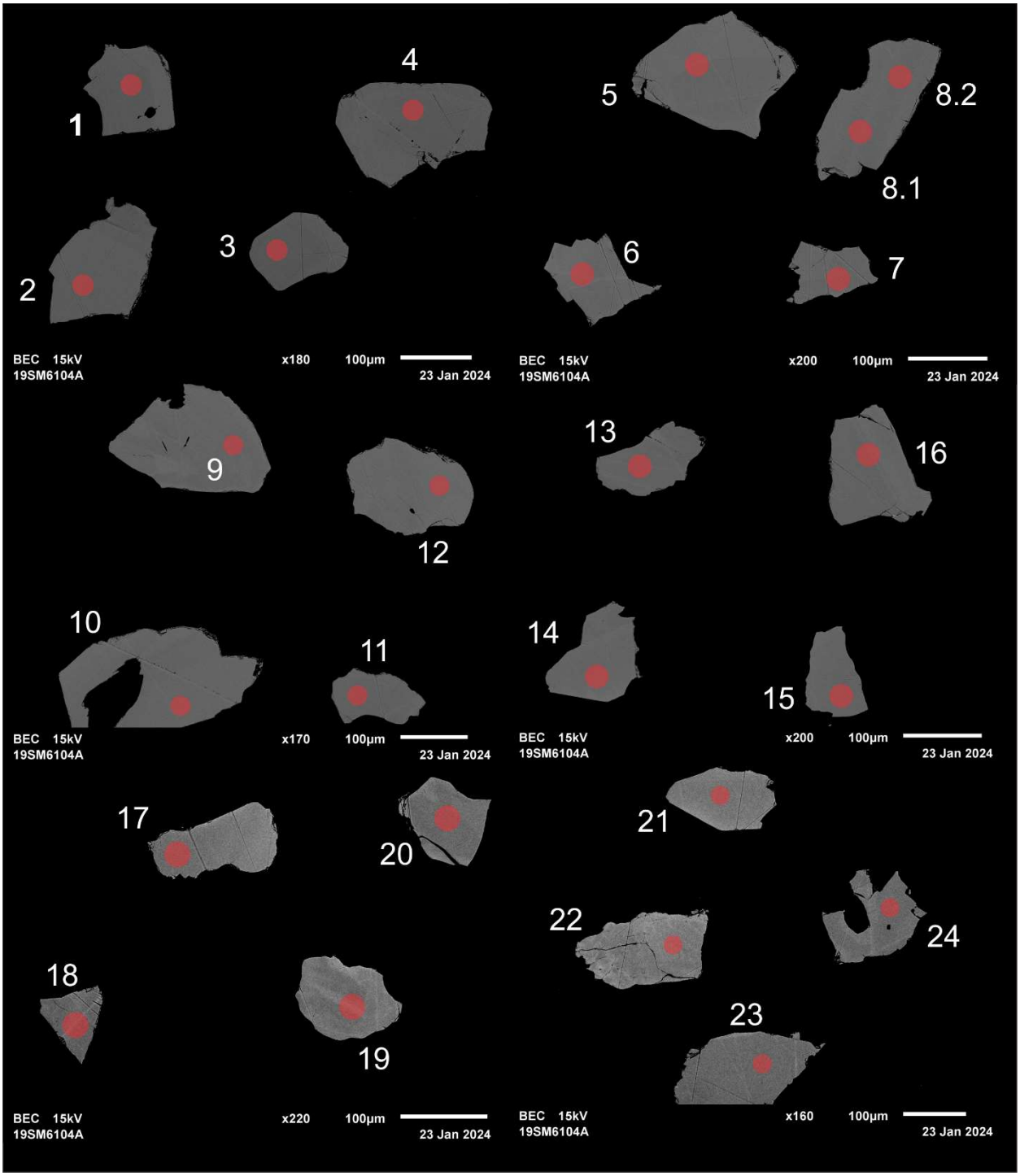

Figure 2.7.2. BSE images of selected grains from sample 2019-SM-6104A. The red circles represent the approximate locations of laser ablation spots.

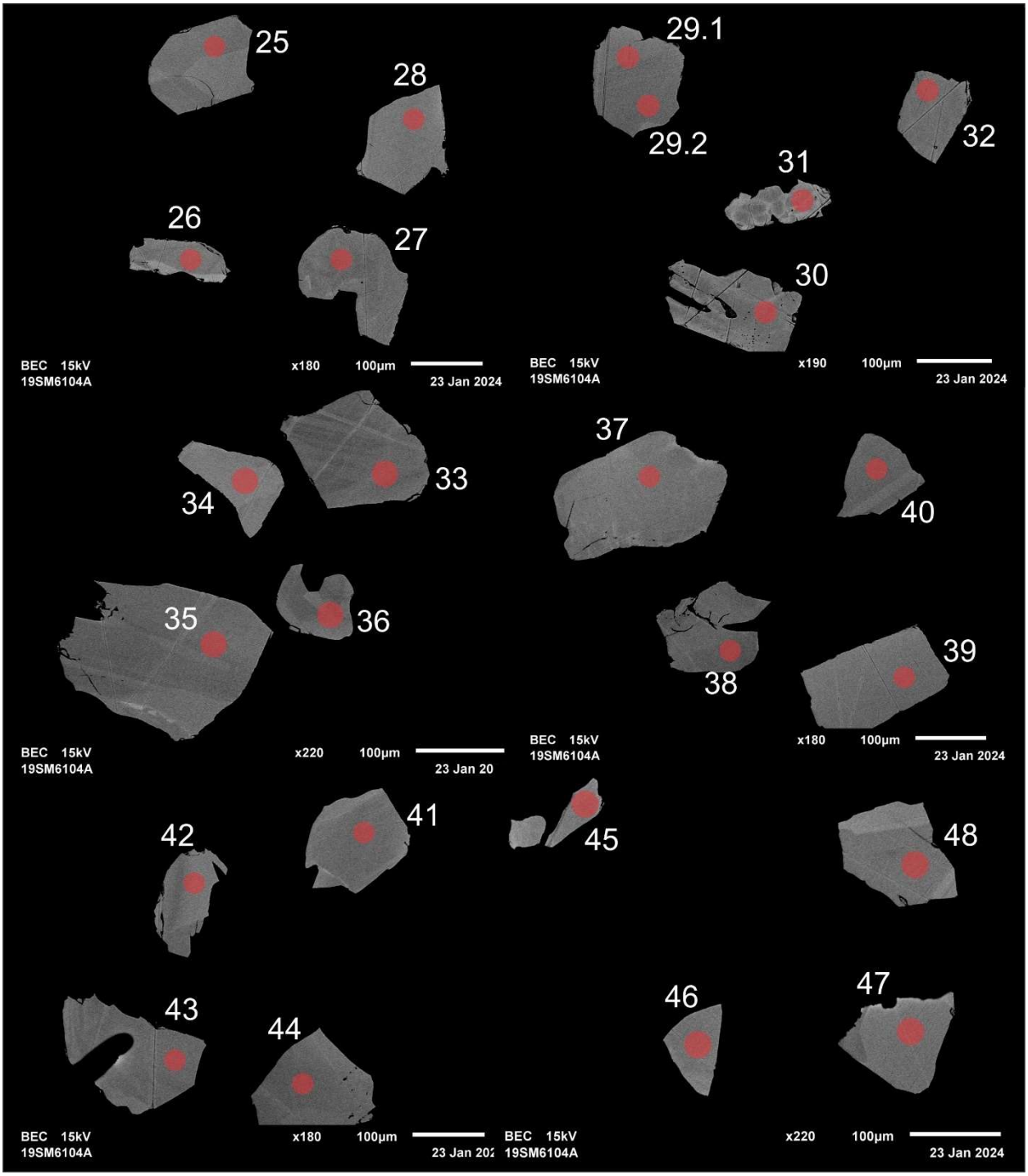

Figure 2.7.2 (cont.). BSE images of selected grains from sample 2019-SM-6104A. The red circles represent the approximate locations of laser ablation spots.

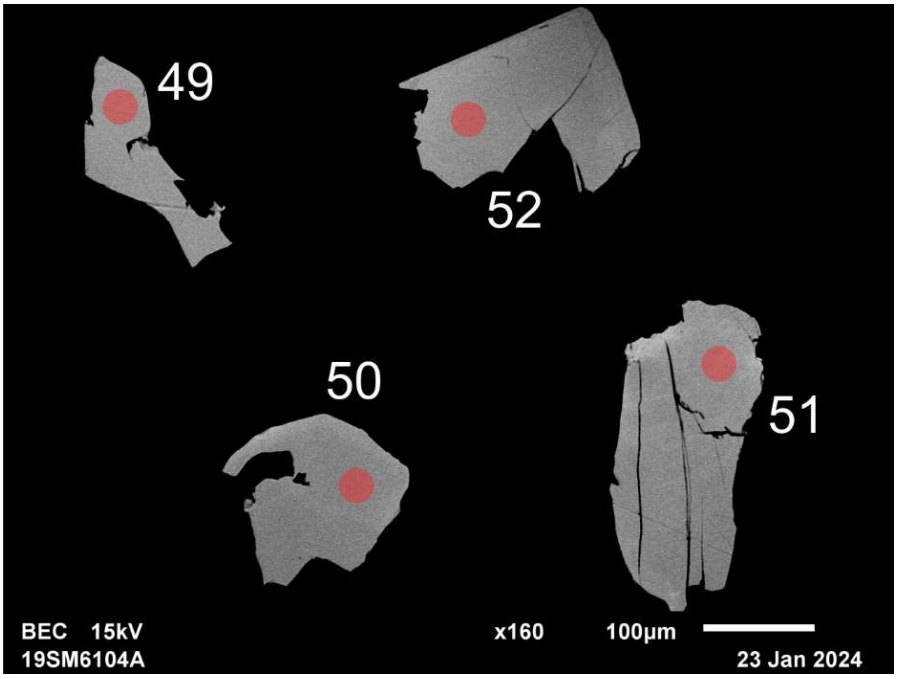

Figure 2.7.2 (cont.). BSE images of selected grains from sample 2019-SM-6104A. The red circles represent the approximate locations of laser ablation spots.

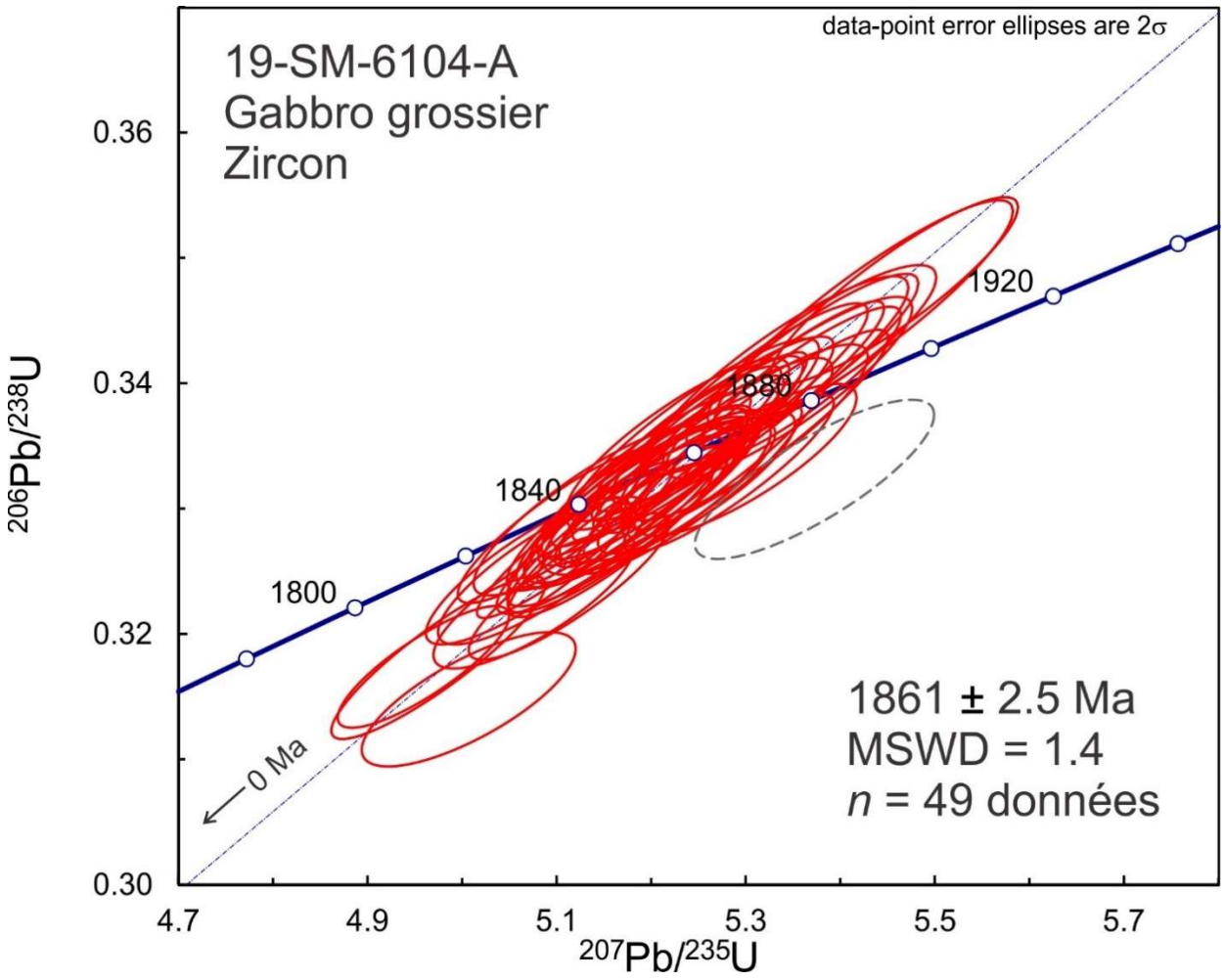

Figure 2.7.3. Concordia plot showing U-Pb isotopic data on polished zircon from gabbro sample 2019-SM-6104A. Red ellipses correspond to spots considered in the age model whereas gray-dashed ellipse corresponds to the omitted spot.

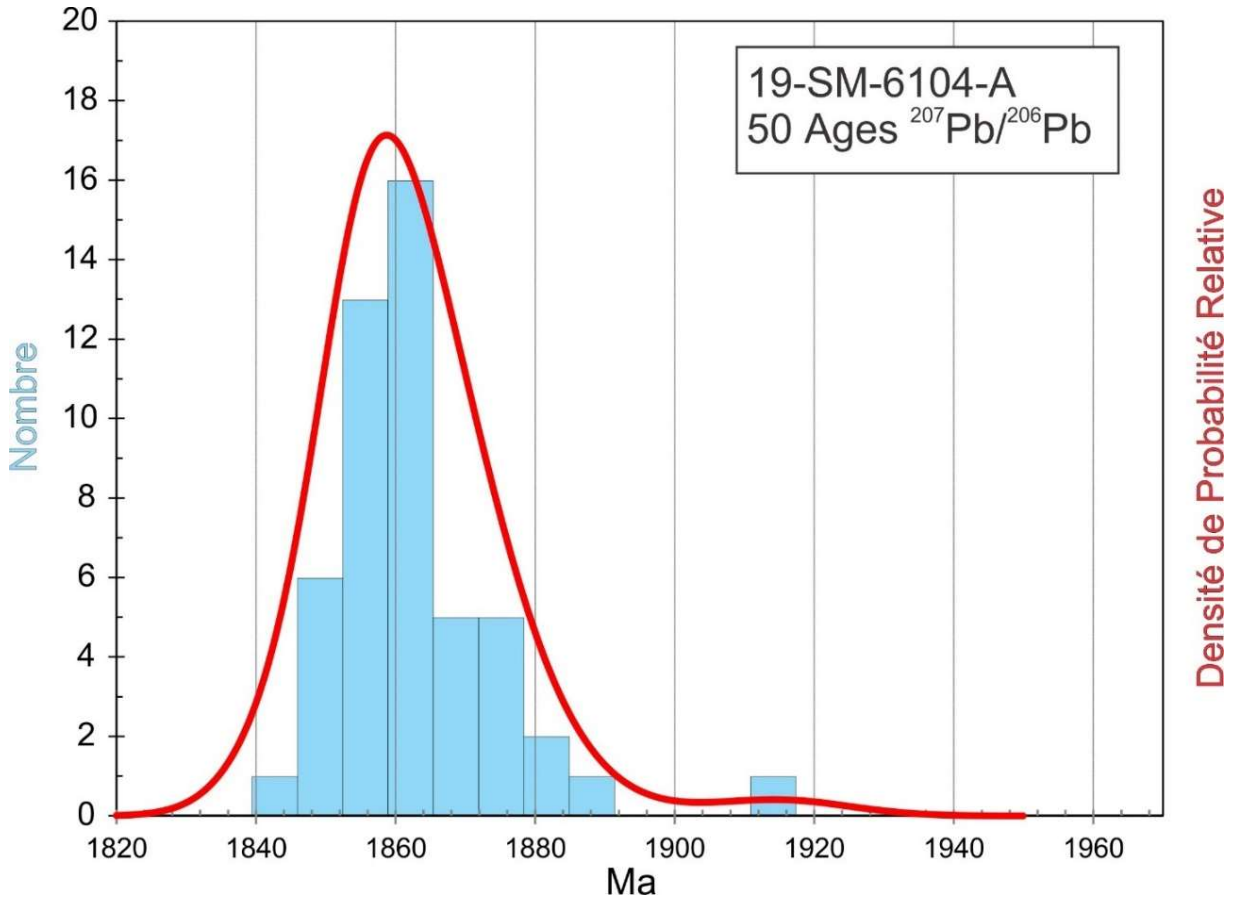

Figure 2.7.4. Combined age relative probability density plot and histogram showing the distribution of $^{207}Pb/^{206}Pb$ ages on polished zircon from gabbro sample 2019-SM-6104A.

2.8. 2022-TD-2084A
Wacke lithique

This sample yielded a zircon population of generally stubby rounded grains (Fig. 2.8.1). BSE images show a range of oscillatory to indistinct zoning patterns (Fig 2.8.2). U-Pb analyses show diverse ages ranging from 1991 Ma to 2754 Ma. Some ages around 1991 Ma to 2200 Ma (Fig. 2.8.3) correspond to rims, however, all analyses show Th/U ratios>0.1, so there is no evidence of metamorphic zircon and all of the zircon appears to be detrital. Five ages about 4000 Ma were omitted because the high Sr signal which suggests intersection of the beam with zones of alteration or inclusions. A relative probability density plot of $^{207}Pb/^{206}Pb$ ages reveals two major age peaks at around 2320 Ma and 2390 Ma (Fig. 2.8.3 and 2.8.4). Depending on the metamorphic grade in the region, the U-Pb data may indicate partial resetting of a diverse Archean detrital population during Paleoproterozoic metamorphism or a population of late Archean to Paleoproterozoic detrital zircon deposited in the Proterozoic.

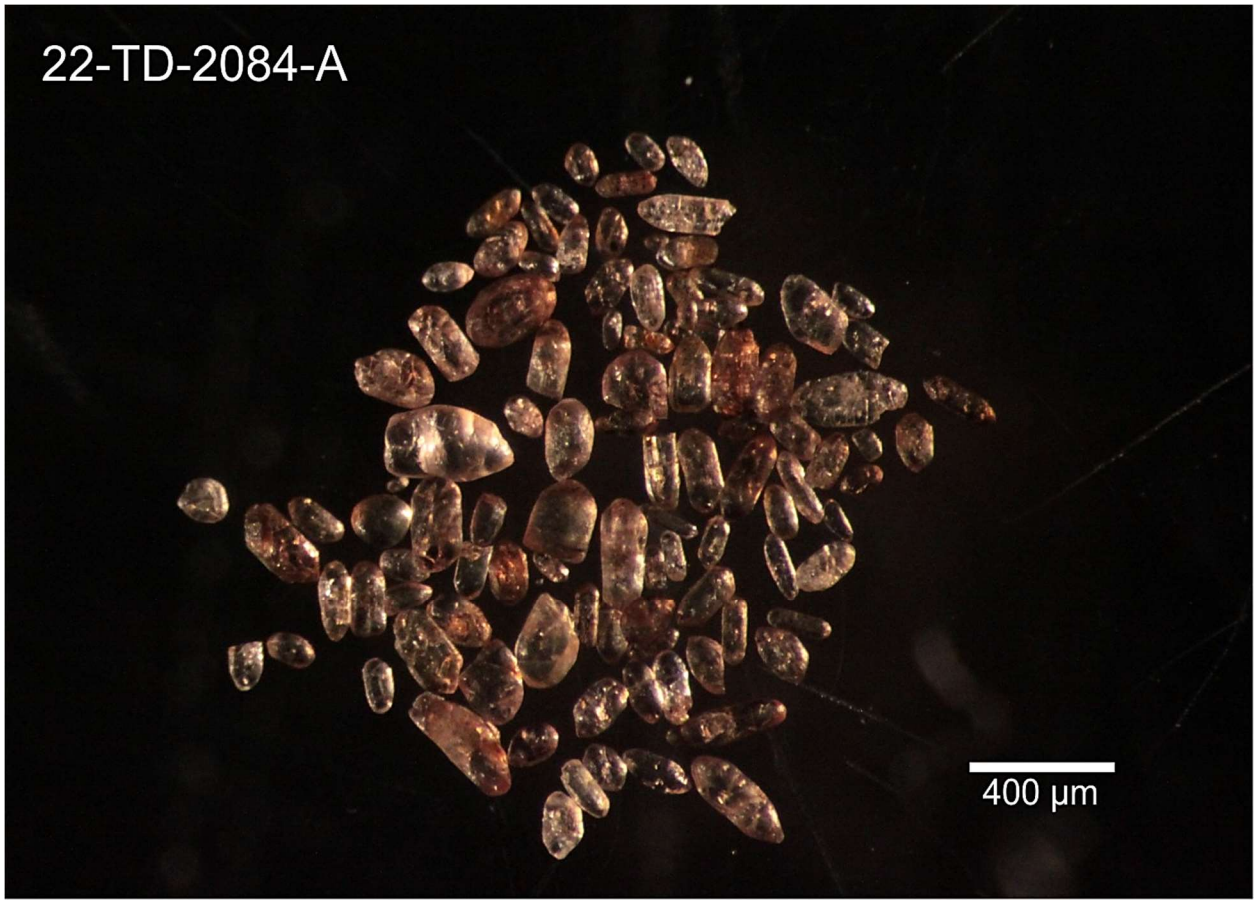

Figure 2.8.1. Picked zircon from wacke sample 2022-TD-2084A.

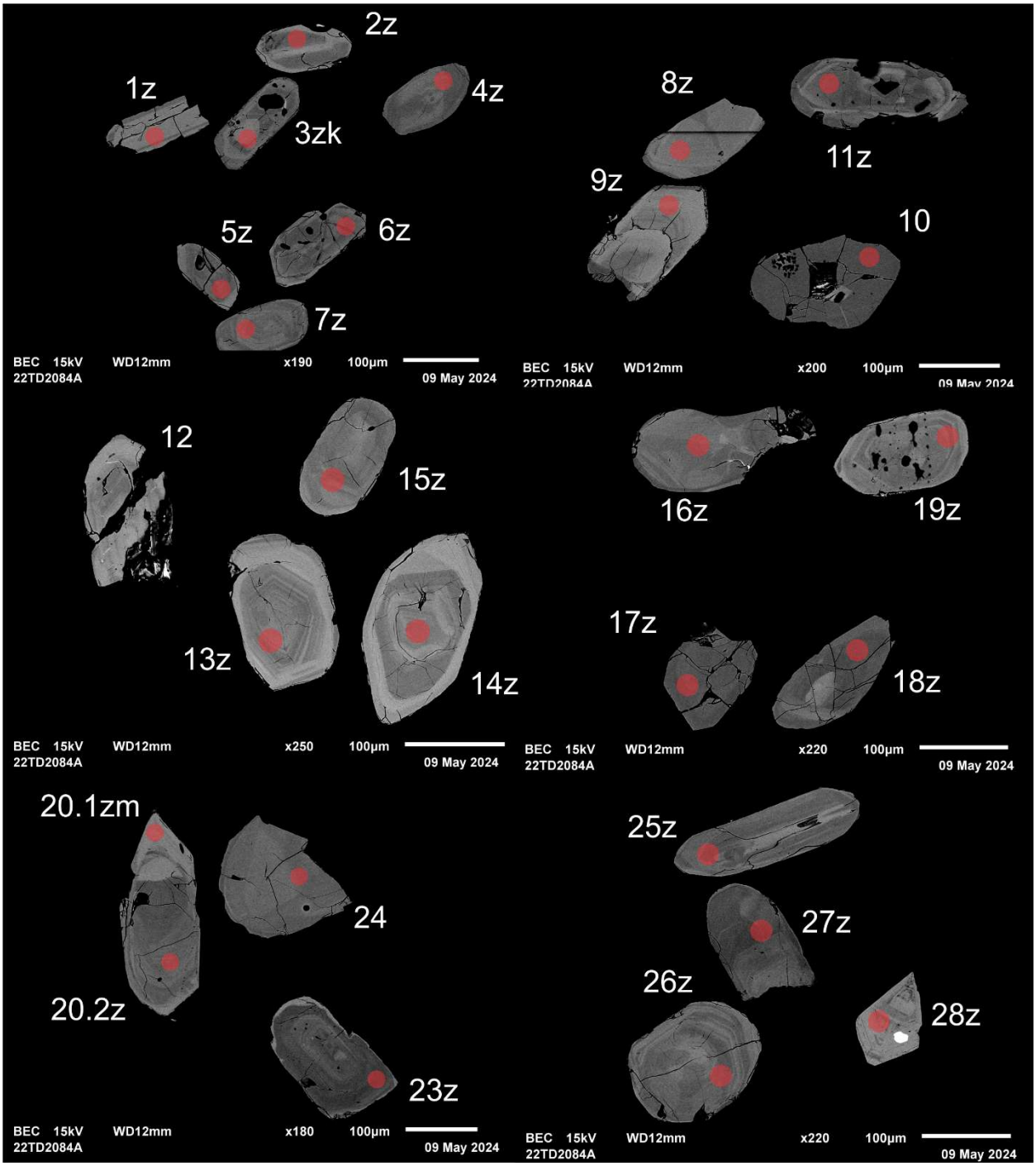

Figure 2.8.2. BSE images of selected grains from sample 2022-TD-2084A. The red circles represent the approximate locations of laser ablation spots.

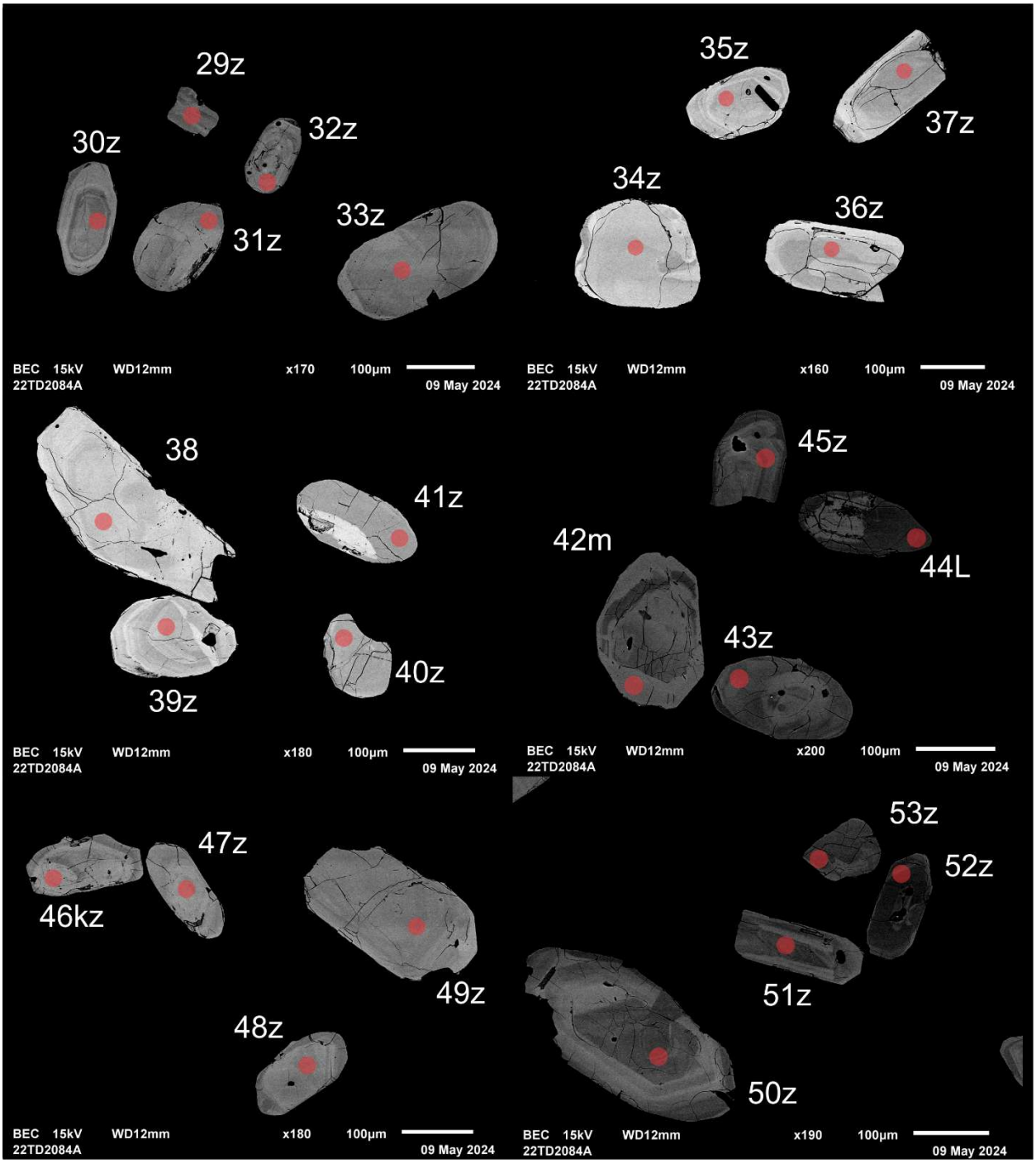

Figure 2.8.2 (cont.). BSE images of selected grains from sample 2022-TD-2084A. The red circles represent the approximate locations of laser ablation spots.

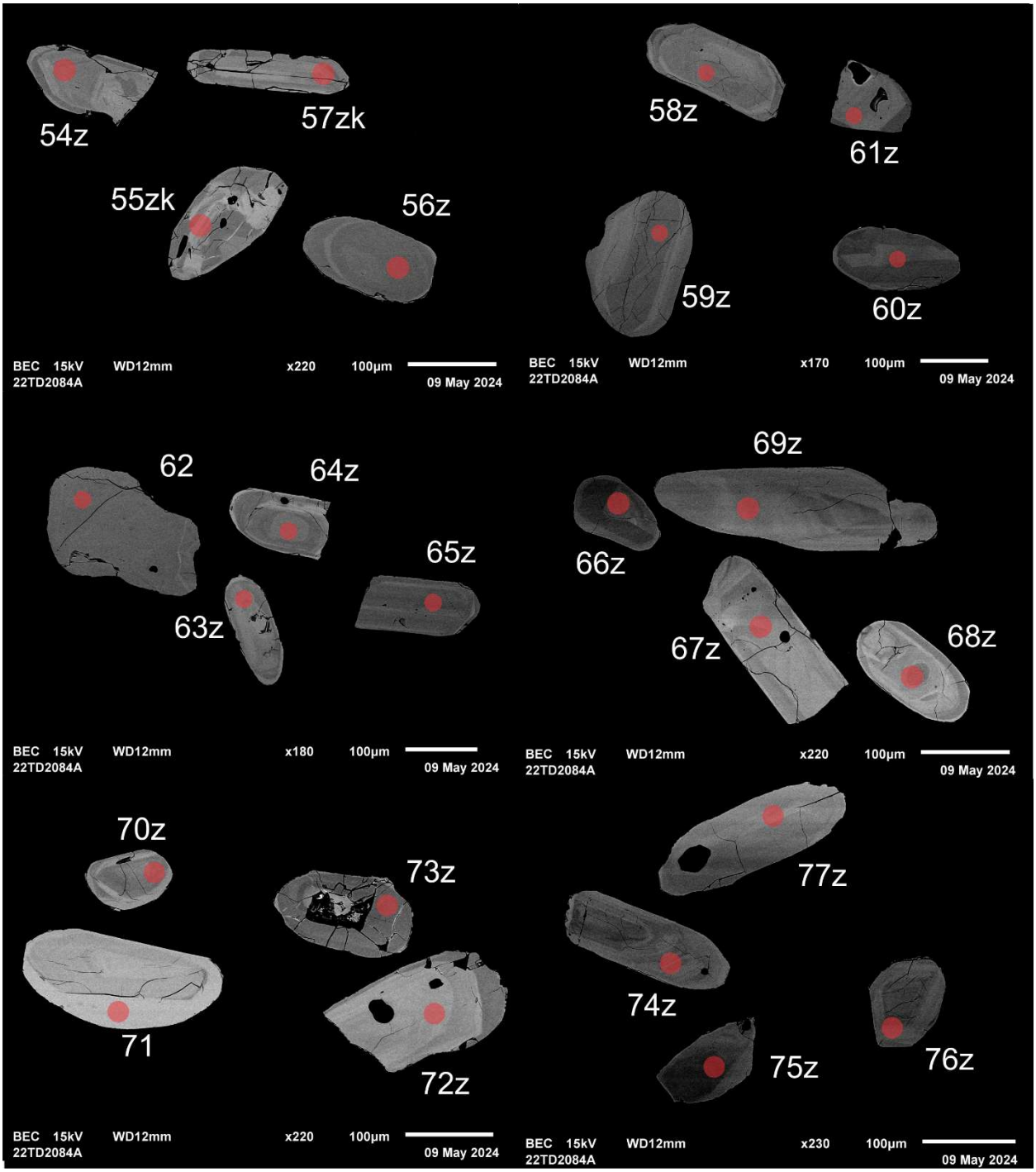

Figure 2.8.2 (cont.). BSE images of selected grains from sample 2022-TD-2084A. The red circles represent the approximate locations of laser ablation spots.

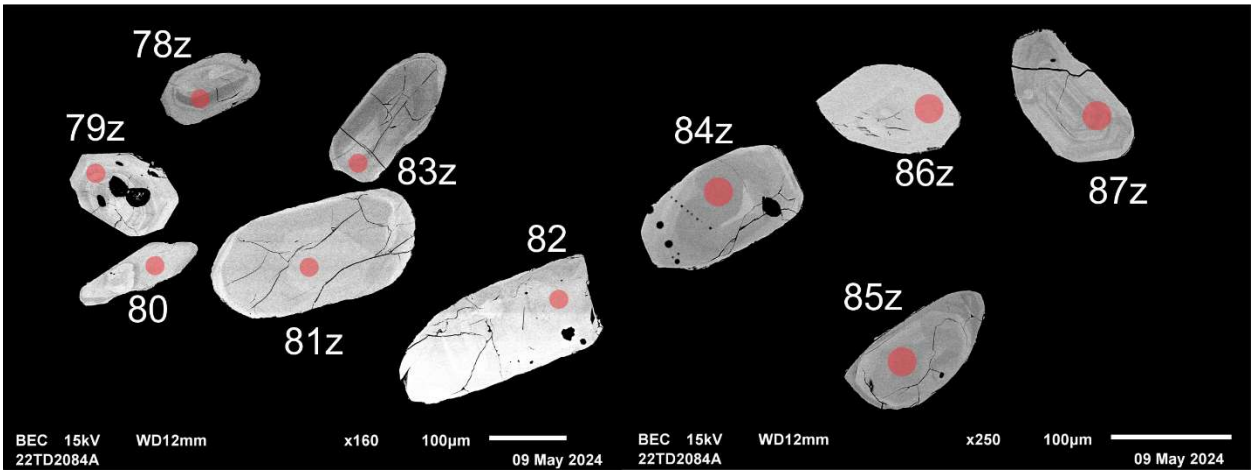

Figure 2.8.2 (cont.). BSE images of selected grains from sample 2022-TD-2084A. The red circles represent the approximate locations of laser ablation spots.

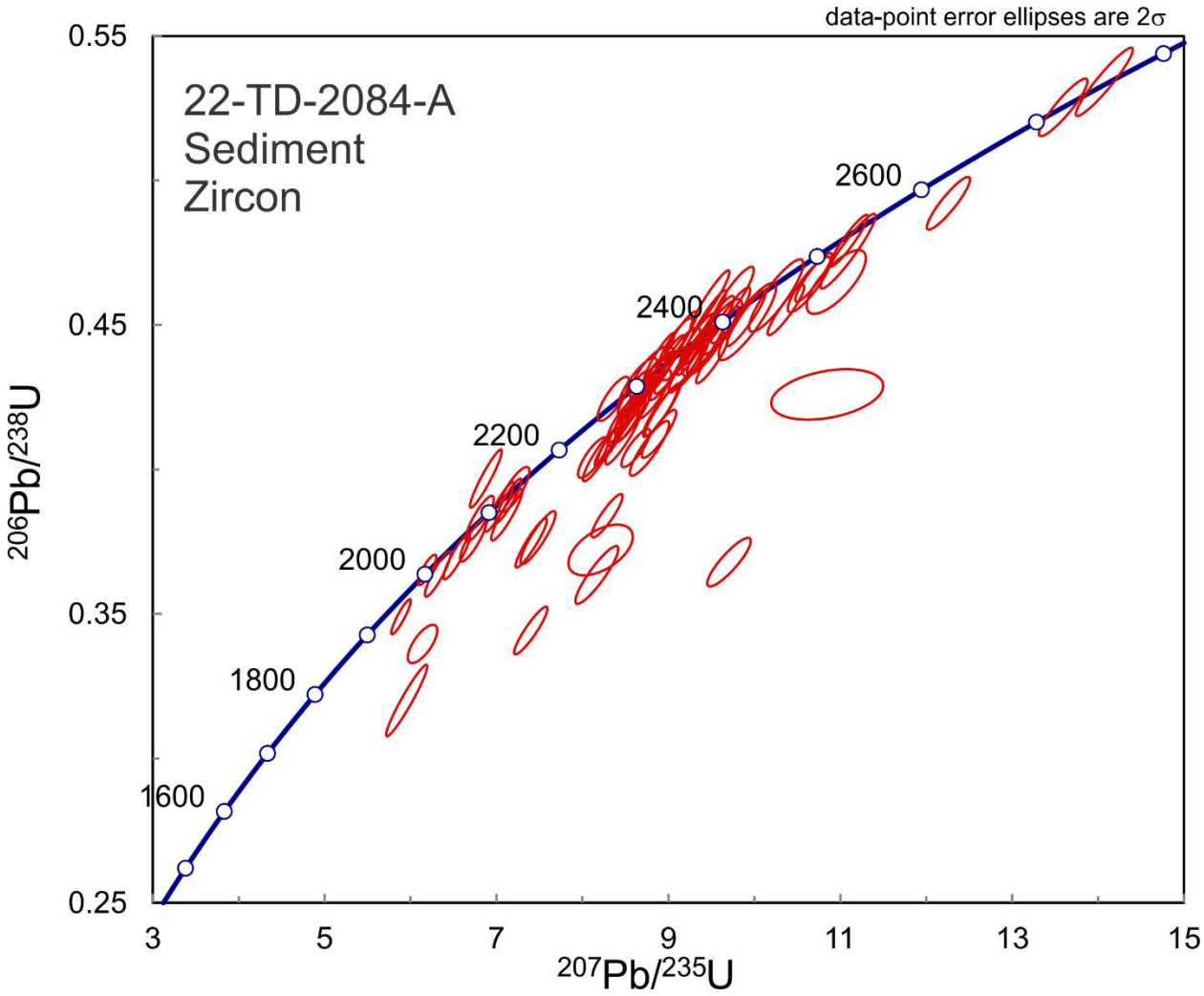

Figure 2.8.3. Concordia plot showing U-Pb isotopic data on polished zircon from wacke sample 2022-TD-2084A.

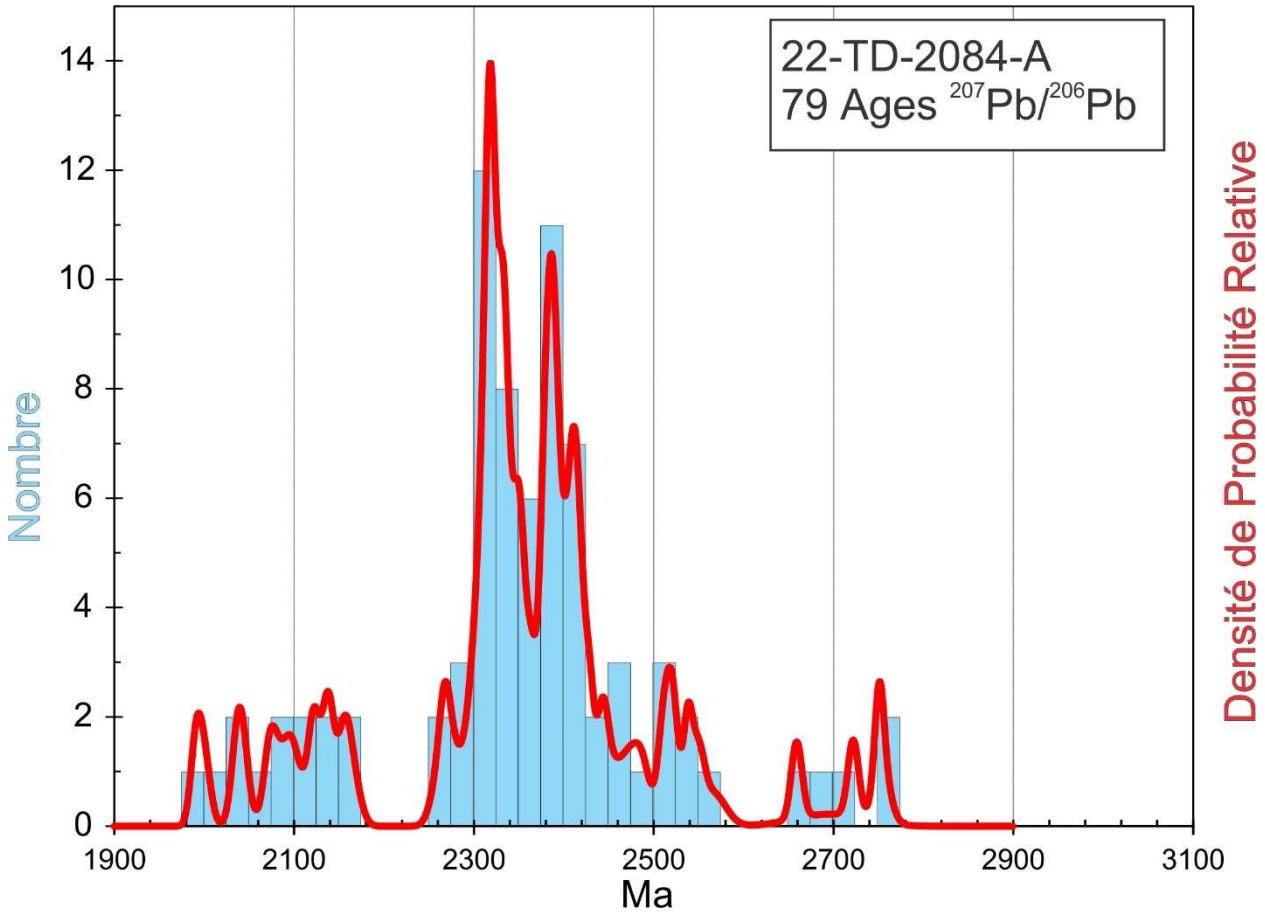

Figure 2.8.4. Combined age relative probability density plot and histogram showing the distribution of $^{207}Pb/^{206}Pb$ ages on polished zircon from wacke sample 2022-TD-2084A.

2.9. 2022-MV-1044-B
Arkose lithique

This sample yielded a small amount of zircon consisting of subhedral to well-rounded stubby grains (Fig. 2.9.1). BSE images show broad zoning patterns with the possibility of some cores and overgrowths (Fig. 2.9.2). U-Pb analyses show diverse ages ranging from 1967 Ma to 2726 Ma (Fig. 2.9.3 and 2.9.4) very similar to the previous sample in that ages are concentrated over the range 2250-2750 Ma (Fig. 2.9.4) with a minor group over the range 1950-2100 Ma. All of the zircon appears to be magmatic and should represent a detrital population, but the degree to which ages may have been reset depends on the metamorphic grade of the sample.

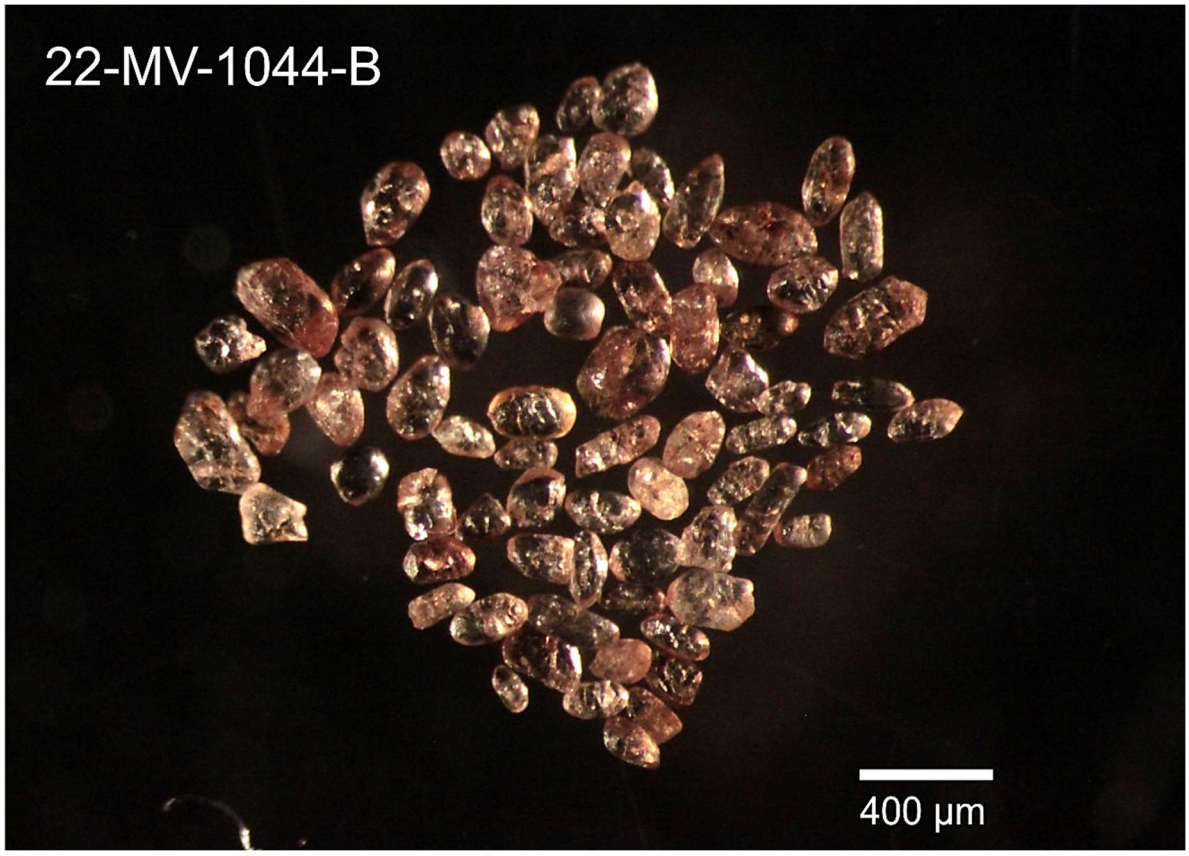

Figure 2.9.1. Picked zircon from arkose lithique sample 2022-MV-1044B.

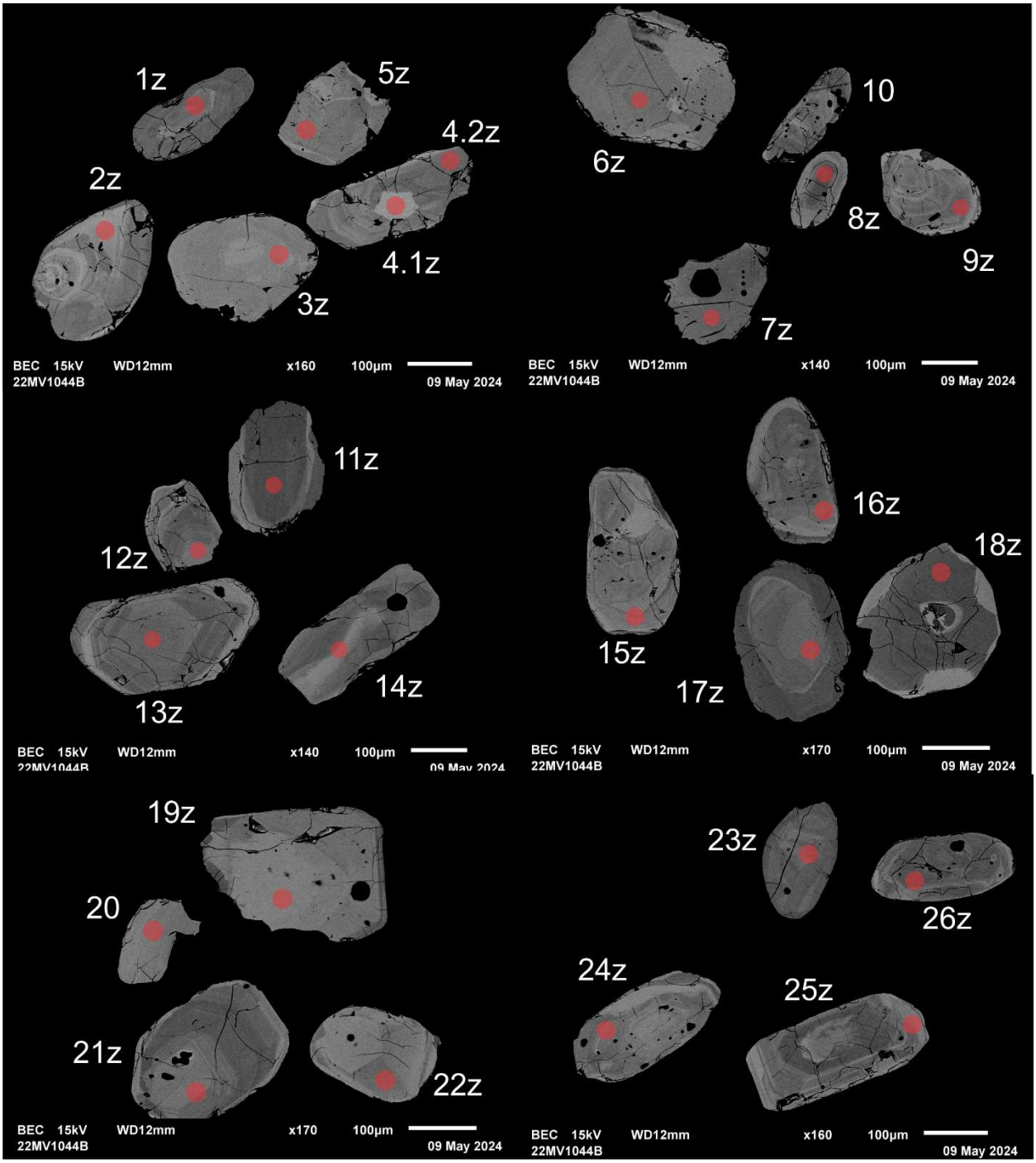

Figure 2.9.2. BSE images of selected grains from arkose lithique sample 2022-MV-1044B. The red circles represent the approximate locations of laser ablation spots.

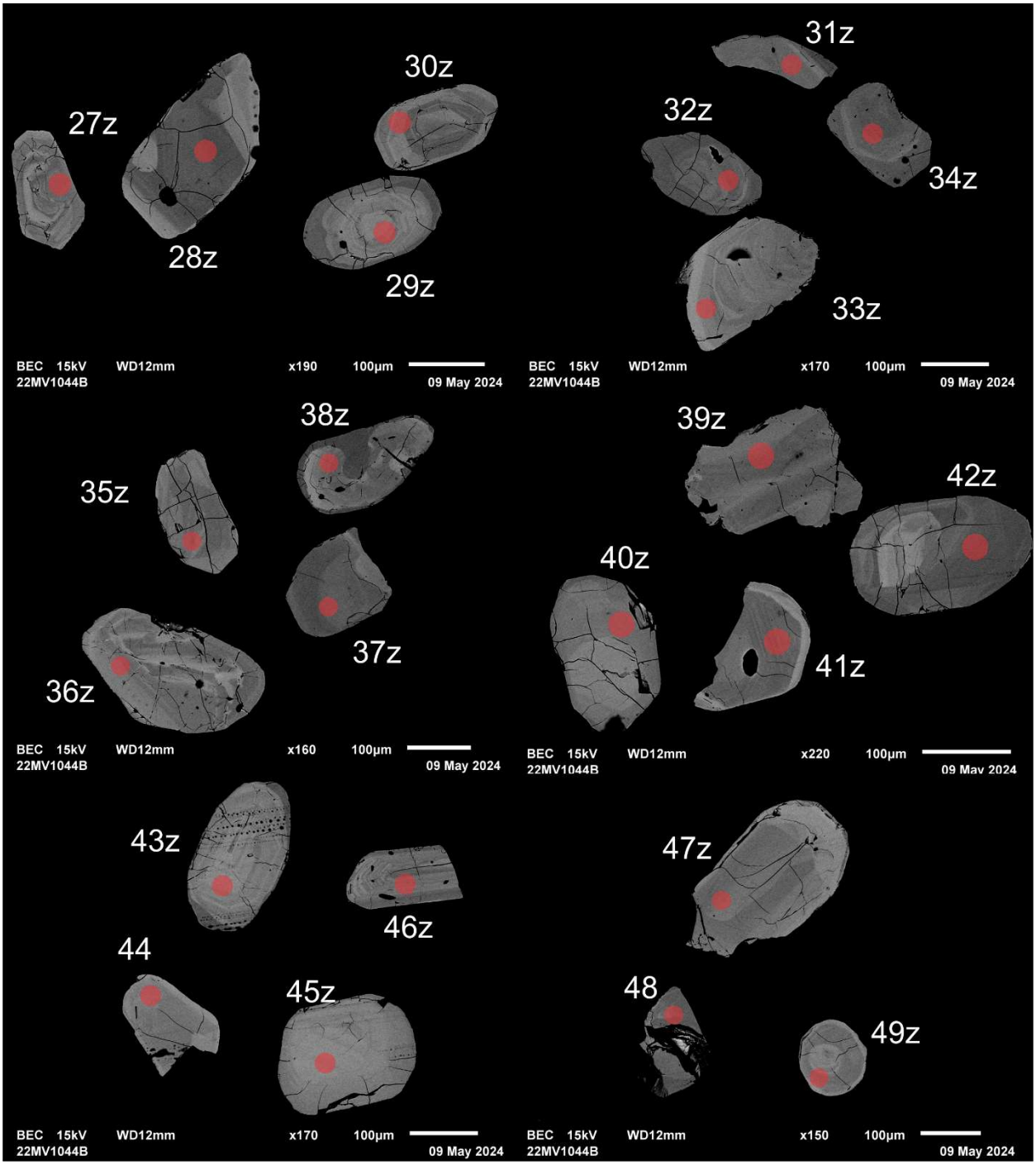

Figure 2.9.2 (cont.). BSE images of selected grains from arkose lithique sample 2022-MV-1044B. The red circles represent the approximate locations of laser ablation spots.

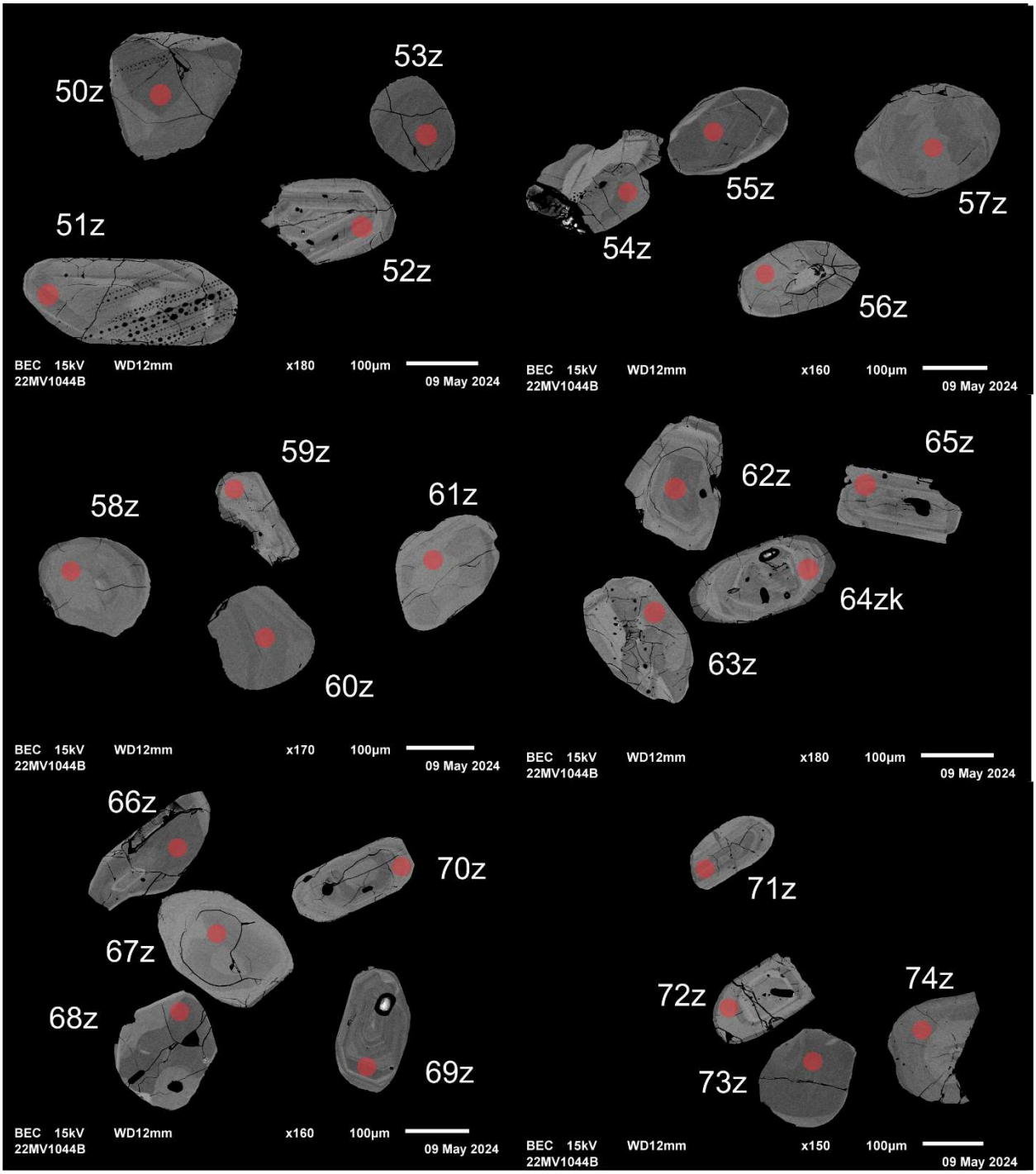

Figure 2.9.2 (cont.). BSE images of selected grains from arkose lithique sample 2022-MV-1044B. The red circles represent the approximate locations of laser ablation spots.

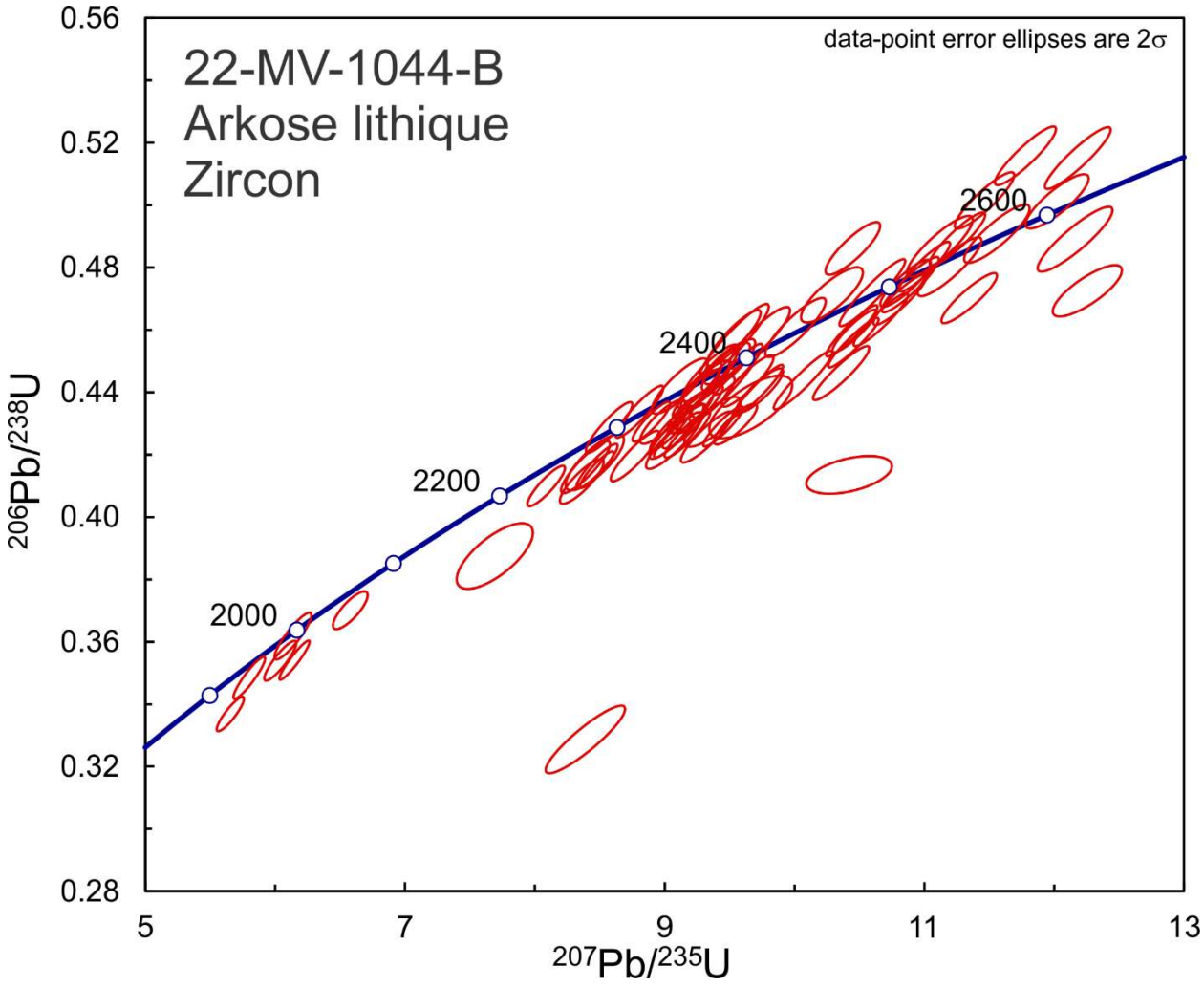

Figure 2.9.3. Concordia plot showing U-Pb isotopic data on polished zircon from arkose lithique sample 2022-MV-1044B.

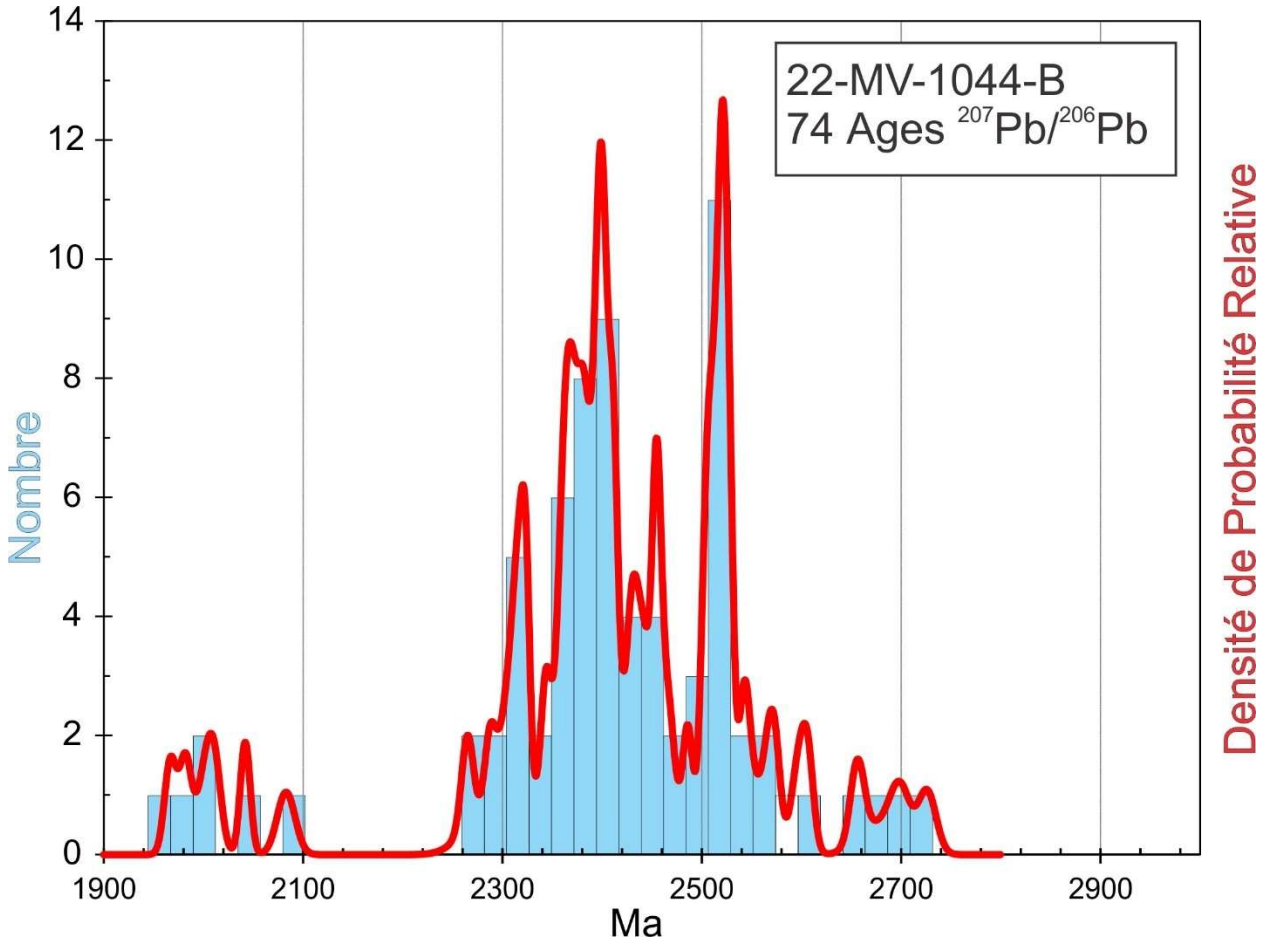

Figure 2.9.4. Combined age relative probability density plot and histogram showing the distribution of $^{207}Pb/^{206}Pb$ ages on polished zircon from arkose lithique sample 2022-MV-1044B.

3. Baie-James - Lac Michaux

3.1. 2023-GS-4071A
Volcanoclastite intermédiaire

This sample yielded only a small amount of zircon as tiny rounded grains (Fig. 3.1.1). Due to their size, the grains were mounted on double-sided tape and analyzed on natural surfaces. $^{207}Pb/^{206}Pb$ ages show a polymodal distribution between 2596 Ma and 2713 Ma but with most ages around 2640 Ma (Fig. 3.1.2 and 3.1.3), U concentrations are relatively high and Th/U ratios (Table 3) are mostly in the range for metamorphic zircon (<0.1). Examination of the individual analytical profiles shows that the two oldest ages have consistently high Th/U ratios with pit depth, suggesting that they are entirely within magmatic zircon. The oldest gives a $^{207}Pb/^{206}Pb$ age of 2713 ±12 Ma, which should be a minimum estimate for the age of volcanism. Many of the other profiles show generally low Th/U with a narrow peak, near the middle, suggesting penetration of the beam through a small igneous core. We conclude that igneous zircon in the felsic volcanic consisted of small grains that acted as nuclei for growth of metamorphic zircon. U-Pb data of 24 analyses give $^{207}Pb/^{206}Pb$ scatter within error resulting in an average age of 2642 ±3 Ma (MSWD = 2.2). The best estimate for the age of metamorphism is the youngest resolvable age peak, which is roughly estimated to be 2639 ±3 Ma (MSWD = 1.3, Fig. 3.1.2).

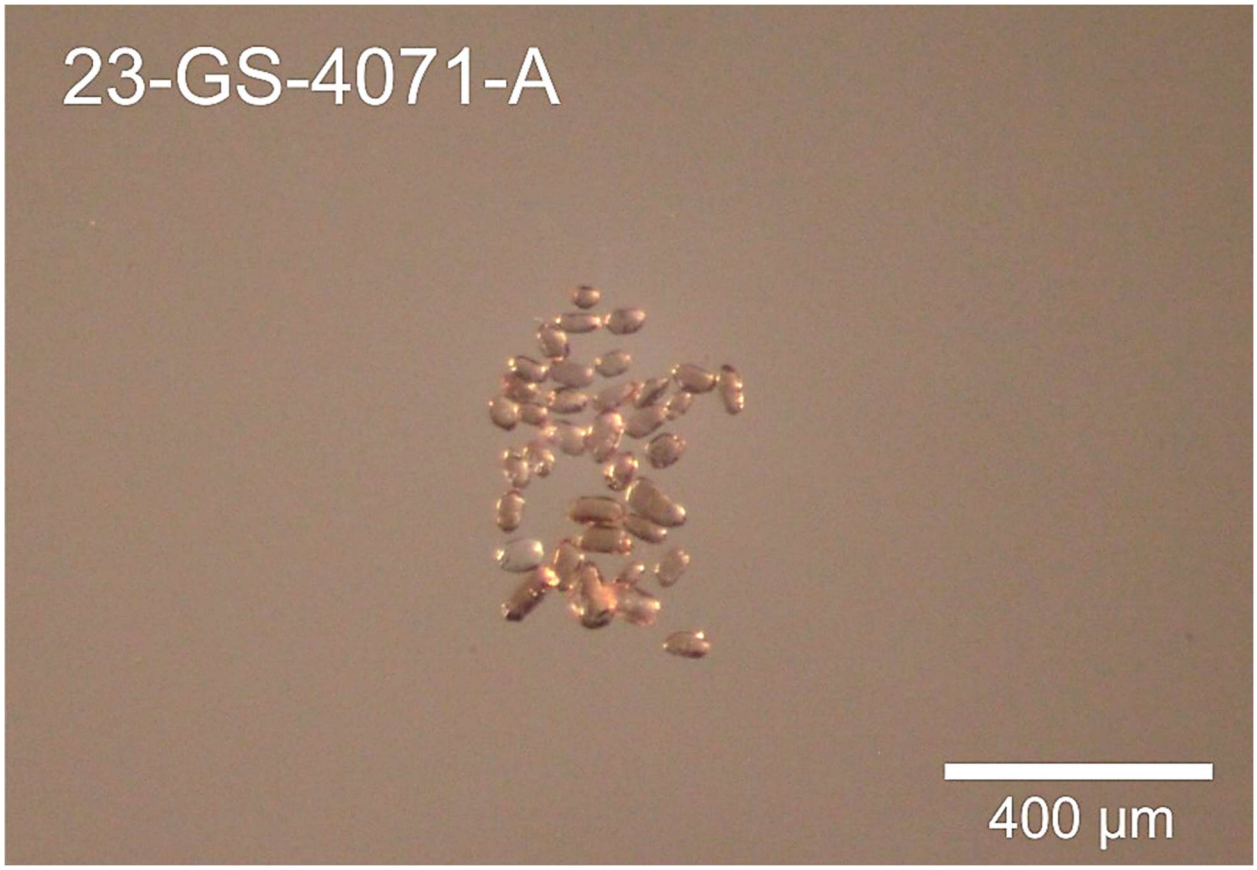

Figure 3.1.1. Picked zircon from volcanoclastite intermédiaire sample 2023-GS-4071A.

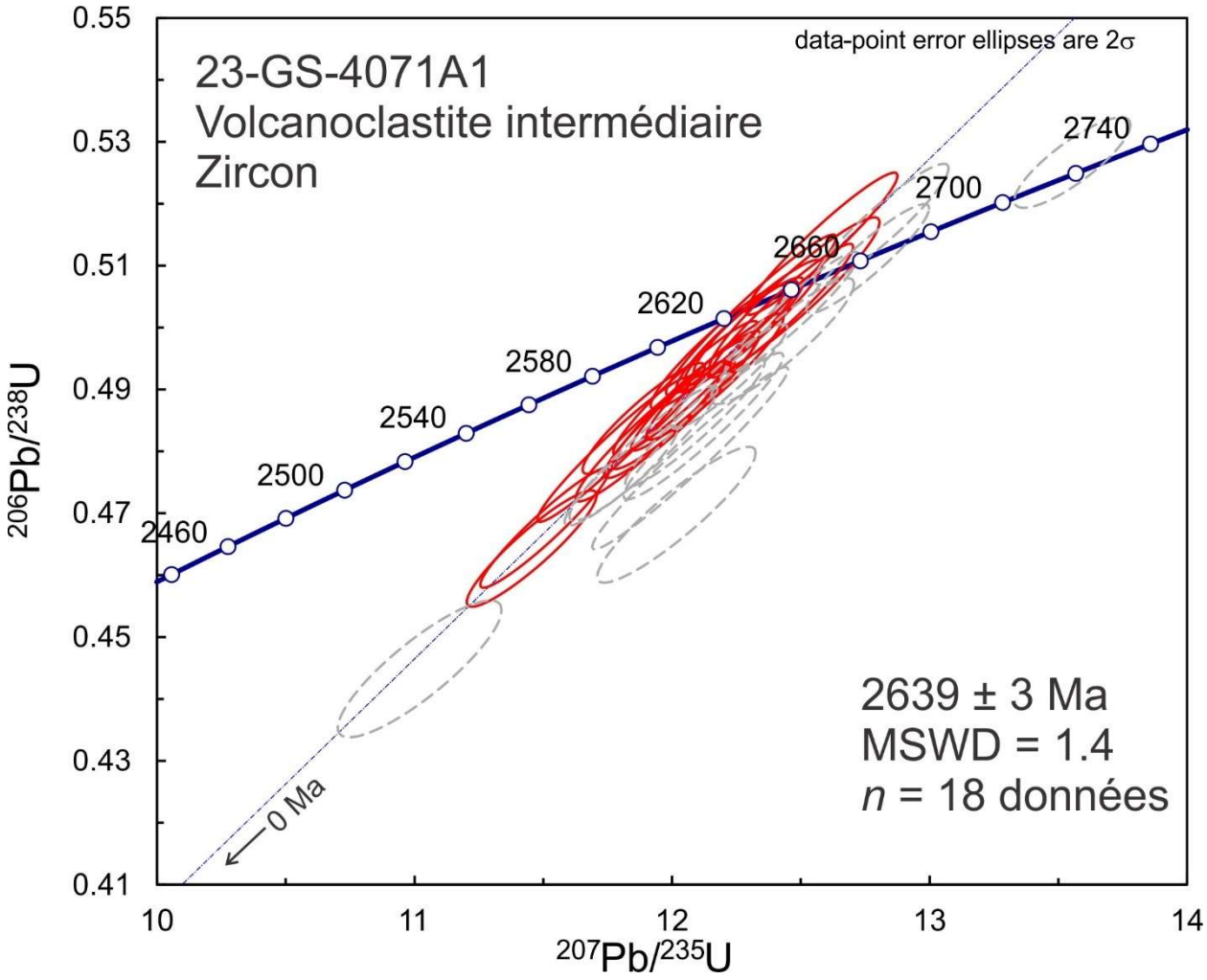

Figure 3.1.2. Concordia plot showing U-Pb isotopic data on polished zircon from volcanoclastite intermédiaire sample 2023-GS-4071A. Red ellipses correspond to spots considered in the age model whereas gray-dashed ellipses correspond to the omitted spots.

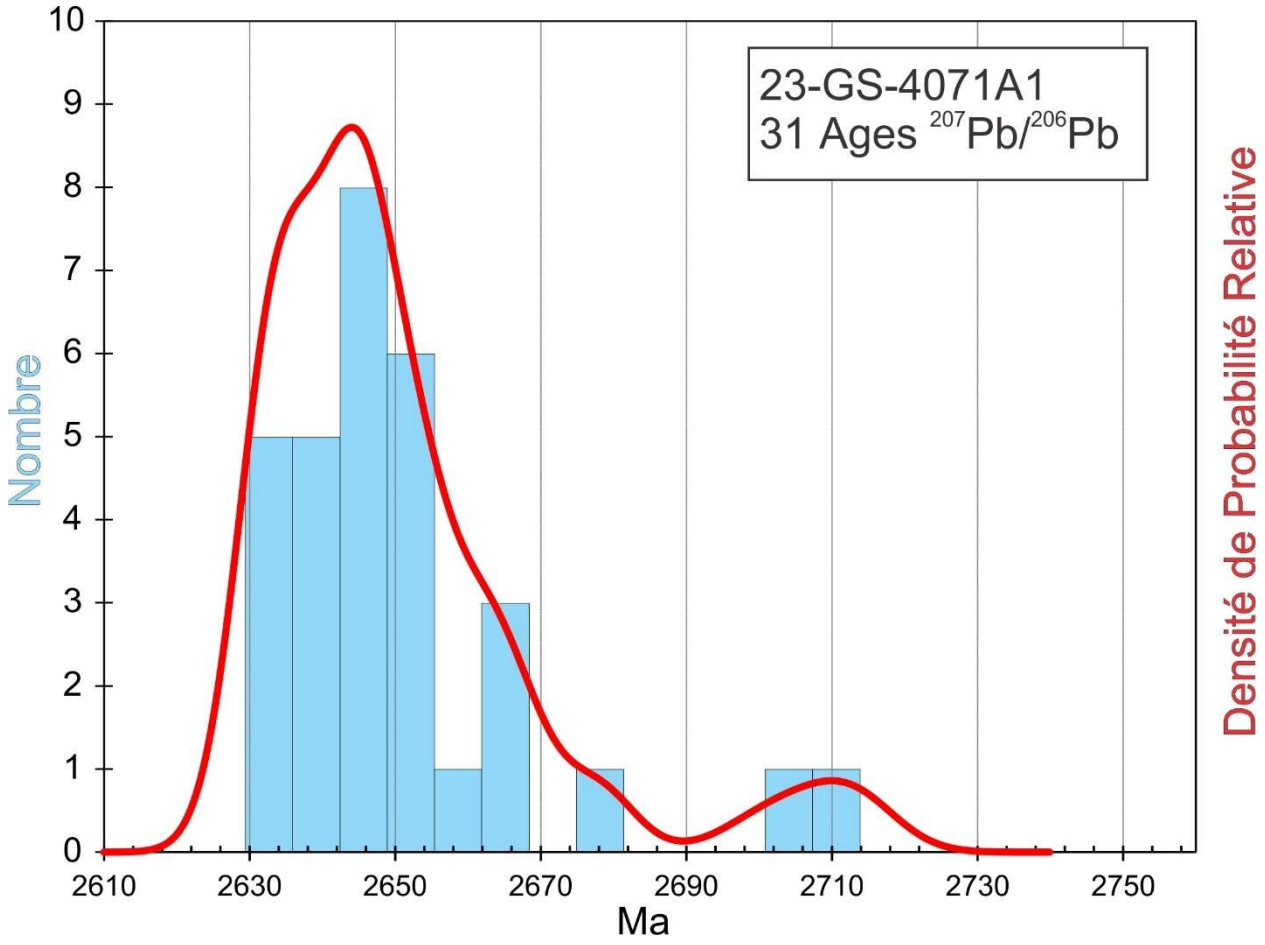

Figure 3.1.3. Combined age relative probability density plot and histogram showing the distribution of $^{207}Pb/^{206}Pb$ ages on polished zircon from volcanoclastite intermédiaire sample 2023-GS-4071A.

3.2. 2023-DB-1059A
Quartzite

This sample shows stubby rounded zircon grains (Fig. 3.2.1). The largest grains show cloudy-white colors (alteration) whereas the smallest are clear, therefore only the smallest and clearest grains were selected for U-Pb dating. The grains were mounted on double-sided tape and analyzed on natural surfaces. U-Pb analyses show ages between 2504 Ma and 2844 Ma (Fig. 3.2.2 and 3.2.3), the youngest and oldest dates correspond to grains showing high Sr signal so are omitted, as are the next 3 youngest grains, which show evidence that the beam intersected metamorphic overgrowth and igneous core phases. This sample also shows monazite grains and give an age of 2550 ±4 Ma (MSWD = 2.6, Fig. 3.2.4). This is likely to represent the approximate age of peak metamorphism. The scatter in ages may reflect growth of different-sized monazite grains during the period of metamorphism.

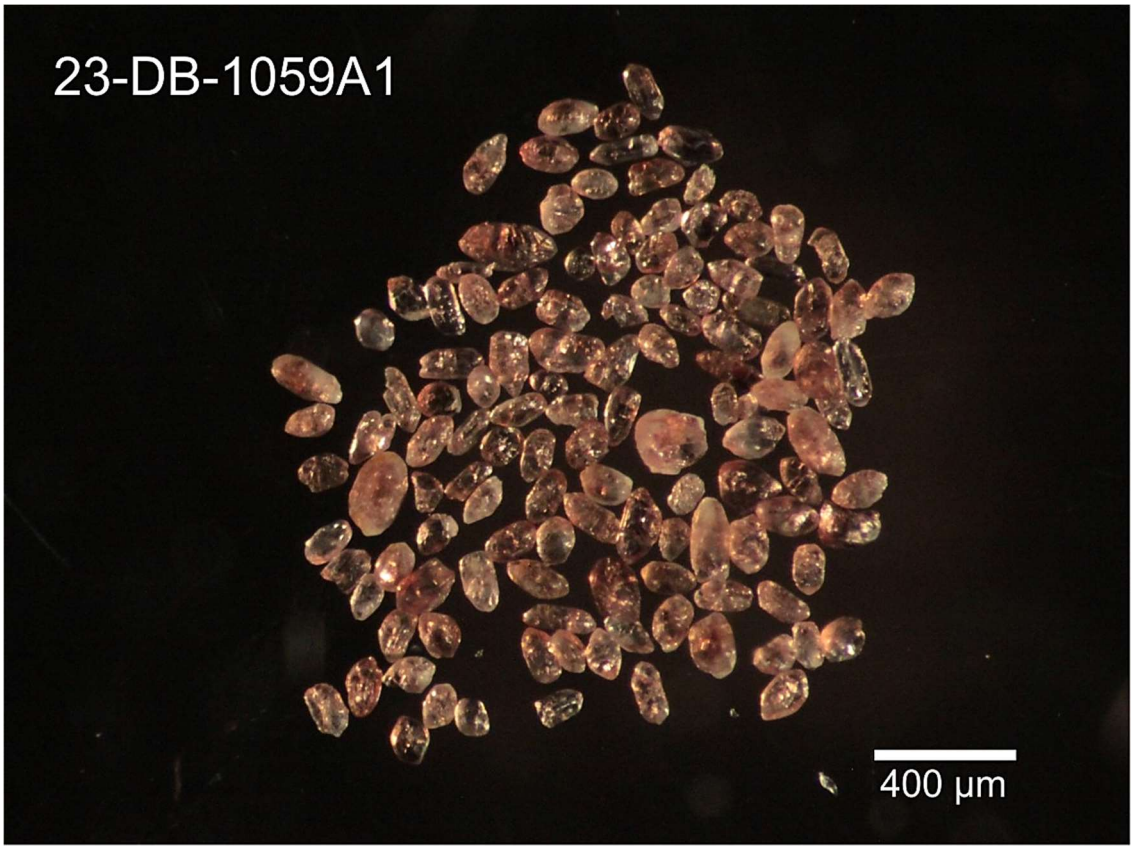

Figure 3.2.1. Picked zircon from quartzite sample 2023-DB-1059A.

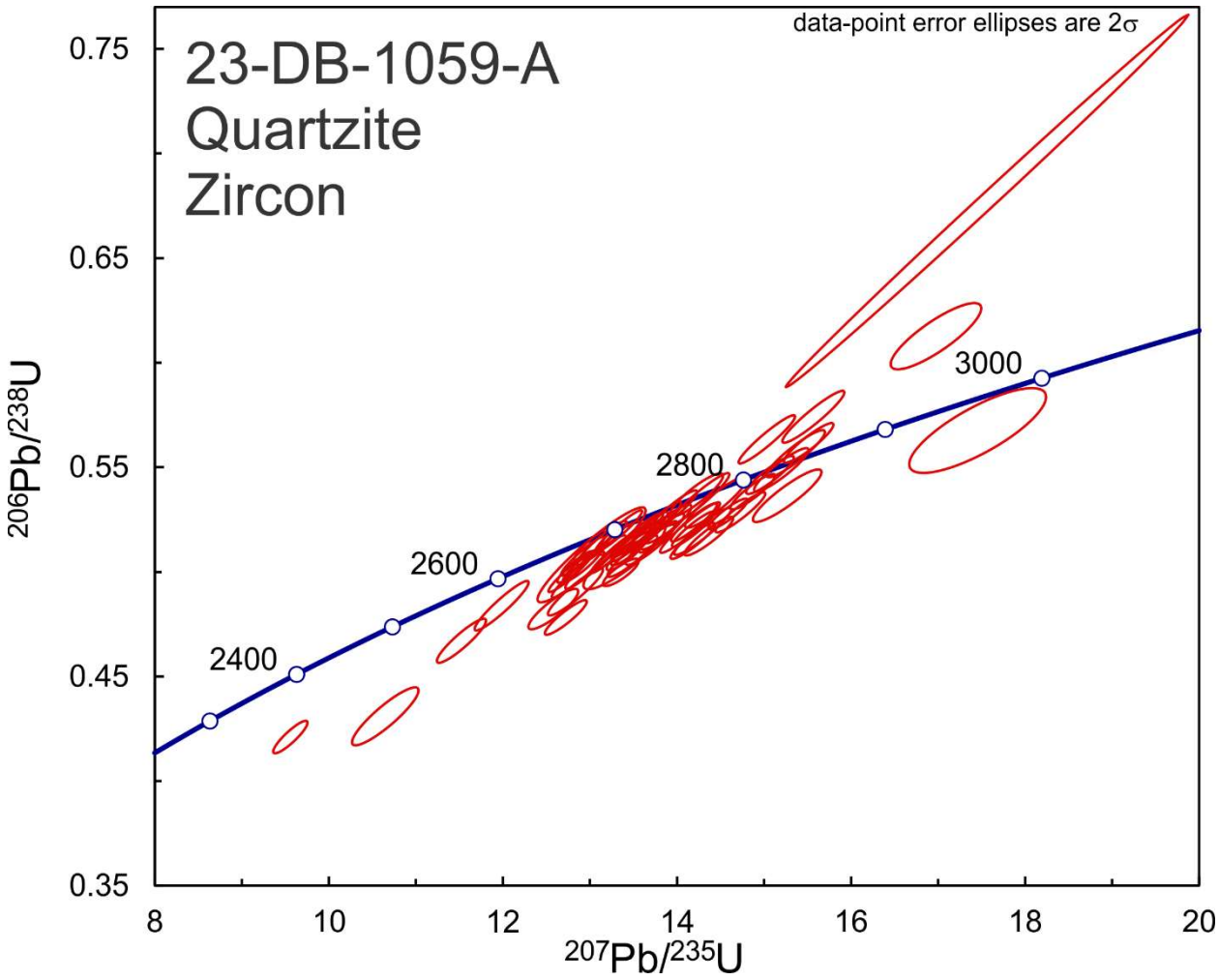

Figure 3.2.2. Concordia plot showing U-Pb isotopic data on zircon from quartzite sample 2023-DB-1059A.

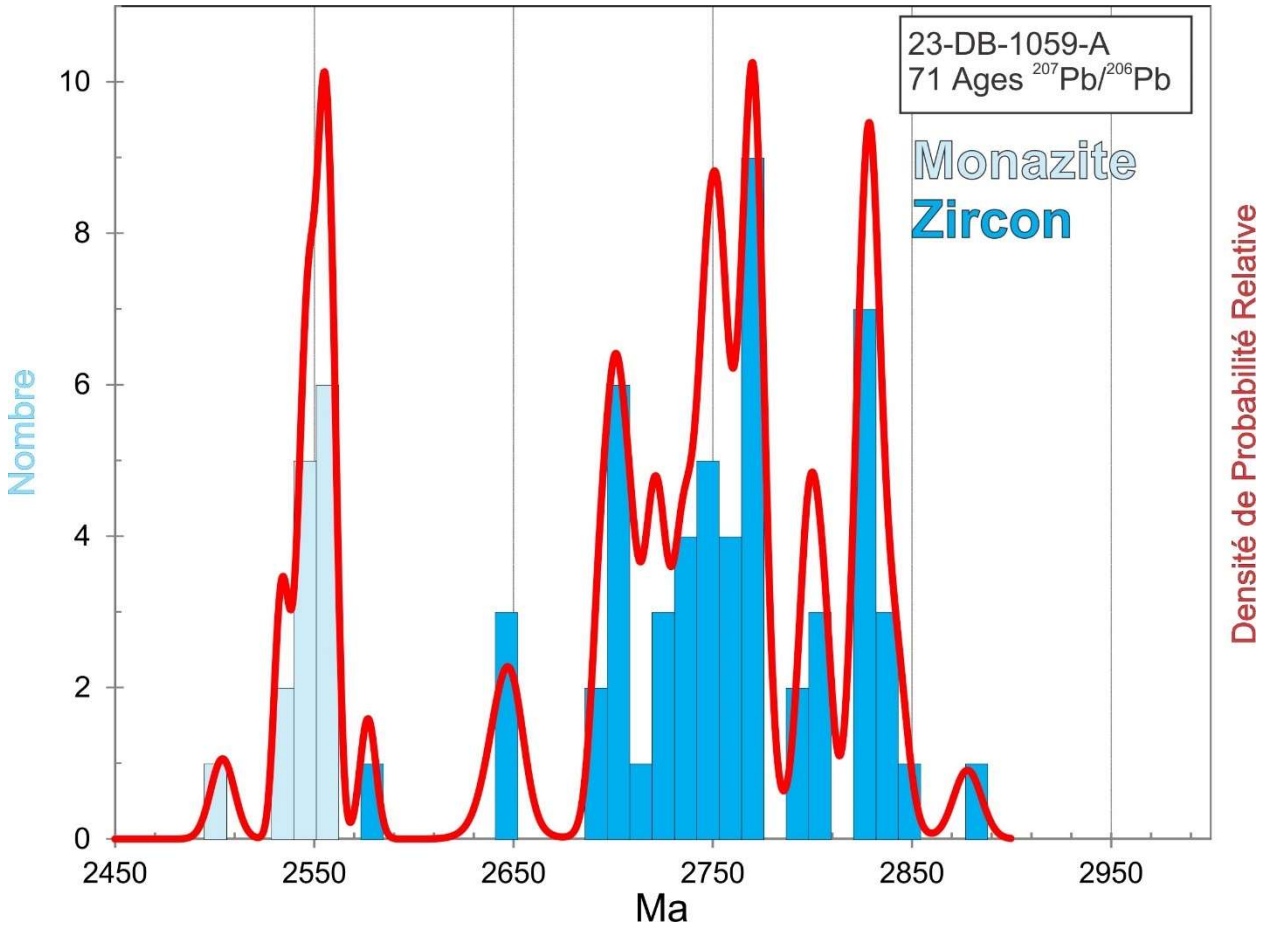

Figure 3.2.3. Combined age relative probability density plot and histogram showing the distribution of $^{207}Pb/^{206}Pb$ ages from quartzite sample 2023-DB-1059A.

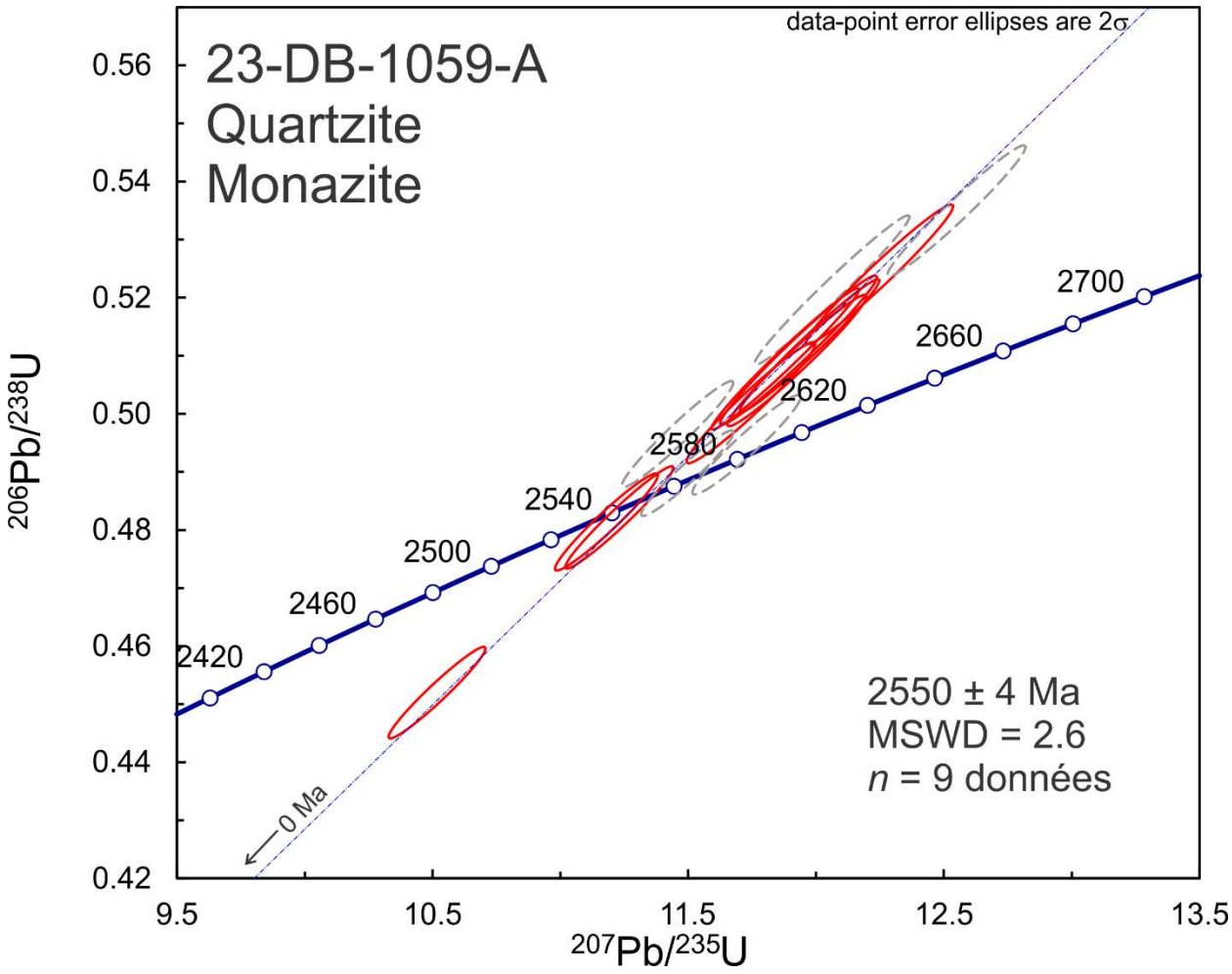

Figure 3.2.4. Concordia plot showing U-Pb isotopic data on monazite from quartzite sample 2023-DB-1059A. Red ellipses correspond to spots considered in the age model whereas gray-dashed ellipses correspond to the omitted spots.

3.3. 2023-NT-2078A
Gneiss tonalitique

No zircon grains were found in this sample; however, the sample contains a few titanite crystals (Fig. 3.3.1). BSE images show zoning patterns, altered zones, and cracks (Fig. 3.3.2). U-Pb analyses show overlapping ages between 2335 Ma to 2821 Ma. A relative probability density plot of $^{207}Pb/^{206}Pb$ ages reveals a resolved age peak at around 2570 Ma. Th/U ratios are <1 suggesting the titanite is metamorphic. Minerals like titanite contain a common Pb component so the Tera and Wasserburg (T-W) diagram is often more convenient. Analyses of a number of undisturbed samples that all share the same age and initial Pb isotopic ratios should be collinear. In the T-W diagram the lower intercept of the mixing line gives the age of the radiogenic component whereas the upper intercept gives the $^{207}Pb/^{206}Pb$ ratio of the common Pb component. Excluding the outliers, the age regression model suggests an age of 2574 ±28 Ma (2σ, MSWD = 2.0) with a $^{207}Pb/^{206}Pb$ ratio of the initial common Pb component of 0.683 (Fig. 3.3.3). The $^{207}Pb/^{206}Pb$ ratio of the initial common Pb component for an age of 2600 Ma should be close to 1.04 as predicted by the Stacey and Kramers (1975) Pb evolution model for average crust. The $^{207}Pb/^{206}Pb$ ages of 11 spots scatter within error resulting in an average age, using the $^{207}Pb/^{206}Pb$ ratio of the initial common Pb component from Stacey and Kramers (1975), of 2587 ±9.5 Ma (2σ, MSWD = 2.1) which agrees within error with the age regression model. In this case, the age error is smaller because the upper intercept of the mixing line is anchored to a “known value” but this might not be as accurate as the free regression model (free fit).

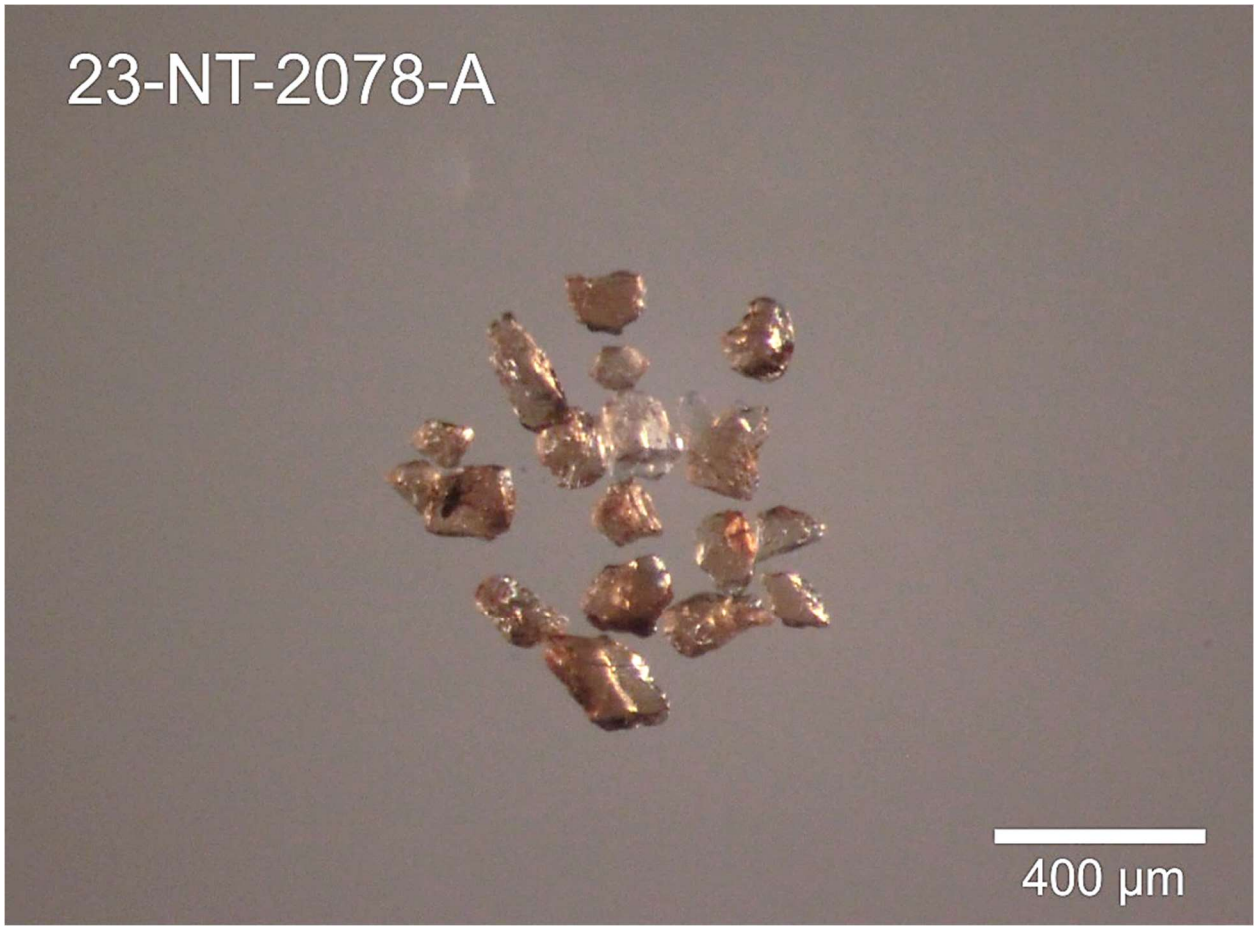

Figure 3.3.1. Picked titanite from gneiss tonalitique sample 2023-NT-2078A.

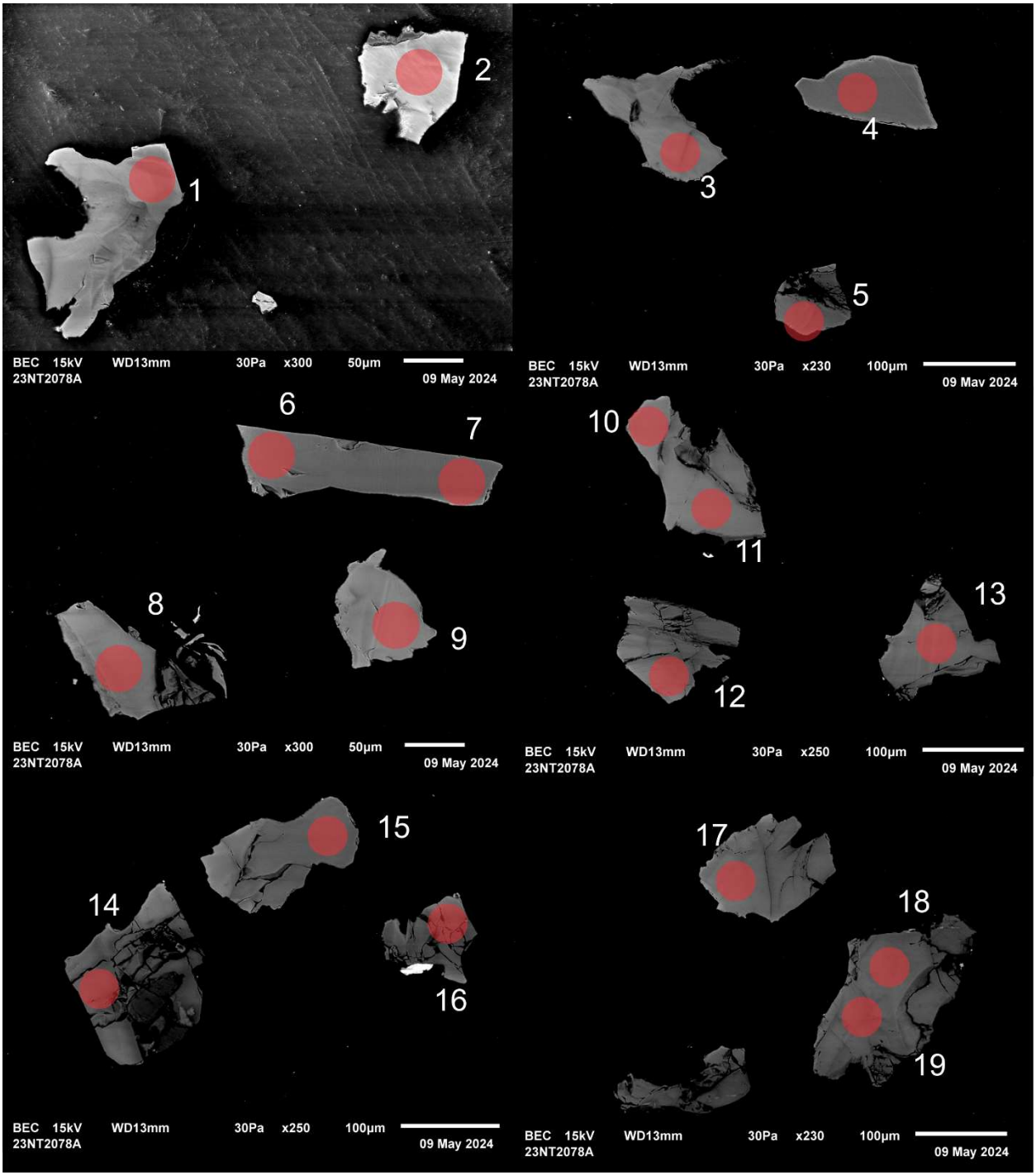

Figure 3.3.2. BSE images of selected titanite grains from gneiss tonalitique sample 2023-NT-2078A. The red circles represent the approximate locations of laser ablation spots.

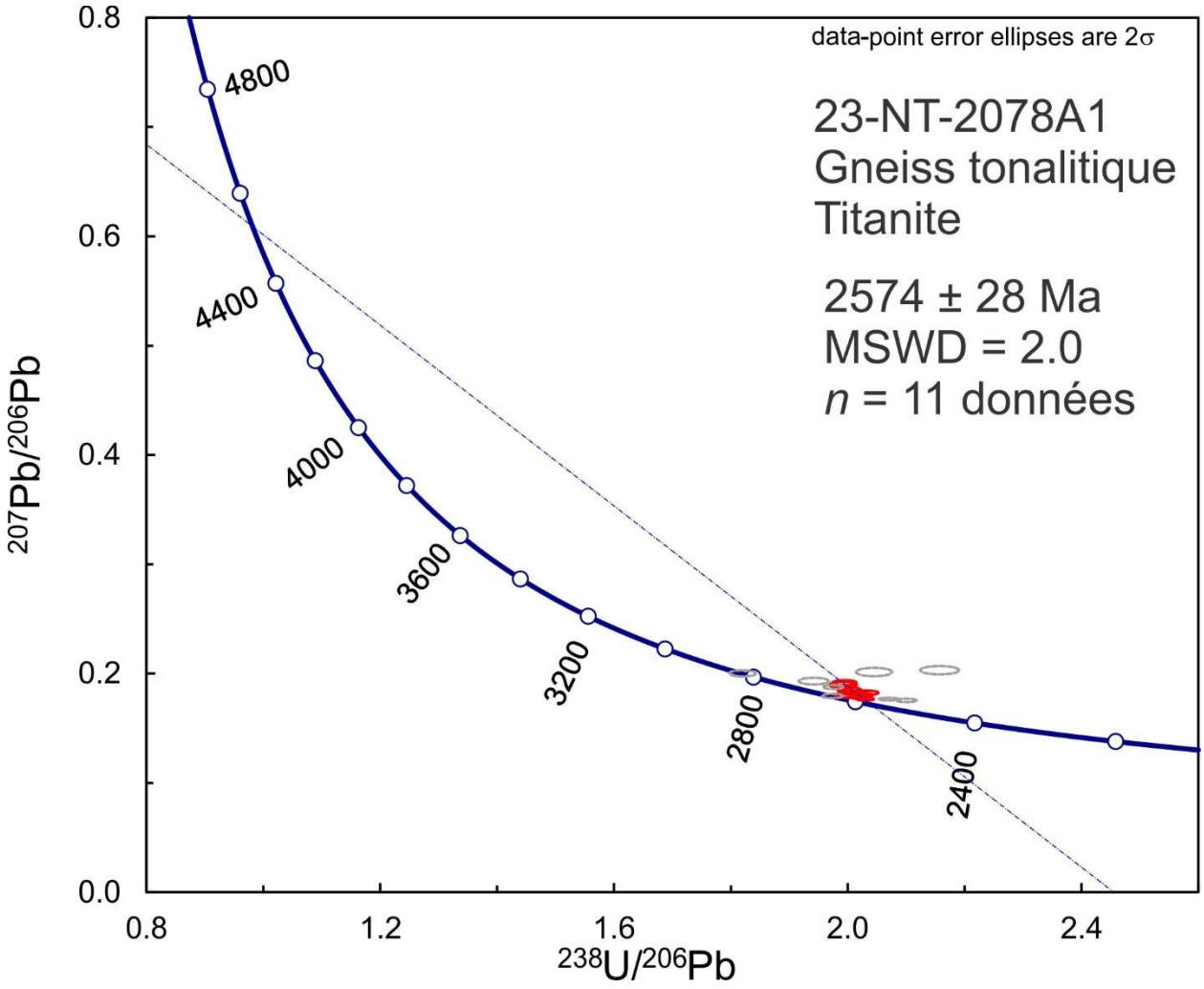

Figure 3.3.3. T-W Concordia plot showing U-Pb isotopic data on titanite grains from gneiss tonalitique sample 2023-NT-2078A. Grey ellipses are omitted from the average age calculation.

3.4. 2023-DB-1057A
Diatexite dérivée de paragneiss

No zircon grains were found in this sample; however, the sample contains a few monazite grains with diverse morphologies (Fig. 3.4.1). BSE images confirm that the grains show fractures, and zoning (Fig. 3.4.2). U-Pb analyses show diverse ages ranging from 2587 Ma to 2683 Ma (Fig. 3.4.3 and 3.4.4). Th/U profiles suggest the presence of at least 2 phases of monazite. The most common shows Th/U around 30 but 3 spots (2, 6 and 13) seem to record phases with Th/U well below this. However, there is no systematic relationship with age or U concentrations. It may be that partial melting and crystallization of monazite occurred over an extended period of time with a peak of monazite formation around 2660 Ma.

Figure 3.4.1. Picked monazite from diatexite dérivée de paragneis sample 2023-DB-1057A.

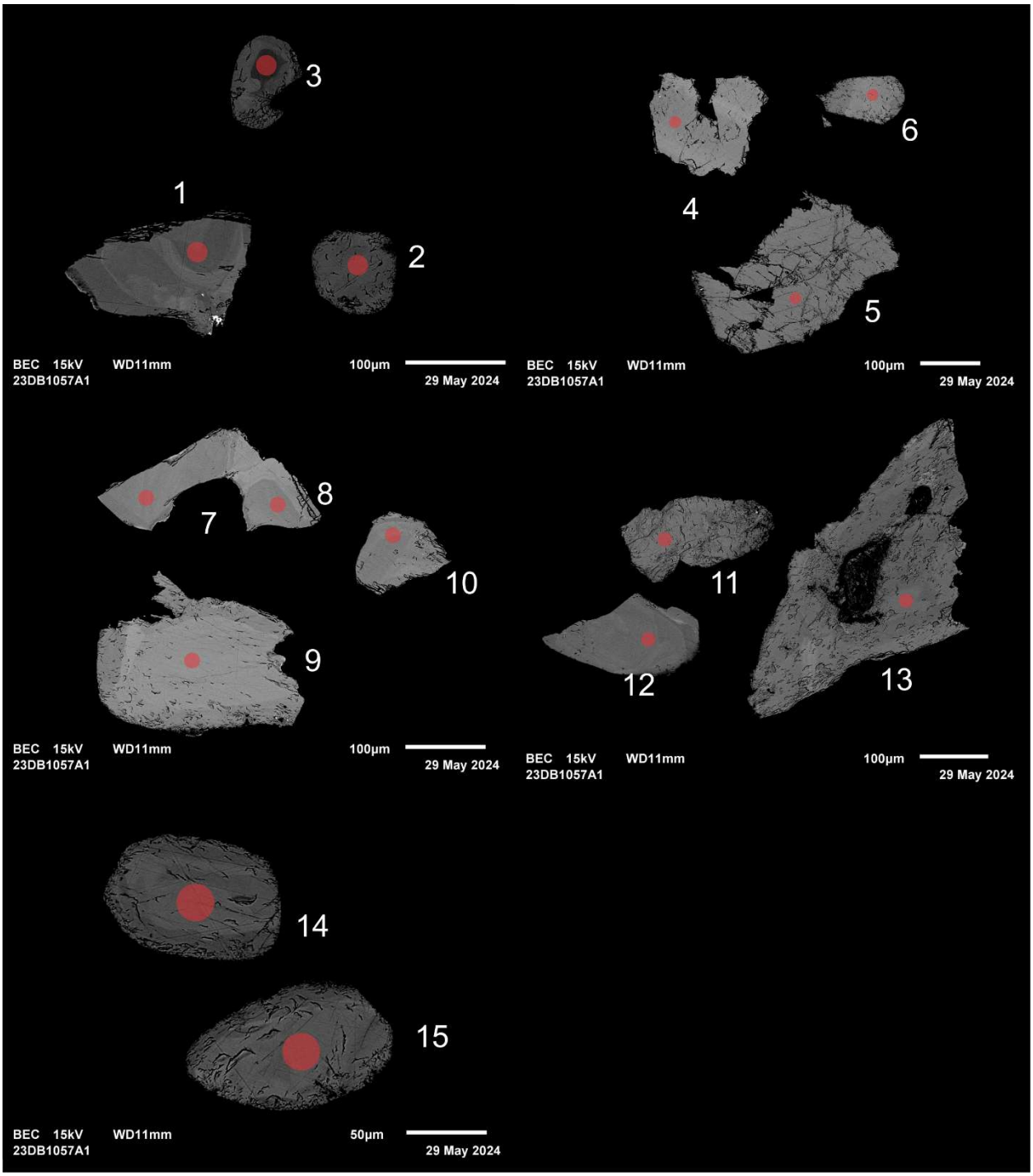

Figure 3.4.2. BSE images of selected grains from sample 2023-DB-1057A. The red circles represent the approximate locations of laser ablation spots.

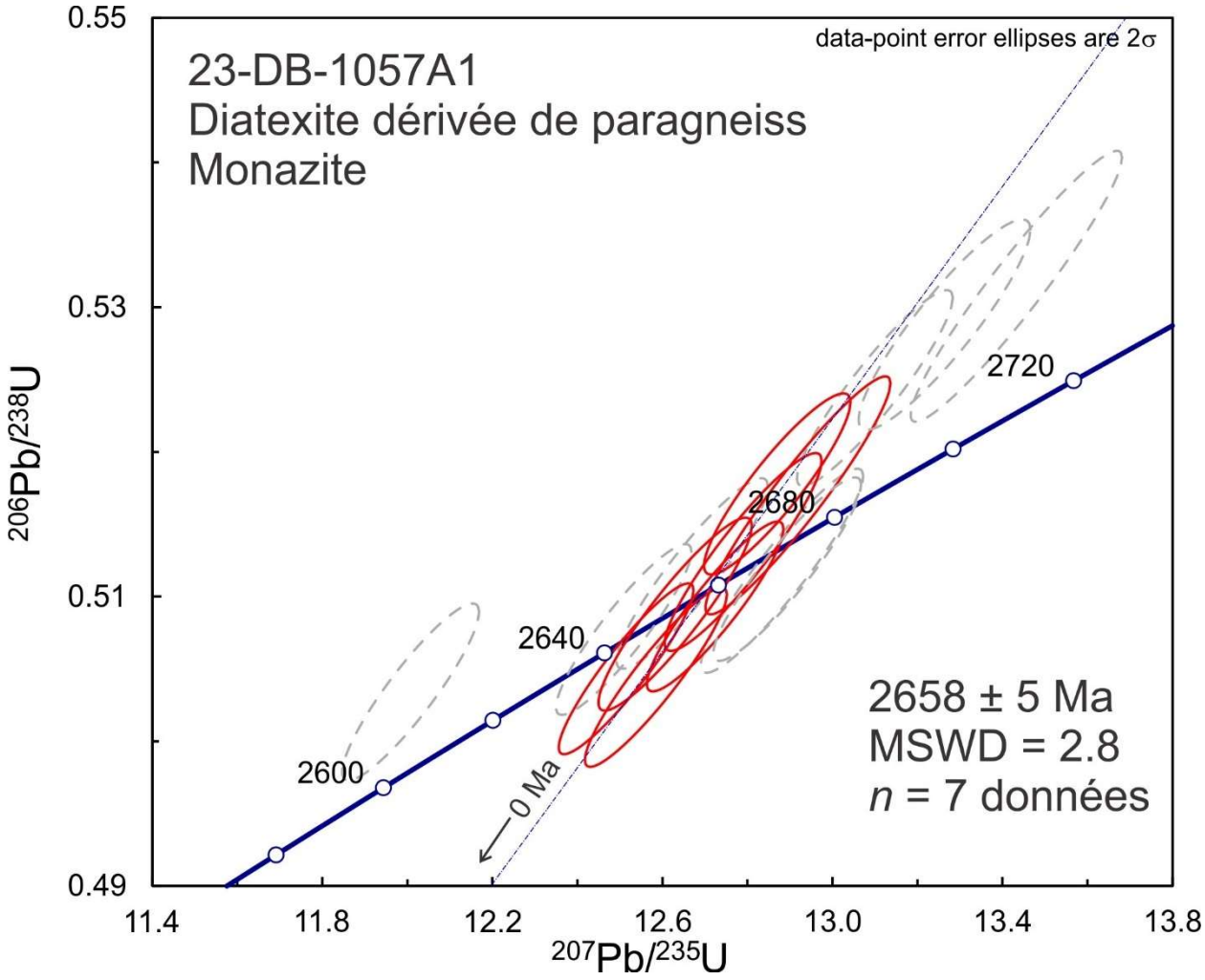

Figure 3.4.3. Concordia plot showing U-Pb isotopic data on polished monazite from diatexite sample 2023-DB-1057A. Red ellipses correspond to spots considered in the age model whereas gray-dashed ellipses correspond to the omitted spots.

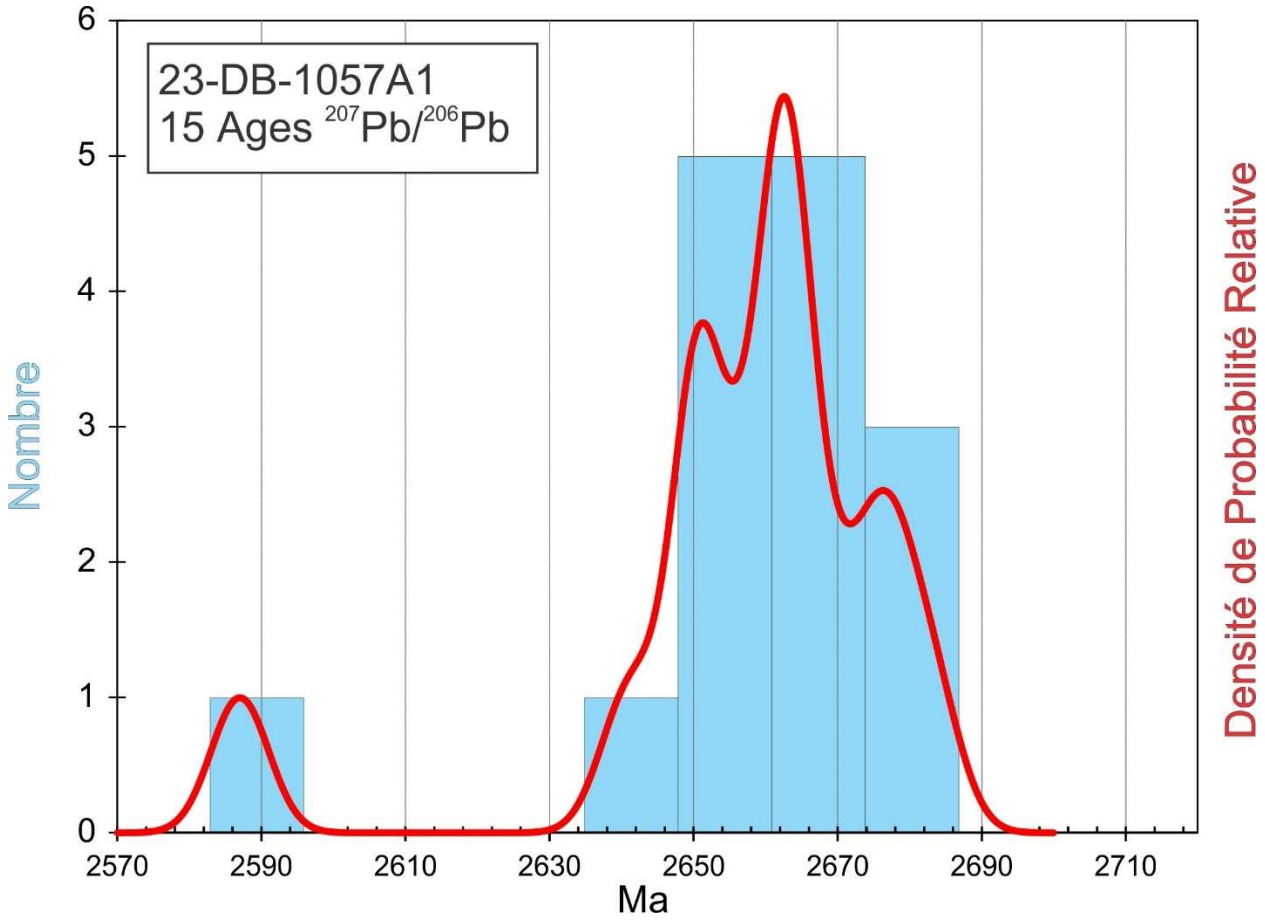

Figure 3.4.4. Combined age relative probability density plot and histogram showing the distribution of $^{207}Pb/^{206}Pb$ ages on polished monazite from diatexite sample 2023-DB-1057A.

REFERENCES

Jaffey, A.H., Flynn, K.F., Glendenin, L.E., Bentley, W.C. & Essling, A.M., 1971. Precision measurement of half-lives and specific activities of 235U and 238U. Physical Review 4: 1889-1906.

Ludwig, K.R., 2003. User's manual for Isoplot 3.00 a geochronological toolkit for Excel. Berkeley Geochronological Center Special Publication 4, 71 p.

Ludwig, K.R., 1998. On the treatment of concordant uranium-lead ages. Geochimica et Cosmochimica Acta 62: 665-676.

Stacey, J.S., and Kramers, J.D., 1975, Approximation of terrestrial lead isotope evolution by two stage model: Earth and Planetary Science Letters, v. 26, p. 207–221.